

OPTIMISATION OF GAS COOLERS FOR CO₂ REFRIGERATION APPLICATION

A thesis submitted for the degree of
Doctor of Philosophy

By

I Dewa Made Cipta Santosa, M.Sc.



Department of Mechanical, Aerospace and Civil Engineering
College of Engineering, Design and Physical Science
Brunel University

December 2015

ABSTRACT

Carbon dioxide (CO₂) is a natural, low cost refrigerant with good thermo-physical properties. CO₂ is a good alternative for replacing HFC refrigerants that possess high global warming potential and reducing the direct impacts of refrigeration systems on the environment. However, CO₂ refrigeration systems operate at relatively high condenser/gas cooler pressures and this imposes special design and control considerations. The gas cooler is a very important part of the system and can have significant influence on its performance. In sub-critical operation, good gas cooler/condenser design can reduce the condenser pressure and delay switching to supercritical operation which increases system efficiency. In supercritical operation optimum design and control can enable the system to operate at pressures that maximise system efficiency.

In air cooled systems, gas coolers/condensers are of the finned-tube type. This type of heat exchanger is well established in the HVAC and refrigeration industries. The large changes in the CO₂ properties in the gas cooler, however, during supercritical operation impose special design and manufacturing considerations. This research project considered the influence of the unique heat transfer characteristics of CO₂ on the design and performance of finned tube air cooled condensers/gas coolers for CO₂ refrigeration applications. A combined experimental and modelling approach using Computational Fluid Dynamics (CFD) was employed. A CO₂ condenser/gas cooler test facility was developed for the experimental investigations. The facility employs a 'booster' hot gas bypass CO₂ refrigeration system, with associated condenser/gas cooler test rig and evaporator load simulation facility. A series of experimental tests were carried out with two gas coolers which incorporated horizontal and horizontal-vertical slit fins and was obtained adequate experimental data concerning gas cooler performance.

CFD modelling was used to study the performance of the gas coolers. The model was validated against test results and was shown to predict the air outlet temperature and heat rejection of the gas cooler with an accuracy of within $\pm 5\%$. The model was subsequently used to evaluate the effect of a fin slit between the 1st and 2nd row of tubes of the gas cooler as well as a vertical slit on the 1st row before the last tube of the section. The results showed a 6%-8% increase in the heat rejection rate of the gas cooler compared to the performance without the horizontal slit. The vertical slit in the fin of the last tube has resulted in an additional increase in heat rejection over and above that for the horizontal slit of 1%-2%.

CFD modelling was also used to investigate the variation of the refrigerant side, air side and overall heat transfer coefficient along the heat exchanger. The results showed that the refrigerant heat transfer coefficient increases with the decreasing of bulk refrigerant temperature and reaches its maximum when the specific heat of the refrigerant is highest. Furthermore, increasing the refrigerant mass flux, increases the refrigerant side heat transfer coefficient and heat rejection. This can reduce the size of the gas cooler for a given capacity at the expense of higher pressure drop and compressor power consumption. Air side and overall heat transfer coefficient correlations were developed for the specific gas cooler designs which were investigated and showed the heat transfer coefficients increase with increasing Reynolds Number .

PUBLICATIONS

Published journal papers:

Y.T. Ge, S.A. Tassou, **I. Dewa Santosa**, K. Tsamos, 2015. Design optimisation of CO₂ gas cooler/condenser in a refrigeration system. *Applied Energy* xxx, xxx–xxx.

Published conference papers:

ID.M.C. Santosa, IN. Suamir, Y.T. Ge, K. Tsamos, S.A. Tassou, 2013, Modelling and analysis of CO₂ gas coolers for commercial refrigeration applications, *Proc. 2nd IIR Conference on Sustainability and the Cold Chain*, Paris, France, ISBN978-2-913149-97-7, paper no.S12-P2, 8 pgs.

ID.M.C. Santosa, K.M.Tsamos, S.A. Tassou, Y.T. Ge, S. Jones, N. Atkins, 2014, Experimental investigation of the performance of finned tube CO₂ refrigeration gas coolers, *Proc. 3rd IIR Conference on Sustainability and the Cold Chain*, London, UK, ISBN 978-2-36215-003-6, paper ID 216, page 589-605.

Y.T. Ge, S.A. Tassou, **IDewa Santosa**, K.Tsamos, S. Jones, N. Atkins (2014). Design and integration of CO₂ condenser/gas cooler in a refrigeration system, *Proc. 3rd IIR Conference on Sustainability and the Cold Chain*, London, UK, ISBN 978-2-36215-003-6 paper ID 206, page 555-562.

Y.T. Ge, S.A. Tassou, **ID. Santosa**, K.Tsamos (2014). Design optimisation of CO₂ condenser/gas cooler in a refrigeration system, *Proc. The 6th of International Conference on Applied Energy-ICAE 2014*, Taiwan.

IDewa M.C. Santosa, Baboo L. Gowreesunker, Savvas A. Tassou, Konstantinos M. Tsamos, Yunting Ge, 2015, Investigation of refrigerant side-heat transfer coefficient of finned-tube CO₂ gas coolers using Computational Fluid Dynamics (CFD), *Proc. 3rd Sustainable Thermal Energy Management International Conference (SusTEM2015)*, Newcastle Upon Tyne, UK, page 320-329.

Konstantinos M. Tsamos, Yunting Ge, **ID.M.C. Santosa**, S.A.Tassou, Experimental investigation of CO₂ gas cooler/condenser in a refrigeration system, 2015, *Proc. 14th International Conference on Sustainable Energy Technologies (SET 2015)*, Nottingham, UK.

Yunting Ge, Savvas Tassou, Konstantinos Tsamos, **IDewa Santosa**, Effect of geometry on the performance of CO₂ gas cooler/condenser and its associated refrigeration system, 2015, The 24th IIR International Congress of Refrigeration (ICR 2015), Yokohama, Japan.

CONTENTS

ABSTRACT	ii
PUBLICATIONS	iii
CONTENTS	iv
LIST OF FIGURES	ix
LIST OF TABLES	xvi
ACKNOWLEDGEMENTS	xvii
NOMENCLATURE.....	xviii
ABBREVIATION AND GLOSSARY	xx
CHAPTER I - INTRODUCTION.....	1
1.1 Use of carbon dioxide (CO ₂) as refrigerant	3
1.2 Refrigeration systems in supermarket and GHG emissions	3
1.3 Finned-tube condenser/gas coolers in CO ₂ refrigeration systems	5
1.4 Research aim and objectives.....	6
1.5 Structure of the thesis	7
CHAPTER II - LITERATURE REVIEW	9
2.1 Introduction.....	9
2.2 CO ₂ refrigeration system	10
2.2.1 CO ₂ refrigeration system with booster bypass gas system.....	10
2.2.2 CO ₂ refrigeration system with internal heat exchanger (IHX).....	11
2.2.3 CO ₂ refrigeration system using ejector	12
2.3 Supercritical CO ₂ refrigeration system performance and optimum pressure correlation.....	13
2.4 Control system for optimum performance in supercritical operation.....	15
2.5 Heat transfer coefficient and refrigerant pressure drop of supercritical CO ₂	17
2.5.1 Supercritical CO ₂ heat transfer coefficient.....	17
2.5.2 CO ₂ pressure drop correlation	21
2.5.3 Air side heat transfer coefficient-finned and tube heat exchanger	22
2.6 Finned and tube gas cooler simulation	25
2.7 Effect of the thermal conduction in gas coolers	27
2.8 Summary.....	30
CHAPTER III - TEST FACILITIES	33
3.1 Introduction.....	33
3.2 Mechanical system and components	34
3.2.1 CO ₂ compressors (HT and LT compressors).....	37
3.2.2 Refrigeration load system.....	37
3.2.2.1 MT display cabinet.....	38

3.2.2.2	Air cooler.....	39
3.2.2.3	MT Additional load.....	39
3.2.3	Standstill condensing unit.....	40
3.2.4	CO ₂ receiver	41
3.2.5	Expansion devices (ICMT valve, ICM valve and AKV)	41
3.2.5.1	ICMT valve	42
3.2.5.2	ICM valve.....	43
3.2.5.3	AKV expansion valve	44
3.2.6	Oil management system and components	44
3.2.7	Gas cooler test rig.....	46
3.2.7.1	Gas cooler heat exchanger.....	47
3.2.7.2	Electrical air heaters	47
3.2.7.3	Main fans and recirculation fans	48
3.2.8	Auxiliary components	48
3.3	Control systems	49
3.3.1	CO ₂ refrigeration booster hot gas bypass system control strategies.....	52
3.3.2	Gas cooler control strategies	54
3.4	Instrumentation and data logging system	56
3.4.1	Instrumentation devices.....	56
3.4.1.1	Temperature and pressure measurement	56
3.4.1.2	Flow meter.....	57
3.4.1.3	Air pressure difference transmitter.....	58
3.4.1.4	Velocity meter	58
3.4.1.5	Infrared (IR) thermography	59
3.4.2	Data logging system for gas cooler test rig	59
3.5	Summary.....	60
CHAPTER IV - EXPERIMENTAL TEST RESULTS AND DISCUSSION		62
4.1	Overview of CO ₂ refrigeration system test facilities.....	62
4.2	Gas cooler design and specification	63
4.2.1	Gas coolers A and A-with vertical slits (3-row-4-circuit).....	63
4.2.2	Gas cooler B (2-row-2-circuit)	64
4.3	Instrumentation design of gas cooler test rig.....	65
4.4	Gas cooler test condition and procedures	67
4.4.1	Test conditions.....	67
4.4.2	Experimental test procedures	68
4.5	Data collection and processing	68
4.5.1	Data collection.....	68
4.5.2	Data processing	69
4.5.3	Uncertainty in calculation heat rejection in gas cooler (Q).....	71
4.6	Test results of gas cooler and discussion.....	71
4.6.1	Gas cooler heat rejection (Q) and refrigerant mass flow rate (\dot{m}_{ref}) in the system	72
4.6.1.1	Heat rejection and mass flow rate in variable and fixed compressor speed operation	72
4.6.1.2	Investigation of the effects of gas cooler types on heat rejection (Q)	74

4.6.2	Operating pressure of the gas cooler	76
4.6.3	Pressure drop in refrigerant-side and air-side.....	79
4.6.4	Coil temperature profile	82
4.6.4.1	Coil temperature for condenser and gas cooler modes of operation.....	82
4.6.4.2	Coil temperature profile for different compressor speeds.....	83
4.6.4.3	Temperature profile for different type of gas cooler.....	83
4.6.4.4	Effect of vertical slit and heat gain on the tubes by fin conduction	85
4.6.5	Fin surface temperature	87
4.6.6	Air-side temperature difference (TD).....	88
4.6.7	Refrigerant-side temperature difference (TD_{ref}).....	90
4.6.8	Approach Temperature (AT).....	92
4.7	Medium Temperature (MT) refrigeration system test results.....	94
4.7.1	Mass flow rate in the system	94
4.7.2	Thermodynamic cycle of the MT CO ₂ refrigeration system	96
4.8	Summary.....	98
CHAPTER V - CFD MODELLING OF GAS COOLERS AND VALIDATION.....		99
5.1	Introduction.....	99
5.2	Governing equations.....	101
5.3	Turbulence in fluid dynamics	102
5.4	Choosing turbulence model	102
5.5	Realizable k- ϵ turbulence model.....	104
5.6	Shell conduction in heat exchanger fins	105
5.7	Working fluid properties.....	105
5.8	CFD geometry design of gas cooler heat exchanger	106
5.9	Meshing	107
5.10	CFD Boundary Conditions	109
5.11	Validation of the CFD Models against Experimental Results.....	112
5.11.1	Turbulence model (k- ϵ Realizable) validation	112
5.11.2	Fin temperature validation.....	113
5.11.3	Errors in prediction of heat rejection (Q) and air-off temperature ($T_{air-off}$)	115
5.12	Post-Processing.....	116
5.12.1	Fin and pipe temperatures contours in five segments	117
5.12.2	Air temperature and velocity contours	118
5.12.3	Heat Rejection (Q) in the CFD model	122
5.13	Summary.....	123
CHAPTER VI – INVESTIGATION OF THE AIR-SIDE HEAT TRANSFER COEFFICIENT		124
6.1	Introduction.....	124
6.2	Calculation of air side -heat transfer coefficient.....	124
6.3	Air side heat transfer coefficient of gas cooler-B.....	125

6.3.1	Segment air side heat transfer coefficient for gas cooler-B with continuous fin	125
6.3.2	Segment air side heat transfer coefficient for gas cooler-B with slit fin.....	128
6.3.3	Average air-side heat transfer coefficient with respect to air velocity	130
6.3.4	Average air-side heat transfer coefficient correlation for gas cooler-B	131
6.4	Air side -heat transfer coefficient of gas cooler-A	133
6.4.1	Segment air side heat transfer coefficient of gas cooler –A continuous fin	133
6.4.2	Segment air side heat transfer coefficient of gas cooler-A with horizontal slit fin.....	136
6.4.3	Segment air side heat transfer coefficient of gas cooler-A with vertical and horizontal slit fin.....	137
6.4.4	Average air-side heat transfer coefficient correlation for gas cooler-A	138
6.5	Comparison of the average air-side heat transfer coefficient for gas cooler-A and gas cooler-B	140
6.6	Summary.....	140
CHAPTER VII - INVESTIGATION OF THE REFRIGERANT AND OVERALL HEAT TRANSFER COEFFICIENTS OF GAS COOLERS		
7.1	Introduction.....	142
7.2	Refrigerant-side heat transfer coefficient (h_{cr}).....	142
7.2.1	Refrigerant-side heat transfer coefficient of gas cooler-B	143
7.2.2	Refrigerant-side heat transfer coefficient of gas cooler-A	145
7.2.3	Comparison of h_{cr} for gas coolers-A and B with previous studies.....	147
7.3	Overall heat transfer coefficient (U)-Log Mean Temperature Difference (LMTD) of gas coolers	149
7.3.1	The U-LMTD from the experimental results	152
7.3.2	The U-LMTD from the CFD model results	153
7.3.2.1	The U-LMTD for gas cooler-B with continuous fin	153
7.3.2.2	U-value for gas cooler –B horizontal-slit fin segments.....	154
7.3.2.3	U-LMTD value for gas cooler-A continuous fin segments.....	155
7.3.2.4	U-LMTD value in segment of gas cooler-A with horizontal slit fin.....	157
7.3.2.5	U-LMTD value for gas cooler-A with horizontal and vertical slit fin segments.....	158
7.3.3	Variation of mean U-value with air velocity in entire gas coolers.....	159
7.4	Summary.....	160
CHAPTER VIII - CONCLUSIONS AND RECOMMENDATIONS FOR FUTURE WORK.....		
8.1	Conclusions	163
8.2	Recommendations for future work	166
REFERENCES		168

Appendix A: Mechanical components of test rig.....	173
Appendix B: Instrumentation and data logging systems of gas cooler test rig.....	177
Appendix C: Operational procedures.....	189
Appendix D: Examples of test results.....	194
Appendix E: Uncertainty analysis.....	198
Appendix F: CFD model input data and calculation.....	200

LIST OF FIGURES

Figure 1.1	Percentage of Electric Energy Consumption, by use category, of typical large supermarket.....	4
Figure 1.2	Direct and indirect emissions in food chain refrigeration	5
Figure 2.1	CO ₂ expansion and phase change	9
Figure 2.2	A typical CO ₂ booster system in a supermarket	10
Figure 2.3	Variation of COP with high side refrigeration pressure and ambient air temperature for the supercritical CO ₂ booster system	11
Figure 2.4	Optimum discharge pressure formula at different exit gas cooler temperatures (T ₁).....	14
Figure 2.5	Optimum gas cooler pressure control	16
Figure 2.6	On-line optimal pressure control concept.....	17
Figure 2.7	Variation of heat transfer coefficient with bulk temperature.....	20
Figure 2.8	Heat transfer coefficient of CO ₂ mixed with oil	20
Figure 2.9	Blasius and Petrov-Popov's pressure drop correlation	22
Figure 2.10	Measured pressure drop variation with T _{bulk} at different oil concentrations	22
Figure 2.11	Fin configuration	23
Figure 2.12	Variation of heat transfer coefficient and pressure drop with average inlet velocity of the fluid for the different fin types	24
Figure 2.13	Two design fin and tube heat exchangers.....	24
Figure 2.14	Comparison of refrigerant temperature profile from simulation and experiment	26
Figure 2.15	Temperature profile from model and experimental results	26
Figure 2.16	Schematic of the gas cooler with two cut configurations	28
Figure 2.17	Cut fin configuration.....	29
Figure 2.18	Infrared image of gas cooler surface with and without cut fins	29
Figure 3.1	Schematic diagram of the CO ₂ test facilities	33
Figure 3.2	P-h diagram of the CO ₂ refrigeration system with booster hot gas bypass (supercritical mode)	35
Figure 3.3	CO ₂ refrigeration system in the Refrigeration Laboratory	35
Figure 3.4	Schematic diagram of CO ₂ refrigeration system in the Refrigeration Laboratory.....	36

Figure 3.5	HT CO ₂ compressor with specification data	37
Figure 3.6	MT display cabinet	38
Figure 3.7	Air cooler	39
Figure 3.8	Schematic diagram of the MT additional load	40
Figure 3.9	Standstill condensing unit.....	40
Figure 3.10	CO ₂ vessel (liquid receiver).....	41
Figure 3.11	Diagram showing valve positions in the system	42
Figure 3.12	Expansion devices	43
Figure 3.13	Schematic diagram of the oil management system and some of its main components	45
Figure 3.14	Construction of gas cooler test rig	46
Figure 3.15	Finned tube gas cooler	47
Figure 3.16	Electrical heater location	48
Figure 3.17	Gas cooler main fan	48
Figure 3.18	The auxiliary components.....	49
Figure 3.19	Electronic control components	50
Figure 3.20	Electrical control panel of CO ₂ refrigeration system.....	51
Figure 3.21	Control strategy of the CO ₂ booster system	53
Figure 3.22	Gas cooler test rig control system.....	55
Figure 3.23	Control strategy for the air-on temperature	55
Figure 3.24	Flow meter	58
Figure 3.25	Air pressure difference transmitter	58
Figure 3.26	Infrared (IR) thermal imaging camera.....	59
Figure 3.27	Measurement instrumentation and Data logging system.....	60
Figure 4.1	Schematic diagram of MT CO ₂ refrigeration system booster hot gas bypass.....	62
Figure 4.2	Gas cooler A (3-row-4-circuit) designs	64
Figure 4.3	Gas cooler B (2-row 2-circuit) designs.....	65
Figure 4.4	Schematic of measurement points on gas cooler test rig.....	66
Figure 4.5	Photograph of measurement points on gas cooler test rig	66
Figure 4.6	Fin surface temperature measurements	67
Figure 4.7	Correlation between velocity and volume flow rate with % of full fan speed	69

Figure 4.8	Variation of heat rejection and \dot{m}_{ref} with air-on temperature at varied compressor speed	73
Figure 4.9	Variation of heat rejection and \dot{m}_{ref} with air-on temperature at fixed compressor speed	73
Figure 4.10	Variation of heat rejection and mass flow rate with air-on temperature of gas cooler A and gas cooler B	74
Figure 4.11	Variation of heat rejection and \dot{m}_{ref} with air-on temperature of gas cooler A and A-with vertical slits	75
Figure 4.12	Variation of heat rejection and \dot{m}_{ref} with air-on temperature.....	76
Figure 4.13	Comparison of optimum pressure correlations with experimental results	77
Figure 4.14	Variation of operating pressure with air-on temperature.....	77
Figure 4.15	Variation of discharge pressure with air- on temperature for different \dot{m}_{ref}	78
Figure 4.16	Variation of discharge pressures with air on temperature for different gas cooler types and sizes	79
Figure 4.17	Variation of pressure drop with discharge pressure for different gas cooler designs	80
Figure 4.18	Variation of pressure drop with discharge pressures	81
Figure 4.19	Correlations of air side pressure drop with air face velocity for Gas cooler A and B	81
Figure 4.20	Temperature profiles along the gas cooler- A and gas cooler-B	82
Figure 4.21	Temperature profiles along the coil of gas cooler B.....	83
Figure 4.22	Temperature profile along the tubes for different gas cooler types.....	84
Figure 4.23	Temperature profile for gas cooler A and A-with vertical slits with pipe numbers.....	85
Figure 4.24	Temperature profile for gas cooler B.....	86
Figure 4.25	Thermal image of gas cooler	87
Figure 4.26	Fin surface temperature and coil temperatures for gas cooler A	88
Figure 4.27	Air-side temperature difference (TD) for different gas cooler types.....	88
Figure 4.28	Variation of air side-TD with air-on temperature for different air velocity.....	89

Figure 4.29	Variation of air-side-TD with air-on temperature for different refrigerant mass flow rate	89
Figure 4.30	Variation of refrigerant-side- TD_{ref} with discharge pressure for different gas cooler types	90
Figure 4.31	Variation of refrigerant-side TD_{ref} with discharge pressure for vertical slit fin	90
Figure 4.32	Variation of inlet refrigerant temperature with discharge pressure for various test conditions	91
Figure 4.33	Variation of enthalpy difference and temperature difference with discharge pressure	91
Figure 4.34	Variation of approach temperature with air face velocity of gas cooler B.....	92
Figure 4.35	P-h diagram for several discharge pressure conditions of gas cooler B	92
Figure 4.36	Variation of approach temperature with air face velocity for different gas cooler types.....	93
Figure 4.37	Variation of heat rejection with approach temperature	93
Figure 4.38	Schematic diagram of MT CO ₂ refrigeration cycle test results for 100% compressor speed.....	95
Figure 4.39	Schematic diagram of MT CO ₂ refrigeration cycle test results for 130% compressor speed.....	95
Figure 4.40	P-h diagram of MT CO ₂ refrigeration system-2K sub cooling.....	97
Figure 4.41	P-h diagram of MT CO ₂ refrigeration system-0.3K sub cooling.....	97
Figure 5.1	Basic programme structure	99
Figure 5.2	Schematic diagram of the gas cooler physical model simulation.....	100
Figure 5.3	Variation of c_p and thermal conductivity of CO ₂ with temperature for several working pressures	106
Figure 5.4	Variation of density and viscosity of CO ₂ with temperature for several working pressures (Derived : EES®Program)	106
Figure 5.5	CFD Gas cooler geometry (i.e. gas cooler- A)	107
Figure 5.6	Mesh of gas cooler-A.....	108
Figure 5.7	Mesh of gas-cooler B.....	108
Figure 5.8	Segment positions along the 1600 mm length gas cooler.....	109
Figure 5.9	Boundary condition for gas coolers-A and B	111

Figure 5.10	Coil tube temperature for inlet refrigerant boundary condition for gas cooler-A and gas cooler-B at identical test procedure	111
Figure 5.11	Turbulence model errors	113
Figure 5.12	Fin temperature measurement positions – experimental tests	113
Figure 5.13	Fin temperature investigation with CFD	114
Figure 5.14	Temperature profile along each fin - LINE A	114
Figure 5.15	Temperature profile of fin collar-LINE B	114
Figure 5.16	Model validation using heat rejection and air-off (outlet) temperature parameters	116
Figure 5.17	Temperature contour, velocity vector and path line of the CFD-post processing	117
Figure 5.18	Fin temperature contour in each segment (gas cooler A)	117
Figure 5.19	Fin temperature contour in each segment (gas cooler B)	118
Figure 5.20	Air temperature contour and plot of gas cooler-A	119
Figure 5.21	Air temperature contour and plot of gas cooler-B	119
Figure 5.22	Velocity vector of gas cooler-B and A at air velocity inlet of 2 m/s	121
Figure 5.23	Average air - off temperature in each segment	121
Figure 5.24	Average heat rejection (Q) at each segment	122
Figure 6.1	Schematic diagram of gas cooler-B design	125
Figure 6.2	CFD post processing results and calculation methods for each segment	126
Figure 6.3	Average air, wall temperature and heat rejection in each segment for continuous fin	127
Figure 6.4	Air side heat transfer coefficient of the continuous fin configuration	128
Figure 6.5	Air side CFD post processing results of gas cooler-B with horizontal slit fin	128
Figure 6.6	Average air, wall temperature and heat rejection in each segment of slit fin design	129
Figure 6.7	Segment air side heat transfer coefficient for circuit -1 and -2 for the slit fin	130
Figure 6.8	Variation of average air-side heat transfer coefficient with air inlet velocity	131

Figure 6.9	Average air side heat transfer coefficient correlation of gas cooler-B for horizontal slit fin and continuous fin	131
Figure 6.10	Schematic diagram of gas cooler-A.....	133
Figure 6.11	Temperature contour and segment investigation of gas cooler-A.....	134
Figure 6.12	Heat rejection at pipe-reference segment	134
Figure 6.13	Variation of wall temperature, bulk temperature and temperature difference (TD) with segment number of gas cooler-A.....	135
Figure 6.14	Air-side heat transfer coefficient at segment.....	136
Figure 6.15	Post processing of CFD simulation results for gas cooler-A with horizontal slit	136
Figure 6.16	Air-side heat transfer coefficient for the gas cooler-A with horizontal slit fin	137
Figure 6.17	Post processing of CFD simulation results for gas cooler-A with horizontal and vertical slit fin	137
Figure 6.18	Air-side heat transfer coefficient of gas cooler-A with vertical and horizontal slit fins	138
Figure 6.19	Correlation of average air-side heat transfer coefficient of gas cooler-A	138
Figure 6.20	Variation of average air-side heat transfer coefficient of gas cooler-B and gas cooler-A	140
Figure 7.1	Refrigerant- side post processing results for a segment	143
Figure 7.2	Variation of refrigerant side-heat transfer coefficients with refrigerant bulk temperature of gas cooler-B.....	144
Figure 7.3	Variation of CO ₂ c _p with temperature at a pressure: 82 bar _g	144
Figure 7.4	The hc _r profile in segment of gas cooler-B.....	145
Figure 7.5	Variation of refrigerant-side heat transfer coefficient with bulk temperature of gas cooler-A	146
Figure 7.6	Variation of CO ₂ c _p with temperature at pressure: 83 bar _g	146
Figure 7.7	Variation of refrigerant- side heat transfer coefficient at segment of gas cooler-A.....	147
Figure 7.8	The heat transfer coefficient from Oh and Son (2010), Dang et al. (2012), Jun and Yung (2013) and this study's results	148
Figure 7.9	Overall heat transfer area.....	150

Figure 7.10 Schematic diagram of heat transfer area (A_o) of gas cooler-B and gas cooler-A from experimental result.....	151
Figure 7.11 Experimental U-LMTD results for gas cooler-A and B with horizontal slit fin.....	152
Figure 7.12 U- LMTD profile in gas cooler-B with continuous fin configuration.....	154
Figure 7.13 U-LMTD of gas cooler - B with horizontal-slit fin.....	155
Figure 7.14 U-LMTD of gas cooler-A with continuous fin.....	156
Figure 7.15 U-LMTD of gas cooler-A with horizontal-slit fin.....	157
Figure 7.16 U-LMTD of gas cooler- A with horizontal and vertical slit fin	158
Figure 7.17 Variation of air side heat transfer coefficient with air-velocity for different gas cooler types	159
Figure 7.18 U Value errors of the CFD results compared with the experimental results	160

LIST OF TABLES

Table 1.1	Comparative refrigerant performance.....	2
Table 2.1	Carbon dioxide gas cooler specification.....	27
Table 2.2	Carbon dioxide gas cooler test condition.....	28
Table 2.3	Measured capacity and CO ₂ temperature of the gas cooler	30
Table 4.1	Specification of finned and tube gas cooler -A.....	63
Table 4.2	Specification of finned and tube gas cooler -B.....	64
Table 4.3	Experimental results of fin surface temperature	87
Table 5.1	Air properties	105
Table 5.2	Comparison between experimental and model results for fin temperature	115
Table 6.1	Comparison heat exchanger specification between the CFD model and Wen and Ho (2009) experiment	130

ACKNOWLEDGEMENTS

I would like to express my gratitude to Professor Savvas Tassou, for his assistance, great guidance and enthusiastic support throughout the project. His advice and encouragement have strongly inspired me to complete the project successfully. I would also like to thank Dr Baboo Lesh Gowreesunker for his excellent guidance for the CFD modelling and Professor Maria Kolokotroni and Dr Yunting Ge for support during my PhD studies.

I am delighted to acknowledge the financial support and PhD scholarship received from Directorate General of Higher Education (DGHE)-DIKTI, Indonesian Government and also the excellent support received from staff of the RCUK Centre for Sustainable Energy use in Food Chains (CSEF)-Brunel University and staff from GEA-Searle.

I also express my gratitude to colleagues and technical staff in CSEF, Konstantinos Tsamos, Dr INyoman Suamir, Wesley Welcome, Demitris Parpas, Costas Xanthos and others as well as my colleagues in the Mechanical Engineering Department of Bali State Polytechnic for all their support and encouragement.

Finally, I would like to express my very special gratitude to my wife, Ni Luh Putu Yudiarini, and my children: Desak Putu Wikania Anjani, Dewa Made Bagus Paradhita, Desak Ayu Yuvika Kharisma and my parents for their patience during the most demanding time of my PhD studies.

NOMENCLATURE

A	Area (m^2)
A_f	Fin surface area (m^2)
A_o	Heat transfer area (m^2)
A_t	Tube outside surface area (m^2)
C_p	Specific heat (kJ/kg. K)
d	Diameter (m or mm)
DC	Collar diameter at air side of a finned tube coil (m or mm)
dT	Temperature difference (K)
G	mass velocity (kg/s. m^2)
GWP	Global warming potential (kgCO ₂ /kg)
hc_a	Air side heat transfer coefficient (W/ m^2 .K)
hc_r	Refrigerant side heat transfer coefficient (W/ m^2 .K)
h	Specific enthalpy (kJ/kg), heat transfer coefficient (W/ m^2 .K)
k	Thermal conductivity (W/m.K)
L	Length (m)
$LMTD$	Log mean temperature difference (K)
m	Mass (kg)
\dot{m}	Mass flow rate (kg/s)
N	Number of rows or circuits
P	Pressure (kPa or Pa or bar _g or bar _a)
q	Heat flux (W/ m^2)
Q	Heat transfer rate in gas cooler (Watt, kW)
RH	Relative Humidity (%)
SE	Energy source term (W/ m^2)
SM	Mass source term (kg/ m^3)
T	Temperature ($^{\circ}C$ or K)
t	Time (s)
T_{film}	Film temperature ($^{\circ}C$, K)
U	Overall heat transfer coefficient (W/ m^2 .K)
u	Velocity in x direction (m/s)
v	Velocity in y direction (m/s)
w	Velocity in z direction (m/s)
W	Electrical power/energy (kW or kWh)
<i>Air-off</i>	Air outlet heat exchanger (-)
<i>Air-on</i>	Air inlet heat exchanger (-)
C	Constant (-)
COP	Coefficient of performance (-)
f	friction factor (-)
Nu	Nusselt number (-)
ODP	Ozone depletion potential (-)
Pr	Prandtl number (-)

Re	Reynolds number (-)
Re_{DC}	Reynolds Number based on collar diameter (-)

Greek symbols

η	Efficiency
μ	Dynamic viscosity (N.s/m ²)
ρ	Density (kg/m ³)
f	Friction factor (-)

Subscript

a	Air or air-side, absolute
amb	Ambient
app	Approach
avg	Average
b	Bulk
comp	Compressor
cond	Condensing, condenser
crit	Critical point
DC	Collar diameter
evap	Evaporating, evaporator
f	Fin, film
g	Gauge
gc	Gas cooler
i	Inner
in	Inlet
int	intermediate
j	Depth axis
k	Height axis
LMTD	Log means temperature difference
m	Mean
o	Outer
opt	Optimum
out	Outlet, out
PAG	lubrication/oil type of R-744
pc	Pseudo critical
ref	Refrigeration, refrigerant, refrigerant-side
sat	Saturated
sc	Sub-cooling
sh	Superheating
t	Tube
w	wall

ABBREVIATION AND GLOSSARY

AK-CC	Adap-Kool cabinet controller: a cabinet controller manufactured by Danfoss
AKV	Adap-Kool valve: an electrically operated expansion valve manufactured by Danfoss
ASHRAE	American society of heating refrigerating and air-conditioning engineers
AT	Approach temperature
BV	Ball valve
BVP	Bypass valve
CD	Condenser mode
CFC	Chloro-fluoro-carbon
CFD	Computational Fluid Dynamics
CO ₂	Carbon dioxide
CSEF	Centre for Sustainability Energy use in Food chains-Brunel University
DX	Direct expansion
EDM	Electrical Discharge Machining
EES	Engineering equation solver
FPM	Number of fins per metre
GC	Gas cooler mode
GHG	Green House Gases
GWP	Global warming potential
HCFC	Hydro-chloro-fluoro-carbon
HFC	Hydro-fluoro-carbon
HP	High pressure
HT	High temperature
HX	Heat exchanger
HVAC&R	Heating, ventilating, air conditioning and refrigeration
ICAD	Industrial Control Actuator with Display
ICM	Industrial control motor valve
ICMT	High pressure expansion valve
IHX	Internal heat exchanger
IR	Infrared
kg	Kilo gram
kJ	Kilo joule
kW	Kilowatt
kWh	Kilowatt hour
LP	Low pressure

LT	Low temperature
M.W.P	Maximum work pressure
MOP	Maximum operating pressure
MOPD	Maximum operating pressure difference
MPa	Mega Pascal
MT	Medium temperature
OD	Outer diameter
ODP	Ozone depleting potential
PI	Proportional integral
PID	Proportional integral differential
RCUK	Research Council United Kingdom
RNG	Renormalisation Group
SV	Solenoid valve
TAT	Transition Air Temperature
TD	Temperature difference
TXV	Thermostatic expansion valve

CHAPTER I - INTRODUCTION

Carbon dioxide (CO₂) is most commonly known as the product of respiration or combustion of fossil-fuels, and its high level in the atmosphere is a contributing factor to global warming. Its concentration in the atmosphere is mainly controlled through natural sinks like forests, but the increasing pattern of deforestation is resulting in further increased concentration of CO₂ in the earth's atmosphere. Another method of controlling CO₂ concentration is through the use of carbon capture technologies to transfer CO₂ to storage spaces, such as underground geological reservoirs, which however have limited capacity. In this regards, in order to reduce the amount of CO₂ that has to be stored, it can be employed as an alternative to other commonly used fluids. For instance, CO₂ can be used in the pharmaceutical and chemical industries industry as a chemical reagent or solvent. Furthermore, CO₂ can be used as a working fluid in refrigeration systems.

This study focuses on the potential of using CO₂ as a natural refrigerant (refrigerant code: R744). The use of CO₂ refrigeration systems began in the 1890s and has become a refrigerant for freezing and transporting fresh food products around the world. Marine CO₂ refrigerated shipping rapidly became very popular for its reliability in the distribution of several food products to many countries around the world. Initially, the requirements of high operating pressure condition were detrimental to the development and growth of CO₂ refrigeration, whereby the availability of synthetic refrigerants and refrigeration systems, such as chlorodifluoromethane (R-22) in the 1940s, halted the progress of CO₂ systems such that by the 1960s, it had been almost entirely replaced in all marine and land-base system (ASHRAE,2010).

In recent years due to environmental pressures, the use of R-22 is now prohibited for new systems, whilst its production has been completely stopped because of very high global warming potential (GWP). Similarly, synthetic refrigerants (R134a, R404a and R507) are also gradually being phased out as also declare in Kyoto Protocol, promoting the use of natural refrigerants (CO₂, ammonia and hydrocarbons) in recent years. CO₂ as a natural refrigerant has zero Ozone Depletion Potential (ODP) and negligible Global

Warming Potential (GWP). It is non-flammable and nontoxic, with no known carcinogenic, mutagenic, or other toxic effects, and no dangerous products of combustion (IIR Guide, 2014).

Beside the environmental issues, CO₂ is also a refrigerant of great interest since it has attractive thermo-physical properties: low viscosity, good thermal conductivity, high vapour density and high specific heat capacity. Table 1.1 shows thermo-physical and performance comparison of various refrigerants and CO₂ (R744) where it can be seen that it has good thermo-physical properties but also higher evaporating and condensing pressures than the other refrigerants. It also can be seen from the table that CO₂ has the lowest pressure ratio, and a very small suction gas specific volume. These are indicating that CO₂ can provide better volumetric and isentropic efficiencies and require smaller compressor dimensions and suction pipe diameters. However, CO₂ has lower refrigerant effect than R22, R290 and R717 but still higher than R 404A.

Table 1.1 Comparative refrigerant thermo-physical and performance

Thermo-physical properties (T, P _{cond})						
Refrigerant	P _{evap} (bar _a)	P _{cond} (bar _a)	Viscosity x 10 ⁻⁵ (kg/ms)	Thermal conductivity x 10 ⁻³ (W/mK)	Vapour density (kg/m ³)	Specific heat capacity (J/kgK)
R-22	3.8	11.3	1.359	12.19	47.99	898.4
R-404A	4.7	13.6	12.09	67.1	72.3	1579
R-290	3.7	10.3	9.532	93.48	22.37	2770
R-717	3.2	11.0	12.79	476.9	8.54	4810
R-744	28.0	68.9	2.224	61.51	288.9	16387
Refrigerant performance						
Refrigerant	P _{evap} (bar _a)	P _{cond} (bar _a)	Pressure ratio -	Refrigeration effect (kJ/kg)	Refrigerant mass flow rate x 10 ⁻³ (kg/s)	Suction gas specific volume x 10 ⁻³ (m ³ /kg)
R-22	3.8	11.3	3.0	170.1	5.9	62.6
R-404A	4.7	13.6	2.9	124.2	8.1	42.8
R-290	3.7	10.3	2.9	300.5	3.3	126.1
R-717	3.2	11.0	3.5	1134.1	0.9	396.8
R-744	28.0	68.9	2.6	153.1	6.5	13.9

Operating conditions:

Refrigeration capacity 1 kW, degree of superheat 5 K, no sub-cooling, evaporating temperatures of -8 °C (Medium temperature refrigeration systems) and condensing temperature of 28 °C.

(Derived using EES, 2014)

CO₂ is also considered a very low cost refrigerant compared with other common refrigerants in use today and is projected to have a good future in mechanical refrigeration systems, serving as both primary and secondary refrigerant (ASHRAE, 2010).

1.1 Use of carbon dioxide (CO₂) as refrigerant

CO₂ can be used in almost all refrigeration system applications and is now becoming common in supermarket applications (IIR Guide, 2014). As primary refrigerant, CO₂ has been proposed for use in mobile air conditioners, supermarket display cases, and vending machines. In the application in heat pump water heaters for example, the supercritical operation (i.e., rejection of heat above the critical point) is beneficial because it allows good temperature matching between the water and supercritical CO₂, which improves the coefficient of performance (ASHRAE, 2010). As a secondary refrigerant, CO₂ can be used as the low temperature stage refrigerant in cascade systems, typically with ammonia or R-507A as the high temperature refrigerant, in large industrial systems. Medium-sized commercial systems can also use CO₂ as the low temperature stage refrigerant in cascade arrangements with HFCs or hydrocarbons as the high temperature stage refrigerant. In early CO₂ refrigeration systems for supermarket applications, the cascade arrangement was also preferred to avoid high pressures and supercritical operation (Tassou, 2011).

1.2 Refrigeration systems in supermarket and GHG emissions

In modern retail food stores, the energy use is mostly by refrigeration systems. The energy-use per unit area is defined as the energy intensity of a supermarket (Tassou, 2011). It was found, through detailed review of energy consumption of UK supermarkets that the energy intensity could vary from around 700 kWh/m² sales area per year in hypermarkets to over 2000 kWh/m² sales area per year in convenience stores (Tassou, 2011). The refrigeration systems accounted for between 30% and 60% of the electricity used. Figure 1.1 shows an example from a supermarket where refrigeration systems accounted for roughly 50% of the electrical energy consumption, followed by lighting at 38% (ASHRAE, 2014)

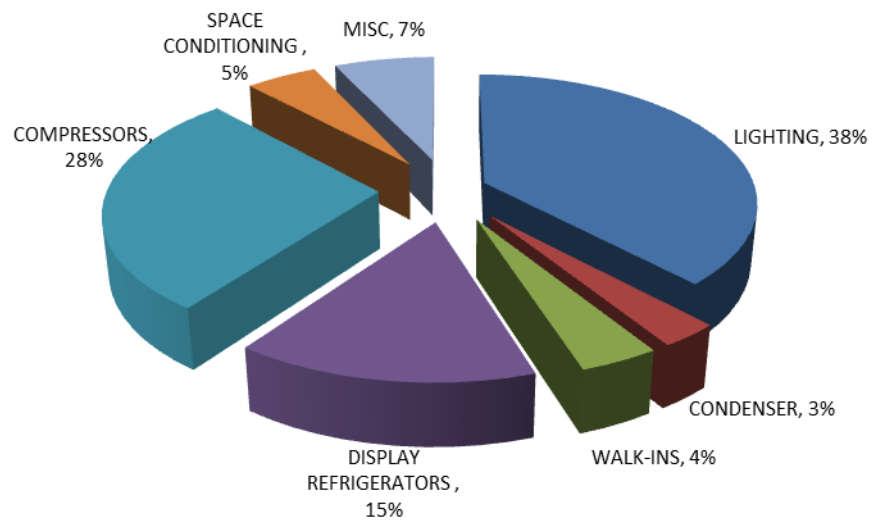


Figure 1.1 Percentage of Electric Energy Consumption, by use category, of typical large supermarket
(Source : ASHRAE, 2014)

Refrigeration systems in supermarkets contain substantial amounts of refrigerant and are responsible for direct Greenhouse Gas (GHG) emissions through leakage, even though significant progress has been made in recent years to reduce leakage through better system design and leakage sensing (Tassou, 2011).

In the cold food chain as a whole, direct emissions are dominated by those from supermarkets (63%), larger industrial systems in food / drink manufacture (18%), the food service sector (9%) and cold storage (4%), Figure 1.2 (Tassou, 2002). The R404A with its very high GWP is the dominant HFC refrigerant used in supermarkets and industrial systems. R404A was estimated to represent 80% of HFC emissions and 60% of total direct emissions. Using a refrigerant with a very low or zero GWP in the cold chain will lead to a significant reduction in direct GHG emissions.

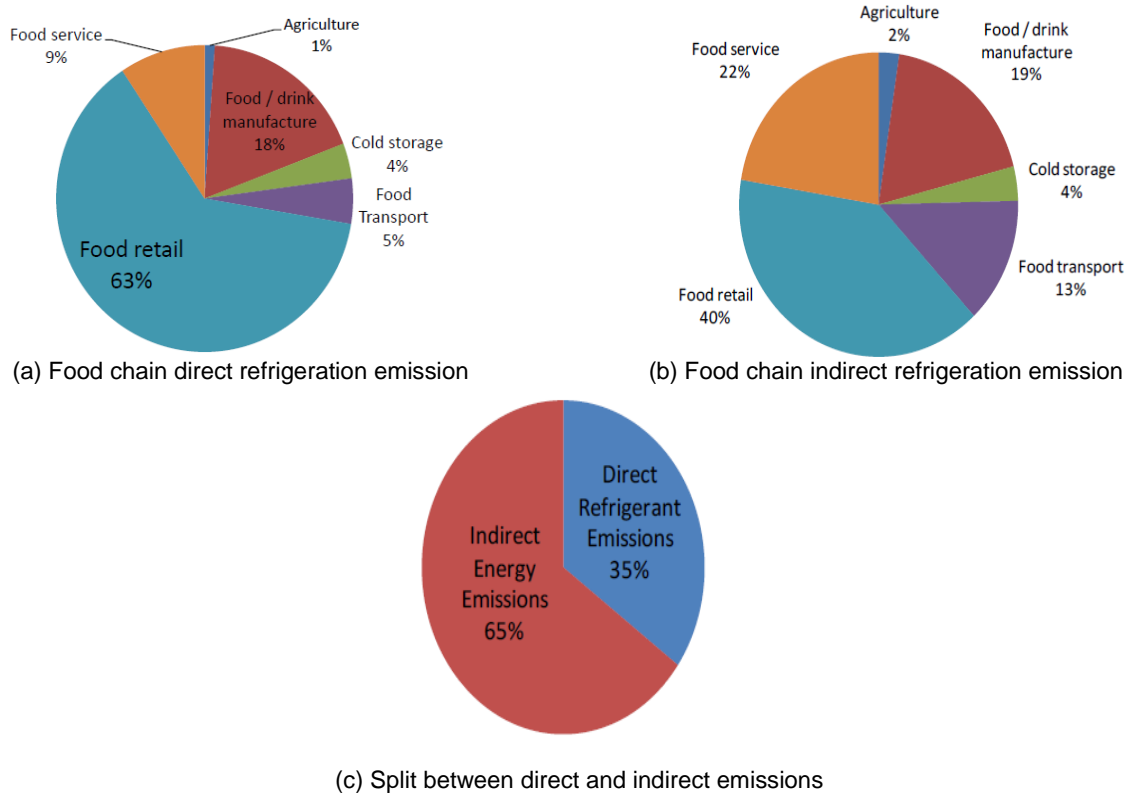


Figure 1.2 Direct and indirect emissions in food chain refrigeration
(Source : Tassou Report for IEA Annex, 2002)

More recently, Finckh et al. (2011) investigated the energy consumption of alternative refrigeration systems in several supermarkets and several supermarkets and concluded that CO₂ system operation was more efficient than R-404A systems at subcritical operating conditions, when ambient temperatures were below about 24°C. However, in supercritical operation the CO₂ systems had equivalent COP with that of R-404A systems, especially at ambient temperatures above about 30°C. The efficiency of CO₂ systems in supercritical operation could be improved through the introduction of a number of improvements such as the introduction of an ejector to replace the expansion valve.

1.3 Finned-tube condenser/gas coolers in CO₂ refrigeration systems

In CO₂ refrigeration systems, the system can operate in the subcritical or supercritical mode depending on ambient temperature. In supercritical operation the heat exchanger rejects heat from the superheated refrigerant gas to the ambient air without condensation (single phase heat transfer). In this case the heat exchanger is known as a gas cooler

(Santosa et al., 2013). In subcritical operation, the heat exchanger behaves in a very similar way to a standard condenser, condensing CO₂ refrigerant gas by rejecting heat to the ambient air. Two main air-coupled gas coolers have been developed in recent years (Gupta et al., 2010): macro-tube and micro-channel. Each type of gas coolers has advantages and shortcomings for specific applications.

The micro-channel gas cooler, developed rapidly for automobile air conditioning applications, consists of tube hydraulic diameters less than 2 mm (Fillipini and Merlo, 2011). The advantage of a higher heat transfer coefficient compared to conventional tube geometries, allows a more compact design of heat exchanger. An optimized design of the flow channels and the refrigerant distribution (distribution manifold) are important factors to realise improved efficiency, lower refrigerant charge, as well as low internal pressure losses.

In spite of the advantages, the micro-channel heat exchanger also has some disadvantages. Micro-channels have very rigid construction which makes it difficult to provide special circuiting for large coils. They also have the tendency to accumulate dirt in the air flow passages requiring frequent maintenance (Fillippini and Merlo, 2011).

On the other hand, macro-tube fin and tube heat exchangers have good reliability low air flow resistance and low dirt accumulation in the field. They also offer manufacturing flexibility and reduced capital and maintenance costs compared to micro-channel gas coolers (Ge and Cropper, 2009). For these reasons, the macro-finned tube gas cooler is the most favourable type in industrial applications compared to the micro-channel gas cooler (Sun and Zang, 2014). However, the design of macro-finned tube gas coolers for CO₂ refrigeration systems has evolved from the design of standard finned tube HVAC coils and further research and development is required to optimise their design for operation in the condensing and gas cooling modes at high pressures for the unique properties of CO₂ (Pongsoi at al., 2012).

1.4 Research aim and objectives

The aim of the research in this thesis is to investigate and improve the performance of finned tube gas coolers in CO₂ refrigeration applications. The main objectives of the project are:

- Conduct literature review on the design and performance characteristics of gas cooler coils during subcritical and supercritical operation.
- Carry out experimental investigations on the performance of different finned tube gas cooler with a slit fin configuration designs using a ‘booster’ CO₂ refrigeration system with hot gas by-pass.
- Employ and validate Computational Fluid Dynamics (CFD) modelling to investigate the performance of a three row and two row finned tube gas coolers and influence of design modifications. The design including continuous and slit fin configuration.
- Evaluate and investigate refrigerant, air and overall heat transfer coefficients in gas coolers for use in design and overall refrigeration system modelling and optimisation.

1.5 Structure of the thesis

The thesis comprises of eight chapters. **Chapter 1** provides an introduction of the work in the thesis and details the aims, objectives and structure of the thesis. **Chapter 2** presents an overview of CO₂ as a refrigerant and describes several CO₂ refrigeration systems. The chapter also outlines recent investigations on optimum pressure, pressure drop and heat transfer coefficients in a gas cooler heat exchangers, and efforts to improve the performance of gas coolers in CO₂ refrigeration systems.

Chapter 3 discusses the construction of the test facilities implemented for the experimental investigations on gas cooler performance. The facilities comprise a ‘booster’ refrigeration system and associated refrigeration load equipment and a specially designed gas cooler test rig.

Chapter 4 presents test results and analysis of the gas cooler performance which covers heat rejection, refrigerant mass flow rate, pressure drop, variation of gas cooler operating pressure with air-on temperature, temperature profile along the gas cooler coil, temperature difference (TD) and approach temperature (AT) analyses for the different gas cooler designs and operating conditions.

Chapter 5 details CFD modelling to simulate gas cooler heat exchanger performance. The model has been validated against experimental data obtained from the test results. The k- ϵ turbulence models were found to produce better performance than k- ω models with the Realizable k- ϵ turbulence model producing best performance among the k- ϵ turbulence models (Standard and RNG). The CFD results showed that by modelling individual segments of the gas cooler, the overall performance of the heat exchanger can be simulated with adequate accuracy, as depicted by the mean errors obtained.

In Chapter 6, the air-side heat transfer coefficient in the gas cooler was investigated and correlations were developed for the determination of the heat transfer coefficient.

Chapter 7 presents investigations on the refrigerant-side heat transfer coefficient and overall heat transfer coefficient and the development of correlations for use in design and optimisation studies.

Finally, **Chapter 8** presents overall conclusions for the study and identifies areas for further investigations to improve further gas cooler performance.

CHAPTER II - LITERATURE REVIEW

2.1 Introduction

The supercritical system is an excellent option for CO₂ system because the critical point of CO₂ is at a relatively low temperature at 31°C, at relatively high pressure (73.8 bar_a), with the triple point occurs at -56.6°C at a pressure of 5.2 bar as shown in Figure 2.1.

The use of environment benign natural refrigerant substituting chlorofluorocarbons (CFCs) and hydrochlorofluorocarbons (HCFCs) has been widely investigated recently. Among the natural refrigerants (carbon dioxide, ammonia, hydrocarbon, etc.), carbon dioxide (CO₂) satisfies a lot of thermal characteristics, such as low viscosity, high volumetric capacity, excellent heat transfer coefficients, no toxicity and being inflammable. At the same time, CO₂ has zero Ozone Depletion Potential (ODP), negligible Global Warming Potential (GWP) and relatively low cost. So CO₂ is an excellent alternative to the conventional refrigerants (ASHRAE, 2010).

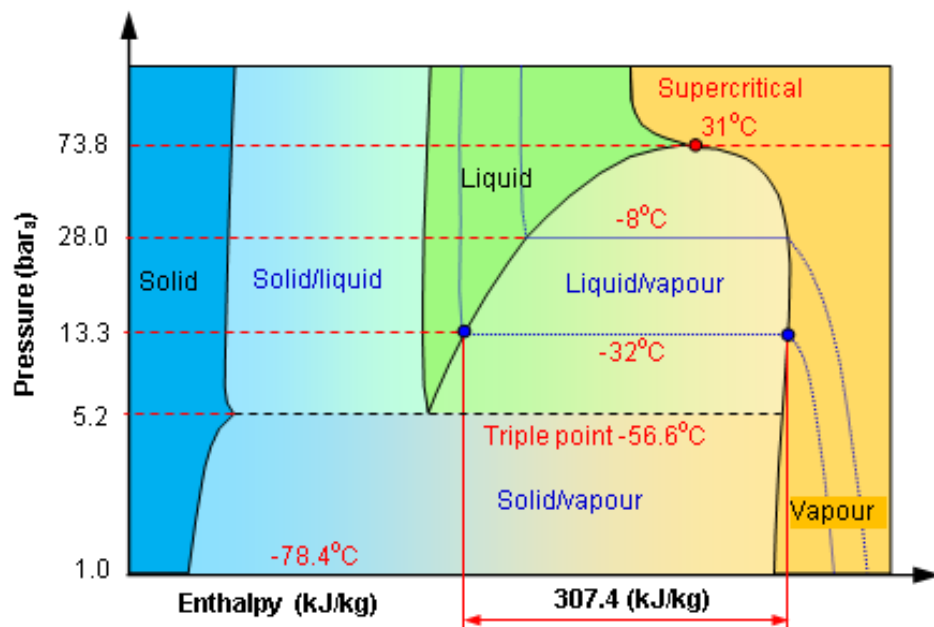


Figure 2.1 CO₂ expansion and phase change
(Adapted from: ASHRAE, 2010)

2.2 CO₂ refrigeration system

This section explains the CO₂ refrigeration with a booster bypass gas system and two common designs to improve performance of the CO₂ refrigeration system comprise: 1) internal heat exchanger (IHX) and 2) ejector system.

2.2.1 CO₂ refrigeration system with booster bypass gas system

Being environmentally friendly systems, supercritical or sub-critical booster refrigeration systems are widely used in supermarkets (Ommen and Elmegaard, 2012). Figure 2.2 shows a typical booster cycle for supermarket application adapted from (Ge and Tassou, 2011a) which is identical with the test rig used in this study. The system has four pressure regions: high, intermediate, medium and low, with two stage compressors (low stage and high stage compressor) and two evaporating systems which are Medium Temperature (MT) and Low Temperature (LT) evaporators. The system also comprises two bypass valves (BPV). The first valve mixes the expanded vapour from the receiver with refrigerant from the low stage compressor (Comp LP) and MT evaporator. The mixture then flows through an internal heat exchanger (IHX) before entering the high stage compressor (Comp HP). In this system, a second bypass valve (BPV-2) is included to bypass. This situation may occur at the system operates in the sub-critical condition.

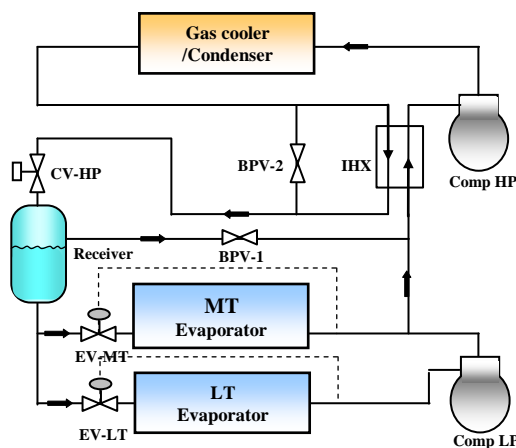


Figure 2.2 A typical CO₂ booster system in a supermarket
(Source: Ge and Tassou, 2011a)

The coefficient of performance (COP) of the booster system was investigated using a simulation model by Ge and Tassou (2011b) with the investigation was conducted

depend on supercritical condition with the ambient temperature vary from 25° C to 40° C as described in Figure 2.3. It was obtained that the optimum discharge pressure in order to get maximise COP increases at higher ambient temperature.

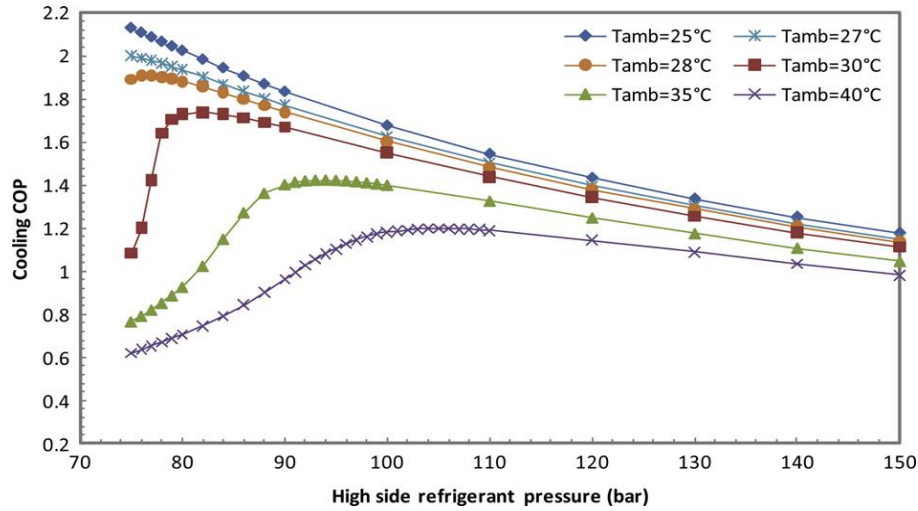


Figure 2.3 Variation of COP with high side refrigeration pressure and ambient air temperature for the supercritical CO₂ booster system
(Source: Ge and Tassou, 2011b)

2.2.2 CO₂ refrigeration system with internal heat exchanger (IHX)

The internal heat exchanger (IHX), one of the most commonly alternative used to improve cooling capacity and COP in a CO₂ refrigerating plant working in supercritical conditions (Sánchez et al., 2014). Generally, the cooling of the refrigerant flowing out of the gas cooler prevents flash gas at the expansion valve, and the superheating of the suction gas avoids that liquid refrigerant from the evaporator entering into the compressor, so the IHX is set up between the refrigerant of the compressor suction and the refrigerant of the exit of the gas-cooler. Aprea and Maiorino (2008), Torrella et al. (2011) conducted experiments investigating the influence of the internal heat exchanger (IHX) on carbon dioxide supercritical refrigerating plants and the performance of the system. It was confirmed that the use of the IHX increases the COP of the system by 10%. In addition, the use of the IHX was associated with an increase on compressor discharge temperature, reaching increments up to 10°C at the evaporating temperature of 15°C. Moreover, Rigola et al. (2010) added that there are specific conditions to reach maximum performance of a CO₂ supercritical refrigeration system using internal heat exchanger. The first condition, when ambient temperature of 35°C and the optimal discharge pressure is between 95 and 100 bar, the COP increases by 20%. Secondly,

when the ambient temperature increases become 43°C, so the optimal gas cooler pressure is between 105 and 110 bar, with IHX the COP can be increased up to 30%.

The position of the internal heat exchanger (IHX) also become challenging to be investigated. Sánchez et al. (2014) studied experimentally about several position configuration of the IHX: the classical position (gas cooler exit, liquid receiver exit), and new position in both positions at the same time. A maximum increment of 13% on COP has been registered working with two IHX at the same time.

2.2.3 CO₂ refrigeration system using ejector

A basic supercritical CO₂ refrigeration system suffers from large expansion loss because of huge pressure difference between discharge and evaporating pressure. To improve performance of the CO₂ refrigeration system, the ejector works as an expansion valve and it can mitigate the expansion losses (Chen et al, 2012). There are a lot of researches investigating ejectors system for supercritical CO₂ refrigeration systems. Elbel & Hrnjak (2008) and Lucas & Koehler (2012), compared an ejector and expansion valve experimentally. The experimental results showed that with the ejector COP can be improvement significantly up to 18%. Nakagawa et al. (2011) developed two phase ejectors with internal heat exchangers (IHX) and based on the experimental results obtained significantly increased the coefficient of performance (COP) of the ejector system. With the specific conditions which have been used, the ejector system with IHX can enhance the COP of the system up to 27% compared to similar conventional systems.

A thermodynamic-exergy analysis has been developed by Fangtian & Yitai (2011) and Ahammed et al. (2014) to compare a conventional system and ejector system in supercritical mode system. They simulated a vapour compression system and stated that the ejector implementation on CO₂ refrigeration system show positive significant effect to improve the performance of the system because of significant high of discharge pressure comparing with the conventional system. The result has been obtained that there was a COP improvement of 21 %.

2.3 Supercritical CO₂ refrigeration system performance and optimum pressure correlation

In supercritical CO₂ refrigeration system, the gas cooler becomes an important device because it works in a relatively high temperature and pressure in comparison with the conventional system. In general, performance concerning the supercritical mode operation is lower than the performance in sub-critical mode operation (Beaver et al., 1999).

Three major factors which affect the performance of supercritical CO₂ refrigeration systems were pointed out by Gupta et al. (2010): 1) design of gas cooler, 2) gas cooler pressure and 3) gas cooler outlet temperature. The effect of the gas cooler conditions in the system was also investigated by Tao et al. (2010) focusing on average exergy loss. Gas cooler and expansion valve has the higher exergy loss under all working condition, about 30.7% and 24.9%, respectively followed by the exergy losses in evaporator and compressor, which account for 21.9% and 19.5%, respectively. The exergy loss in internal heat exchanger is the lowest (only about 3.0%). Therefore, in the optimization design of the supercritical CO₂ more attention should be paid to the gas cooler and expansion valve.

Gupta et al. (2010) stated that approach temperature is a very important parameter in the design of gas cooler. To reduce the thermodynamic losses the refrigerant exit temperature of gas cooler should approach coolant inlet temperature. Increasing gas cooler outlet temperature (which in turn is dictated by ambient temperature), COP of the system decreases. Furthermore, with increasing pressure, COP decreases up to certain gas cooler outlet temperature after which point COP increases with pressure. Tao et al. (2010) investigated the effects of air inlet temperature and air inlet velocity in gas cooler. The increasing of gas cooler side air inlet temperature, gas cooler side air inlet velocity and evaporating temperature caused the exergetic efficiency of the system increase.

In supercritical mode, the optimum discharge pressure should be controlled in order to get maximum system COP. Chen and Gu (2005), Sawalha (2008), Ge and Tassou (2009), Ge and Tassou (2011b) obtained that the optimum pressure subsequently increases with ambient temperature. Ge and Tassou (2011b) investigated the optimum

pressure for a typical CO₂ booster system refers to Figure 2.2 for the schematic diagram of the system. The results showed that for each ambient temperature there is a high stage pressure that maximises the COP. For ambient temperatures above 27°C, the relationship between ambient temperature and optimum pressure is fairly linear with a correlation as follows:

$$Y = 2.3426 x + 11.541, \text{ with } R^2 = 0.9991 \quad (2.1)$$

Where Y = optimum gas cooler pressure (bar) and x = ambient temperature (°C)

Sawalha (2008) also developed the correlation of the optimum pressure in relation to ambient temperature and temperature of the CO₂ exit of gas cooler (T₁) as shown in Figure 2.4 and equation (2.2), where the approach temperature was assumed constant at 5°C:

$$P_{opt} = 2.7 (T_{amb} + T_1) - 6.1 \quad (2.2)$$

Sawalha's correlation was applicable for the supermarket system, but it's still need to be improved in the mobile air conditioning and heat pump applications.

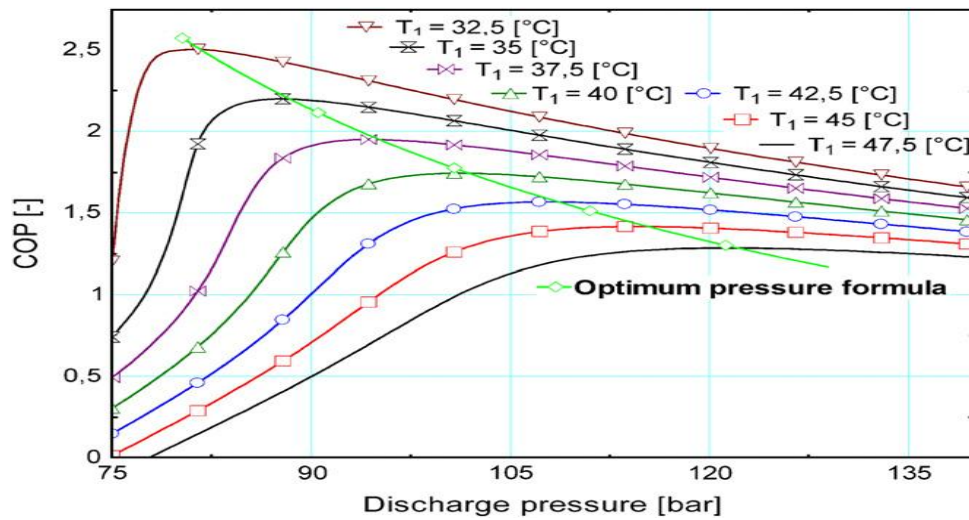


Figure 2.4 Optimum discharge pressure formula at different exit gas cooler temperatures (T₁)
(Source: Sawalha, 2008)

Chen and Gu (2005) also developed a correlation of optimum pressure in a typical CO₂ refrigeration system with an internal heat exchanger (IHX). The correlation was performed between optimum pressure and ambient temperature (T_{amb}) or gas cooler exit

temperature (T_3). Some assumptions are considered in this correlation, including: 1) CO_2 properties are according to pure CO_2 properties, 2) gas cooler and evaporator pressure is constant and 3) approach temperature is constant at 2.9°C . The optimum pressure was predicted with deviations less than 3.6 %. The correlation is described as follows:

$$P_{opt} = 2.68 T_{amb} + 0.975 = 2.68 T_3 - 6.797 \quad (2.3)$$

Liao et al. (2000) implies that the optimal heat rejection pressure for a supercritical CO_2 cycle depends on three major parameters: 1) the outlet temperature of the gas cooler; 2) the evaporation temperature; and 3) the performance of the compressor used in the system. They found correlation of optimal heat rejection pressure (P_{opt}) in terms of the outlet temperature of the gas cooler (T_{gc}) and evaporation temperature (T_{evap}) as follows:

$$P_{opt} = (2.778 - 0.0157 T_{evap}) \cdot T_{gc} + (0.381 T_{evap} - 9.34) \quad (2.4)$$

Liao's correlation as explained in equation (2.4) is more precise for CO_2 air conditioning cycle.

2.4 Control system for optimum performance in supercritical operation

To achieve an optimum performance in supercritical mode, optimum operation conditions need to be controlled as explained in Section 2.3. Various control strategies have been implemented dependent upon the operation condition of the system. Danfoss (2010) developed a valve and its controller to maintain the optimum pressure to get maximum COP when in the supercritical range. The valve is an ICMT valve which is an expansion device for gaining a high pressure. The valve regulates pressure on the gas cooler and the optimum pressure can be achieved by a controller with a proportional integral differential (PID) controller. The gas cooler pressure and outlet CO_2 temperature provide a signal for the controller. Otherwise, in the subcritical mode the ICMT will regulate the pressure to get sub cooling degree as a setting condition. The control system is shown in Figure 2.5.

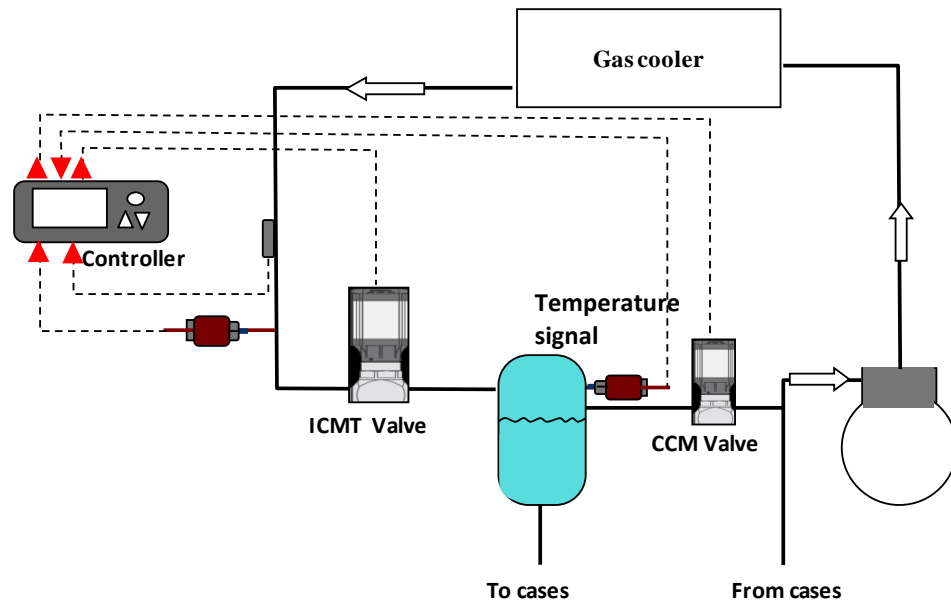


Figure 2.5 Optimum gas cooler pressure control
(Source: Danfoss, 2010)

Ge and Tassou (2009) developed a CO₂ medium temperature (MT) model to simulate a control procedure and strategies for food retail refrigeration applications. The control strategies are according to the mode operation of the system, supercritical and sub critical mode. When the system operates in supercritical mode, the optimum refrigerant pressure is predicted from the correlation which explained in equation (2.1). When the system operates in the subcritical mode, the control strategy is using a conventional control strategy as also described by Danfoss (2010). To assess the effectiveness of control strategy with the saving energy, Ge and Tassou (2009) determined the mode of operation using Transition Air Temperature (TAT). Two ambient temperatures consider for switch point subcritical to supercritical which are 16 °C and 21 °C. These switch point primary depend upon the effectiveness of the gas cooler and for the better gas cooler performance the point should be increased. As a result, with transition temperature of 21°C was obtained an energy saving of 18% over the TAT 16°C. This means that increasing the transition temperature can improve the performance system and the gas cooler performance has an important role in this condition.

The on-line optimal pressure control concept presented by Zhang and Zhang (2011) derives an on-line correction formula of optimal heat rejection pressures for supercritical refrigeration systems. This can replace the traditional empirical optimal pressure correlation which was described in Section 2.3. The correction formula and the

PI controller take different duties and work together to track the optimal pressures as shown in Figure 2.6. The optimal pressure set point $P_{2,opt}$ is updated by the correction formula periodically and the formula module accepts T_1 , T_3 , P_2 and P_3 as input signals to evaluate electrical work (w) and heat flow (q) using thermodynamic property sub-routines. Following on from this, the PI controller accepts the optimal set point from the correction formula module as reference set point and pushes the pressures to approach the set point (Zhang and Zhang, 2011). However, this online system was not implemented in our experimental rig as the rig was already set-up by Danfoss®.

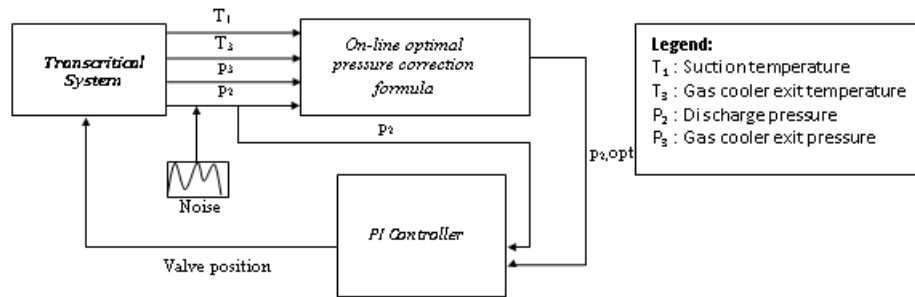


Figure 2.6 On-line optimal pressure control concept
(Source: Zhang and Zhang, 2011)

2.5 Heat transfer coefficient and refrigerant pressure drop of supercritical CO₂

The heat transfer coefficient of finned and tube heat exchanger was investigated based on air side and refrigeration side by several researches. The air side heat transfer coefficient was also influenced by the design of the gas cooler such as the fin design and number of rows (Wang et al, 1999). In following Section 2.5.1 and 2.5.2 are explained the refrigeration side heat transfer coefficient and pressure drop based on horizontal long pipe investigation in supercritical condition and it was also compared between the heat transfer coefficient of pure CO₂ and CO₂-oil mixture. Furthermore, the air-side heat transfer coefficient of a finned and tube heat exchangers are presented in Section 2.5.3.

2.5.1 Supercritical CO₂ heat transfer coefficient

Pitla et al. (2002), Dang and Hihara (2004), and Oh and Son (2010) investigated experimentally the heat transfer coefficient of pure CO₂ in horizontal long pipe with the effect of the mass flux and pressure during supercritical condition under cooling

conditions. The mass flux and the temperature of CO₂ have significant effects on the heat transfer coefficient, especially near the pseudo-critical region and Pitla et al. (2002) stated that “Pseudo-critical region is the region of the maximum in heat transfer coefficient and coincides with the region where the specific heat has a maximum”. The heat transfer coefficient decreases as the cooling pressure increases but otherwise increases as mass flux increases. Furthermore, Dang et al. (2012), and Jung and Yung (2013) investigated the heat transfer coefficient of CO₂ and oil mixture in a horizontal pipe. The heat-transfer coefficients of CO₂ with the different oil concentrations are compared with that of pure CO₂ near the pseudo-critical temperature.

The pure CO₂ heat transfer coefficient correlations developed by Pitla et al. (2002) are defined as shown in equation (2.5):

$$Nu = \left(\frac{Nu_{wall} + Nu_{bulk}}{2} \right) \frac{k_{wall}}{k_{bulk}} \quad (2.5)$$

Where Nu_{wall} and Nu_{bulk} are Nusselt Numbers that are evaluated based on the thermo-physical properties at the wall and bulk temperatures, respectively.

In each case, the Gnielinski’s correlation, as shown in equation (2.6), is used to calculate the respective Nusselt Number:

$$Nu = \frac{f/8(Re-1000)Pr}{12.7\sqrt{f/8(Pr^{2/3}-1)}+1.07}, \text{ where } f: \text{ friction factor} \quad (2.6)$$

To obtain the local mean velocity, the length of the test section was divided into finite lengths (finite sections) and the mean velocity was evaluated in each finite section using equation (2.7):

$$U_{avg} = \frac{\dot{m}}{A\rho_{bulk}} \quad (2.7)$$

In addition, equation (2.6) requires the knowledge of the friction coefficient, ζ . Appropriate results were obtained by using Filonenko’s correlation as shown in equation (2.8).

$$f = (0.79 \ln(Re) - 1.64)^{-2} \quad (2.8)$$

Once the mean Nusselt Number has been obtained, the heat transfer coefficient can be computed as shown in equation (2.9):

$$h = \frac{Nu}{D} k_{bulk} \quad (2.9)$$

Dang and Hihara (2004) modified the Gnielinski correlation (equation 2.6) become a new correlation as described in equation (2.10). Effects of parameters such as mass flux, pressure, heat flux, and tube diameter on the heat transfer coefficient and pressure drop were analysed. The correlation predicted experimental data with an accuracy of 20%.

$$Nu = \frac{(f_f / 8)(Re_b - 1000) Pr}{1.07 + 12.7 \sqrt{f_f / 8} (Pr^{2/3} - 1)} \quad (2.10)$$

Oh and Son (2010) improved Dang and Hihara (2004) correlation with more precise prediction. Two terms were considered especially near the pseudo-critical region. 1) The density ratio, representing the effect of density gradient and buoyancy. 2) The other is the specific heat ratio, representing the effect of variable specific heat along the cross section of the tube. Accordingly, the new correlation introduces the density ratio and the specific heat ratio evaluated at T_b (bulk temperature) and T_w (wall temperature), respectively. The exponents in the proposed heat transfer correlation are shown in equation (2.11).

$$Nu_b = 0.023 Re_b^{0.7} \cdot Pr_b^{2.5} \cdot \left(\frac{C_{p,b}}{C_{p,w}} \right)^{-3.5} \quad \text{for } T_b / T_{pc} > 1 \quad (2.11)$$

Where $C_{p,b}$ and $C_{p,w}$ indicate the specific heat evaluated at T_b and T_w , respectively and T_{pc} is temperature of maximum $C_{p,b}$.

Oh and Son (2010) stated that most of the experimental data can be predicted by the correlation of equation (2.11) with a mean deviation of 12.5%.

In the range of $T_b / T_{pc} \leq 1$, the exponents in equation (2.12) were obtained by the same method.

$$Nu_b = 0.023 Re_b^{0.6} \cdot Pr_b^{3.2} \cdot \left(\frac{\rho_b}{\rho_w}\right)^{3.7} \cdot \left(\frac{C_{p,b}}{C_{p,w}}\right)^{4.6} \quad \text{for } T_b / T_{pc} \leq 1 \quad (2.12)$$

Oh and Son (2010) clearly explained in Figure 2.7 that the maximum heat transfer coefficient at operating pressure 7.5 MPa until 10 MPa occur at between 30°C-45°C. This variation coincides with the specific heat (c_p) of the refrigerant.

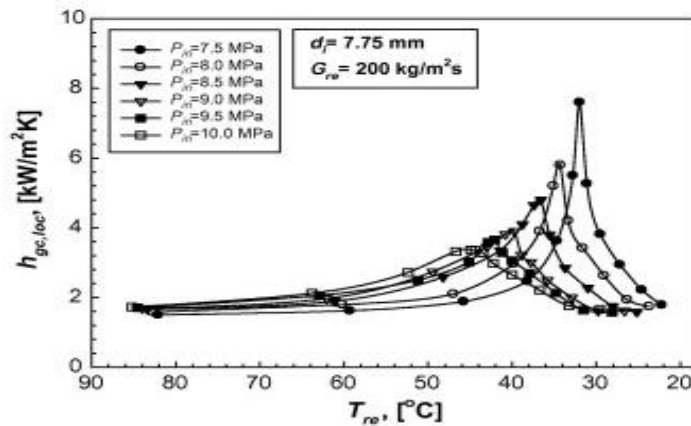


Figure 2.7 Variation of heat transfer coefficient with bulk temperature (Source: Oh and Son, 2010)

For the CO₂ mixed with oil, Dang et al. (2012) and Jung and Yung (2013) found there was a significant drop in the heat-transfer coefficient caused by the oil. Oil with good CO₂ solubility has a higher heat transfer coefficient. The oil percentage in CO₂ has significant effect when the percentages reach 5%, it causes the pseudo critical area disappear as shown in Figure 2.8.

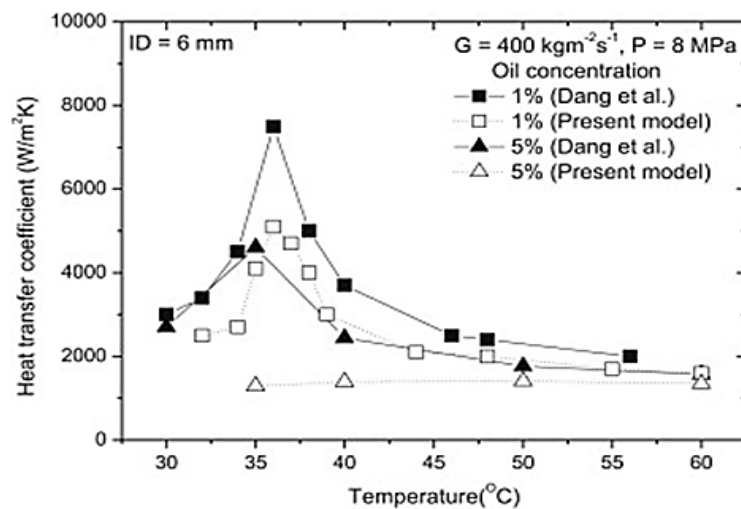


Figure 2.8 Heat transfer coefficient of CO₂ mixed with oil (Source: Jun and Yung, 2013)

The gas cooling heat transfer coefficient of the CO₂ and oil mixture decreases with the increase of working pressure because of the increased oil droplet entrainment in the CO₂ core flow. The thermo-physical properties deteriorate compared to pure CO₂ when the working pressure is increased (Jun and Yun, 2013).

2.5.2 CO₂ pressure drop correlation

As heat transfer coefficient investigation is during supercritical gas cooling condition, the CO₂ pressure drops in pipe also distinguish between pure CO₂ and an effect of the lubrication oil mixture. Generally, the pressure drop increases as the mass flux increases and as the system pressure decreases. This is because the density of CO₂ is higher if the system pressure is higher. The pressure drop decreases if the density increases at constant mass flux. In terms of pure CO₂, Yoon et al. (2003) and Son and Park (2006) measured the pressure drop between the inlet and outlet as less than 1 kPa m⁻¹ and it has been found that the pressure drop will increase sharply when the oil concentration increases (Dang et al., 2007).

Yoon et al. (2003) compared the experiment results with the frictional pressure drop for a fully developed turbulent single-phase flow in a smooth tube which is shown in equation (2.13).

$$\Delta P = f \frac{G^2 L}{2\rho D_i} k_{bulk} \quad (2.13)$$

Several equations have been developed for the friction factor (f). Blasius' equation is most widely used for the turbulent flow in smooth tubes and is calculated by:

$$f = 0.316 \text{Re}^{-1/4} \quad \text{for } \text{Re} \leq 2 \times 10^4 \quad \text{and} \quad f = 0.184 \text{Re}^{-1/5} \quad \text{for } \text{Re} \geq 2 \times 10^4 \quad (2.14)$$

Yoon et al. (2003) recommended the Blasius's correlation for carbon dioxide pressure drop prediction. The correlation shows good agreement with the experimental result with the average deviation only as 3.7%. Son and Park (2006) also found only 4.6 % of the mean deviation from the Blasius correlation compared with Petrov–Popov's correlation mean deviation as high as 64%, as shown in Figure 2.9(a) and (b).

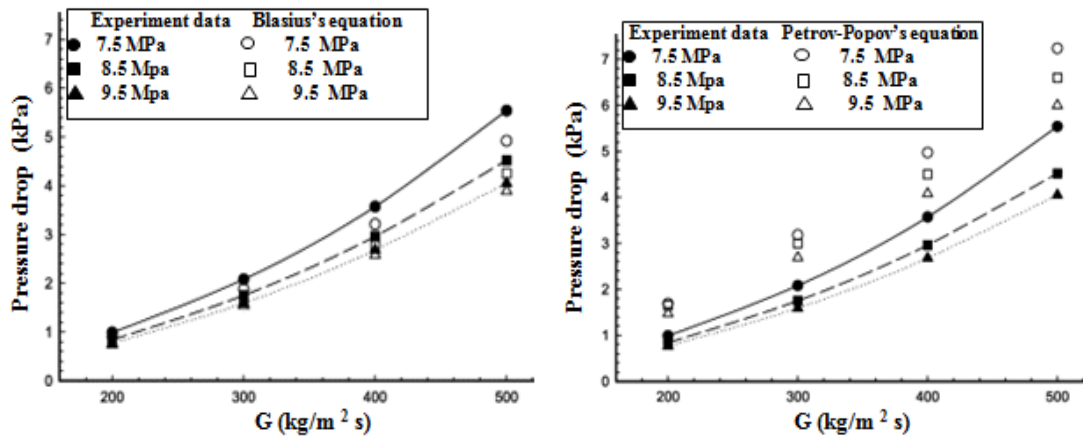


Figure 2.9 Blasius and Petrov-Popov's pressure drop correlation
(Source: Son and Park, 2006)

Dang et al. (2007) carried out an experiment to investigate the effects of lubricating to the pressure drops which measured for 2 mm tubes diameter at oil content from 1% to 5%. Figure 2.10 shows the variation of pressure drop (kPa) with bulk temperature ($^{\circ}\text{C}$). It can be seen that the effect of oil concentration is not linear, and there is significant effect of the oil content of 3% and 5%. It can be recommended that to keep the system has good performance the oil concentrations should be limited up to 1%

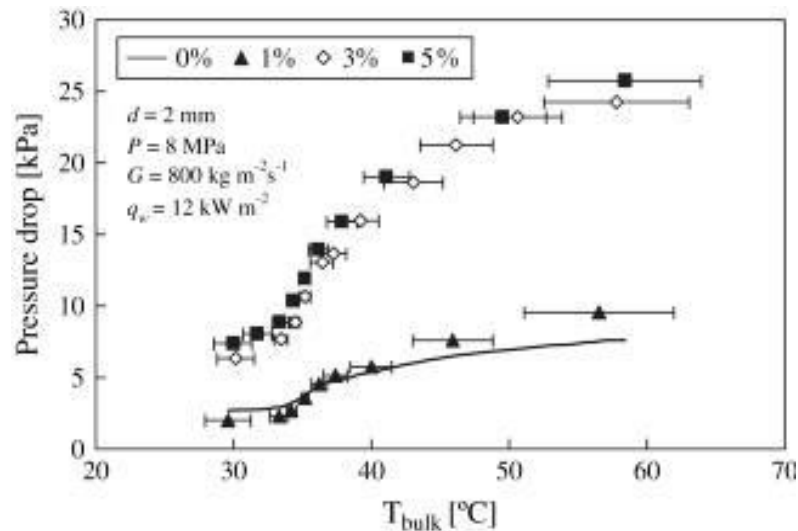


Figure 2.10 Measured pressure drop variation with T_{bulk} at different oil concentrations
(Source: Dang et al., 2007)

2.5.3 Air side heat transfer coefficient finned and tube heat exchanger

The air side heat transfer coefficient calculations and correlation were adopted from Wen and Ho (2009) and Chang and Kim (2006). The equation (2.15) and (2.16) will be used to define air side heat transfer coefficient in this study as explained in Chapter 6.

Wen and Ho (2009) carried out an experimentally investigated the air side heat transfer coefficient in finned and tube heat exchangers. The experiment was carried out with improved fin design to enhance heat transfer in fin-and-tube heat exchangers. Three different fins (plate fin, wavy fin, and compounded fin – see Figure 2.11) were investigated in a wind tunnel.



(a) Plate fin



(b) Wavy fin



(c) Compound fin

Figure 2.11 Fin configuration

(Source: Wen and Ho, 2009)

The heat transfer coefficients are defined from the total heat-transfer rate (Q), the total of tubes and fin surface area ($A_t + A_f$) and the average wall-to-fluid bulk temperature difference ($T_w - T_b$). The heat transfer coefficient is defined as follows:

$$h = \frac{Q}{(A_t + A_f)(T_w - T_b)} \quad (2.15)$$

$$Q = \dot{m} c_p (T_{\text{out}} - T_{\text{in}}) \quad (2.16)$$

Where, T_{out} = air outlet temperature and T_{in} = air inlet temperature

The thermo-physical properties of air were obtained at a film temperature (T_{film}) = $0.5(T_w + T_b)$. Where, T_w is average of tube and fin wall temperature. The bulk temperature T_b is the mean temperature between inlet and outlet air temperature.

Figure 2.12 shows the heat transfer coefficient and pressure drop of the different test fins with respect to air velocity. It can be seen that as the air velocity increases, the heat-transfer coefficients also increase. The wavy and compound fin have significant higher

heat transfer coefficient than plate fins, this is due to higher velocity fluctuations and higher acceleration in the circulation regions for the wavy and the compounded fins than those of the plate fin (Wen and Ho, 2009).

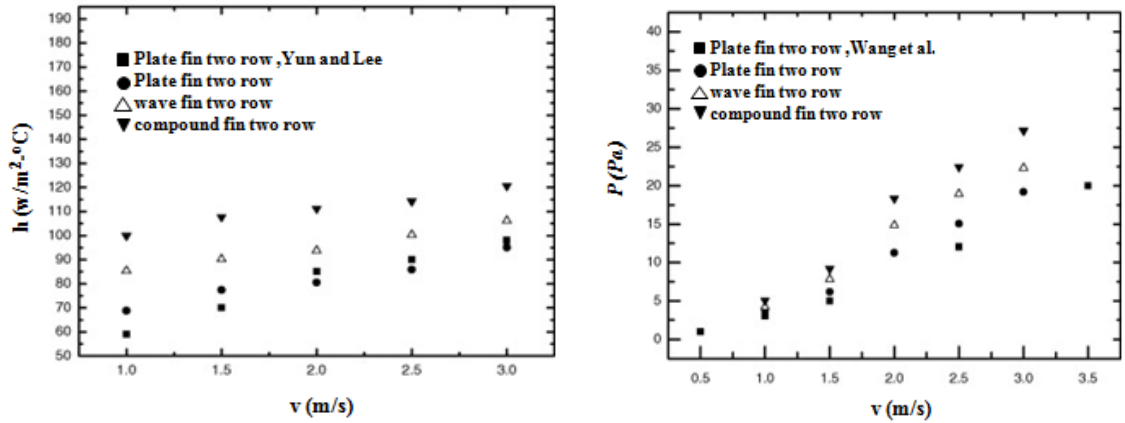


Figure 2.12 Variation of heat transfer coefficient and pressure drop with average inlet velocity of the fluid for the different fin types
(Source: Wen and Ho, 2009)

Chang and Kim (2006) developed an air side heat transfer correlation according to air velocity-Reynold Number of three row and two row gas coolers with louver fin type (see Figure 2.13). The correlation template is expressed in equation (2.17) as follows:

$$Nu = C Re_D^m Pr^{1/3} \quad (2.17)$$

Where, Re_D is Reynolds Number for tube diameter. In this study, this template will be used to develop air side heat transfer correlation.

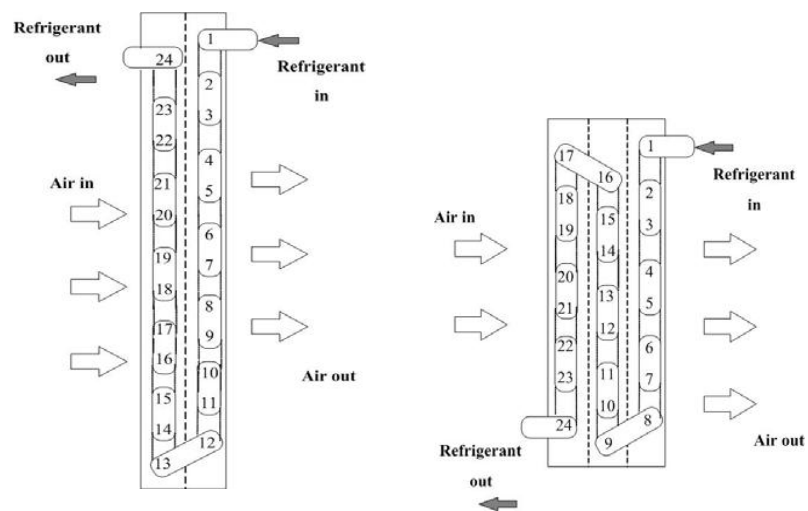


Figure 2.13 Two design fin and tube heat exchangers
(Source: Chang and Kim, 2006)

2.6 Finned and tube gas cooler simulation

The Computational Fluid Dynamics (CFD) is a common and valuable tool to investigate the finned and tube heat exchanger improvement. For instance, Yaïci et al.(2014) and Singh et al. (2011) simulate inlet air flow mal-distribution using two and three-dimensional (2D-3D) CFD. The validation shows a good agreement against experimental results within 4% errors of the overall predicted heat load and also demonstrates that 3D CFD simulation is a useful tool for analysing, designing and optimising heat exchangers.

The CFD model also showed satisfaction results to investigation heat transfer coefficient of fin improvement with the vortex generation (He et al., 2013), investigation of the average heat transfer coefficient for the air of plate fin and tube heat exchanger using CFD with the modified method, which is similar to the technique used for experimental data reduction (Taler & Oclo, 2014), and also the ability of CFD code to predict flow patterns and thermal fields allows determining the heat transfer characteristics by performing ‘numerical experiments’. However, even if an offset is noticed between CFD calculations and the experimental results, the trends are comparable and CFD permits to reach local information, leading to better understanding of the physical phenomena involved in compact heat exchangers (Perrotin & Clodic, 2004).

The air and refrigerant side - heat transfer coefficient correlations are very important in order to obtain a gas cooler design precisely, since high variation temperature entire the gas cooler lead fluctuation thermo-physical properties of the working fluid (R744). Gupta and Dasgupta (2014) developed a numerical steady-state model that examines the performance of an air-cooled gas cooler using the Effectiveness-NTU method. The model employed the Gnielinski (1976) and Pitla et al. (2002) correlation to simulate the refrigerant-side heat transfer (as described in Section 2.5.1), while the air-side heat transfer was obtained from the Incropera and DeWitt (1996) correlation. The model was validated with experimental results, however, only the CO₂ outlet temperatures were compared. In addition, Ge and Cropper (2009) developed a distributed model which calculates the local overall heat transfer coefficients for the gas cooler, in order to account for the rapid changes in the CO₂ temperatures for different tubes. The model was validated with errors of up to 2°C, with a general trend similar to the test results as

shown in Figure 2.14. Whilst, Zilio et al.(2007) obtained errors of up to 30°C in the first tubes of an air-cooled gas cooler as shown in Figure 2.15.

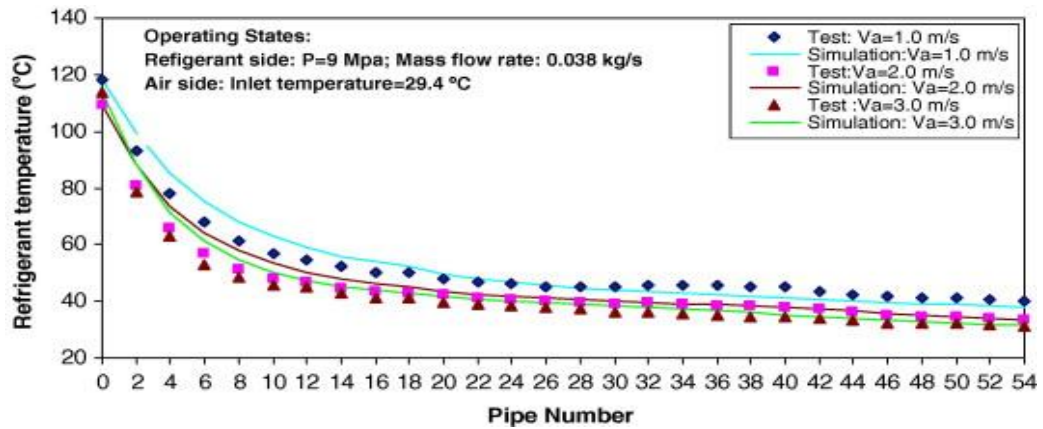


Figure 2.14 Comparison of refrigerant temperature profile from simulation and experiment (Source: Ge and Crooper, 2009)

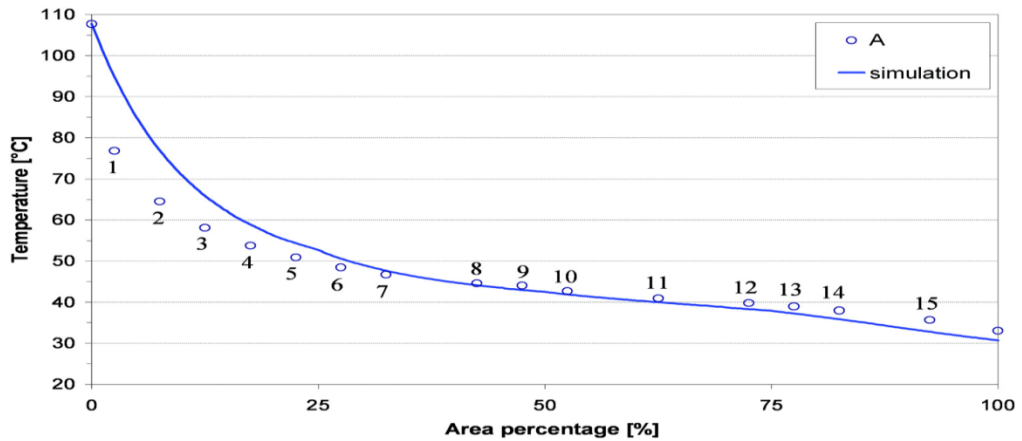


Figure 2.15 Temperature profile from model and experimental results (Source: Zilio et al., 2007)

Generally, these errors have been attributed to the use of average values rather than the local value of the heat transfer coefficients both on the refrigerant and air-side of the gas cooler (Ge and Crooper, 2009). The refrigerant side heat transfer coefficients are usually obtained from established correlations such as, Pitla et al. (2002) and Dang and Hihara (2004), and these different correlations often predict similar results for CO₂ gas coolers (Zilio et al., 2007).

2.7 Effect of the thermal conduction in gas coolers

A gas cooler of CO₂ refrigeration system is operating at a significant higher temperature and pressure than other conventional refrigeration systems and also found that the gas temperature is decreased with the highest rate at the beginning along the pipe from refrigerant inlet to outlet because of the thermo-physical properties (Santosa et al., 2013). This condition leads heat conduction from the hot tube to adjacent cold tube through the fin and causes performance reduction of the gas cooler. To reduce the conduction effect, it was introduced a slit or cutting fin design to block the heat spread between tubes through fins. Zilio *et al.* (2007), Singh *et al.* (2010) introduced a finned tube heat exchanger model improvement with a cutting fin configuration and validated by their experimental results. Park and Hrnjak (2006) carried out an experimental investigation for cutting fin toward a microchannel gas cooler, whilst Asinari et al. (2004) developed a model of effects of heat conduction in microchannel gas coolers.

Zilio's model results obtained heat flux improvement of 3.7% up to 5.6% for the separated fin design in each row comparing with the continuous fin for the gas cooler application and contributed better performance (COP) of the system by 5.7% to 6.6%. Singh et al. (2010) investigated not only the effect of the cut fin with the performance but also material can be saving by the cutting. The gas cooler specification and test condition of Singh' studies are shown in Table 2.1 and Table 2.2.

Table 2.1 Carbon dioxide gas cooler specification

PARAMETERS		
Number of segments	10	--
Tube configuration		Staggered
Number of tubes per bank	18	--
Number of tube banks	3	--
Tube length	0.61	M
Tube OD	0.0084	M
Tube thickness	0.406	Mm
Tube vertical spacing	1	In
Tube horizontal spacing	0.625	In
Fpi	17	Fpi
Fin thickness	0.0043	In
Fin type	Slit	---
Coil face air velocity	Variable	ms ⁻¹

(Source: Singh *et al.*, 2010)

Table 2.2 Carbon dioxide gas cooler test condition

No	Inlet Air temp [°F(°C)]	Ref MFR [lbmin ⁻¹ (gs ⁻¹)]	Inlet pressure [psia (Mpa)]	Air Frontal Velocity [fpm (ms ⁻¹)]
1	85 (29.4)	5(38)	1,300 (9.0)	200,400,600 (1.0,2.0,3.0)
2			1,450 (10.0)	200,400,600 (1.0,2.0,3.0)
3			1,600 (11.0)	200,400,600 (1.0,2.0,3.0)
4			1,300 (9.0)	200,400,600 (1.0,2.0,3.0)
5			1,450 (10.0)	200,400,600 (1.0,2.0,3.0)
6			1,600 (11.0)	200,400,600 (1.0,2.0,3.0)
7	95 (35)	10 (76)	1,300 (9.0)	200,400,600 (1.0,2.0,3.0)
8			1,450 (10.0)	200,400,600 (1.0,2.0,3.0)
9			1,600 (11.0)	200,400,600 (1.0,2.0,3.0)
10			1,300 (9.0)	200,400,600 (1.0,2.0,3.0)
11			1,450 (10.0)	200,400,600 (1.0,2.0,3.0)
12			1,600 (11.0)	200,400,600 (1.0,2.0,3.0)

(Source: Singh et al., 2010)

Figure 2.16 shows two configurations of cutting fin were modelled, the best cut configuration design would impact on the optimum performance of the gas cooler. The configuration is according to pipe number. Number 1 refers to the inlet and number 36 refers to the outlet and the cut length follow the sequence number of tubes. In general it was found that more length the configuration cutting, the gain in heat load increases. And the maximum heat load gain can be up to 12% over the baseline. In terms of fin material savings, at a specific capacity and operating condition the fin cuts configuration can be save as high as 45% (Singh et al. 2010).

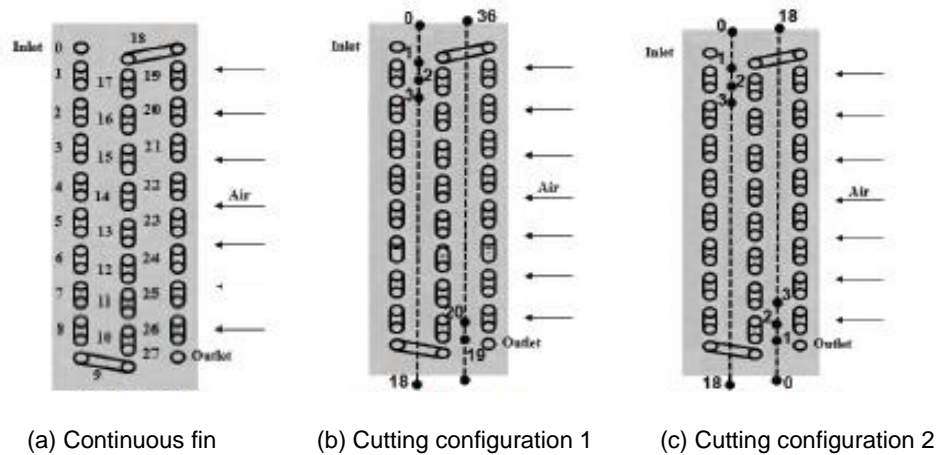


Figure 2.16 Schematic of the gas cooler with two cut configurations

(Source: Singh et al., 2010)

In term of microchannel heat exchanger, Park and Hrnjak (2006) carried out experimental test toward a serpentine gas cooler which was employed in a supercritical CO₂ system for air conditioning. In these experimental procedures, Figure 2.17 shows some sections of the fin, where the conduction from hotter tube was significant, were

cut by EDM (Electrical Discharge Machining). The tube surface temperature of the gas cooler was measured at some points and Figure 2.18 shows the temperature contour from infrared images which can display clearly the heat conduction spread for the continuous fin and then block after cutting fins.

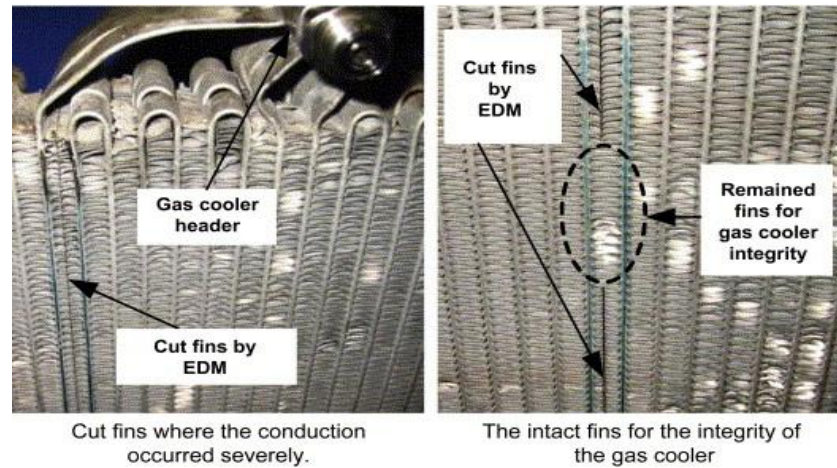


Figure 2.17 Cut fin configuration
(Source: Park and Hrnjak, 2006)

Park and Hrnjak (2006) investigated the cutting fin effect towards the gas cooler performance with several important parameters, comprise: gas cooler capacity (Q), approach temperature (temperature difference between air inlet and refrigeration outlet) and COP of the system. It was found that gas cooler capacity was improved up to 3.9% and approach temperature was reduced by 0.9-1.5°C. Furthermore, by using simulation depend on the better approach temperature, system COP could be improved by 5%.

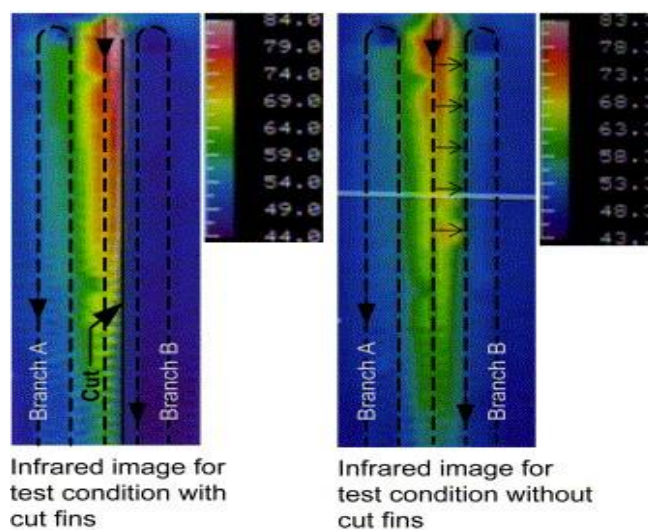


Figure 2.18 Infrared image of gas cooler surface with and without cut fins
(Source: Park and Hrnjak, 2006)

Park and Hrnjak (2006) also tabulated the representative test results as shown in Table 2.3. The test procedures are using a variation of refrigerant mass flow rate (\dot{m}_{ref}) and air face velocity. It can be seen that approach temperature ($T_{ref,o} - T_{air,i}$) decreases, whilst Q increases with cut fins and the uncertainty is less than 2.5%

Table 2.3 Measured capacity and CO₂ temperature of the gas cooler

\dot{M}_{ref} (gs ⁻¹)	Item	Face V_{air} 1.2 (ms ⁻¹)		Face V_{air} 1.8 (ms ⁻¹)	
		With cut	Without cut	With cut	Without cut
20	Q(kW)	3.19	3.13	3.38	3.30
	$(Q_w - Q_{wo}) \times 100/Q_{wo}$		1.9%		2.4%
	$T_{ref,i} - T_{ref,o}$ (°C)	69.1	67.3	68.1	66.6
	$T_{ref,o} - T_{air,i}$ (°C)	2.1	3.6	1.0	1.9
	Uncertainty	2.5%	2.2%	2.0%	2.0%
25	Q(kW)	4.01	3.86	4.35	4.20
	$(Q_w - Q_{wo}) \times 100/Q_{wo}$		3.9%		3.6%
	$T_{ref,i} - T_{ref,o}$ (°C)	73.5	71.5	71.9	70.2
	$T_{ref,o} - T_{air,i}$ (°C)	2.0	3.3	1.2	2.1
	Uncertainty	2.4%	1.9%	2.0%	1.8%

(Source: Park and Hrnjak, 2006)

Asinari et al. (2004) investigated a typical minichannel gas cooler and it was found that the bad conduction can be diminished by its tube circuits. In this case the cutting fin design can be neglected. A similar study by Ge and Cropper (2009) obtained that with increased pipe circuits, the gas cooler heat transfer coefficients inside the pipes will be increased and therefore the approach temperature will be decreased and the heating load will be increased. Therefore, in the gas cooler optimal design, more circuit numbers need be considered. As a result, for the next better design of gas cooler should be consider also the optimal tube arrangement and circuits to avoid severe conduction effect among the tubes.

2.8 Summary

Internal heat exchanger (IHX) and ejector systems are a common system to improve a supercritical CO₂ refrigeration system. During supercritical operation, the gas cooler should be controlled at an optimum pressure in order to get the optimum COP of the system and the optimum gas cooler pressure correlations were developed by several researchers.

CO₂ heat transfer coefficients in a long pipe during gas cooling process were investigated experimentally and developed correlations in respect with Re and Pr

Numbers. Air side heat transfer coefficient increases as the fin design improvement. This chapter also provide a correlation template from previous study which will be used to develop the air side heat transfer coefficient correlation in this study.

The literature summary of heat transfer and pressure drop on the refrigerant side and air side shows at following table.

Author	Refrigerant side heat transfer coefficient	Explanation
Gnielinski (1976)	$Nu = \frac{f/8(Re-1000)Pr}{12.7\sqrt{f/8(Pr^{2/3}-1)}+1.07}$	Because of the CO ₂ thermophysical properties, so the results showed high deviation in pseudo critical area (highest cp)
Pitla et al. (2002)	$Nu = \left(\frac{Nu_{wall} + Nu_{bulk}}{2} \right) \frac{k_{wall}}{k_{bulk}}$	Nusselt Number calculated by Gnielinski's correlation, the results quite precision, except for pseudo critical area.
Dang and Hihara (2004)	$Nu = \frac{(f_f/8)(Re_b-1000)Pr}{1.07 + 12.7\sqrt{f_f/8(Pr^{2/3}-1)}}$	Modified from Gnielinski correlation, the accuracy is approximately 20%
Oh and Son (2010)	$Nu_b = 0.023 Re_b^{0.7} \cdot Pr_b^{2.5} \cdot \left(\frac{C_{p,b}}{C_{p,w}} \right)^{-3.5}$ for $T_b/T_{pc} > 1$ $Nu_b = 0.023 Re_b^{0.6} \cdot Pr_b^{3.2} \cdot \left(\frac{\rho_b}{\rho_w} \right)^{3.7} \cdot \left(\frac{C_{p,b}}{C_{p,w}} \right)^{-4.6}$ for $T_b/T_{pc} \leq 1$	<p>For $T_b/T_{pc} > 1$</p> <p>For $T_b/T_{pc} \leq 1$</p> <p>The mean deviation with experimental data up to 12.5 %</p>
Dang et al.(2012), Jun and Yung (2013)	Conducted experimentally investigation of CO ₂ mixed with oil to the heat transfer coefficeint.	Thermophysical properties of CO ₂ with oil deteriorate compared with pure CO ₂ , especially in pseudo critical area and the oil has significant effect when the percentage reach 5%
Author	Refrigerant side pressure drop	Explanation
Blasius equation	Pressure drop equation of refrigerant side $\Delta P = f \frac{G^2 L}{2\rho D_i} k_{bulk}$ $f = 0.316 Re^{-1/4}$ for $Re \leq 2 \times 10^4$ and $f = 0.184 Re^{-1/5}$ for $Re \geq 2 \times 10^4$	Blasius equation for CO ₂ pressure drop was investigated by several researchers
Yoon et	The Blasius correlation for the CO ₂ pressure drop	They measured pressure drop less

al. (2003), Son and Park (2006)	prediction showed good agreement with the experimental results, with average deviation 3.7% - 4.6%	than 1 kPa m ⁻¹ and were recommended that the Blasius correlation for the CO ₂ pressure drop is precision
Dang et al.(2007)	Conducted experimental test for the lubricating effect to the pressure drop and it was found that there is significant effect of the oil content of 3% and 5%	It can be recommended that to keep the system has good performance the oil concentration should be limited up to 1%
Author	Air side heat transfer coefficient	Explanation
Wen and Ho (2009)	Air side heat transfer coefficient was investigated experimentally and calculated using equation : $h = \frac{Q}{(A_t + A_f)(T_w - T_b)}$	This experiment for finned tube heat exchanger with hot water as the hot working fluid. The equation is to calculate the air side heat transfer coefficient from experimental results. Also it will be used to calculate air side heat transfer coefficient from the CFD results in this study
Chang and Kim (2006)	Gas cooler (CO ₂) air side heat transfer coefficient was expressed in general equation as follows: $Nu = C Re_D^m Pr^{1/3}$	An air side heat transfer coefficient correlation only eligible for one specific design of the finned tube gas cooler, and this correlation template will be used in this study

The optimisation of gas cooler was investigated by several researchers by simulation models and experiments. The gas cooler improvement has been found with a cutting fin method and also optimal design can be considered by a higher number of circuits.

The following chapter will explain test facilities and will include the mechanical and electrical component, refrigeration load, control components and strategies and also data logging system.

CHAPTER III - TEST FACILITIES

3.1 Introduction

Figure 3.1 shows a schematic diagram of the CO₂ refrigeration system test facilities in the refrigeration laboratory of the Research Council United Kingdom (RCUK) Centre for Sustainable Energy use in Food chains (CSEF), Brunel University. The main parts of the system comprise a refrigeration system, an environmental chamber with Medium Temperature (MT) display cabinet as well as an MT air cooler and gas cooler test rig. Additionally, there is a load system using glycol as the heat transfer medium, a standstill condensing unit, which is positioned on the plant roof of the machine room, as well as electrical control panels.

The control system for the refrigeration is a commercially available system with automatic controls. However, the other systems are controlled separately including the additional load, gas cooler test rig and the environmental chamber.

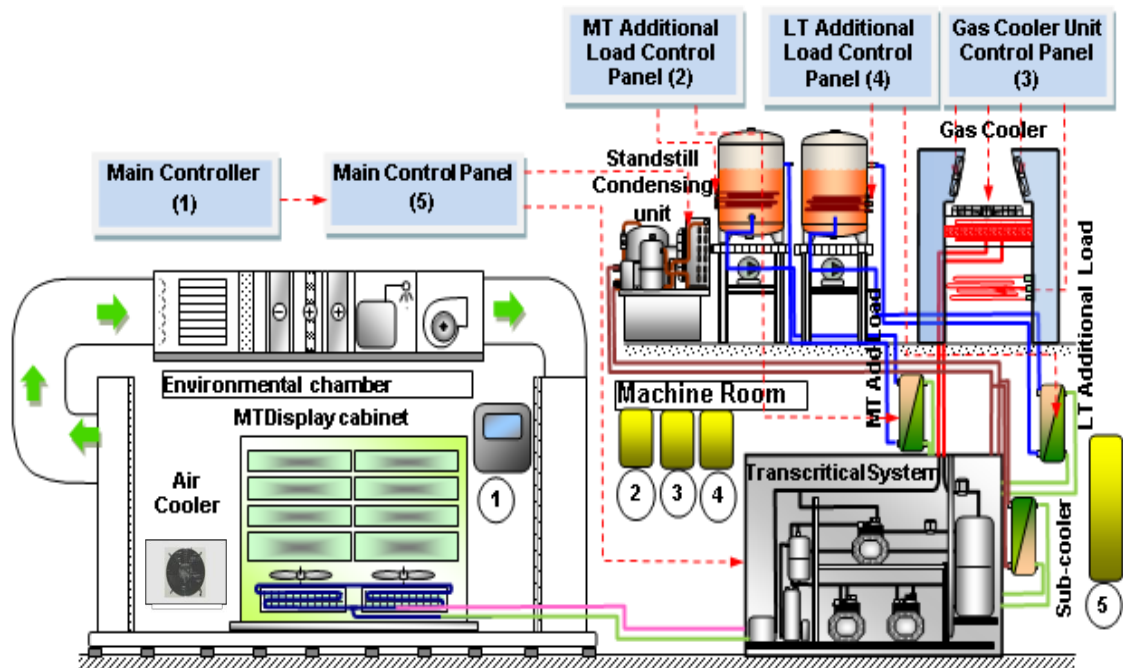


Figure 3.1 Schematic diagram of the CO₂ test facilities
(CSEF- Brunel University Laboratory)

Some modifications and improvements have been made to the refrigeration system in order to satisfy the gas cooler testing objectives: an added sub-cooler system, MT additional load and an MT air cooler. The Low Temperature (LT) additional load was suspended and LT display cabinet was removed from the environmental chamber. The internal heat exchanger (IHX-3) was modified to become an indirect mass flow rate measurement to validate the mass flow rate calculation from the air-side with heat balance calculation in the gas cooler. The existing gas cooler from LUVE was replaced with some newly tested gas coolers from GEA-Searle. This system is a two stage system, with medium temperature (MT) and low temperature (LT) stages. However, for the gas cooler test procedures only medium temperature has been operated. The whole schematic diagram of the system after modification is described in Figure 3.4.

3.2 Mechanical system and components

Figure 3.3 shows the CO₂ refrigeration system which was installed in Brunel University and Figure 3.4 illustrates a detailed schematic diagram of the mechanical system after modifications and improvements. Drawing of the identification and numbering of the mechanical component of the CO₂ refrigeration system, with all of the valve number and measurement point also can be found in Appendix A. The refrigeration system is a booster bypass system which has four pressure regions, high, intermediate, medium and low pressure. The main components of the high pressure region include two high temperature (HT) compressors in a parallel arrangement, an accumulator downstream of the suction line, an oil separator, a gas cooler and an internal heat exchanger (IHX-3).

The ICMT valve reduces the pressure from the high pressure to the intermediate pressure region. Mechanical components for the intermediate pressure region include a CO₂ vessel/liquid receiver with cooling coil for the standstill condensing unit, an ICM valve which controls the pressure in the receiver and reduces the pressure of refrigerant vapour from the receiver to the medium pressure level of the system. In the medium pressure region there is a sub-cooler and internal heat exchanger (IHX-2) used as an intercooler for LT discharge. The liquid line is equipped with a sight glass downstream of the receiver-sub-cooler, a mass flow meter and a liquid line filter. The medium pressure region also includes a medium temperature refrigerated display cabinet, and electronic expansion valve (AKV-MT) as well as components for additional load on the system when needed.

The LT region comprises five main components which include: LT compressor, expansion valve (AKV-LT), LT display cabinet, an LT additional load and an internal heat exchanger (IHX-1). The p-h diagram indicates pressure levels in the system, and is shown in Figure 3.2.

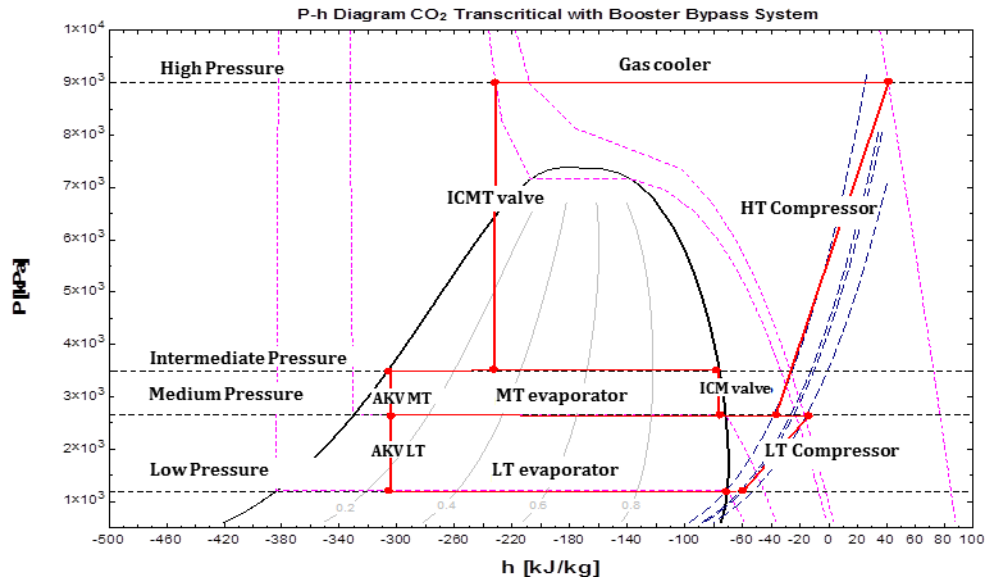


Figure 3.2 P-h diagram of the CO₂ refrigeration system with booster hot gas bypass (supercritical mode)

The receiver of the CO₂ refrigeration system during standstill is cooled down by a small condensing unit to maintain a constant pressure in the system at the intermediate level. The system is also equipped with an oil management system to maintain a relatively constant oil level in the compressor and to ensure the compressors are adequately lubricated.

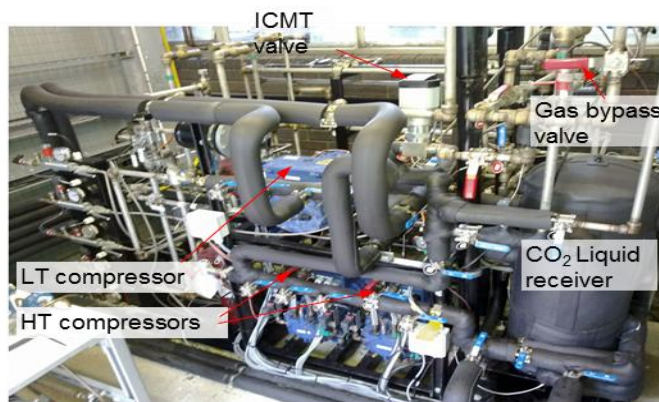


Figure 3.3 CO₂ refrigeration system in the Refrigeration Laboratory (CSEF- Brunel University Laboratory)

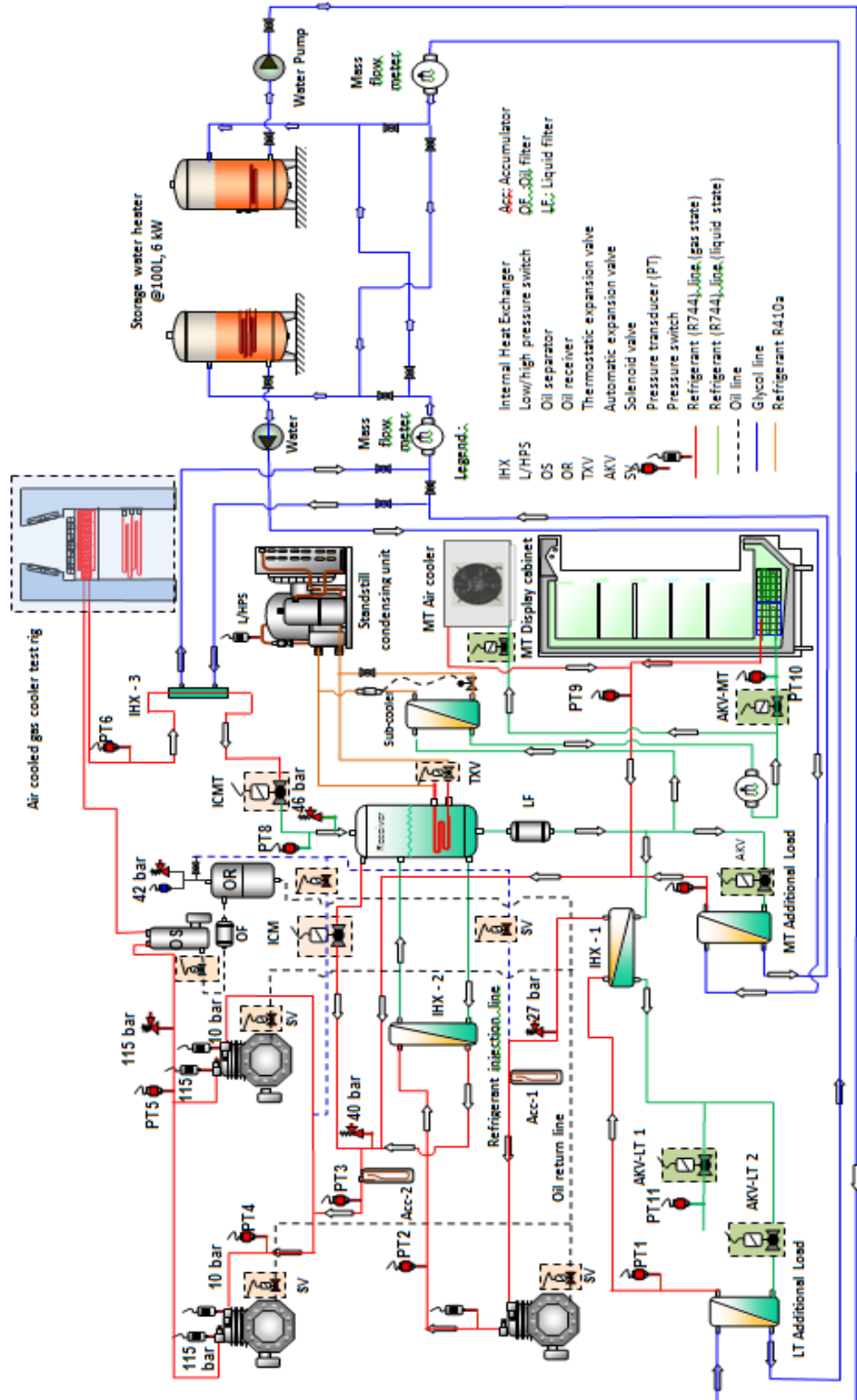


Figure 3.4 Schematic diagram of CO₂ refrigeration system in the Refrigeration Laboratory

3.2.1 CO₂ compressors (HT and LT compressors)

The specifications of the two parallel HT compressors are shown in Figure 3.5. The compressors are BOCK RKX 26/31-2 CO₂T, performance at -10/35; cooling: 9.93kW; power: 6.34kW. Performance at -35/-1; cooling: 8.281 kW; power: 1.98kW. The compressors were equipped with a variable speed controller to enable some variation of capacity.

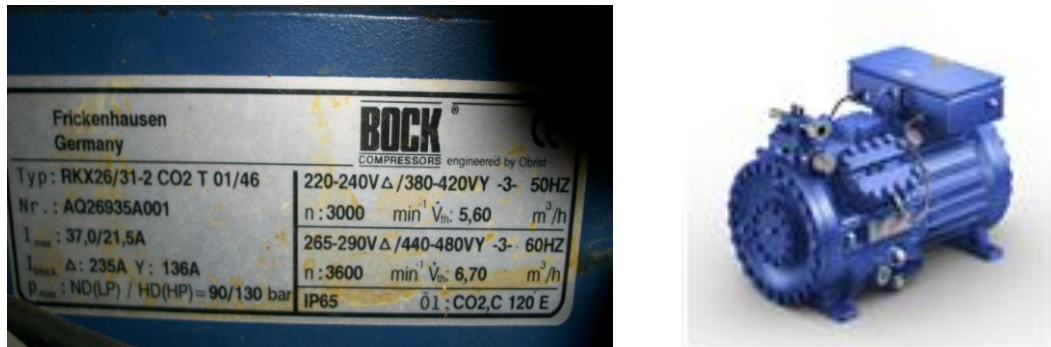


Figure 3.5 HT CO₂ compressor with specification data

To ensure safe operation, the compressor was equipped with several safety controls, which included an oil safety switch, low and high pressure switches, a motor temperature switch and a time delay relay. The oil safety switch protects the compressor from running without sufficient lubrication by switching it off if the oil level drops below a certain limit. The low and high pressure switches are used to stop the compressor when the suction pressure drops below 20 bar and the discharge pressure rises above 115 bar.

The LT compressor used is type BOCK HGX 12P/60-4CO₂, with performance at -35/-10 cooling: 9.394kW, power: 2.23kW. The LT and HP pressure switches off the compressor when discharge pressure rises above 40 bar and suction pressure decreases below 5 bar.

3.2.2 Refrigeration load system

The refrigeration load system consists of medium temperature refrigerated display cabinet with a full load capacity of 5 kW, an additional load with full load capacity of 6kW and an air cooler with full load capacity of 3.5kW. Therefore, the total that can be applied to the system for Medium Temperature (MT) operation is around 14.5kW.

3.2.2.1 MT display cabinet

The refrigerated display cabinet used was a 2.5m long chilled open vertical multi-deck MT cabinet (Carter ELFM). The height of the cabinet was 2.05m, the depth 1.13m and total display area (TDA) was 4.2m².

Evaporator coil used in the loading system was direct expansion (DX) coil with finned tubes designed to operate with CO₂ refrigerant. The coil was made of copper tubes of 12.7mm nominal outside diameter and corrugated aluminium fins of 0.22mm thickness, and fin spacing of 158fins per metre (FPM). The coil consists of 4 circuits in staggered arrangements with 4 rows high, 6 rows deep and a total tube length of approximately 50m. The MT coil can contain about 4.6 litres CO₂ refrigerant. The MT DX evaporator coil is placed adjacent to the MT flooded evaporator coil (which is for subcritical CO₂ refrigeration system). The two evaporator coils which are not used simultaneously are separated by a 25mm gap.

The cabinets were loaded with test packages stacked on the shelves. The test packages of the MT cabinet were 0.8 litre plastic containers filled with water –glycol mixture (50%/50%) and also M-Packages. The MT display cabinet and the loaded products as well as evaporator construction are shown in Figure 3.6.

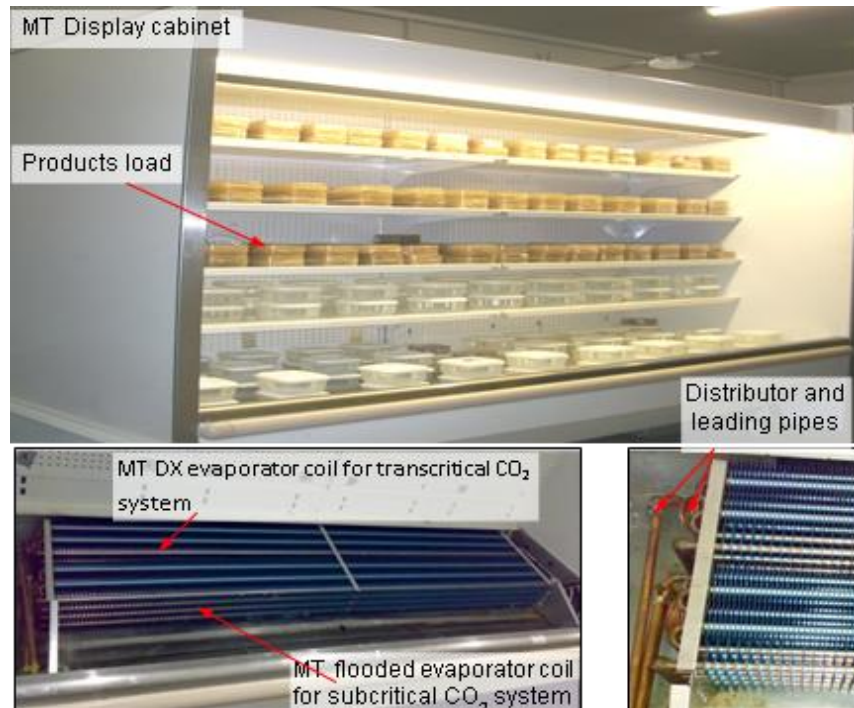


Figure 3.6 MT display cabinet
(CSEF- Brunel University Laboratory)

3.2.2.2 Air cooler

This air cooler (see Figure 3.7) was arranged in parallel with the MT display cabinet. The type of air cooler used was a KEC 30-6L from GEA Searle. The evaporator coil used aluminium fins with fin spacing 6mm with the air flow constant at $0.42\text{m}^3/\text{s}$ and coil volume 3.83l refrigerant. The air cooler has cooling capacity of 3.16 kW for R404 at liquid sub-cooling temperature of 2K and temperature difference between of air-entering temperature and refrigerant saturated suction temperature at the outlet of the cooler was 8K.



(a) Air cooler front view



(b) Air cooler back view

Figure 3.7 Air cooler

The expansion valve and controller for the air cooler are the Danfoss AKV valve size – number 2 and AK-CC-550 controller. It is important that the expansion is correctly sized. The expansion size was determined using the maximum design capacity and the minimum valve pressure drop.

3.2.2.3 MT Additional load

A schematic diagram of the MT additional load is shown in Figure 3.8. The system is used to increase the cooling load of the refrigerant system over and above that provided by the display cabinet and air cooler. A water heater in a storage vessel is used to heat up a water-glycol mixture. This is then circulated through a plate evaporator coil. The evaporating temperature and degree of superheat are controlled by using AK-CC-550 (a cabinet controller from Danfoss-Dean & Wood), AKV Valve, pressure transducer (AKS-32 max WP: 55 bar) and three temperature sensor –AKS 11. The evaporator coil is a plate HX:B15Hx30/1P-SC-M from SWEP International with capacity 6kW at evaporating temperature -8°C , and 10K superheat.

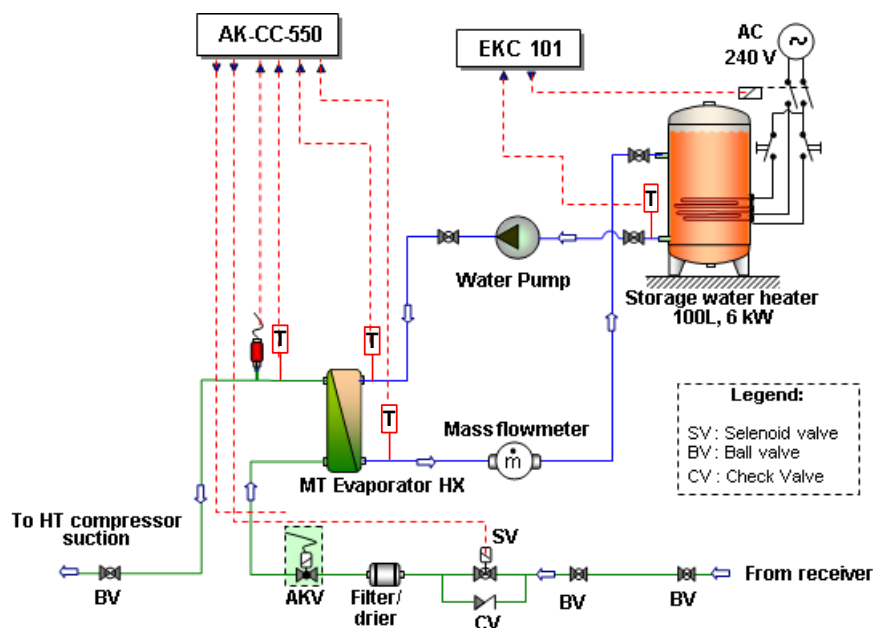


Figure 3.8 Schematic diagram of the MT additional load

3.2.3 Standstill condensing unit

The condensing unit is used to control the pressure in the system at standstill conditions. It consists of a hermetic scroll compressor with a capacity of 1.5HP, accumulator, thermostatic expansion valve, condenser, fan, oil filter and filter dryer and a pressure switch for compressor safety from extremely high and low pressures. A thermostatic expansion valve size of 3/8x1/2, type TES2 is used as the expansion device. The condensing unit is connected to a coil in the CO₂ receiver.

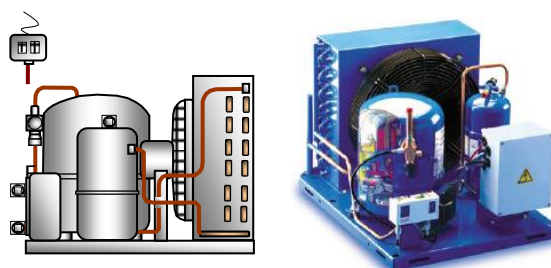


Figure 3.9 Standstill condensing unit
(source: Danfoss-Optyma OP-MCHC034GSA01G)

The unit uses refrigerant R-410A and it has a refrigerant charge of 8.4kg. The condensing unit is controlled from the control system of the CO₂ refrigeration system. The control system automatically regulates the operation of the condensing unit depending on the pressure setting on the receiver, which was set at 31 bar during the system operation and, 26 bar during stand still.

3.2.4 CO₂ receiver

The CO₂ receiver is a vertical receiver manufactured by Klimal- Italia Srl product type RCO.273.80.40.50 + WT65.3II-R(K). It has a volume of 40.8 litres, a test pressure of 71.5 bar and operates at intermediate pressures of around 30-31 bar .The receiver is fitted with three sight glasses, which are on the top, middle and bottom of the vessel to detect the CO₂ liquid level.

The liquid receiver in the CO₂ refrigeration system has three main purposes. One is to provide pump-down storage capacity when other components of the system must be serviced or the system must be shut down due to the tests having been completed. The second is to accommodate a fluctuating refrigerant demand which varies with load and ambient conditions. The third is to provide adequate liquid flow to the MT and LT evaporator. Figure 3.10 shows the dimensions of the liquid receiver.

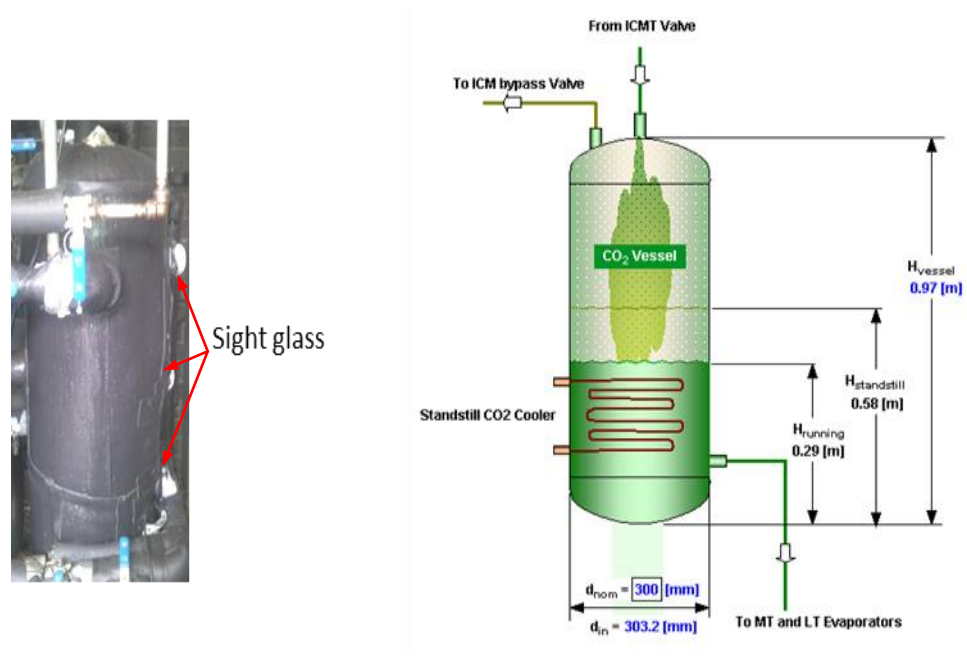


Figure 3.10 CO₂ vessel (liquid receiver)

3.2.5 Expansion devices (ICMT valve, ICM valve and AKV)

Figure 3.11 shows a simple diagram of the position of the valves in the system. Figure 3.12 shows the expansion devices of the CO₂ refrigeration system which include an ICMT valve, an ICM valve and an AKV valve. The ICMT valve can regulate the pressure in supercritical and subcritical mode and the ICM valve is used as a bypass valve. This is one of the differences between a CO₂ system and a conventional system.

In addition, an AKV valve is a common expansion device which is used for the DX evaporator.

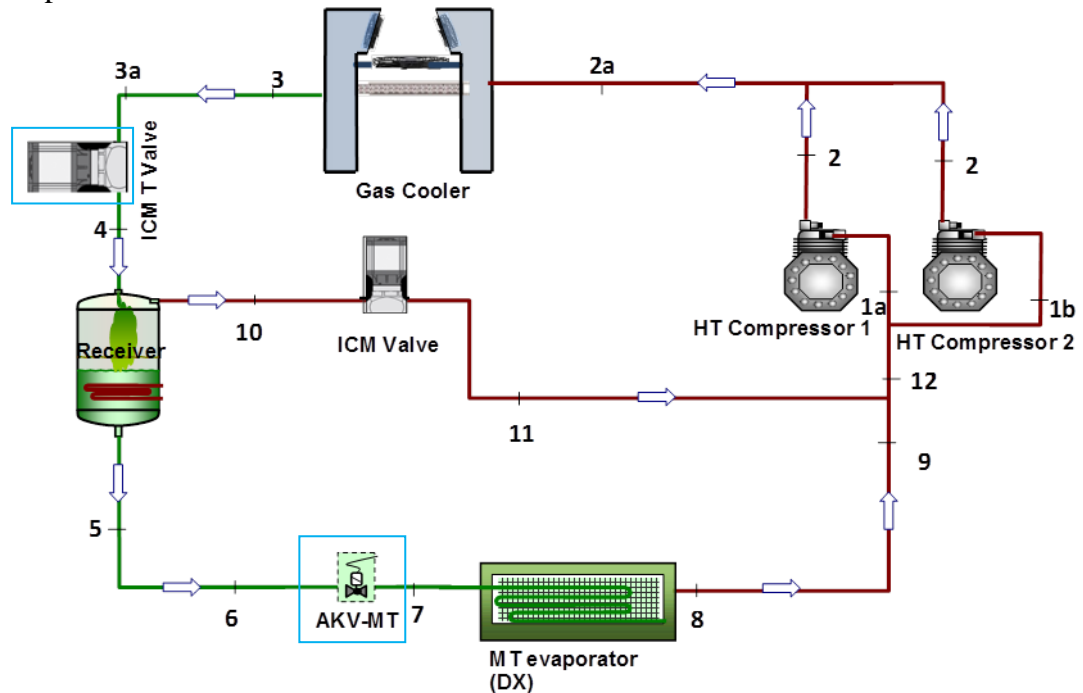


Figure 3.11 Diagram showing valve positions in the system

3.2.5.1 ICMT valve

The ICMT is a valve which has been specially developed for the pressure conditions that exist in a supercritical CO₂ system and it is installed at the outlet of the gas cooler. The ICMT Valve is controlled by an EKC 326 controller, which provides a signal from gas cooler pressure and temperature which are fitted in the outlet immediately after the gas cooler. The controller module at the ICMT valve opening will maintain the optimum pressure to get maximum COP, when in supercritical range. In sub-critical mode the valve will regulate the pressure to get dT-sub-cooling as a setting condition. The ICMT is designed to regulate the flow of supercritical gas or sub-critical liquid from the gas cooler in CO₂ refrigeration systems.

The ICMT is a direct operated motorised valve driven by actuator type ICAD 600TS, and the valve is designed so that the opening and closing forces are balanced. The ICMT valve and ICAD (Industrial Control Actuator with Display) are shown in Figure 3.12(a).

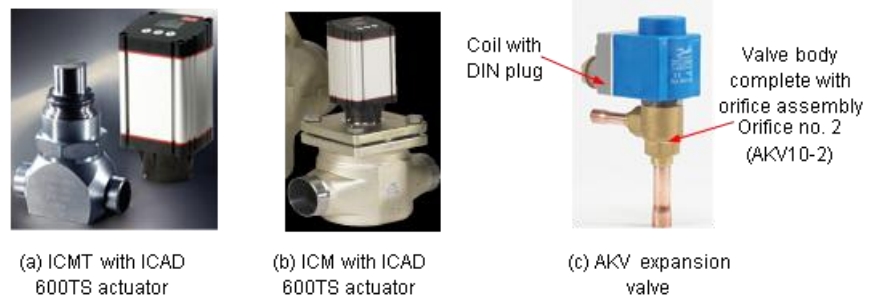


Figure 3.12 Expansion devices
(Source: Danfoss,2009)

The ICMT valve can be used in systems with flash gas bypass, parallel compression as well as for stand-alone applications. The most typical application is with flash gas bypass. This design provides the possibility to optimise gas cooler pressure and intermediate receiver pressure independently. The pressure in the receiver is one important parameter, but the design of the receiver is also important. It typically acts as a liquid separator as well. In order to keep the intermediate pressure low, flash gas is expelled through a gas bypass valve to the suction side of the compressor. The two phase mixture from the ICMT valve has to be separated before gas enters the gas bypass.

3.2.5.2 ICM valve

The ICM valve has two main functions: to control the receiver pressure and expanded hot gas and reduce the pressure to match with medium region pressure from the intermediate region. The valve is controlled by EKC 347 with the signal coming from the pressure transmitter in the receiver and in this system the valve can open simultaneously from 0-100% opened.

Figure 3.12(b) shows the motor valve comprises of four main components: 1) Valve body, 2) top cover, 3) function module and 4) Actuator. The ICM is a direct operated motorised valve driven by actuator type ICAD. ICM valves are designed to regulate the expansion process in liquid lines with or without phase change, or control the pressure or temperature in dry and wet suction lines and hot gas lines. The ICM motorised valve and ICAD actuator assembly offers a very compact unit with small dimensions. ICAD actuators can also operate the ICM valve as an On/Off from a digital input.

3.2.5.3 AKV expansion valve

In the refrigeration system, an electrically operated expansion valve was used for the DX evaporator as shown in Figure 3.12(c).

The electronic expansion valve has a wider range and flexibility for refrigerant flow control compared to the traditional thermostatic expansion valve (TXV). It also offers the possibility to integrate its control with the cabinet controller to make it easier to change the operational settings for system investigations.

The valve is pulse-width-modulated, which is an on/off solenoid valve with special features that allow it to operate as a variable metering device by rapidly pulsing the valve open and closed. The duration of each pulse is regulated by an electronic controller. Thus, the application of this valve requires a controller and control sensors which include a pressure transducer and a temperature sensor. The expansion valve was specified to have a maximum operating pressure difference (MOPD) across it of 18 bar and maximum operating pressure (MOP) of 52 bar.

3.2.6 Oil management system and components

Figure 3.13 illustrates a schematic diagram of the oil management system. The main components of the oil system comprise an oil separator, an oil reservoir, an oil strainer, an oil level regulator, a pressure relief valve and a controller driven by the integrated refrigeration control system. The oil management system ensures that most of the oil in the system returns back to the compressors for proper lubrication.

The oil separator is a *Temprite* model 133A with a capacity of 25 l, maximum design pressure 130 bar, maximum operational temperature 135°C and minimum 0°C. The oil separator removes some oil from the refrigerant and reduces the rate of oil circulation through the refrigeration system. The oil reservoir has a total volume of 8.2 l and is manufactured by Henry Technology Ltd, type: SH-9109-CE, M.W.P 42 bar, temperature range -110 to +110°C. It receives the returned oil from the oil separator and also provides a reserve supply of oil for the compressor. The oil reservoir also incorporates two sight glasses and two service valves. The sight glasses are used to ensure that there is enough oil in the reservoir, while the service valves are used for charging/draining the oil to/from the reservoir. The oil supply to the compressor is

regulated by the oil level regulator. The regulator comprises an oil level sensor and a solenoid valve. The solenoid valve allows the lubricating oil to flow to the compressor from the oil reservoir when the oil level reaches its lower limit and stops the oil supply when the oil level reaches the upper limit. The oil level regulator is also equipped with a relay which is integrated with the compressor controller. The relay switch stops the compressor when the oil level drops below the lower limit.

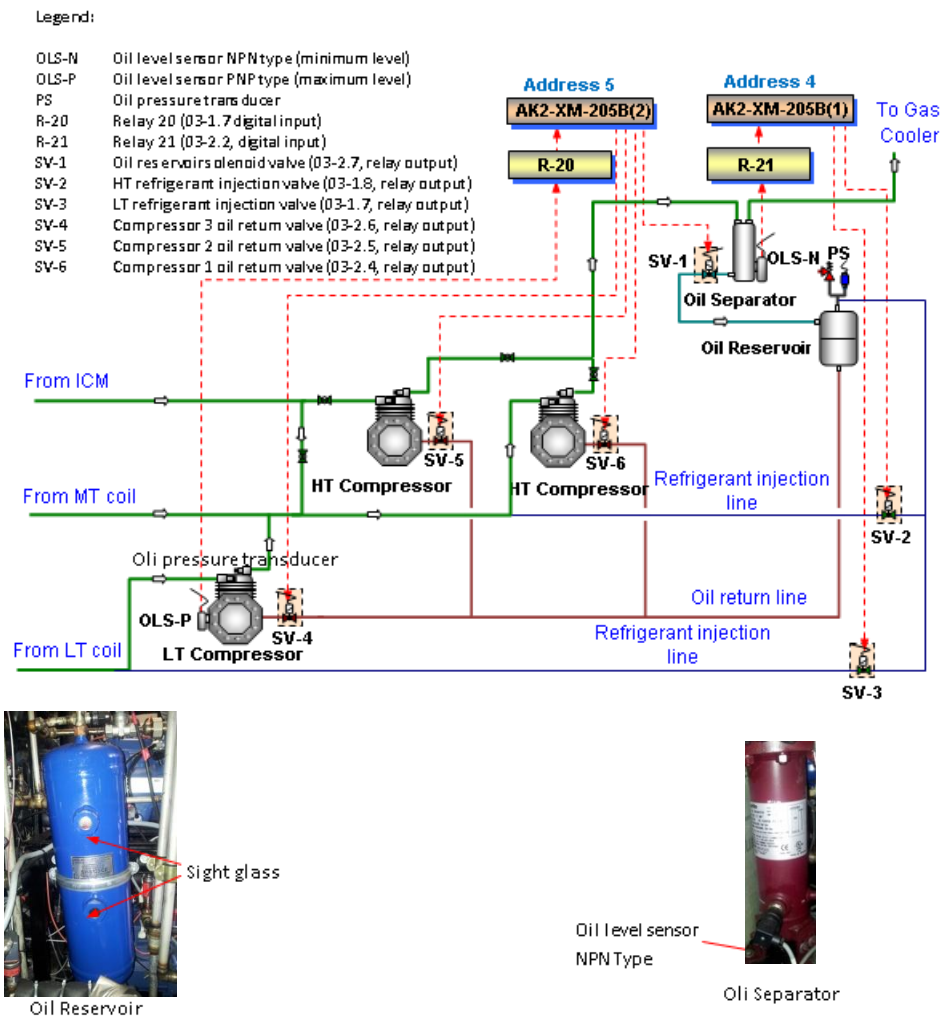


Figure 3.13 Schematic diagram of the oil management system and some of its main components

3.2.7 Gas cooler test rig

The gas cooler test rig is a specially designed test rig with the following mechanical components: a finned tube heat exchanger, an electric air heater, two main fans, and four recirculation fans (see Figure 3.14). The test rig was designed to enable simulation of different air conditions for the gas cooler heat exchanger. The gas coolers were produced by GEA-Searle. Four different designs were tested: 1) three rows with horizontal slit fins, 2) two rows with horizontal slit fins, 3) three rows with horizontal-vertical slit fins and 4) two rows with horizontal slit fins -0.8m coil length.

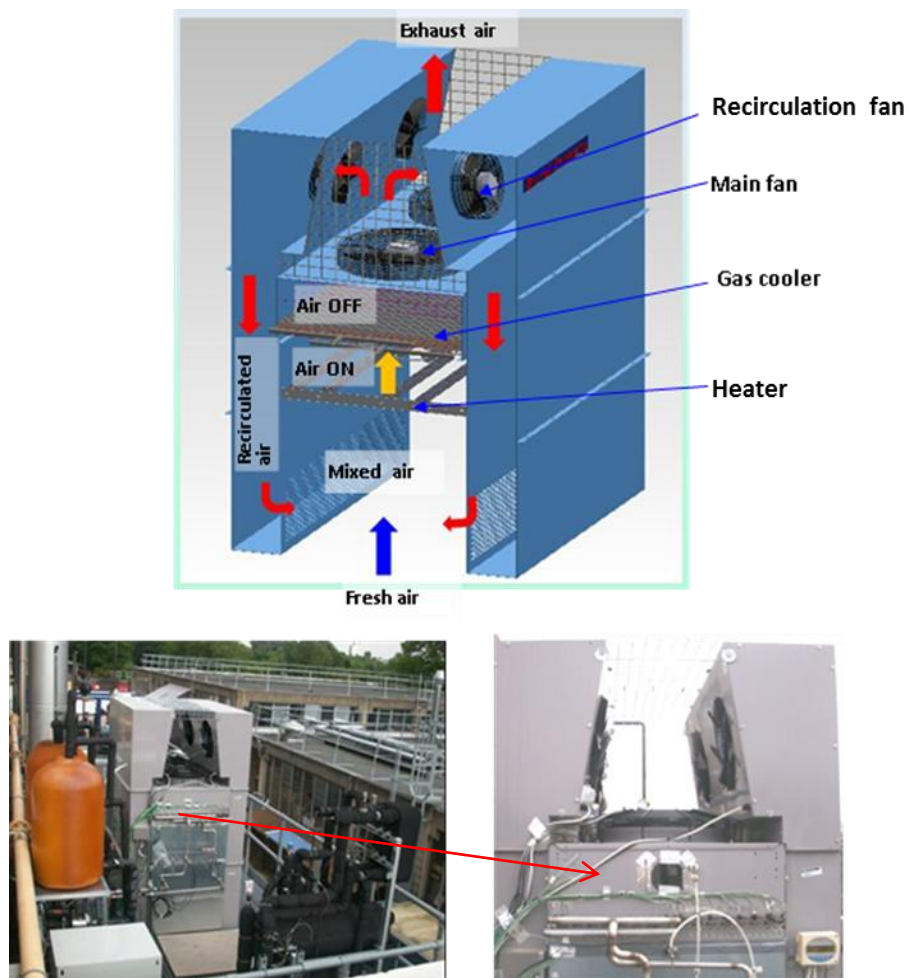


Figure 3.14 Construction of gas cooler test rig
(source: CSEF - Brunel University Laboratory)

3.2.7.1 Gas cooler heat exchanger

Figure 3.15 provides about the finned tube gas cooler/condenser coils used for the tests and the details of the gas coolers are explained in the next Section 4.2.1 and Section 4.2.2. Refer to Table 4.1 and Table 4.2 for the dimensions and specifications of the gas coolers.

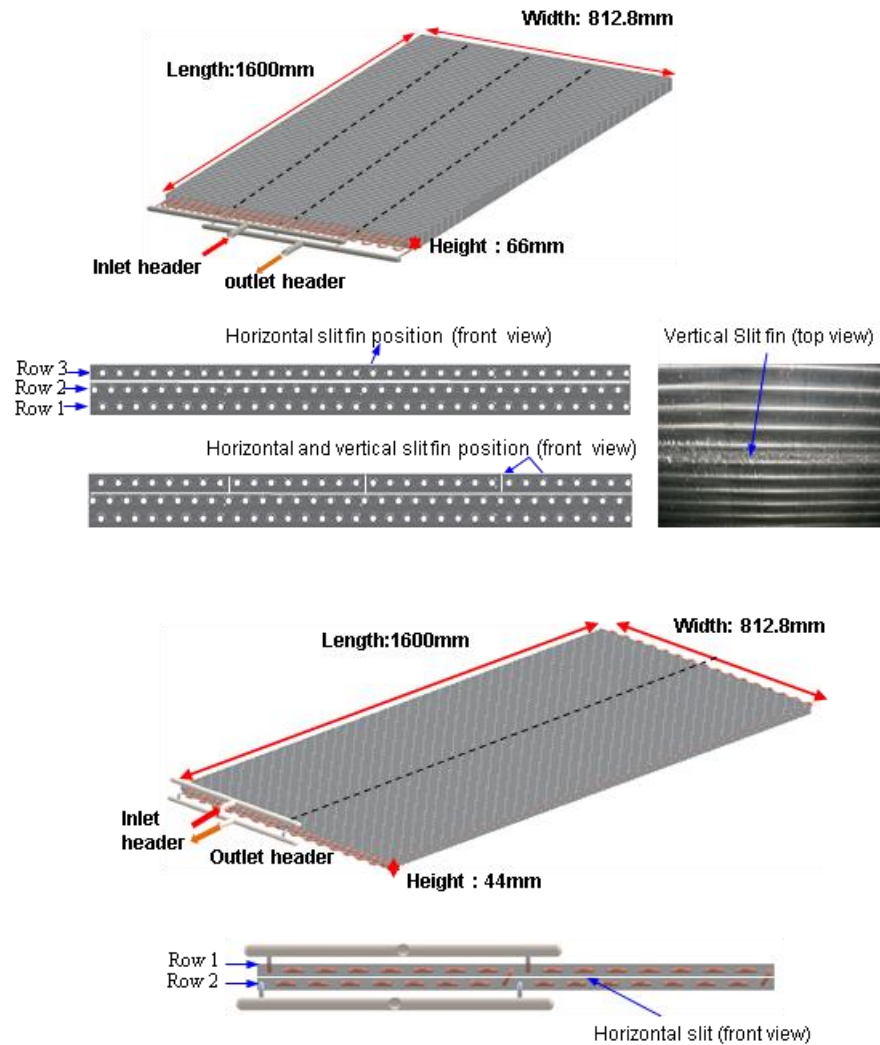


Figure 3.15 Finned tube gas cooler

3.2.7.2 Electrical air heaters

Air heaters are used to control the temperature of the air entering the gas cooler coil alongside recirculation of air from coil discharge to coil inlet. Four heaters of 3kw capacity each were used, giving a total capacity of 12 kW. Figure 3.16 shows the location of the air heater on the test rig.



(a) View from top rear



(b) View from bottom rear

Figure 3.16 Electrical heater location

3.2.7.3 Main fans and recirculation fans

The gas cooler test rig employs two main fans and four recirculation fans. The main fans are type S3G500-AE33-11, manufactured by ebm-papst Mulfingen GmbH & Co. KG with 690W power input, and a nominal fan speed of 1250 min^{-1} . The fan speed can be controlled from 0 % to 100% of full speed with an inverter.



Figure 3.17 Gas cooler main fan

The recirculation fans are used to circulate the ‘hot air’ from air off of the heat exchanger to the air-on, mixing with the fresh air this reduces the power input to the heater and overall power consumption.

3.2.8 Auxiliary components

Some auxiliary components are shown in Figure 3.18. These components include an accumulator, sight glass, filter drier and pressure gauges. The accumulator protects the compressor from damage by preventing liquid droplets from entering the compressor. The system is also equipped with two sight glasses. One was installed on the liquid line

of the LT DX circuit to monitor the presence of flash gas upstream of the expansion valve and another on the MT DX circuit.

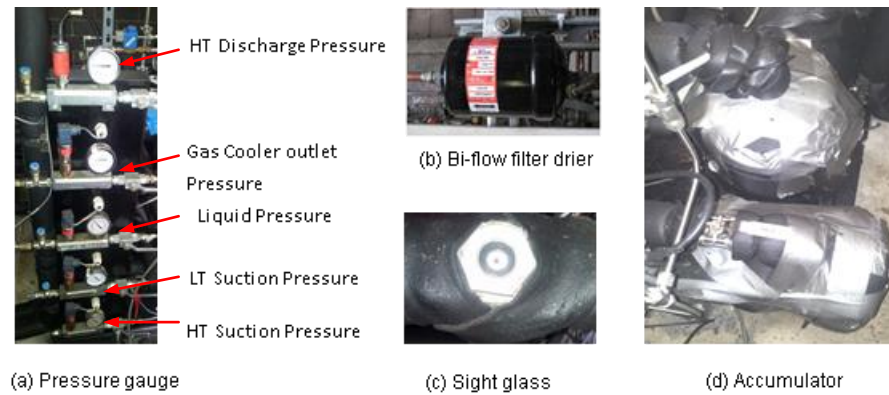


Figure 3.18 The auxiliary components

A filter drier is installed on the liquid line upstream of the expansion valve to prevent any debris within the system from reaching the expansion valve. In order to monitor the pressure fluctuations during charging and operation, the test system was also equipped with five pressure gauges. The gauges were installed on the HT discharge, gas cooler outlet, liquid receiver and HT and LT suction as shown in Figure 3.18. The gauges are Omega Engineering products (PG63-70S) compatible with CO₂ refrigerant. They have a measurement range from 0 to 160 Bar. The gauges are very useful particularly when charging the CO₂ system with refrigerant.

3.3 Control systems

The control system consists of four parts. The first part of a control system is an integrated controller to automatically regulate the operation of the HT and LT compressor, based on signal inputs from the MT and LT suction pressure, high and low pressure switch and oil level regulator. The stand still condensing unit energises the standstill condensing unit based on the pressure of the liquid receiver during standby conditions. The ICMT valve is automatically regulated based on the temperature and pressure signal from the gas cooler outlet, and ICM valve operation gets signal input from receiver pressure.

Secondly, the gas cooler test rig controller, which automatically regulates an electrical air heater and recirculation fan. However, the main fan speed can be controlled manually according to the test condition and procedures. Thirdly, the MT control

system which regulates the MT cabinet, MT air cooler and MT additional load. Finally, the LT control system, which regulates an LT additional load and LT cabinet depending on the pressure and superheat temperature signal, and temperature sensor from the evaporator for defrost control. The control action for both MT and LT system is to regulate AKV opening.

The control system consists of an electrical control system and electronic control system. The main function of the electrical control system is to connect and to disconnect power supply to the electrical components as well as the electronic control system. The electrical control panel is shown in Figure 3.20

Figure 3.19 shows the electronic controllers used, which consist of a main controller with its communication modules and several device controllers. The electronic control system employed is a commercially available electronic control system manufactured by Danfoss. The main controller of CO₂ refrigeration system (AK-SC-255) is connected to the communication module which is divided into two types, which are the Universal Analog Input Module (AK2-CM-101A) and the Digital Output & Combination Digital Output Universal Analog Input Module (AK2-XM-205B). Each communications module in the system has an address from 1 to 8. Several electronic controllers are used which consist of an ICMT valve controller (EKC-362A), ICM valve controller (EKC-347), MT cabinet controller with MT and LT Additional load as well as air cooler use AK-CC-550, water-glycol temperature controller (EKC-101) and air on temperature controller (EKC-101).



Figure 3.19 Electronic control components

The electrical and electronic control system was installed in an electrical control panel which was placed in the plant room. A front view of the control panel showing controller displays, switches and indicator light and also illustrates the VLT (inverter) of the compressors as well as the arrangement of the components inside the panel is shown in Figure 3.20.

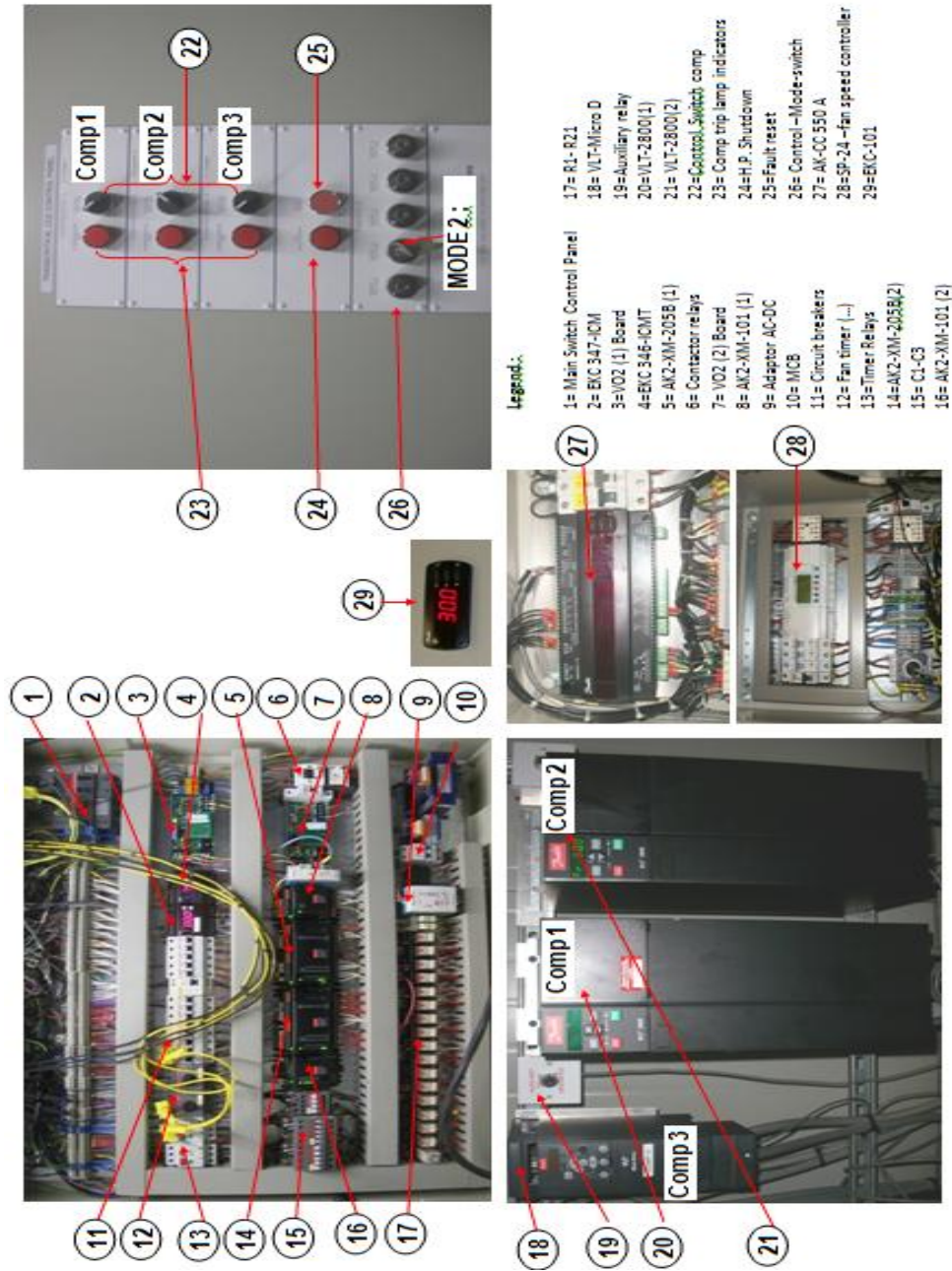


Figure 3.20 Electrical control panel of CO₂ refrigeration system

3.3.1 CO₂ refrigeration booster hot gas bypass system control strategies

The CO₂ refrigeration booster system control strategy is to satisfy the gas cooler experimental objectives. However, the original control strategy of the hot gas booster by pass mode is used to get optimum operation. According to gas cooler test procedure the system was only operated at medium temperature (MT) or single stage system which was the system only generated by both of the HT compressors. The block diagram of operational control strategy which was applied to the test rig is shown in Figure 3.21.

The ICMT valve is regulated by a EKC 326 controller, which provides a signal from both outlet gas cooler pressure and temperature sensors. Both are fitted in the outlet immediately after the gas cooler. EKC 326 will regulate a maximum COP control throughout by maintaining optimum pressure in the supercritical range. When sub-critical range conditions are present, the degree of sub-cooling will be based on pressure difference (dP) or temperature difference (dT) will be used in controller base. The controller modulates the valve opening which was set at maximum opened at 100% and minimum 0%. The percentage of the ICMT valve opening is also one of the test variables to see the effect of the ICMT opened to the gas cooler operation. The original setting was set at maximum 30% and minimum 0%. The sub-cooling degree of the experimental test was set between 0.3-2K, whereas the original operation was set at 2K.

The ICM valve is controlled by an EKC 347 controller which provides signals from receiver (vessel) pressure. The controller modulates the valve opening which was set at maximum opening 40% in order to maintain the target pressure in receiver of 32 bar and then decrease expanded hot gas pressure to meet the MT pressure at 27 bar.

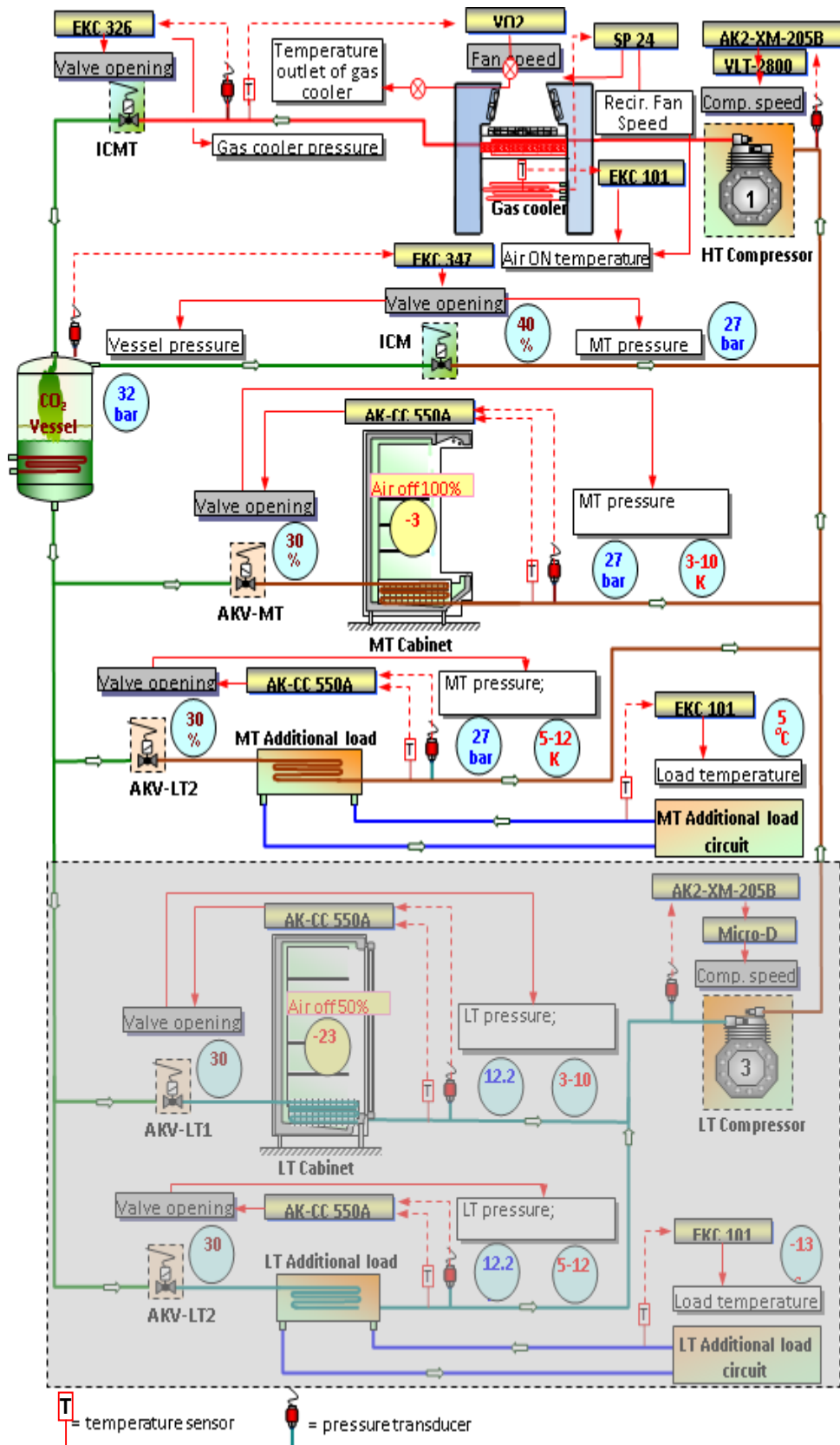


Figure 3.21 Control strategy of the CO₂ booster system

MT Compressor operation is controlled by the main controller and AX2-XM-205 module control, which is regulated based on the suction pressure and temperature. In addition, the on-off compressor according to suction and discharge pressure (between 115 bar-10 bar) and 40 bar discharge pressure for the MT compressor and the LT compressor, respectively. The controller modulates the compressor speed. For test operation, the compressors speed can be set at fix speed as well as variable speed at the main controller (AK-SC-255), with minimum and maximum percentages speed for safety are 65% and 100% respectively. The suction pressure was set between 25.4 bar up to 29 bar to get the evaporating temperature -7°C to -5°C .

The main fan speed of the gas cooler for this experimental rig can be set constantly at between 0-100% of full speed, and the recirculation fan speed control according to air-on temperature which was set at 60% maximum speed. But, for the original integrated controller control system, the main fan speed regulates by the controller according to temperature outlet of gas cooler.

The MT control strategy involves the control of the MT cabinet and MT evaporator and MT air cooler for additional loads involving controller AK-CC 550 and EKC 101. The controllers modulate the opening of the respective expansion valves to maintain a degree of superheat in the range 5K to 12K. At full load conditions, the valve opening was set at 30% of maximum represented by the pulsing frequency of the valve solenoid.

3.3.2 Gas cooler control strategies

Figure 3.22 shows the control system of the gas cooler test rig in isometric view. To achieve the experimental objectives, the gas cooler test rig has a stand-alone independent control system. Two controllers have been used which are Millenium-SP 24 and EKC 101 controller. The control system has two main duties which are to get a reasonable air-on temperature and main fan speed. Air-on temperatures were varied by regulating the air recirculation rate (Millenium-SP24 controller) and modulating the air-on heaters (EKC 101 controller). The main fan speed was set manually on the Millenium-SP24 controller. Air-on temperature range covered both sub-critical and trans-critical range of around 18°C – 36°C .

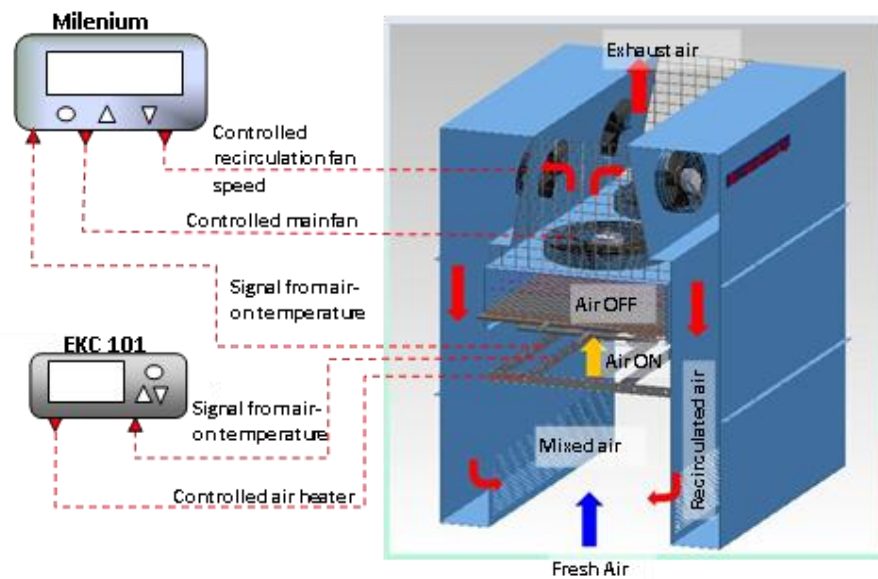


Figure 3.22 Gas cooler test rig control system

Figure 3.23 illustrates the control strategy of the gas cooler test rig. To regulate air-on temperature softly and also to make the heater safe during operation the difference between air heater and recirculation fan set points is 1°C. For instance, setting air – ON 24°C temperature set for recirculation fan and air heater is 25°C and 24°C, respectively and recirculation fan speed set at 0 - 60% of full speed.

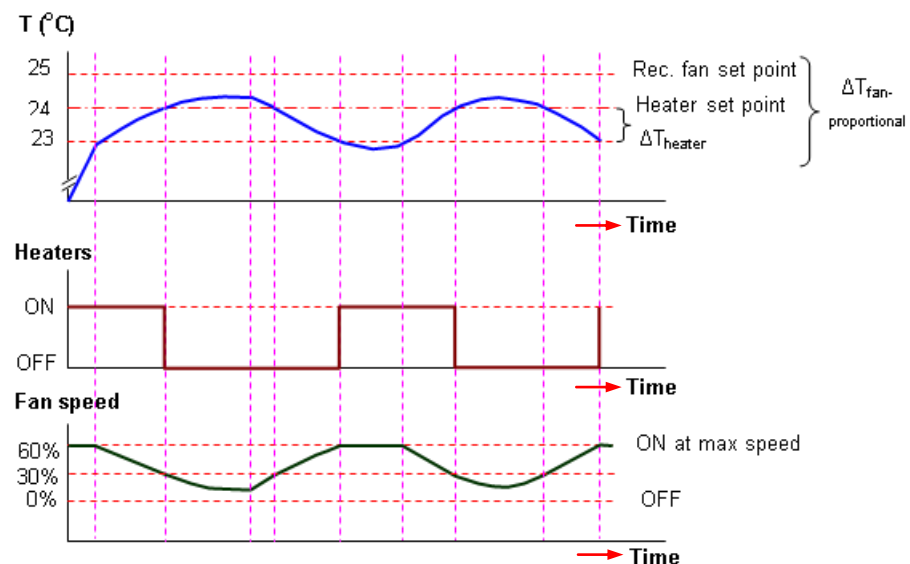


Figure 3.23 Control strategy for the air-on temperature

3.4 Instrumentation and data logging system

The instrumentation is used for both control and performance monitoring. For control, the instrumentation is mainly used to provide signal inputs to the controllers. For monitoring, the instrumentation is used to establish the state and flow conditions of the CO₂ refrigerant such as pressure, temperature and flow rate at different points in the system. The instrumentation is also used to monitor the liquid level in the liquid receiver, temperature and relative humidity of the loading system and test chamber as well as power consumption of the test rig, pressure and temperature of gas cooler. To enable the information to be read and recorded for system analyses and evaluation, the instrumentation is connected to a data logging system.

3.4.1 Instrumentation devices

Generally, this section describes instrumentation devices for the CO₂ refrigeration booster system and details of measurement instrumentation for the gas cooler test rig. The devices comprise temperature and pressure measurement, flow meter, velocity meter, air pressure transmitter and Infrared (IR) Thermography.

3.4.1.1 Temperature and pressure measurement

Temperature measurements used T-type thermocouples and K-type thermocouples for the refrigeration system and gas cooler test rig, respectively. In this study is only described the K-type thermocouple with are used for the gas cooler test rig only. The K-type thermocouples have temperature measurement range -250°C to 350°C with specific error (specified by manufacturer) of $\pm 0.5^\circ\text{C}$. The thermocouples were calibrated using a calibration bath and precision thermometer (ASL type F250 MK II, probe J 100-250-10-NA) of uncertainty $\pm 0.04^\circ\text{C}$. The temperature range of calibration was -30°C to 100°C . It was found that all thermocouples had calibration error within the specifications. Positions of the temperature measurements on the test rig as well as the explanation of each measurement point and the calibration equations of the thermocouples including their calibration errors are given the Appendix B.

Ten pressure transducers were installed on the refrigeration test rig and six transducers on the gas cooler test rig. Pressure transducers on the refrigeration test rig are used for measurement but are also used for the control system. For the gas cooler test rig, the pressure transducers are only for measurement purposes. In this study is described the

six transducers for gas cooler only, since the focus of investigation is in the gas cooler pressure.

The gas cooler pressure transducers have similar type of MBS33 with a measurement range: 0-160 bar (Danfoss products). All of the points should have the ability to measure high pressure conditions in inlet and outlet of header, and inlet and outlet coil in circuit 1 and circuit 2. The pressure transducers have input voltage of 24V d.c. and output current 4mA to 20mA. The output cables of the transducer have to be circuited with 500 Ω resistor to change the output current to become an output voltage since the data logging system requires a voltage input. Each pressure transducer was calibrated using a deadweight pressure gauge calibrator. The voltage outputs were recorded for a series of known pressures. The graphs of the voltage against the pressure were drawn and the best-fit linear equations were derived and used in the data logging system to enable an automatic recording of the measured pressures. The coefficient of correlations of the pressure transducers were above 99.9% with manufacturer uncertainty of $\pm 0.3\%$. The graphs and calibration equations of the transducers can be found in Appendix B.

3.4.1.2 Flow meter

In the refrigeration system a coriolis type flow meter was used for the CO₂ refrigerant, which was fitted on to an upstream MT display cabinet and air cooler. The Optimass-3000-S03 (Figure 3.24) is used, which has a flow rate capacity up to 120kg/h or 0.036kg/s. The flow meter was manufactured by Krohne-Germany and has a measurement uncertainty of $\pm 0.035\%$. The flow meters, however, are also subject to inaccuracies arising from the presence of gas bubbles in the liquid line. To minimise the risk of this occurring, the liquid line was insulated with 25mm of insulation (Armaflex class 0).



Figure 3.24 Flow meter Optimass-3000-S03

Each flow meter provides a current output 4-20mA which is converted into a voltage input in the data logging system. In order to convert the voltage to a flow rate, a calibration was carried out in the laboratory. Best-fit linear equations from the calibration were used in the logging programme to enable automatic recording of flow rate. The calibration graph and equation is provided in Appendix B.

3.4.1.3 Air pressure difference transmitter

The pressure difference is shown in Figure 3.25. The air pressure transmitter used was the KIMO CP 200, unit measurement Pa, accuracy $\pm 1\%$ of reading $\pm 2\text{Pa}$, with overpressure tolerated 1000 Pa.

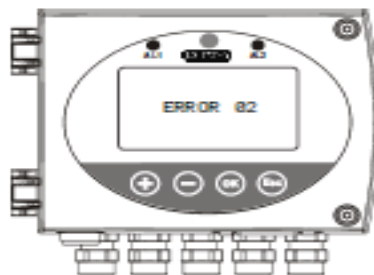


Figure 3.25 Air pressure difference transmitter
(www.kimo.co.uk)

The pressure transmitter using pitot tube placed at air-on and air-off position, output range 4-20mA. The calibration graph and equation is provided in Appendix B.

3.4.1.4 Velocity meter

The velocity meter was used to map the velocity profile of the air flow in air face of the heat exchanger coil which is related to main fan speed (0-100% of full speed). The air

face velocity data is one of the most important performance parameters of the gas cooler. Based on the velocity data a correlation was made between fan speed and air face velocity. Based on air velocity, the air mass flow rate was calculated, which was used to verify the gas cooler capacity from air-side calculation. The velocity meter is Velocicalc Plus 8386A-M-GB, a TSI product, with measurement range 0m/s to 50m/s and uncertainty $\pm 3\%$. The meter can also simultaneously measure the temperature and relative humidity (RH) of the air with measurement range -10°C to 60°C and 0% to 90% RH respectively.

3.4.1.5 Infrared (IR) thermography

The infrared (IR) thermography type Thermal CAMTM S60 infrared camera from FLIR was used as shown in Figure 3.26. The camera was used to investigate the gas cooler temperature contour from top view. This is important in ensuring the temperature difference among the pipes and heat conducted to the fin surface.

The IR thermal imaging camera can provide a proportional temperature contour in fin surface as additional visual data. However, the tube and fin surface temperatures are measured by thermocouples.



Figure 3.26 Infrared (IR) thermal imaging camera

3.4.2 Data logging system for gas cooler test rig

To enable the information to be read and recorded for system analyses and evaluation, the instrumentation was connected to a data logging system (Labtech software and Datascan modules). The output signals from the instrumentation devices are logged by a data logging system which comprises data acquisition modules and a recording and display system. The data acquisition modules utilise the Datascan 7000 series from MSL (Measurement System Ltd.), which include a Datascan measurement processor

7320 and expansion modules 7020. Each Datascan module contains 16 differential input channels, individually configurable for voltage and thermocouple measurements. To cover all the instrumentation devices used, 1 processor and 7 expansion modules were prepared as shown in Figure 3.27(a). The configuration of each module and the channels are detailed in the Appendix B.



(a) Data scan module of gas cooler test rig



(b) Computer display of data logging

Figure 3.27 Measurement instrumentation and Data logging system

The recording and display system is a standard desk top computer. Communication between the Datascan modules and the computer is performed through an RS232 cable. The computer incorporates Labtech software which is fully compatible with the Datascan modules. The software also has the capability to manipulate a complex measurement system into an attractive display so that it can be monitored more easily. The CO₂ refrigeration test rig was recorded and monitored separately using a second computer set. Both computer sets are shown in Figure 3.27(b). A monitoring display set up in the Labtech software is given in Appendix B.

3.5 Summary

A specific design of gas cooler/condenser test rig was built and employed in CO₂ refrigeration system with booster hot gas bypass which are installed in Brunel University. The CO₂ refrigeration system operated in Medium Temperature (MT) system (evaporating temperature -7°C). Refrigeration load of the CO₂ refrigeration system was modified to satisfy the gas cooler investigation, with install a MT display cabinet, an additional load and an air cooler. The gas cooler/condenser test rig enable to

simulate an ambient air temperature range from sub-critical to supercritical mode operation and a range of air face velocities.

The construction of the test facilities have been described in detail, including mechanical, electrical, control, instrumentation and data logging systems. This chapter has also given a brief description of the control strategies of the system in order to get satisfied test condition.

Chapter 4 will present the test results of the gas cooler test rig and some of the refrigeration system test results related to the gas cooler test conditions and procedures. The next chapter also describe about test programme, and discussions of the results.

The refrigeration load comprised of a display cabinet and other additional loads with a total maximum refrigeration load of around 14.5 kW, driven by two parallel compressors with maximum capacity of approximately 10 kW each.

4.2 Gas cooler design and specification

Tests were performed with four designs of gas cooler comprising of gas cooler A (3-rows with horizontal slit fins), gas cooler A-with vertical slits (3-rows with horizontal and vertical slit fins), gas cooler B-1.6m (2-rows with horizontal fins with 1.6m length coils) and gas cooler B-0.8m (2-rows with horizontal slit fins with 0.8m length coils). The specification of the gas coolers are further explained in the following sub-sections.

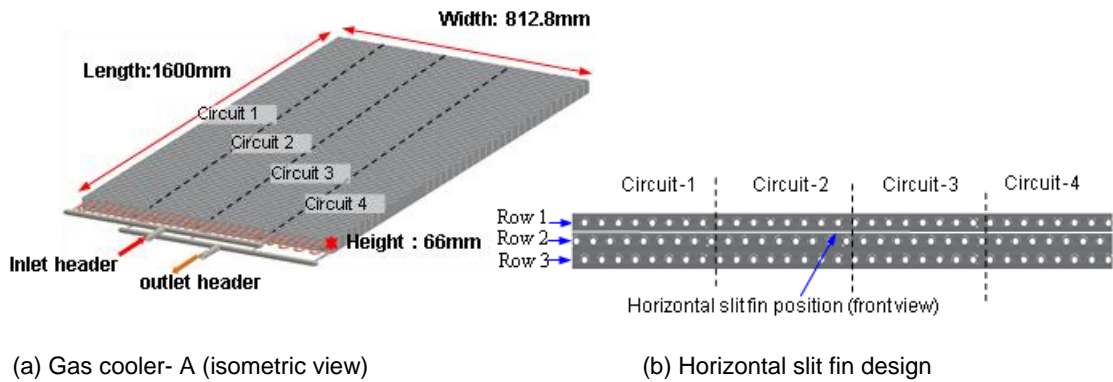
4.2.1 Gas coolers A and A-with vertical slits (3-row 4-circuit)

The gas cooler-A (3-row 4-circuit) investigation considered two fin designs: horizontal slit fins; and a horizontal and vertical slit fin design, as shown in Figures 4.2. In addition, detailed specification of the gas cooler tests is given in Table 4.1.

Table 4.1 Specification of finned and tube gas cooler -A

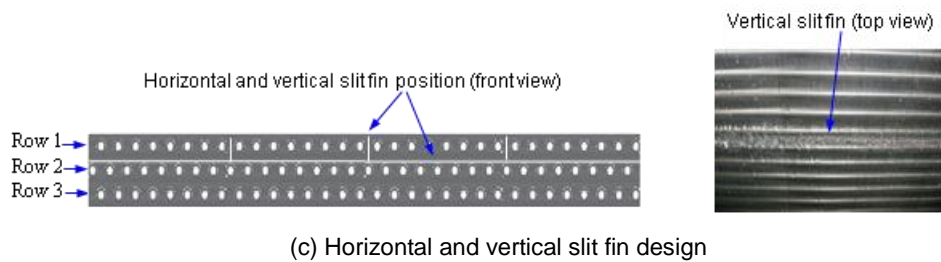
Gas cooler A gas cooler specification			
Number of circuits	4	Tube thickness	0.84mm
Tube configuration	Staggered (Equilateral)	Tube vertical spacing	22.00mm
Number of tubes per row	32	Tube horizontal spacing	25.40mm
Number of rows deep	3 rows	Fin thickness	0.16mm
Tube length	1600mm	Fin gap	2.12mm
Tube OD	8mm	Tube material	Copper
Total number tube	96	Fin material	Aluminium

Horizontal slits cut mid-way along the first and second rows of the tubes, and the vertical slit position on 1st row of tubes before the 1st tube (hottest tube of tube circuit) and cut mid-way between the tubes. The aim of this vertical slit is to reduce heat conduction effects of the first-hottest tube to the cold tube in the previous circuit. The vertical slit is cut only up to the horizontal slit, in the top part of the gas cooler, as shown in Figure 4.2 (c).



(a) Gas cooler- A (isometric view)

(b) Horizontal slit fin design



(c) Horizontal and vertical slit fin design

Figure 4.2 Gas cooler A (3-row-4-circuit) designs

4.2.2 Gas cooler B (2-row 2-circuit)

The specifications of gas cooler-B are described in Table 4.2 and Figure 4.3. Slit fin configuration consists of horizontal slits mid-way between the 1st and 2nd rows of tubes as shown in Figure 4.3 (c). The Gas cooler B includes two different sizes of the gas cooler, which are 1.6m coil length (Gas cooler B-1.6m) as shown in Figure 4.3(a) and 0.8m coil length (Gas cooler B-0.8m), as shown in Figure 4.3 (b).

Table 4.2 Specification of finned and tube gas cooler -B

Gas cooler B specification			
Number of circuits	2	Tube thickness	0.84mm
Tube configuration	Staggered (Equilateral)	Tube vertical spacing	22.00mm
Number of tubes per row	32	Tube horizontal spacing	25.40mm
Number of rows deep	2 rows	Fins gap	2.12mm
Tube length	1600mm & 800mm	Fin thickness	0.16mm
Tube OD	8mm	Tube material	Copper
Total number tube	64	Fin material	Aluminium

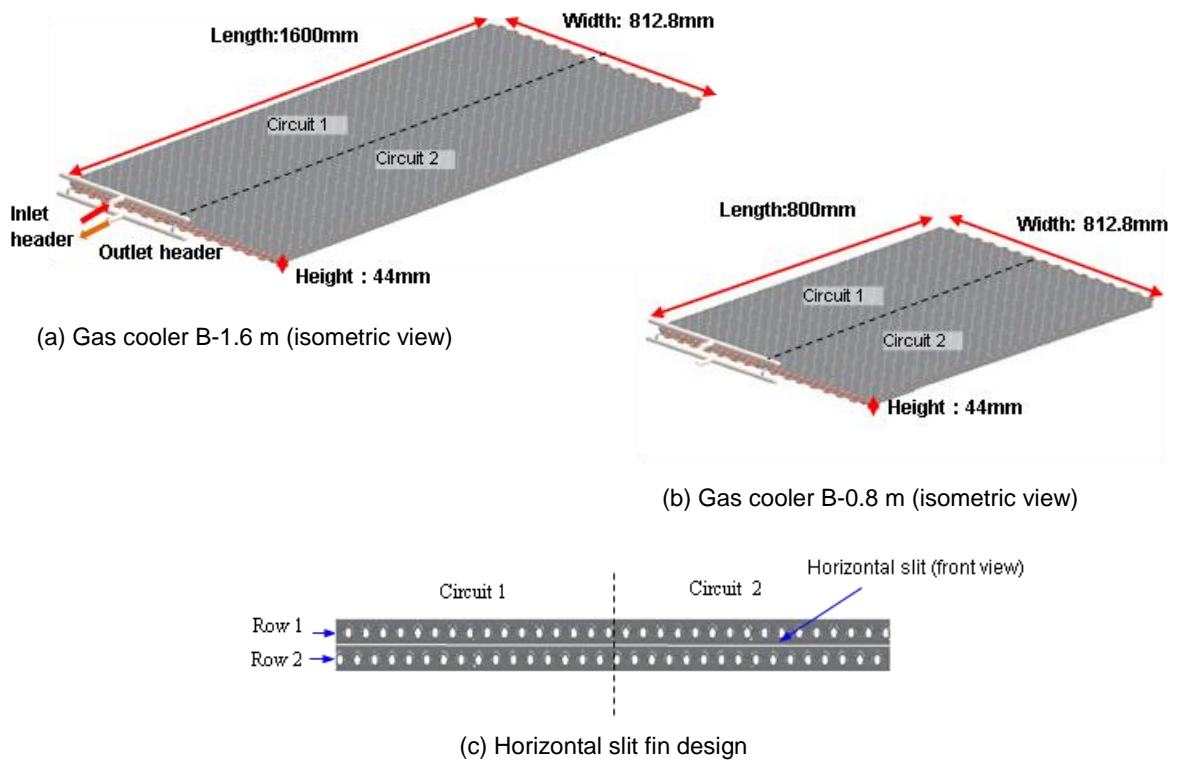


Figure 4.3 Gas cooler B (2-row 2-circuit) designs

4.3 Instrumentation design of gas cooler test rig

The parameters measured during the tests included pressure, temperature and mass flow rate on the R-744-side, and velocity, pressure dropped and temperature on the air-side. The gas cooler measurement design described in this section is used to satisfy the gas cooler test objectives.

The measurement positions on the gas cooler test rig are shown in more detail in Figure 4.4. The air temperature entering the gas cooler/condenser was measured at 24 points along the face of the coil and at 12 points after the coil. In addition, 8 temperature points for the re-circulation air and 4 temperature points for the exhausted air were also measured. The air pressure drop across the coil was measured with a differential pressure transducer. The air velocity, from which the air flow rate was deduced, was measured with a hot wire anemometer. On the refrigerant side, measurements included pressures at different points in the cycle including pressures at the inlet and outlet header of the gas cooler, as well as the inlet and outlet of each section of the coil. On the tube side, temperatures were measured at every bend. The K-Type thermocouples used

had a maximum uncertainty of $\pm 0.5^{\circ}\text{C}$, the pressure transducers had uncertainty of $\pm 0.3\%$, and the air velocity meter had uncertainty of $\pm 3\%$. To enable the information to be read and recorded for system analyses and evaluation, the instrumentation was connected to a data logging system.

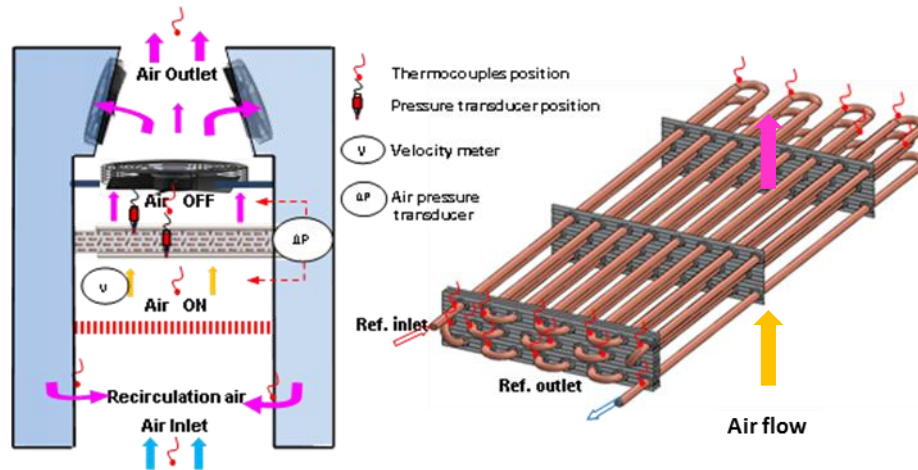


Figure 4.4 Schematic of measurement points on gas cooler test rig

Figure 4.5 shows a photograph of the gas cooler test rig showing where pressure transducers were set up on the inlet and outlet coils, as well as inlet and outlet headers. Some thermocouples and a pressure difference transmitter were positioned to measure the air-side pressure drop. There was also a sight glass to enable the thermal IR imaging camera access.

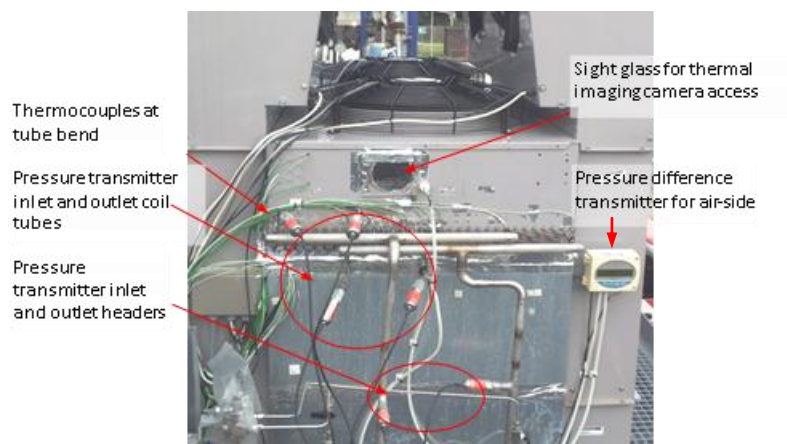


Figure 4.5 Photograph of measurement points on gas cooler test rig

The temperature of the gas cooler fin was also investigated in the experimental test. Figure 4.6 shows the fin surface temperature measurement used K-Type thermocouple. Thermocouples were fastened on to the fin surface at two positions of the fin: at fin tip (T_t) and at fin collar (T_c). There were six thermocouples (Point A- Point F) to measure the fin surface temperature, including four thermocouples for fin tip measurement and two thermocouples for fin collar measurement. Distances from inlet have been measured which are: Point A (70mm), Point B (140mm), Point C (690mm), Point D (710mm), Point E (880mm), and Point F (1530mm) for fin tips and fin collar measurements, respectively. The thermocouples were positioned above the first tube of the circuit-2, and positioned around 2mm from the top of the fins. The fin temperatures measurement positions are explained more in Section 5.12.2 (Fin temperature validation) in Figure 5.11.

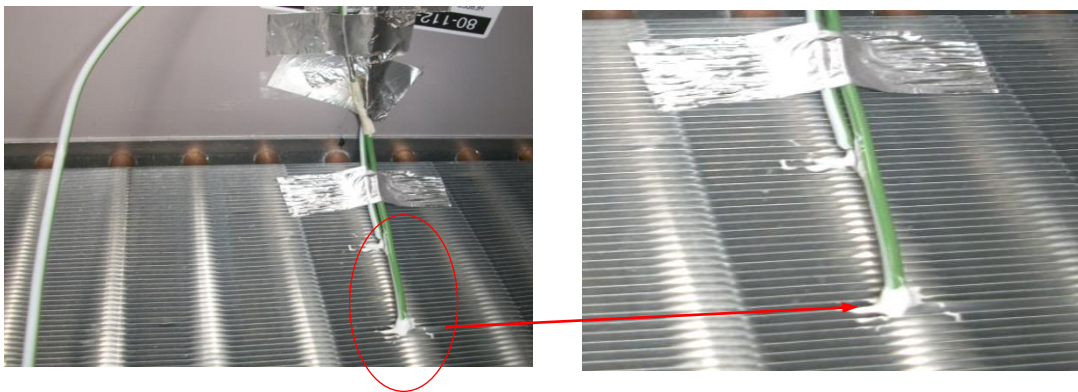


Figure 4.6 Fin surface temperature measurements

4.4 Gas cooler test condition and procedures

4.4.1 Test conditions

Tests were carried out at the refrigeration system set conditions according to the control strategy, which was defined in Chapter 3. The intermediate pressure/vessel pressure set at 32 bar. In order to ensure pressure safety in the vessel, the standstill condensing unit was set at 32.5 bar during running and 26 bar during standstill. The first evaporator load used an MT Display cabinet that was loaded using water and glycol containers to provide the adequate thermal mass. The display cabinet evaporating pressure was set at 27 bar and the superheating condition was 12K. The other loads, which were MT

additional load and an air cooler, were set at similar setting points to the display cabinet. The MT additional load used plate heat exchangers that were loaded by water-glycol circulation with an electrical heater generating the heat load. The environmental chamber was set at relative humidity 60% and temperature 25°C (standard class -3).

4.4.2 Experimental procedures

Test procedures were generally performed for a series of gas cooler types with varied air-on temperatures, percentages of full speed of compressor and cooling fan speed. Air-on temperatures were varied by regulating the air-on heaters and recirculation fan speed of the gas cooler test rig to cover operation both in the sub-critical and supercritical regions. The cooling fan and compressor speed (% of full speed) were regulated to simulate the air face coil flow rate and refrigerant mass flow rate or refrigeration capacity, respectively.

The first test group was performed with variable compressor speeds (65%-100%) and the second group was executed with fixed speed compressor(s). The fixed speed compressor(s) were varied at 80%, 100% and 130% of full speed. Each compressor speed group testing was done for a range the cooling fan fixed speed at 40%, 50%, 60%, and 70% of full speed, corresponding to air velocity, 1.3m/s, 1.7m/s, 2.0m/s and 2.4m/s, respectively. A range of condenser/gas cooler air-on temperatures is from 20°C to 36°C at 2°C steps, corresponding to the discharge pressure on the gas coolers to simulate sub-critical to supercritical mode of operation. The sub-cooling degree was controlled at 2K and 0.3K. The ICMT valve was set with a maximum 100% and minimum 0% open. More details of the operation of the system are given in Appendix C.

4.5 Data collection and processing

Data was collected simultaneously from a data logger and a gas cooler data logger, and was processed in Microsoft Excel®. The properties of the refrigerant and air were derived from the Engineering Equation Solver (EES) software.

4.5.1 Data collection

Measured performance parameters (temperature, pressure and flow rate) from the instrumentation devices were logged at intervals of 20 seconds. Detailed explanations of

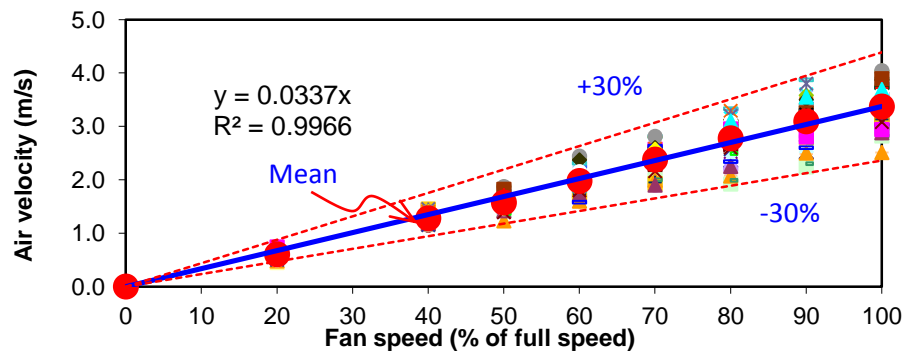
the instrumentation, data logging system and the measurement points can be found in Section 3.4, and some of the test results can be found in Appendix D.

4.5.2 Data processing

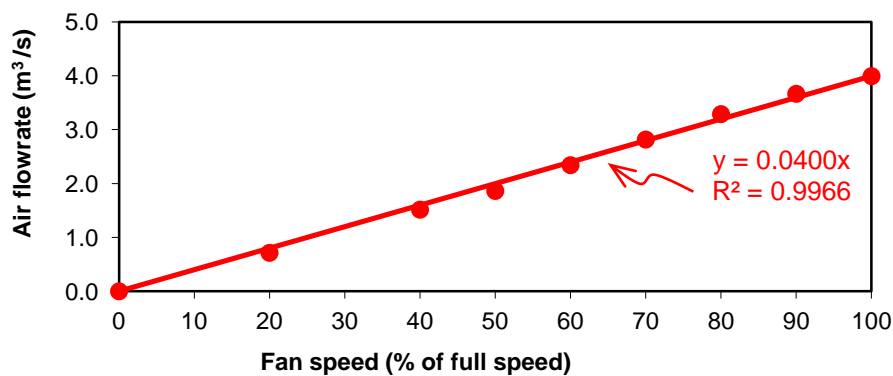
The performance parameters of the gas cooler were calculated and included the gas cooler/condenser heat transfer capacity (Q) and refrigerant mass flow rate (\dot{m}_{ref}). The calculations also involved the determination of the approach temperatures, air side and refrigerant side temperature differences and pressure drops.

Flow rate of air across the face of the gas cooler was calculated based on the percentage of full fan speed. The correlation between % of full fan speed with air velocity (v) and air volume flow rate (\dot{v}_{air}) was obtained from a test which was carried out using hot wire TSI Velocity Meter measurement (TSI-Velocalc Plus 8386A-M-GB).

Figure 4.7(a) describes the correlation of the fan speed and the air velocity (m/s). Figure 4.7 (b) illustrates the air flow rate (m^3/s) correlation with the % of fan full speed.



(a) Correlation of % of fan full speed with velocity (m/s)



(b) Correlation of % of fan full speed with volume flow rate (m^3/s)

Figure 4.7 Correlation between velocity and volume flow rate with % of full fan speed

Hence, air flow rate can be calculated by using:

$$\dot{v}_{air} = 0.04 \times \% \text{ of full fan speed} \quad (4.1)$$

With the correlation coefficient of $R^2 = 0.9966$

So that the air face mass flow rate (kg/s) can be calculated by:

$$\dot{m}_{air} = \dot{v}_{air} \cdot \rho_{air} \quad (4.2)$$

Where, air density (kg/m^3) is as function of temperature, defined from the EES program with correlation as follows:

$$\rho = 360.78.(T+273)^{-1.0034} \text{ with } T=0-150^\circ\text{C}, R^2=0.9987 \quad (4.3)$$

Where, $T=(T_{air\ off} + T_{air\ on})/2$

Heat rejection in the gas cooler / condenser (Q) in kW calculated based on the air-side parameters, as shown below:

$$Q = \dot{m}_{air} \cdot C_p \cdot (T_{air-off} - T_{air-on}) \quad (4.4)$$

Heat rejection was calculated from the refrigerant side on the gas cooler as:

$$Q = \dot{m}_{ref.} (h_{refin} - h_{refout}) \quad (4.5)$$

Refrigerant mass flow rate was calculated according to the energy balance in the gas cooler. Energy balance of the refrigeration system has shown that the refrigerant flow could be calculated indirectly from the energy balance between refrigerant and air-heat transfer across the gas cooler. This method was used to calculate the refrigerant flow rate in the gas cooler/condenser, assuming adiabatic heat transfer.

Energy balance in the gas cooler:

$$\dot{m}_{air} \cdot C_p \cdot (T_{air-off} - T_{air-on}) = \dot{m}_{ref.} (h_{refin} - h_{refout}) \quad (4.6)$$

With *enthalpy* (h) of refrigerant and air specific heat capacity ($C_{p,air}$) of the test results derived by EES program, where C_p is a function of temperature was found to be:

$$C_p = 1.9327 \times 10^{-10} \cdot (T+273)^4 - 7.9999 \times 10^{-7} \cdot (T+273)^3 + 1.1407 \times 10^{-3} \cdot (T+273)^2 - 0.4489 \cdot (T+273) + 1057.5 \quad (4.7)$$

With a regression coefficient $R^2 = 0.998$, with $T = (T_{air\ off} + T_{air\ on})/2$

The approach temperature for a heat exchanger is defined as the minimum temperature difference between the two fluids (for an air-cooled gas cooler, the approach temperature is assumed to be the temperature difference between refrigerant outlet and incoming air inlet as described by Ge and Tassou, (2009).

$$\text{Approach temperature (AT)} = T_{ref\ out} - T_{air-on} \quad (4.8)$$

The switch point between the sub-critical and supercritical behaviour was defined according to the critical pressure of R744, $P_{crit-a} = 73.77\ bar_a$ or $P_{crit-g} \approx 72.77\ bar_g$

Finally, Sub-cooling degree during condenser mode was calculated by:

$$T_{sat} - T_{ref\ out} \quad (4.9)$$

With T_{sat} derived from EES at the outlet pressure of the gas cooler.

4.5.3 Uncertainty in calculation heat rejection in gas cooler (Q)

Considering the uncertainty of the measured variables, which include air velocity, air temperature, refrigerant (coil) temperatures and respective pressures, and assuming that the individual measurements are uncorrelated and random, the uncertainty in the calculation of heat rejection (Q) was determined using the EES software. The uncertainty in the calculations of the Q was found to be $\pm 6.4\%$. The uncertainties are slightly high because in this calculation the K-type thermocouples consider had specific errors in the range of $\pm 0.5\ ^\circ C$. A detailed explanation of the uncertainty analysis is given in Appendix E.

4.6 Test results of gas cooler and discussion

The performance parameters of the gas cooler were examined based on refrigerant side as well as air-side view point. The parameters comprised of heat rejection (Q) ; the discharge pressure trend line with air-on temperature; the air side and refrigerant side pressure drop; the temperature profile along the coil; the air-side and refrigerant-side

temperature difference (TD); and the approach temperature (AT). In addition, the thermodynamically cycle of the supercritical system was also investigated in relation to the gas cooler operational condition to ensure that the test conditions can be obtained based on control strategy. Some of the test results are provided in Appendix D.

4.6.1 Gas cooler heat rejection (Q) and refrigerant mass flow rate (\dot{m}_{ref}) in the system

Since the test conditions were carried out at two compressor speed conditions, with the options of a varied and fixed speed, the discussion of the test results are also made to account for the impact of the compressor speed on heat rejection and mass flow rate.

4.6.1.1 Heat rejection and mass flow rate in variable and fixed compressor speed operation

Refrigerant mass flow rate was regulated by the compressor speed as was explained in Chapter 3. This test condition also highlighted the variation of heat rejection and refrigerant mass flow rate with air-on temperature in the gas cooler as an effect of variable and fixed speed compressor. Figure 4.8 shows the variation of heat rejection and mass flow rate as the system operated with varied compressor speeds ranging from 65%-100% of full speed. This was performed with gas cooler B-1.6m, and in these setting conditions the up and down compressor speed in the range and also on and off, were regulated by load condition.

It can be seen that heat rejection in the gas cooler remains constant at an average 8.7kW, while mass flow rate slightly increases as the air-on increases at an average rate of 0.039kg/s. This implies that to keep the refrigeration load constant at higher air-on temperature, the compressor works at a higher speed, leading to an increase in the mass flow rate. Under realistic operating systems, this condition will keep the system running smoothly with constant load in both sub-critical and supercritical mode.

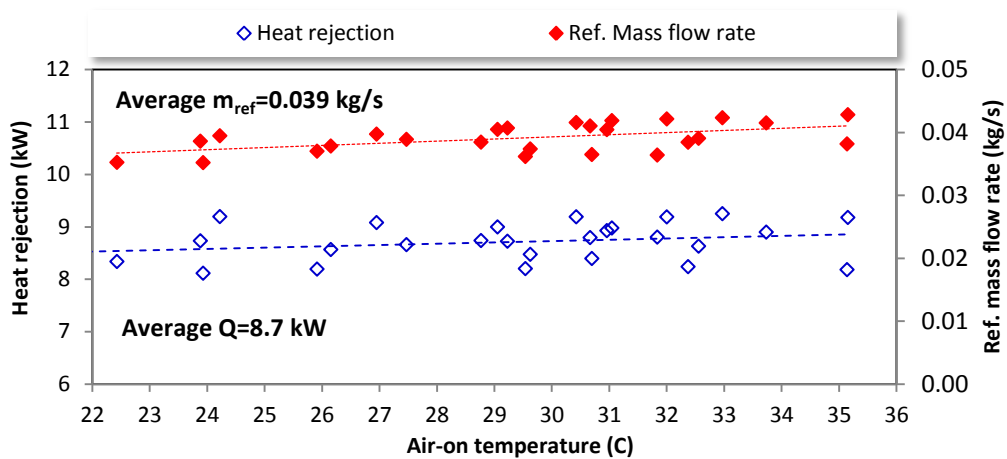


Figure 4.8 Variation of heat rejection and \dot{m}_{ref} with air-on temperature at varied compressor speed (Test conditions at varied compressor speed: 65%-100% and fan speed 50%, 60% & 70%)

For the fixed speed compressor, the controller only regulated the ON and OFF of the compressor. Figure 4.9 shows the heat rejected and mass flow rate in the gas cooler when the system was operated with the fixed speed compressor at 80%, 100% and 130% of full speed for Gas cooler B-1.6 m. It can be seen the heat rejection and mass flow rate increased proportionally when the compressor speed was increased. The heat rejection on average was of the magnitude of 14.5kW, 11.7kW, 9.3kW, and mass flow rates 0.062kg/s, 0.053kg/s, 0.042kg/s. for 130%, 100%, 80% compressor speeds, respectively.

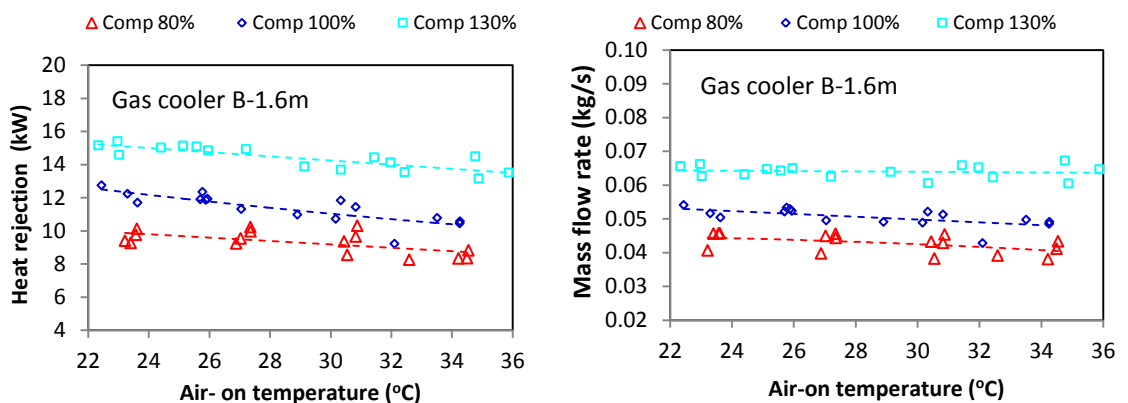


Figure 4.9 Variation of heat rejection and \dot{m}_{ref} with air-on temperature at fixed compressor speed (Test condition at fixed compressor speed and fan speed 50%, 60% & 70%)

The variations of heat rejection and refrigerant mass flow rate with air-on temperature can also be seen in Figure 4.9. The heat rejection seems to reduce as the air-on

temperature increased. This is because with higher air-on temperature the heat transfer rate in the heat exchanger is reduced due to the fact that some important thermal physical properties of CO₂ (such as specific heat, density, viscosity) are strongly dependent on its temperature. Furthermore, the mass flow rate is also seen to reduce slightly during the supercritical mode, due to volumetric efficiency of the compressor reduces when at a higher pressure.

4.6.1.2 Investigation of the effects of gas cooler types on heat rejection (Q)

The first comparison is between gas cooler-A and gas cooler B-1.6m at conditions of varied compressor speed 65%-100%, driving an approximate average of 0.039 kg/s of air. Figure 4.10 shows the variation of heat rejection with ambient temperature (air-on) of the two gas cooler coils. The heat rejections for gas cooler-A and gas cooler B-1.6m were 9.06kW and 8.68kW, respectively. Even though the heat transfer area of gas cooler A was 33% higher than that of gas cooler B the increase in heat rejection was only 4.5% higher. This was due to with the fact that gas cooler A had a greater nominal capacity than the actual heat rejection capacity of the refrigeration system. This is also due to the integrated control in the system.

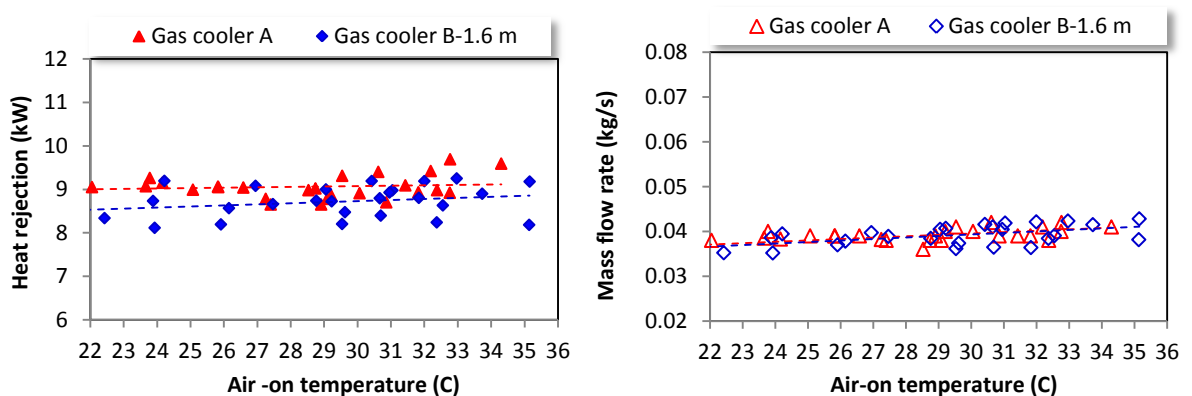


Figure 4.10 Variation of heat rejection and mass flow rate with air-on temperature of gas cooler A and gas cooler B-1.6 m

(Test conditions: varied compressor speed 65%-100%, fan speed 50%, 60%, 70%)

The effects of the vertical slit fin in gas cooler-A at varied compressor speeds 65%-100% were also investigated. It was observed that the average refrigerant mass flow rate and heat rejection of gas cooler-A were 0.039kg/s and 9.06kW, respectively. For gas cooler A-with vertical slits, the refrigerant mass flow rate and heat rejection were 0.042kg/s and 9.93kW, respectively as shown in Figure 4.11. The refrigeration system

in both tests did not work with identical load conditions. Nonetheless, with relatively similar mass flow rates, the effect of slit fin only increased 1.5% of the heat rejection. In this regard, the effect of slit fin was not only investigated by heat rejection parameter but also refrigerant temperature difference and approach temperature parameters, as explained in the next section.

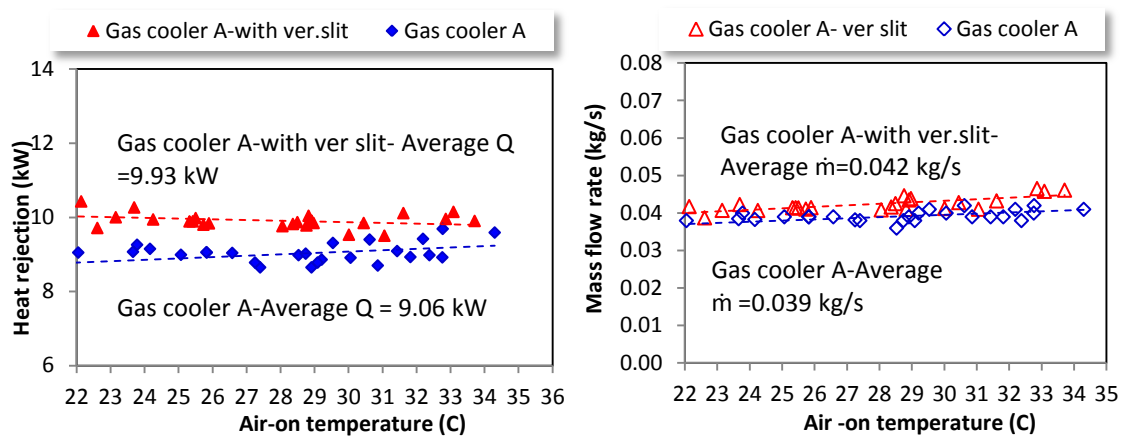
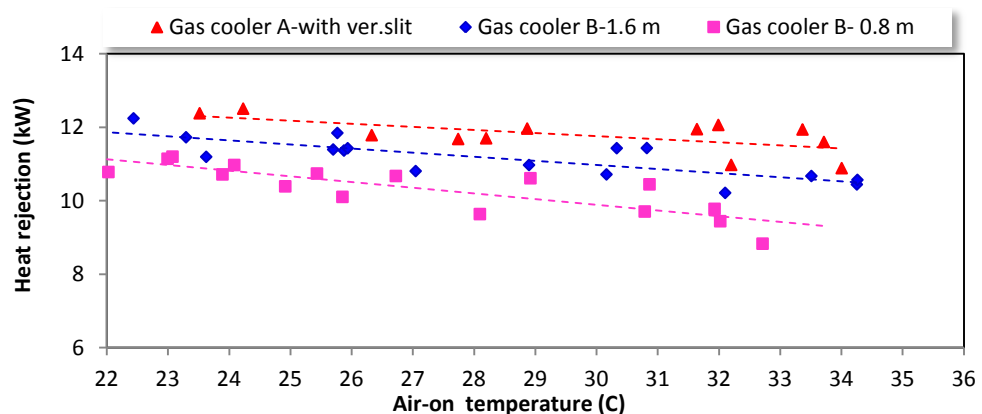
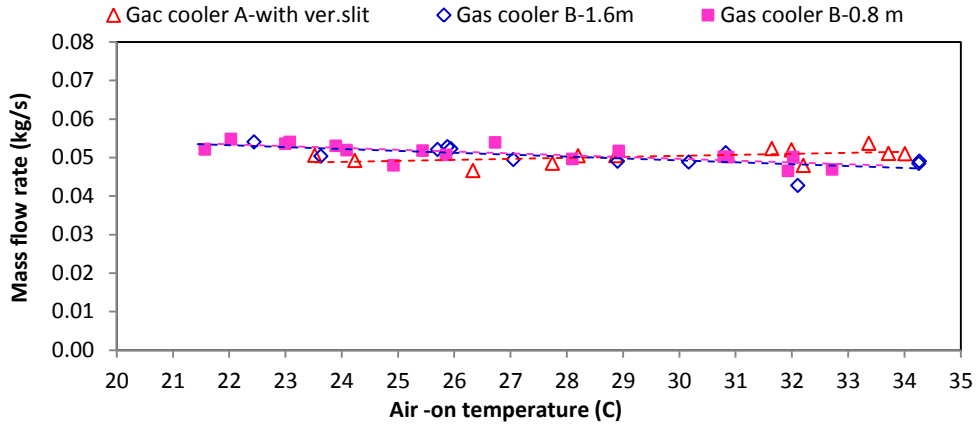


Figure 4.11 Variation of heat rejection and \dot{m}_{ref} with air-on temperature of gas cooler A and A-with vertical slits
(Test condition at varied compressor speed 65% - 100%, fan speed 50%.60% and 70%)

The second comparison is of the three different gas coolers at the fixed 100% compressor speed as shown in Figure 4.12 (a) and (b). It was found that the approximate average heat rejection rates were 11.79kW, 11.15kW and 10.4kW for Gas cooler A-with vertical slits, Gas cooler B-1.6m and Gas cooler B-0.8m, respectively, with similar mass flow rates averaging 0.053kg/s. This is consistent with previous results, however the physical size of gas cooler B-1.6m is doubled that of B-0.8m, but the heat rejection rate only increases by 7.2%, mainly due to the integrated control system and operation conditions of the system.



(a) Variation of heat rejection in gas coolers with air-on temperature



(b) Variation of mass flow rate with air- on temperature

Figure 4.12 Variation of heat rejection and \dot{m}_{ref} with air-on temperature
 (Test condition: fixed compressor speed 100%, fan speed 50%, 60% & 70%)

4.6.2 Operating pressure of the gas cooler

In the supercritical system, the pressure was regulated according to the ambient temperature and outlet temperature of the gas cooler in order to get the optimum performance of the system (as described previously in Chapters 2 and 3). The experimental discharge pressure in supercritical condition was compared with correlations obtained from references. Figure 4.13 shows the operating pressure of the gas cooler-A in certain test conditions, compared with optimum pressure correlations on supercritical condition obtained from Ge and Tassou (2011b), Sawalha (2008) and Chen and Gu (2005), which are explained in Section 2.3. According to these correlations, the optimum pressure is calculated mainly as a function of T_{amb} and refrigerant outlet temperature T_{refout} , approach temperature (AT), evaporating temperature (T_{evap}).

Figure 4.13 shows that the optimum pressures of the correlations have a satisfactory trend with the experiment results in the supercritical mode. Correlation results seem to be linear after the ambient air temperature of 27°C, with a mean deviation of 5% between the correlation and experimental results.

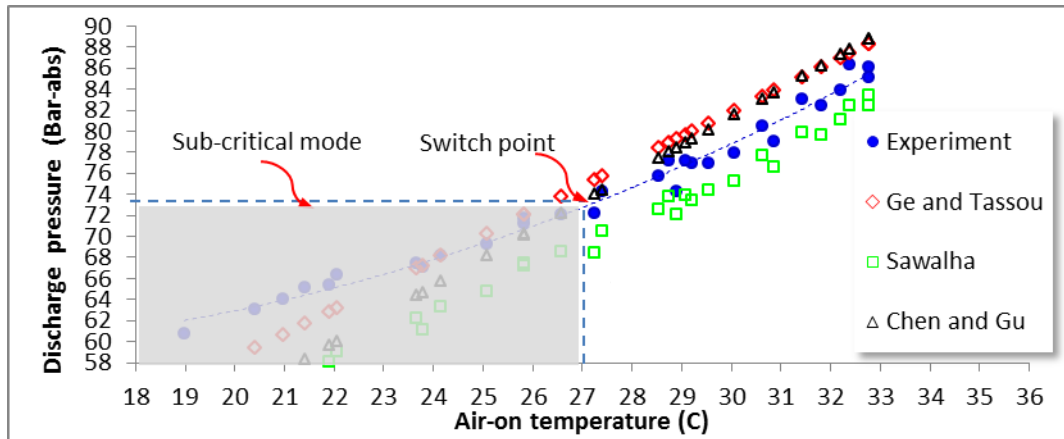


Figure 4.13 Comparison of optimum pressure correlations with experimental results
 (Test conditions: varied compressor speed 65%-100%, fan speed 50%, 60%, 70% of gas cooler- A)

Figure 4.14 shows the variation of discharge pressure with air-on temperature for gas cooler-A and gas cooler B-1.6m in identical test conditions, where the refrigerant mass flow rate is approximately 0.039kg/s, or heat rejection in gas coolers are on average approximately 8-9kW. Figure 4.14 also shows the pressure and temperature corresponding to the critical point of R744, $P_{crit-g} \approx 72.77 \text{ bar}_g$. The footprint (air side-perpendicular surface area) of the gas coolers was the same but gas cooler-A had more rows and circuits than gas cooler B-1.6 m. It also shows that the relationship between pressure and air-on temperature is fairly linear, and the switch from sub-critical to supercritical operation is relatively seamless. This is a function of the control of the ICMT valve and other integrated controls employed.

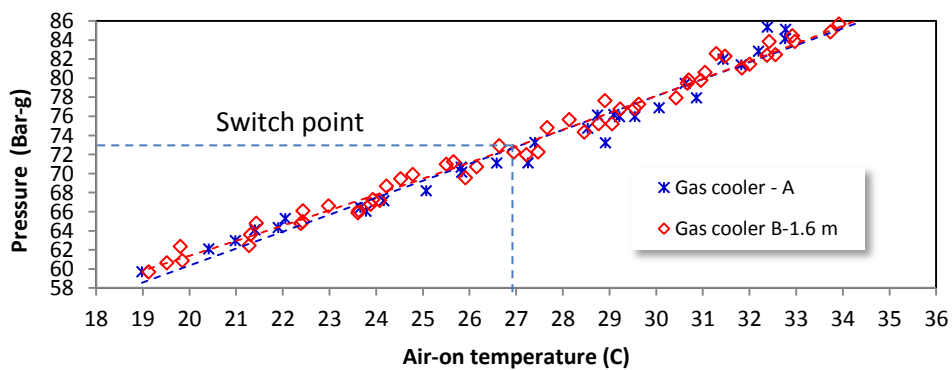


Figure 4.14 Variation of operating pressure with air-on temperature
 (Test conditions: varied compressor speeds 65%-100% $m_{ref} = 0.039 \text{ kg/s}$)

In the subcritical region, the pressure of gas cooler B-1.6 m is slightly higher than gas cooler-A. This is because for sub-critical operation the degree of sub-cooling for both

coils was set at 2K. To achieve this sub-cooling, the higher pressure drop in gas cooler B-1.6 m led to higher gas cooler pressures.

Similarly, the different pressures in sub-critical conditions also occurred when the mass flow rate increased in the similar gas cooler type (i.e. gas cooler A- with vertical slit) as shown in Figure 4.15. The pressure drop increases when the mass flow rate increases from 0.043kg/s up to 0.066kg/s in the entire gas cooler. There is also a slightly higher pressure during supercritical mode of the higher mass flow rate, due to the outlet temperature (T_{refout}) increases which lead the optimum discharge pressure also increases.

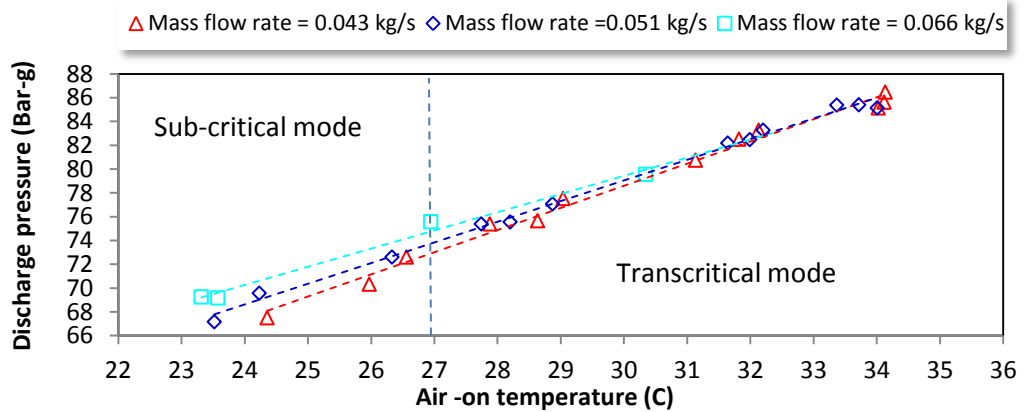


Figure 4.15 Variation of discharge pressure with air- on temperature for different \dot{m}_{ref} (Test conditions: fixed compressor speed)

Figure 4.16 shows three different gas cooler designs and sizes compared at a higher refrigerant mass flow rate of 0.051kg/s. At this mass flow rate, the difference in pressures in the sub-critical mode for gas cooler A-with vertical slits and gas cooler B-1.6m are clearly observed. Gas cooler B-0.8m has higher discharge pressure ranging between sub-critical and supercritical due to the significant lower heat transfer capacity led by the increasing temperature refrigerant outlet (T_{refout}). As the system controlled the optimal pressure of the gas cooler, the pressure of gas cooler B-0.8m was observed to be approximately 1.6 bar higher than both gas cooler A-with vertical slits and gas cooler B-1.6 m.

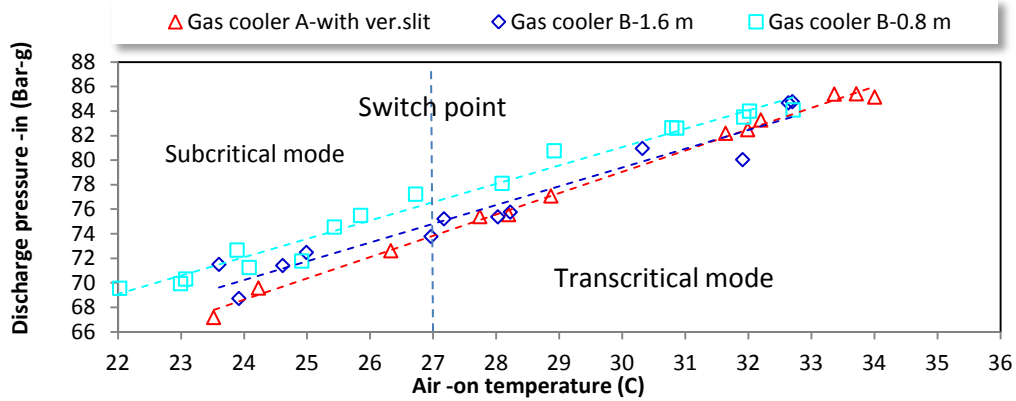


Figure 4.16 Variation of discharge pressures with air on temperature for different gas cooler types and sizes
(Test conditions: fixed speed compressor 100% $\dot{m}_{ref}=0.051$ kg/s)

4.6.3 Pressure drop in refrigerant-side and air-side

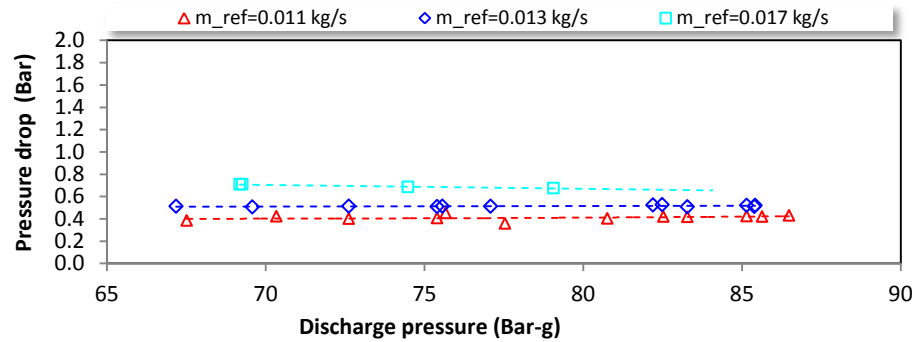
Figure 4.17 shows the variation of the refrigerant pressure drop with gas cooler inlet pressure for the three types of gas coolers at different mass flow rates per gas cooler circuit. It should be noted that this pressure drop also includes the inlet and outlet headers. The pipe length for each circuit was 39.20m for gas cooler A, 52.50m for gas cooler B-1.6 m and 26.25m for gas cooler B-0.8 m.

It can be seen in Figure 4.17(a) that the pressure drop for gas cooler-A increases with the increase in refrigerant mass flow rate as expected, from 0.4 bar to 0.7 bar at refrigerant mass flow rates of 0.011 kg/s and 0.017 kg/s, respectively. It can also be seen that the increase in gas cooler pressure and change from sub-critical to supercritical operation has little effect on the pressure drop at low refrigerant flow rates. At higher flow rates, for example 0.017kg/s, a pressure drop reduction can be observed as operation of the gas cooler moves from sub-critical to supercritical, where gas only flows at supercritical conditions as opposed to two-phase flow in the gas cooler at sub-critical conditions.

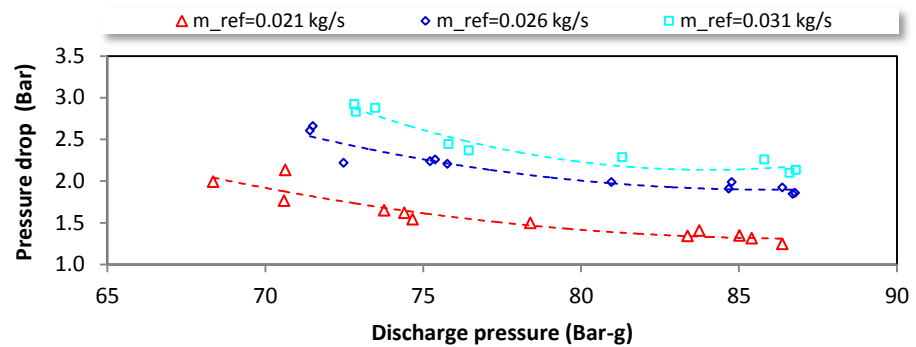
The pressure drop in gas cooler B-1.6m is much higher than in gas cooler-A, due to the lower number of circuits and therefore higher refrigerant mass flux, and also longer coil in gas cooler B. As expected, the pressure drop reduces as the gas cooler pressure increases and operation of the system becomes supercritical (see Figure 4.17b). This is because the density of CO₂ is higher if the system pressure is higher. The pressure drop of gas cooler-B 1.6m is significant higher comparing with the gas cooler-A, this

indicates the importance of suitable sizing and design of gas coolers which can be facilitated by validated design and selection computer simulation models.

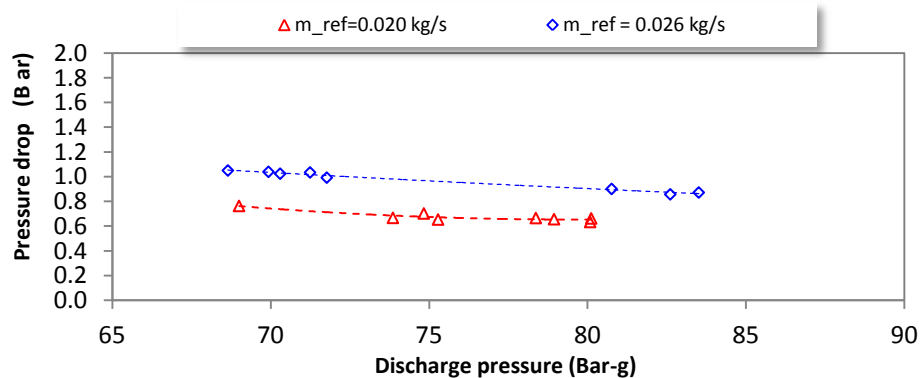
Gas cooler B-0.8m, on the other hand, has a pressure drop lower than the Gas cooler B-1.6m since the pressure drop varies proportionally with the length of the coil. With half the coil length, the pressure drop also approximately halves as shown in the Figures 4.17 (c).



(a) Refrigerant pressure drop of Gas cooler A



(b) Refrigerant pressure drop of Gas cooler B-1.6m



(c) Refrigerant pressure drop of gas cooler B-0.8m

Figure 4.17 Variation of pressure drop with discharge pressure for different gas cooler designs

Figure 4.18 shows the pressure drop obtained between the pressure transmitter position in the header and in the coil which was taken in gas cooler A-with vertical slits. If the pressure drop is compared between header position (total) and tube position, the mean total pressure drop is 0.51 bar, whilst the coil pressure drop is 0.3 bar, depicting the importance of adequately placing the pressure sensors. The difference between those positions is approximately 0.21 bar.

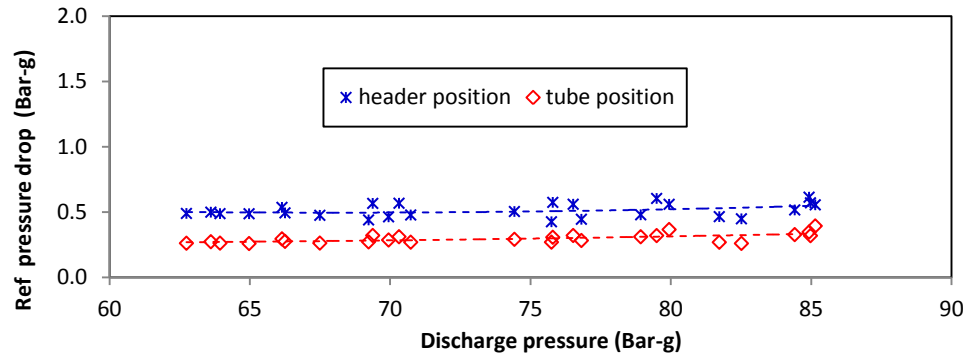


Figure 4.18 Variation of pressure drop with discharge pressures
(Test conditions: different pressure transmitter positions of gas cooler A-with vertical slits)

Figure 4.19 shows the influence of air face velocity on the air side pressure drop for the two gas coolers. The only difference between the gas coolers on the air side is an extra row of tubes for gas cooler A. As expected, the pressure drop increases as a function of the square of the flow velocity and the power consumption of the fan will be a function of the cube of the air flow velocity. It is therefore important to optimise the performance of the gas cooler not only on the refrigerant-side pressure drop but also the air-side pressure drop.

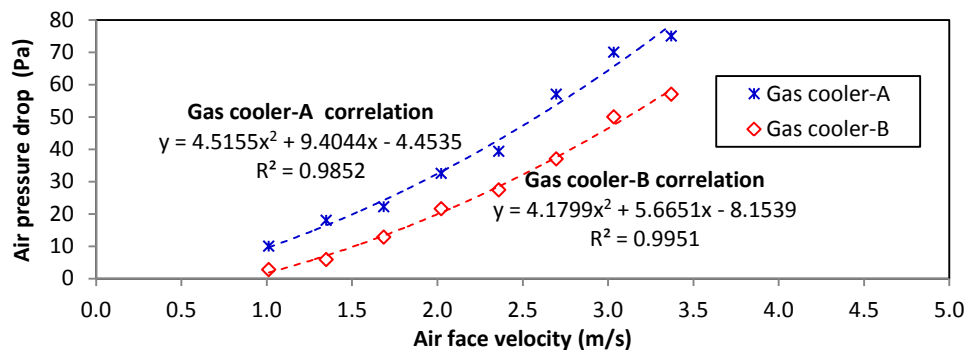


Figure 4.19 Correlations of air side pressure drop with air face velocity for Gas cooler A and B

4.6.4 Coil temperature profile

The coil temperature profiles along the coil were related to the gas cooler size and design, as well as the operating condition. Generally, for all gas cooler temperature profiles, there is a rapid change in temperature in the first tube. The temperature characteristic along the tubes are investigated in each type of gas cooler and operating conditions of sub-critical (condenser mode) and supercritical (gas cooler mode). The performance of each parallel circuit of the coil was found to be similar; hence the temperature data for only one circuit is presented below.

4.6.4.1 Coil temperature for condenser and gas cooler modes of operation

Figure 4.20 shows the variation of refrigerant temperature along the length of the pipes of gas cooler-A and gas cooler-B-1.6m operating as condenser (CD) and gas cooler (GC) with the test conditions of $\dot{m}_{ref}=0.039$ kg/s, fan speed 50% or air face velocity of 1.7 m/s, and heat rejection rate in the gas cooler in the range of 8-9.9 kW.

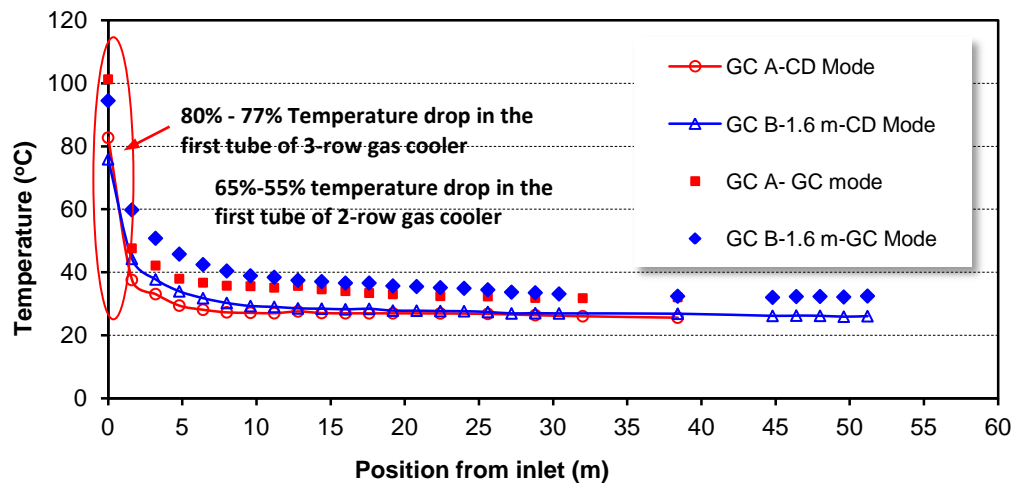


Figure 4.20 Temperature profiles along the gas cooler- A and gas cooler-B
(Test conditions: varied compressor speed 65%-100%, fan speed 50% and $\dot{m}_{ref}=0.039$ kg/s)

It can be seen that in both gas cooler and condenser operating conditions, most of the heat rejection takes place in the first few tubes due to the higher temperature difference between the refrigerant and the incoming air. However, heat transfer continues to take place even in the last few tubes, particularly in the case where the coil operates in the gas cooler mode. For gas cooler A in condenser mode, 80% of the temperature drop on the refrigerant side takes place in the first tube (1.6m length) whereas for the gas cooler

mode the first tube is responsible for 77% of the temperature drop. This indicates that the gas cooler was oversized for the refrigeration capacity. For gas cooler B-1.6m, the temperature drop on the refrigerant side taking place in the first tube is 65% when in condenser mode and 55 % in gas cooler mode.

4.6.4.2 Coil temperature profile for different compressor speeds

The mass flow rate was increased by increasing the compressor speed in the refrigeration system. Figure 4.21 illustrates the temperature profiles at three different mass flow rates in gas cooler B-1.6m. The temperature profiles were proportionally higher as the compressor speed (mass flow rate) increased. The temperature drops on the first tube decreased from 58% up to 48% when the mass flow rate increased from 0.042kg/s up to 0.066kg/s, respectively.

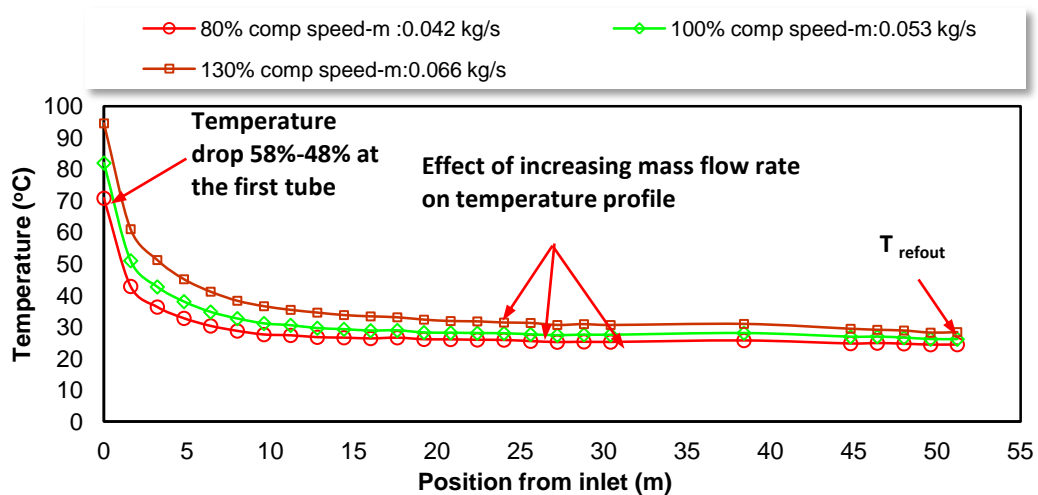
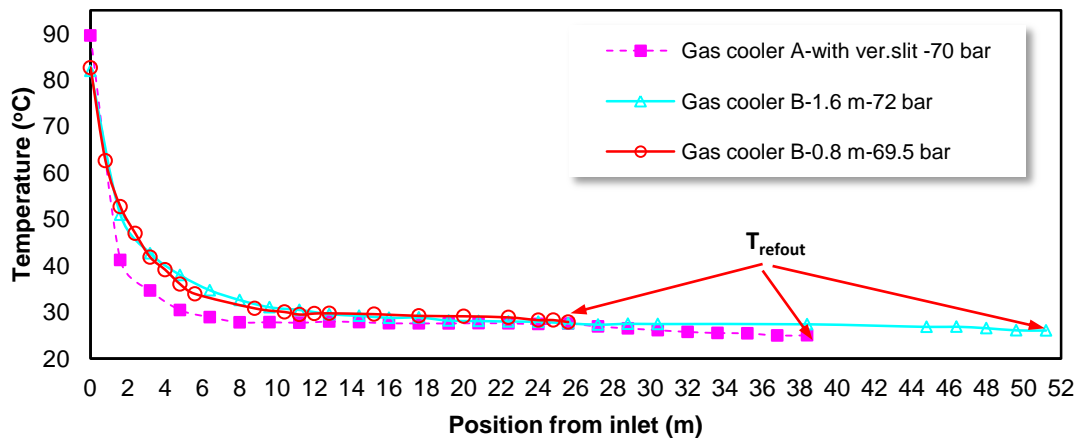


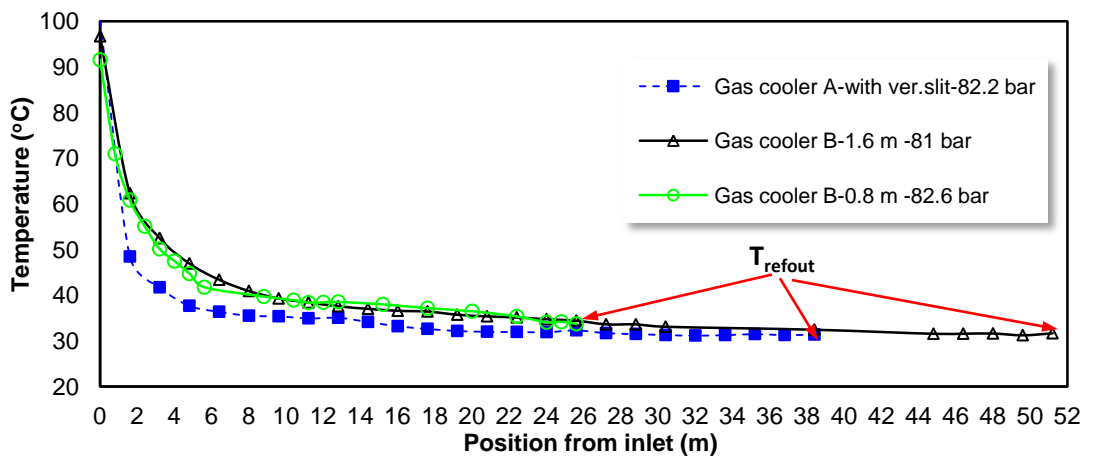
Figure 4.21 Temperature profiles along the coil of gas cooler B
(Test conditions: fan speed 50%; condenser mode)

4.6.4.3 Temperature profile for different type of gas cooler

The temperature profiles of three types of gas coolers (gas cooler A-with vertical slits; B-1.6m; B-0.8m) were compared in Figures 4. 22 (a) and (b). The two main parameters investigated are the temperature drops in the first tube and the temperature outlet (T_{refout}).



(a) Temperature profile in condenser mode



(b) Temperature profile in gas cooler mode

Figure 4.22 Temperature profile along the tubes for different gas cooler types
 (Test conditions: 100% fixed compressor speed; fan speed 50%)

Gas cooler A-with vertical slits shows a significant temperature drop in both the condenser and gas cooler modes and also gas cooler-A with vertical slits has the lowest outlet temperature. This is because of the number of parallel circuits in the gas cooler. Gas cooler B-1.6m and B-0.8m have very similar specifications, with the only difference being the length with gas cooler B-1.6m being double that of gas cooler B-0.8m, and it can be seen that temperature profiles are identical.

4.6.4.4 Effect of vertical slit and heat gain on the tubes by fin conduction

Figure 4.23 illustrates the effects of the vertical slit fins on the temperature profile of the gas cooler. It can be seen that in some cases, the temperature increases rather than decreases from one tube to the next. This is due to heat transfer by conduction across the fins of the adjacent tube; from the hotter to the colder tubes. It can be seen in Figure 4.23 that the temperature gain clearly occurs in pipe 8 and 16 for gas cooler-A.

With the vertical slit fins the temperature gain in pipe 8 does not appear to be significant, and also there is no impact to the temperature for its next row. However, at pipe 16, the heat gain still occurs because the vertical slit only blocks temperature spread from pipe 1 to pipe 8. Regarding the temperature profile in each row, gas cooler A-with vertical slits has a higher temperature in row-1. However, it has a lower temperature for the next row and this means that the heat gain blocking in the pipe 8 can effectively increase the local heat transfer coefficient and could decrease the outlet temperature ($T_{ref\ out}$).

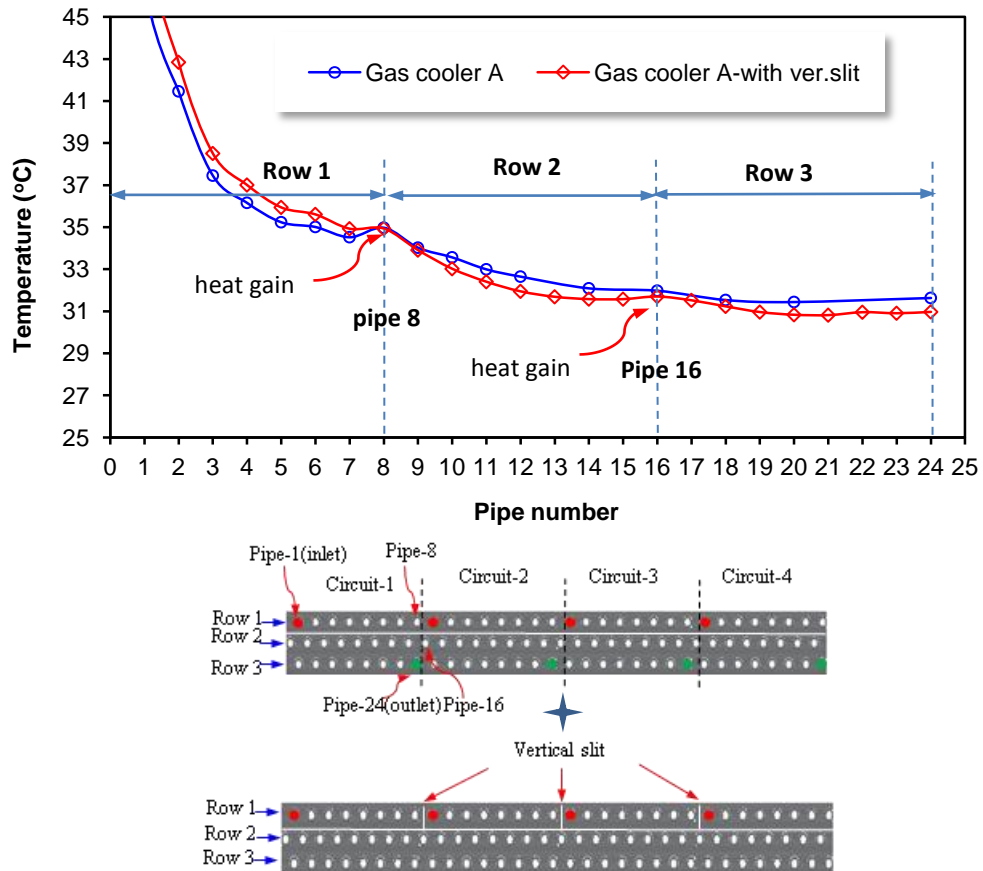


Figure 4.23 Temperature profile for gas cooler A and A-with vertical slits with pipe numbers (Test conditions: 100% fixed compressor speed; gas cooler mode)

Figure 4.24 shows the temperature profile for the gas cooler B-1.6m looking at the heat gain along the tubes, It can be compared the temperature profile between circuit 1 and circuit 2, the heat gain only occurs in the circuit 1 at pipe 16 since there is heat conduction effect through the fin from the hotter adjacent pipe-1 of circuit-2. Also there is slightly higher temperature at the end of coil in circuit-1 because of very close to the header.

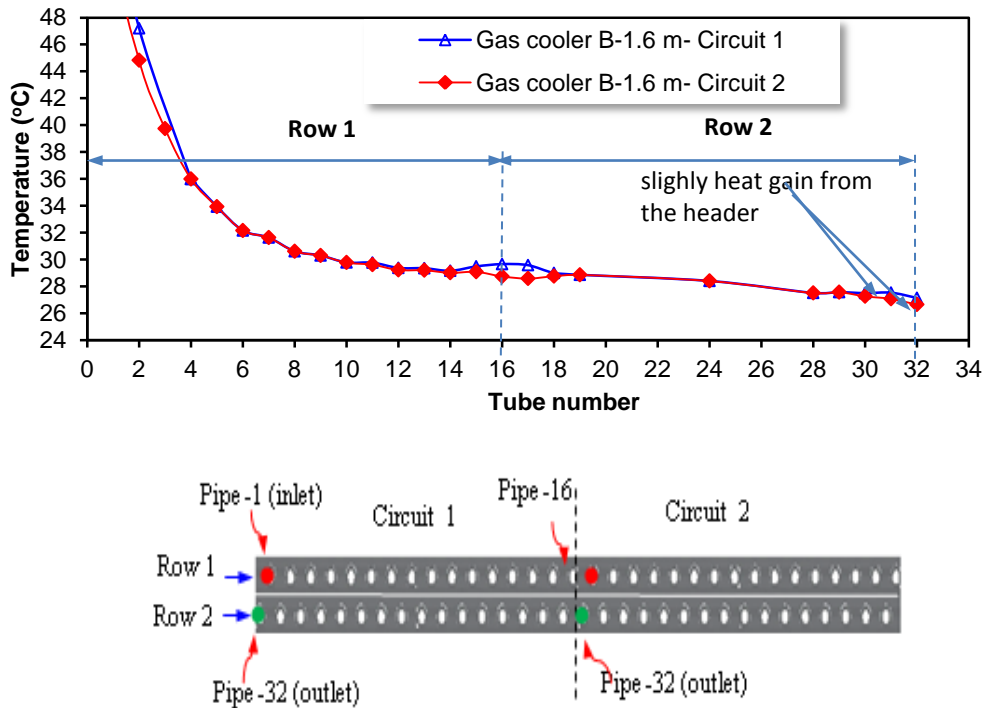


Figure 4.24 Temperature profile for gas cooler B
(Test conditions: 100% fixed compressor speeds; condenser mode)

Figure 4.25 shows the temperature contours in gas coolers, taken using a Thermal IR Imaging Camera. These images confirm the large temperature drop in the first few tubes in the circuit particularly between the first and second tubes. It can also be seen that because of the continuity of the fins between circuits there is heat transfer between adjacent tubes of the parallel circuits which reduces the overall heat transfer effectiveness of the heat exchanger.

In the gas cooler A-with vertical slits, the vertical slit fins can block the heat spread from the hottest pipe to the adjacent colder pipe as shown in Figure 4.25 (c) and (d).

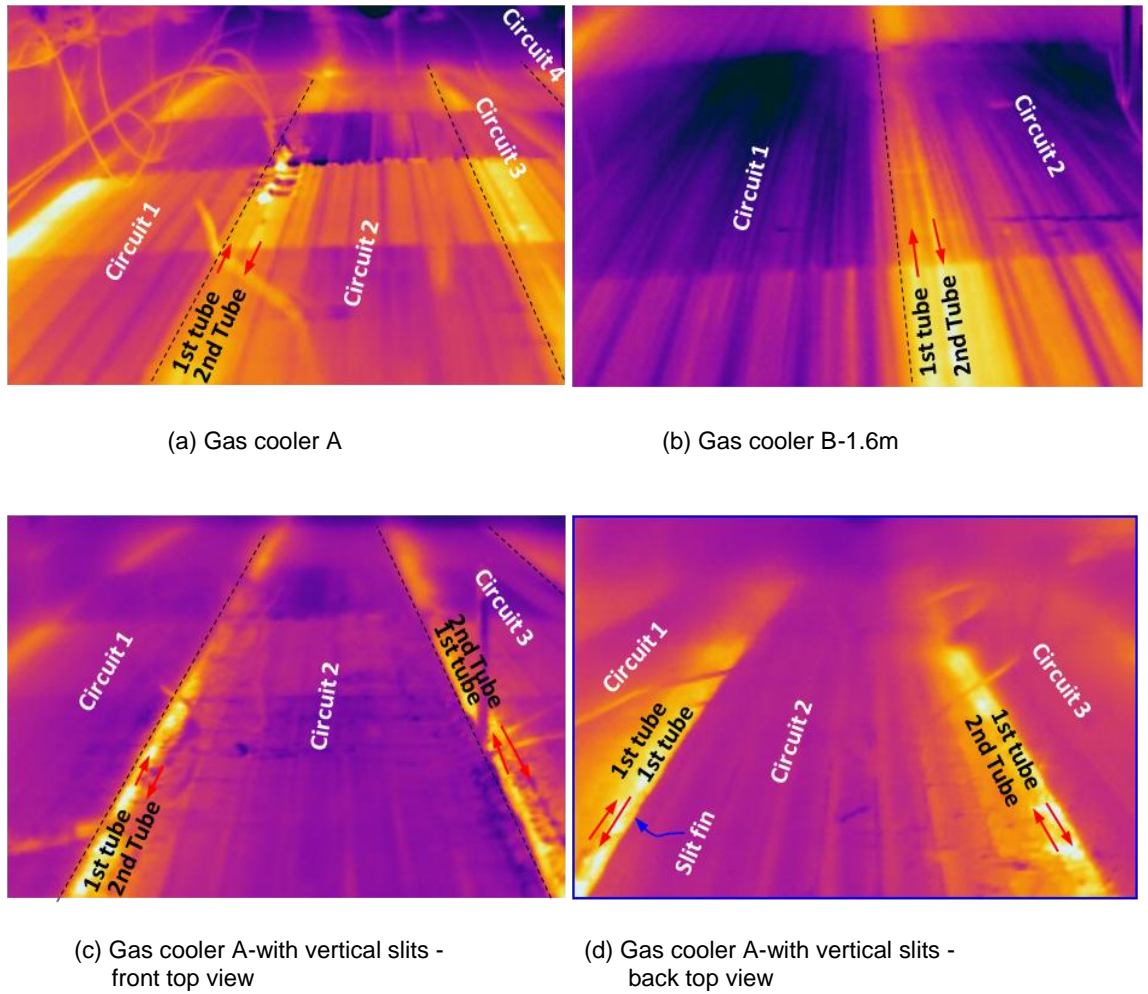


Figure 4.25 Thermal image of gas coolers

4.6.5 Fin surface temperature

Table 4.3 shows the test results, which have been done in controlled conditions with an air-on temperature of 32.8°C and operational pressure of 84 bar.

Table 4.3 Experimental results of fin surface temperature

Points - distance of fin from inlet	Point A (70mm)		Point B (140mm)		Point C (690mm)		Point D (710mm)		Point E (880mm)		Point F (1530mm)	
	Fin tip	Fin collar	Fin tip	Fin collar	Fin tip	Fin collar	Fin tip	Fin collar	Fin tip	Fin collar	Fin tip	Fin collar
Temp. Test results (°C)	56.8	-	-	56.4	47.9	-	-	48.3	45.2	-	41.2	-

Figure 4.26 shows the comparison fin tip and fin collar temperatures with the temperature profile of refrigerant. The fin tip and fin collar temperatures at the two points which were investigated appear to be consistent with the coil (ref) temperature profile. This data was used to CFD model validation.

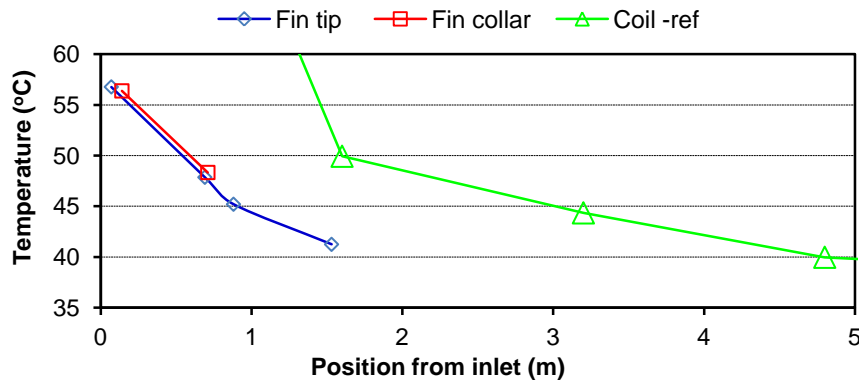


Figure 4.26 Fin surface temperature and coil temperatures for gas cooler A
(Test conditions: fan speed 50% or air face velocity 1.7 m/s; $\dot{m}_{ref}=0.039\text{kg/s}$)

4.6.6 Air-side temperature difference (TD)

This investigation is aimed to show the effect of gas cooler size and design, air face velocity and refrigeration mass flow rate to the air-side temperature difference (TD air-side). Figure 4.27 shows the TD air-side in the two different gas coolers in identical test conditions, which are refrigerant mass flow rate 0.05 kg/s and air face velocity 2.0 m/s.

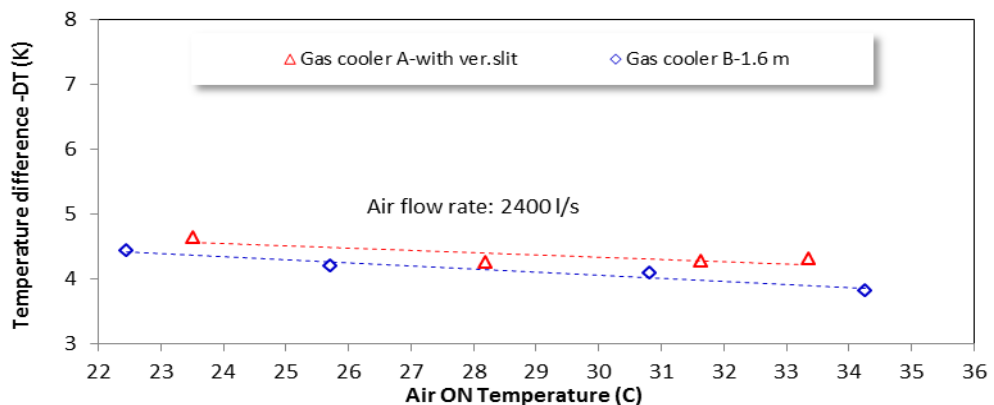


Figure 4.27 Air-side temperature difference (TD) for different gas cooler types
(Test conditions: compressor speed 100%; $\dot{m}_{ref}=0.05\text{ kg/s}$; fan speed 60% or velocity =2 m/s)

For similar air flow rates in this operational condition the gas cooler A-with vertical slits has slightly higher TD on average 4.4 K and the Gas cooler B has an average TD of 4.1K. Since the TD air side is correlated with the heat rejection parameter, it seem that the results consistent with the previous explanation in the Section 4.6.1.2.

In terms of the effect of the air face velocity and the refrigerant mass flow rate on the TD air-side are illustrated in Figure 4.28 and Figure 4.29.

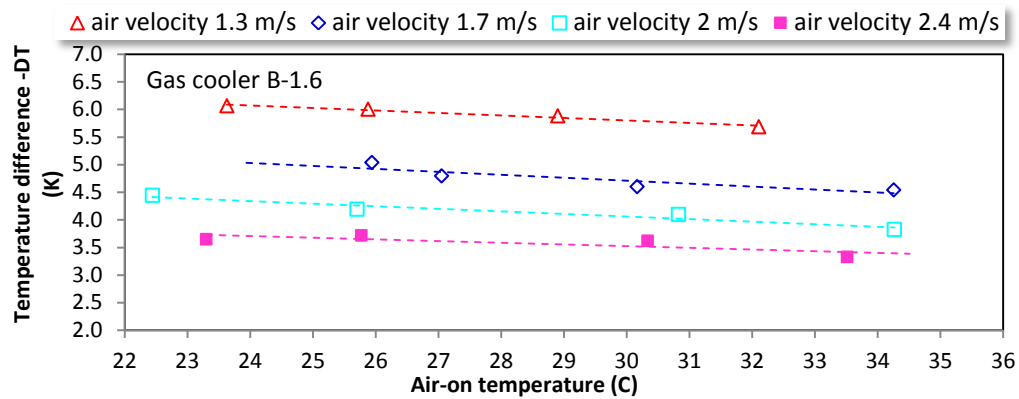


Figure 4.28 Variation of air side-TD with air-on temperature for different air velocity
(Test condition: $\dot{m}_{ref}=0.050$ kg/s /fixed 100% compressor speed - sub cooler -0.3K)

The impact of increasing air face coil velocity and refrigerant mass flow rate can effect to the air side TD proportionally. And with higher air-on temperature TD seems to be slightly decreased. This is because of a lower heat transfer rate at a higher temperature.

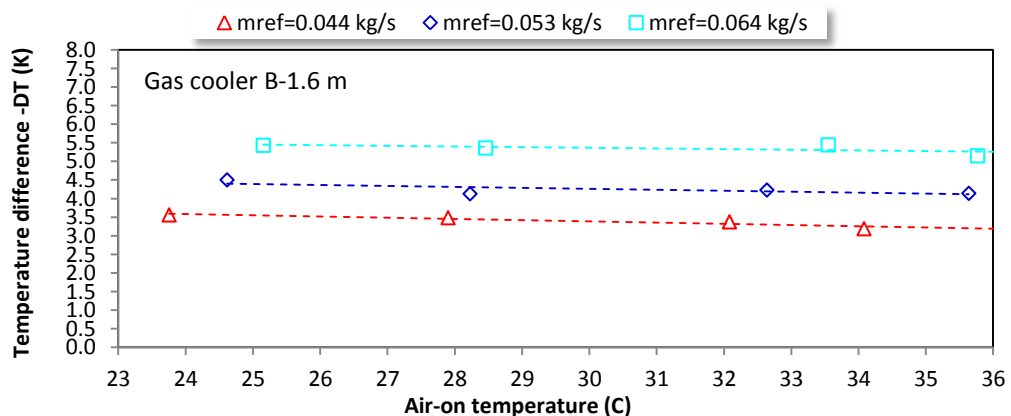


Figure 4.29 Variation of air-side-TD with air-on temperature for different refrigerant mass flow rate
(Test condition: fan speed 60%; sub-cooled 2K)

4.6.7 Refrigerant-side temperature difference (TD_{ref})

First of all, the physical size of the gas cooler, the tube and circuit arrangements are compared with the refrigerant-side temperature differences (TD_{ref}). The three gas coolers were investigated based on the TD_{ref} as shown in Figure 4.30. It can be seen that, consistent with the previous results, gas cooler A-with vertical slits has the better performance compared to both Gas cooler B-1.6 m and B-0.8 m. This is indicated by the TD_{ref} magnitude in identical test conditions.

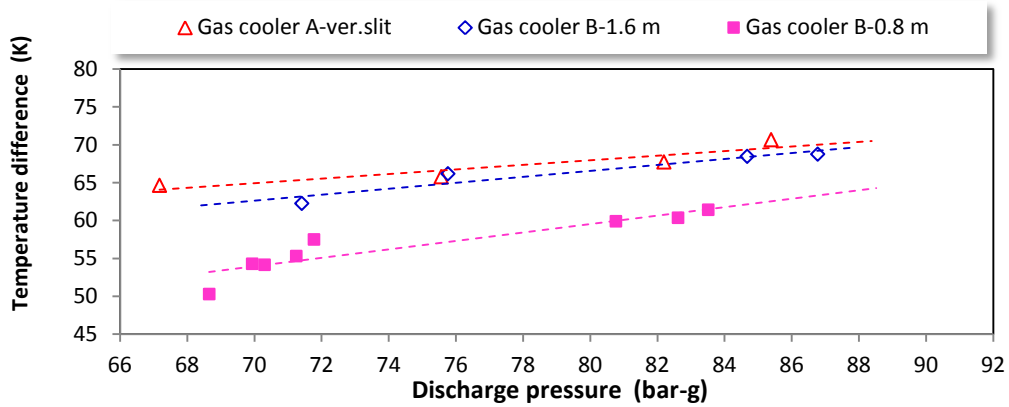


Figure 4.30 Variation of refrigerant-side- TD_{ref} with discharge pressure for different gas cooler types (Test conditions: 100% fixed speed compressor; fan speed 60%)

The second comparison of TD_{ref} is between gas cooler A and gas cooler A-with vertical slit fins as shown in Figure 4.31. The vertical slit fins on the gas cooler A seem to be effective at increasing TD_{ref} . This is indicated by a better overall heat transfer coefficient, which is due to the bad effects from the heat conduction being mitigated through the fins from the hotter tubes to the adjacent colder tubes.

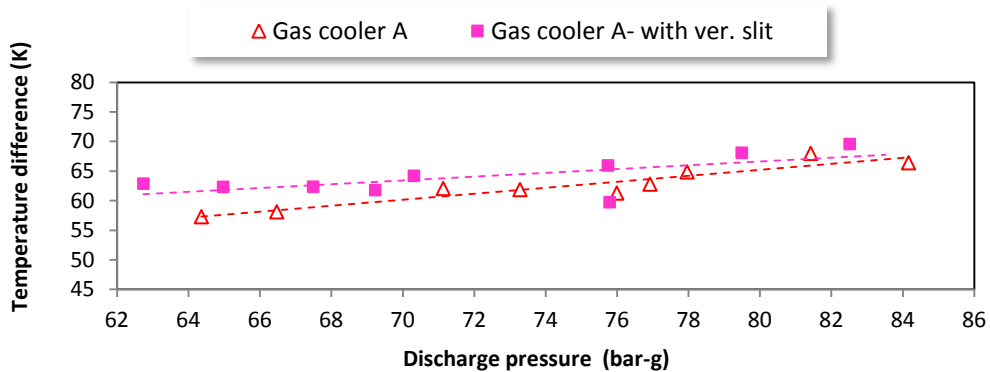


Figure 4.31 Variation of refrigerant-side TD_{ref} with discharge pressure for vertical slit fin (Test conditions: Varied compressor speed 65%-100%; fan speed 60%)

According to both the comparisons, the TD_{ref} trend-line is increased as the discharge pressure increases. This is due to the discharge temperature rising significantly at the

higher pressure. Data recorded from several test conditions is shown in Figure 4.32. The discharge pressure of around 86 bar_g shows the inlet temperature reaches more than 95°C compared to when the pressure is around 62 bar_g and the inlet temperature reaches only around 73°C.

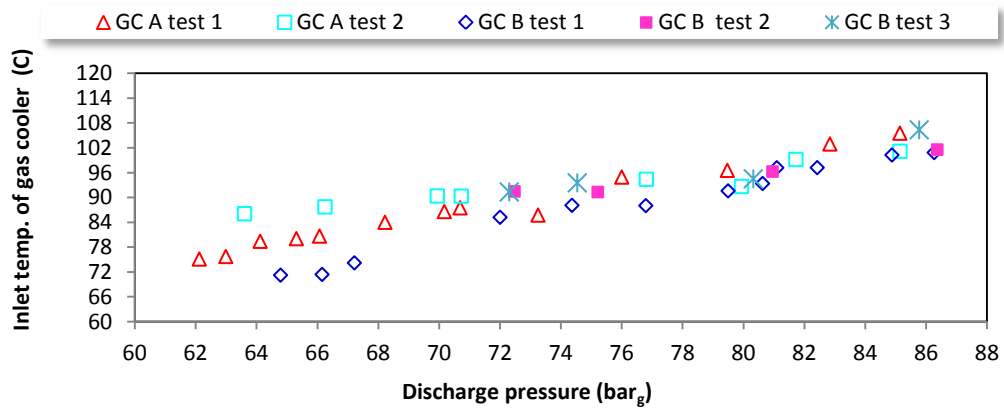


Figure 4.32 Variation of inlet refrigerant temperature with discharge pressure for various test conditions
(Test conditions: Fan speed 50%; compressor speed 100%)

However, the TD_{ref} increases with the increased discharge pressure but the enthalpy difference (Δh) is reduced as shown in Figure 4.33.

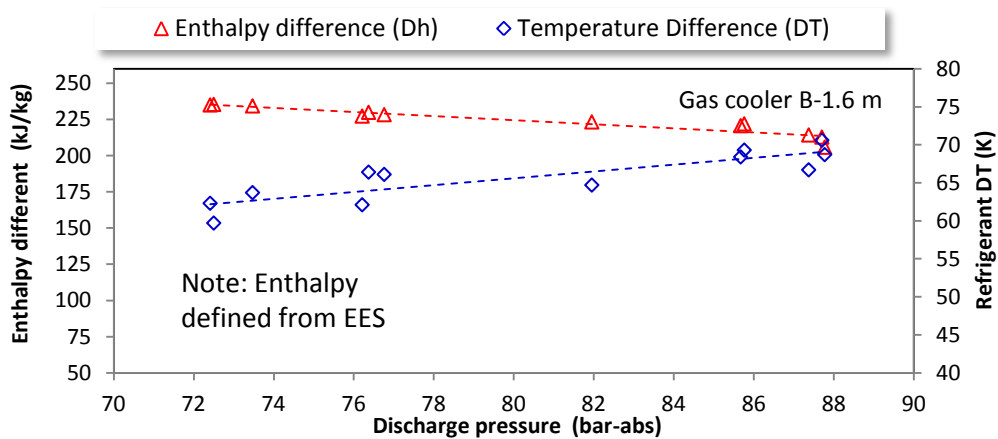


Figure 4.33 Variation of enthalpy difference and temperature difference with discharge pressure
(Test conditions: compressor speed 100%, $m_{ref}=0.052$ kg/s, fan speeds 50%, 60%, 70%)

4.6.8 Approach Temperature (AT)

Approach temperature (difference between refrigerant outlet and air inlet temperature) is a very common parameter used to define gas cooler performance. In this test, the approach temperature can be influenced in a number of ways including air face velocity, pressure (led by ambient temperature) and design of the gas cooler. Figure 4.34 shows the effects of air face coil velocity and ambient temperature (air-on temperature) on gas cooler B-1.6m in certain test conditions and in Figure 4.36 shows the impact of type of gas cooler.

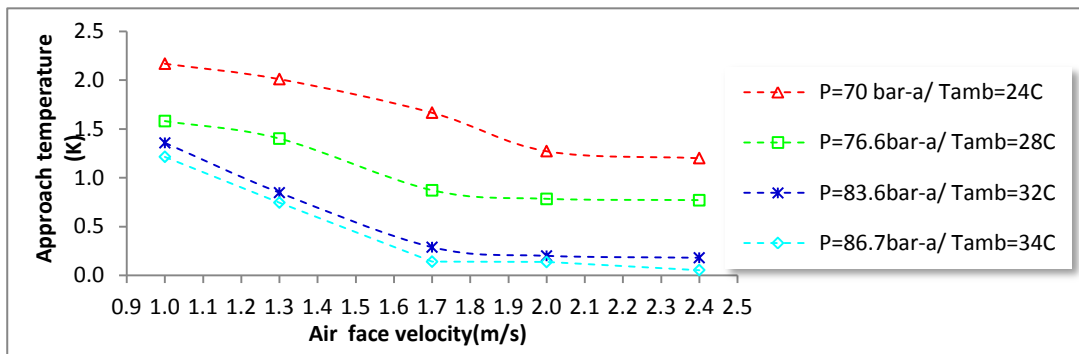


Figure 4.34 Variation of approach temperature with air face velocity of gas cooler B
(Test conditions: $m_{ref} = 0.039$ kg/s, compressor speed 65%-100%)

The approach temperature decreased proportionally as the air velocity and pressure increased. An explanation for this is that this is also related to the discharge pressure, which is automatically controlled by air-on temperature as illustrated by Figure 4.35 showing a P-h diagram. It can be seen that in higher pressure the approach temperature gets lower, however the enthalpy of the fluid is still lower.

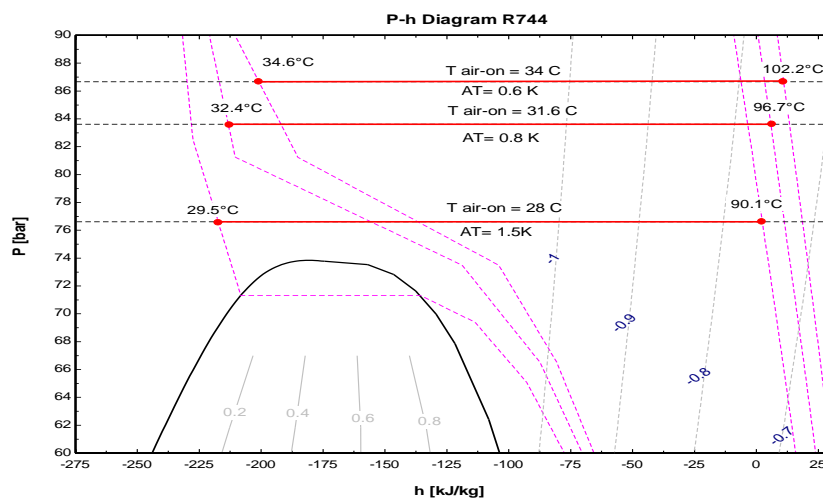


Figure 4.35 P-h diagram for several discharge pressure conditions of gas cooler B
(Test conditions: $m_{ref} = 0.039$ kg/s, compressor speed 65%-100%)

Figure 4.36 shows the variation of approach temperature with air face velocity with three gas cooler different designs. It is clear that type of the gas cooler contribute the significant effect to the approach temperature. Gas cooler A which has biggest physical size has much lower approach temperature than gas coolers- B. It also shows approach temperature decreases as the air velocity increasing.

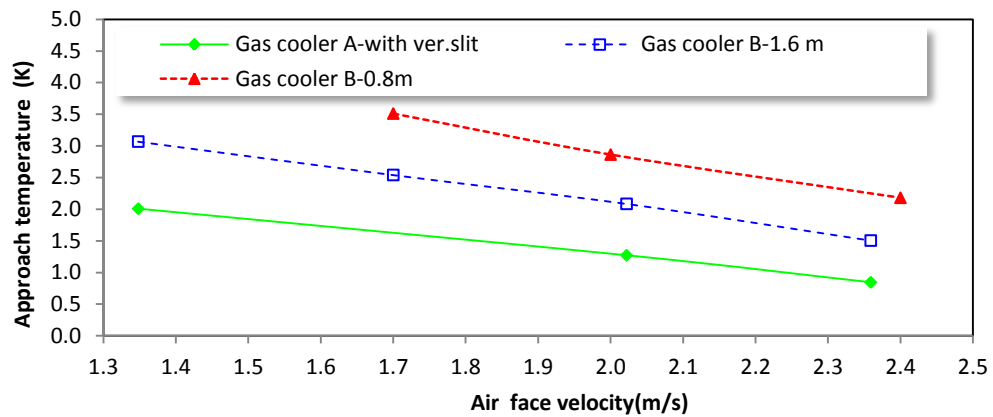


Figure 4.36 Variation of approach temperature with air face velocity for different gas cooler types
(Test conditions: Ambient temperature 28°C or pressure 76 bar_g)

Figure 4.37 shows that influence of the approach temperature on the overall heat rejection of the three gas coolers. Because of its bigger size, for the same approach temperature gas coolers A and A-with vertical slits, led to slightly higher heat rejection compared to gas cooler B for both condensing and gas cooling operation. Furthermore, vertical slit fins in Gas cooler A had better overall heat transfer performance. Figure 4.37 also shows that increasing the approach temperature reduces the heat rejection in the gas cooler.

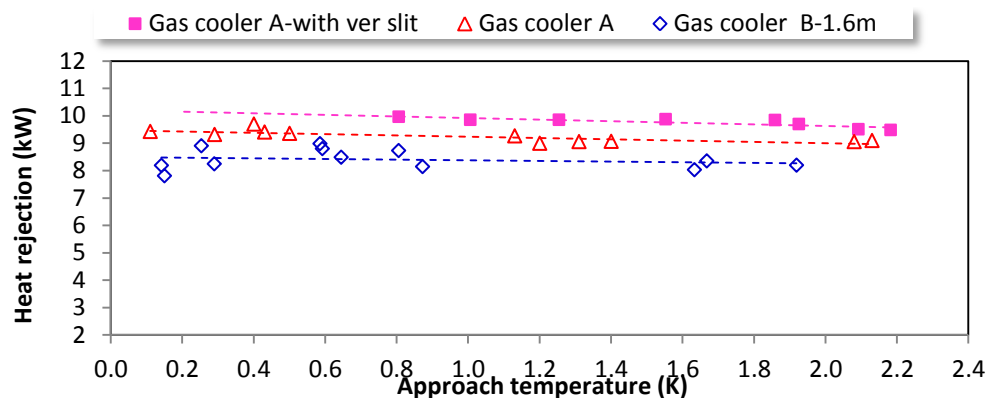


Figure 4.37 Variation of heat rejection with approach temperature
(Test conditions: compressor speed 65%-100%, fan speed 50%, T sub-cooled: 2K)

It can be concluded that the approach temperature is a function of the heat transfer performance of the gas cooler and is dependent on the heat transfer area and air mass flow rates. However, reduction in the approach temperature is limited by the size of the gas cooler coil and power consumption of condenser/gas cooler fan. For maximum performance it is therefore important to maintain the approach temperature as low as possible but without increasing substantially the size and cost of the gas cooler such as, electrical power for fan speed.

Optimisation of the performance of the gas cooler should not be done in isolation. The influence of design and control parameters on the overall performance of the CO₂ refrigeration system should be considered and this can be achieved through a combination of experimentation and system modelling. The data will be used to calculate the heat transfer coefficient in the heat exchanger using CFD.

4.7 Medium Temperature (MT) refrigeration system test results

These results are just to observe that the system has been operated in a way that satisfies the test conditions. The CO₂ refrigeration system and the gas cooler data were collected at the same time when tests were carried out. The results of this investigation correspond with section 4.1 (overview of the test facilities).

4.7.1 Mass flow rate in the system

Figure 4.38 and Figure 4.39 show the test results of an MT CO₂ refrigeration system with 100% compressor speed and 130% compressor speed. The operational condition of the gas cooler was at air-on temperature 24°C and fan speed 40% of full speed with the gas cooler B-1.6m design been used.

The intermediate regions (P4 and T4) and Medium Temperature (MT) regions (P7 and T7) were fairly constant when the refrigerant mass flow rate was increased. The controller employs EKC-326, EKC-347 and AK-CC-550, which were modulated valves to maintain the pressure and temperature to satisfy a setting target. However, the capacity varies by compressor speed. The target pressure and temperature in the intermediate region is 32 bar and the main controller sets the target pressure in the evaporator at around 27 bar, but it seem the evaporation temperature has been approximately 29 bar during the test. This is good condition for the gas cooler testing since compressor able to run on constant condition.

4.7.2 Thermodynamic cycle of the MT CO₂ refrigeration system

Figure 4.40 shows the thermodynamic cycle of the MT CO₂ refrigeration system obtained from one of the test conditions where the compressor speed was 100%. The cycle refers to the schematic diagram shown in Figure 4.38. The compression process (1-2) utilised a semi hermetic reciprocating compressor of isentropic efficiency of around 0.87 – 0.70 with the discharge pressure comprising four pressure levels in condensed and gas cooler mode corresponding to air-on temperatures 24– 35°C. Heat rejection in the condenser / gas cooler (2-3) had a sub-cooling degree (3) around 2K which was thoroughly investigated in the previous section. The expansion process in the ICMT (3-4) was assumed to be isenthalpic. The receiver state (4-5) obtained a saturated liquid condition. Hot gas by pass 4-10 was assumed to be of an isobaric condition and the expansion process in the ICM (10-11) and in the AKV –MT (5-7) was assumed to be isenthalpic as well. The heat extraction process in the MT cabinet (7-8) can be assumed to be at constant temperature and pressure. The intermediate region (4-5; 5-10) and MT region (7-12; 7-11;1-8) were fairly constant, which satisfied the setting point. However, the discharge pressure change corresponds to the air-on temperature. In general, according to the P-h diagram, it can be argued that the gas cooler operational condition (2-3) is very important to optimizing the performance of the system.

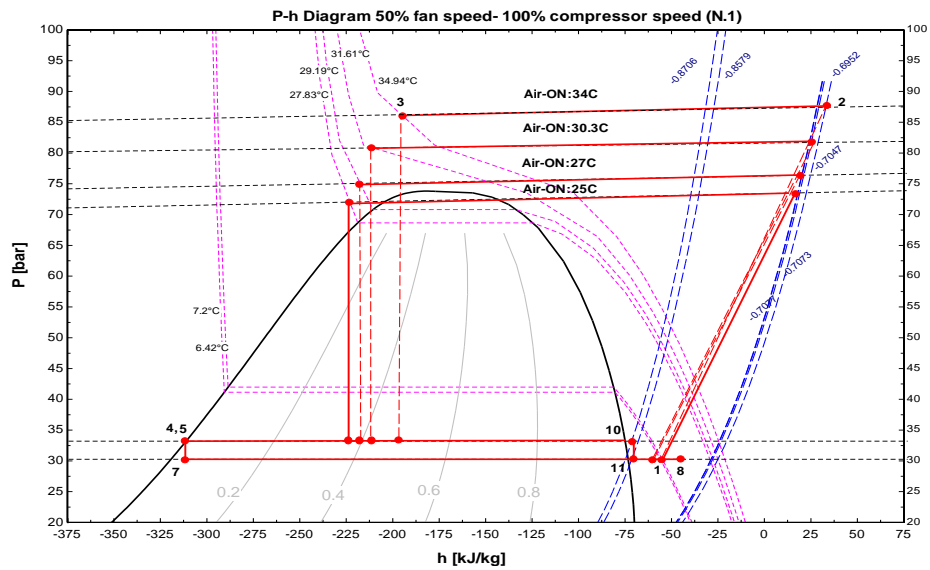


Figure 4.40 P-h diagram of MT CO₂ refrigeration system-2K sub cooling
(Test conditions: 50% fan speed, 100% compressor speed)

In addition, when the sub-cooling degree was set at 0.3K the controller worked well - the sub-cooling degree 0.3 is shown in Figure 4.41.

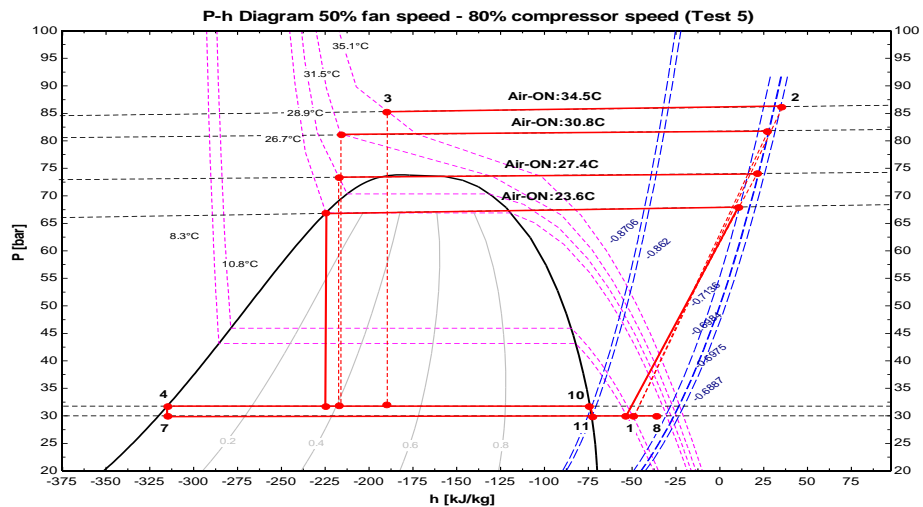


Figure 4.41 P-h diagram of MT CO₂ refrigeration system-0.3K sub cooling
(Test conditions: 50% fan speed, 80% compressor speed)

This test was carried out on the test condition of 80% compressor speed, 50% fan speed and with an air-on temperature of around 24°C, with sub-cooling obtained at 0.216 K. With the intermediated pressure (receiver pressure) constant at 32 bar and medium temperature between 29.8-30 bar, this means that the refrigeration load was too high with a driven 80% compressor speed.

4.8 Summary

Tests have been performed on four of gas cooler design including, gas cooler A (3 row-4 circuit) with horizontal and horizontal and vertical slit fin, gas cooler B (2 row-2 circuit) with horizontal slit fin 1.6 m and 0.8 m length. The K-Type thermocouples used had a maximum uncertainty of $\pm 0.5^{\circ}\text{C}$, the pressure transducers had uncertainty of $\pm 0.3\%$, and the air velocity meter had uncertainty of $\pm 3\%$. The test programmes consist of two test group of compressor speed and three simulated parameters comprise air-on temperature, refrigerant mass flow rate, and air face velocity.

The switch temperature from subcritical and supercritical was found at 23°C until 27°C . Experimental investigation indicated that the gas cooler performance mainly indicated by approach temperature (AT) and heat rejection (Q). The performance of the supercritical mode was found to be lower than the subcritical mode which is indicated by heat rejection (Q). Approach temperature (AT) decreases as the fan speed increasing and the AT are also influenced by gas cooler type. Gas cooler optimum pressure, air side pressure drop correlation and temperature profile along the coil of the gas coolers were also obtained from the experimental results. The result also show that the CO_2 refrigeration system was operated satisfy to the control strategy have been set for the system. In addition, the experimental test results will be significant important to validate CFD model.

Chapter 5 will examine the CFD model of the finned and tube gas cooler and the model is validated against the test results, especially for heat rejection (Q), temperature air-off and fin temperature.

CHAPTER V - CFD MODELLING OF GAS COOLERS AND VALIDATION

5.1 Introduction

The finned and tube gas cooler for supercritical CO₂ refrigeration system with gas cooler-A and gas cooler-B geometry designs were numerically modelled using Computational Fluid Dynamics (CFD), in the commercial package ANSYS FLUENT®. The procedure for setting up a model problem is described in Figure 5.1.

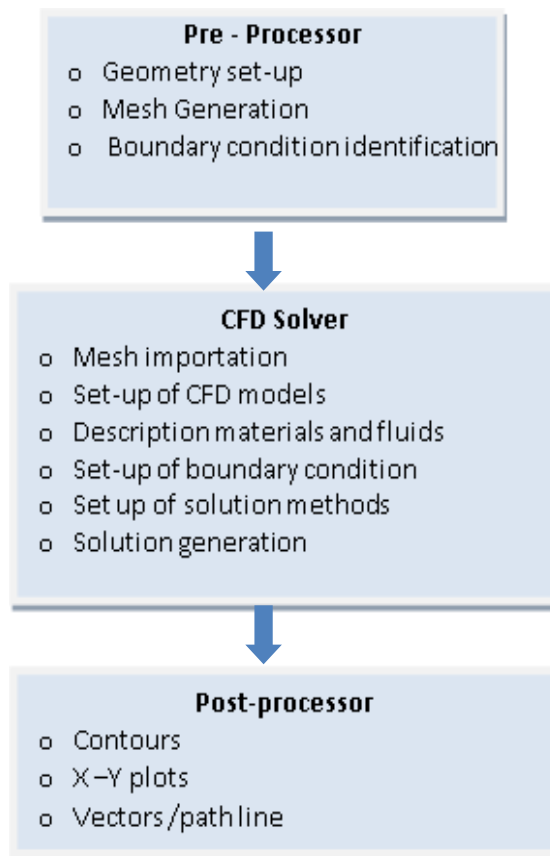


Figure 5.1 Basic programme structure

Figure 5.1 describes the steps required for a CFD problem, i.e. defining the geometry, meshing, and the problem (pre-processor); setting the physical attributes to the problem and assigning the adequate modelling methods required (solver) and; extracting and analysing the results from the model (post-processor). In this study, the three-dimensional model geometry was designed and built in Solid-Works®, which also allows automatic refinement of the grid based on the flow solution, thereby providing

more accurate results. However, this feature should be used properly in order to avoid excessive number of cells which would increase computational time. The resulting set of discrete, non-linear, algebraic matrix equations is solved until the specified convergence criteria are satisfied. For the gas cooler simulation, the physical model is shown in Figure 5.2.

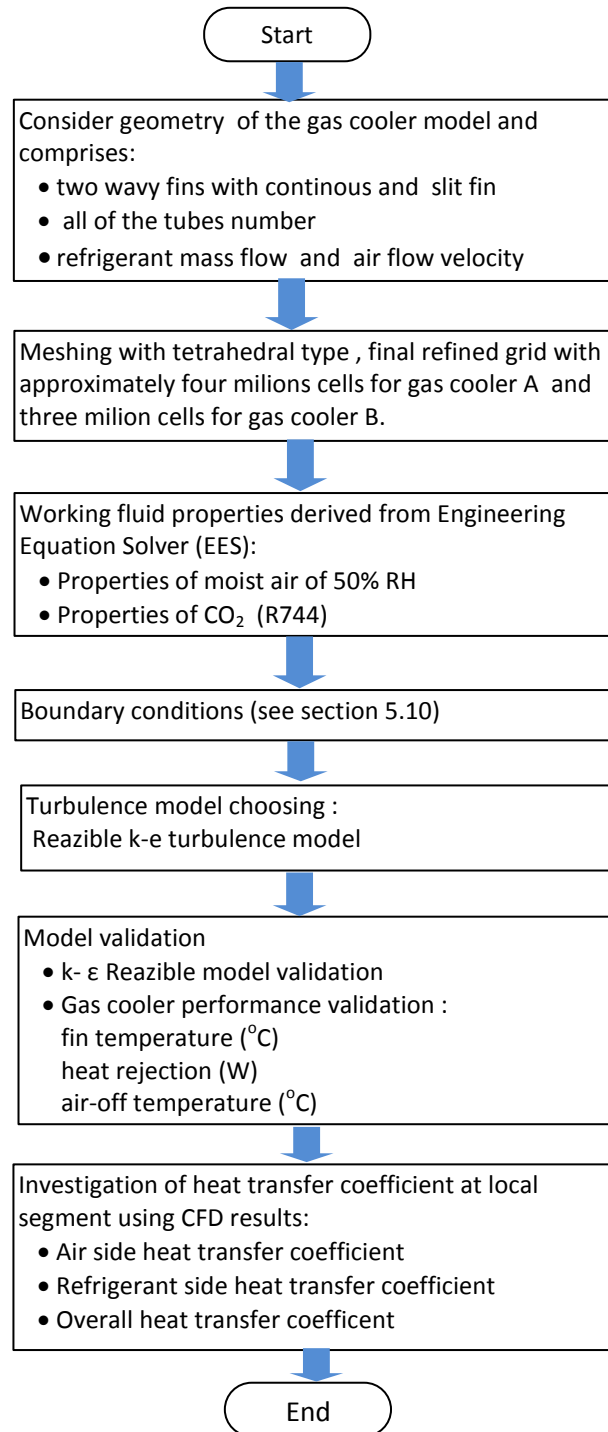


Figure 5.2 Schematic diagram of the gas cooler physical model simulation

5.2 Governing equations

The equations governing the flow and related heat transfer in a fluid are based on the conservation of mass, momentum and energy. These fundamental physical principles are expressed in the Navier-Stokes set of equations (equation 5.1-5.3), and because these are non-linear second-order equations, the solution procedure is complex. CFD therefore applies and solves the discretised form of these equations for a domain, through iterations, where the pressure (p), temperature (T), density (ρ) and velocity components (u , v , w) at each grid cell can be predicted with high accuracy (Gowreesunker and Tassou, 2013).

Continuity equation:

$$\frac{\partial \rho}{\partial t} + \frac{\partial}{\partial x_j} (\rho u_j) = S_M \quad (5.1)$$

Momentum equation:

$$\frac{\partial}{\partial t} (\rho u_j) + \frac{\partial}{\partial x_j} (\rho u_i u_j) = -\frac{\partial}{\partial x_j} (P) + \frac{\partial}{\partial x_j} (\bar{\tau}) + \rho g_j + F_j \quad (5.2)$$

Energy Equation:

$$\frac{\partial}{\partial t} (\rho H) = -\frac{\partial}{\partial x_j} (\rho u_j c_p T) + \frac{\partial}{\partial x_j} \left[\lambda \frac{\partial T}{\partial x_j} \right] + S_E \quad (5.3)$$

One of the challenging aspects of modelling systems where the thermodynamics of different fluids interact is to be able to appropriately distinguish between the different flows regimes of the different fluids. CO₂ and air flows consist of high- or low-turbulence regimes, especially important as the geometry of the heat exchanger and surface topologies become more complex. High Reynolds number flows provide higher heat transfer rates, compared to lower Reynolds flows, and the model needs to be able to capture this difference. The following section describes the required considerations for turbulence models in order to provide adequate results.

5.3 Turbulence in fluid dynamics

Turbulent flows are characterised by fluctuating velocity fields. These fluctuations affect transported quantities such as momentum, energy, and species concentration, and cause the transported quantities to fluctuate as well. Reynolds (1895) stated that any instantaneous value of the physical variables such as velocity, pressure, enthalpy, etc. can be expressed by its average value plus the fluctuating component.

For velocity this becomes:

$$u = \bar{u} + u' \quad (5.4)$$

The barred character is the mean velocity at a point in space defined by x, y and z coordinates and averaged over a time step t, (Reynolds, 1895):

$$\bar{u}_i = \lim_{t \rightarrow \infty} \frac{1}{\Delta t} \int_t^{t+\Delta t} u_i(t).dt \quad (5.5)$$

By equating each velocity component to a mean and fluctuating part, for example u' , Reynolds modified the classical governing equations into a time-averaged form. However, this averaging process also introduced some additional terms, known as the Reynolds stresses, which represent the rate at which momentum is transported or diffused by turbulent fluctuations. In their full form they can be presented as:

$$-\rho u'^2, -\rho v'^2, -\rho w'^2 \quad \text{Normal Stresses}$$

$$-\rho u'v', -\rho v'w', -\rho u'w' \quad \text{Shear Stresses}$$

The original Navier-Stokes equations form a closed set of simultaneous equations. The unknown Reynolds stresses, introduced by the averaging procedure, however, make the equations unsolvable, without introducing turbulent models.

5.4 Choosing turbulence model

Turbulent and laminar flow conditions are indicated by the Reynolds Number of the fluid flow and in this study the Reynolds Number calculated based on the fin collar diameter (D_c) for air side investigation this is because of the complex nature of the air

flow between the fins and over the tubes and the collar diameter directly contact to the air flow and influence most of the turbulence inside heat exchanger (Chang and Kim, 2006; Pu et al., 2009; Yun et al., 2009; Pongsoi et al, 2012). And then Wang et al.(1999) also built their fin geometry correlation with Reynolds Number depend on the collar diameter (D_c) as a characteristic length since they found that the correlation experimental data use of the hydraulic diameter (D_h) was not successful.

Hence, Reynolds Number depends on collar diameter (Re_{D_c}) is obtained from:

$$Re_{D_c} = \frac{\textit{inertia forces}}{\textit{viscous forces}} = \frac{\rho u^2 D_c^2}{\mu u D} = \frac{\rho u D_c}{\mu} \quad (5.6)$$

The heat exchanger in this study has collar diameter (D_c) of 8.32 mm and inner diameter (D_i) of 6.8 mm. The air side Reynold Number (Re_{D_c}) was found to be approximately 500 – 1200 corresponding to inlet air velocities 1 – 2.4 m/s. The Reynold Number for the refrigerant side was found approximately 3.5×10^4 up to 1.5×10^5 with corresponding to inlet mass flow rates of 0.01 kg/s to 0.02 kg/s. Conventionally, flows with $Re < 2000$ are considered laminar, while $Re > 4000$ implies turbulent flow. In this respect, the air flow can be considered laminar, while the refrigerant flow is turbulent. It is however difficult to find a universal turbulence model that exactly defines the flow regimes of both turbulent and laminar flows. Hence, the validity of the turbulence models is often evaluated with respect to the difference of the models with experimental data.

Previous studies have evaluated the performance of turbulence models for a variety of finned-tube heat exchanger problems. Butta et al. (2012) reviewed the application of CFD in various heat-exchanger design and optimisation studies and concluded that the $k-\varepsilon$ turbulence models have been most commonly used in previous studies, providing good agreement with experimental test results. The others model also most popular are $k-\omega$ standard and SST, but the option is dependent on the design heat exchanger being investigated. Singh et al. (2008) investigated the steady-state air-side heat transfer of a finned tube heat exchanger using the realizable $k-\varepsilon$ models with enhanced-wall function. The validation of the CFD numerical results with experimental data, provided with temperature and heat-transfer rate errors in the range of 4%. Bilirgen et al. (2013) used the RNG $k-\varepsilon$ model, where the air-flow is assumed to be incompressible and

steady-state. The model was mainly employed to investigate different fin thicknesses, heights, materials and air-flow Reynold Numbers. They concluded that as the thermal conductivity and fin height increase, heat transfer rate also increases, whilst the fin thickness had minor impact on the heat transfer and pressure drop. The model was however not experimentally validated. Sun and Zhang (2014) applied the realizable k-ε turbulence model, and found that the numerical results agree well with the reported experimental data for a finned-tube heat exchanger. The validation process was performed based on heat transfer coefficients and pressure drops in the heat-exchanger, and the errors were found to be in the range of 4.7-13.2%, respectively.

Nonetheless, the studies obtained relating to finned-tube heat exchangers were found to suggest that the realizable k-ε model has been more popular, as well as predicting valid results. Hence, for this study, the realizable k-ε model is employed, where its validity is investigated with respect to experimental data.

5.5 Realizable k-ε turbulence model

This section describes the Realizable k-ε model equation which is used in this study. Following the Boussinesq approach for the k-ε turbulence models, two additional sets of equations are to be solved: one for the turbulent kinetic energy (k); and one for the dissipation rate of kinetic energy (ε) (Launder and Spalding, 1972), which are then used to obtain the turbulent/eddy viscosity (μ_t) of the flow. The transport equations for k and ε in realizable k-ε model are:

$$\frac{\partial}{\partial t}(\rho k) + \frac{\partial}{\partial x_j}(\rho k u_j) = \frac{\partial}{\partial x_j} \left[\left(\mu + \frac{\mu_t}{\sigma_k} \right) \frac{\partial k}{\partial x_j} \right] + G_k + G_b - \rho \epsilon - Y_M + S_k \quad (5.7)$$

$$\frac{\partial}{\partial t}(\rho \epsilon) + \frac{\partial}{\partial x_j}(\rho \epsilon u_j) = \frac{\partial}{\partial x_j} \left[\left(\mu + \frac{\mu_t}{\sigma_\epsilon} \right) \frac{\partial \epsilon}{\partial x_j} \right] + \rho C_1 S \epsilon - \rho C_2 \frac{\epsilon^2}{k + \sqrt{v \epsilon}} + C_{1\epsilon} \frac{\epsilon}{k} C_{3\epsilon} G_b + S_\epsilon \quad (5.8)$$

Where,

$$C_1 = \max \left[0.43, \frac{\eta}{\eta + 5} \right], \eta = S \frac{k}{\epsilon}, S = \sqrt{2 S_{ij} S_{ij}} \quad (5.9)$$

In these equations, G_k represents the generation of turbulence kinetic energy due to the mean velocity gradients, calculated as described in modelling turbulence production in

k- ϵ models. G_b is the generation of turbulence kinetic energy due to buoyancy, calculated as described in effect of buoyancy on turbulence in the k- ϵ models. Y_M represents the contribution of the fluctuating dilation in compressible turbulence to the overall dissipation rate, calculated as described in effects of compressibility on turbulence in the k- ϵ models. C_2 and $C_{1\epsilon}$ are constants. σ_k and σ_ϵ are turbulence Prandtl numbers for k and ϵ , S_k and S_ϵ are user-defined source terms. The k equation is the same as that in the standard k- ϵ and the RNG k- ϵ model, except for the model constants. However, the form of the ϵ equation is different from those in the standard and RNG based k- ϵ model. One of the noteworthy features is that the production term in the ϵ equation does not involve the production of k (ANSYS FLUENT Theory Guide, 2013).

5.6 Shell conduction in heat exchanger fins

The thin wall shell conduction property in ANSYS FLUENT® was employed in order to compute the heat conduction through the fin. This shell conduction allows to more conveniently model heat conduction on walls where the wall thickness is small with respect to the overall geometry (e.g., finned heat exchangers). Meshing these walls with solid cells would lead to high-aspect-ratio meshes and a significant increase in the total number of cells (ANSYS FLUENT theory guide, 2013).

5.7 Working fluid properties

The properties of the fluid used in the heat exchanger are moist air and CO₂ (R744) properties, derived from the Engineering Equation Solver (EES®) numerical package, the air properties are described in Table 5.1.

Table 5.1 Air properties

Temperature (K)	Density ρ (kg/m ³)	Specific heat c_p (J/kg-K)	Viscosity μ (kg/m-s)	Thermal conductivity k (W/m-K)
0	1.248	1031	1.73e-5	0.02368
100	0.9138	1035	2.18e-5	0.03106

Properties values were derived from EES program at pressure 103.3 kPa

Furthermore, the properties of the CO₂ refrigerant were also derived from EES® over a temperature range between 40 °C and 160 °C. The properties are described as a function of pressure and temperature as shown in Figure 5.3 and 5.4. These properties were used in ANSYS for the simulations and configured as piecewise-linear.

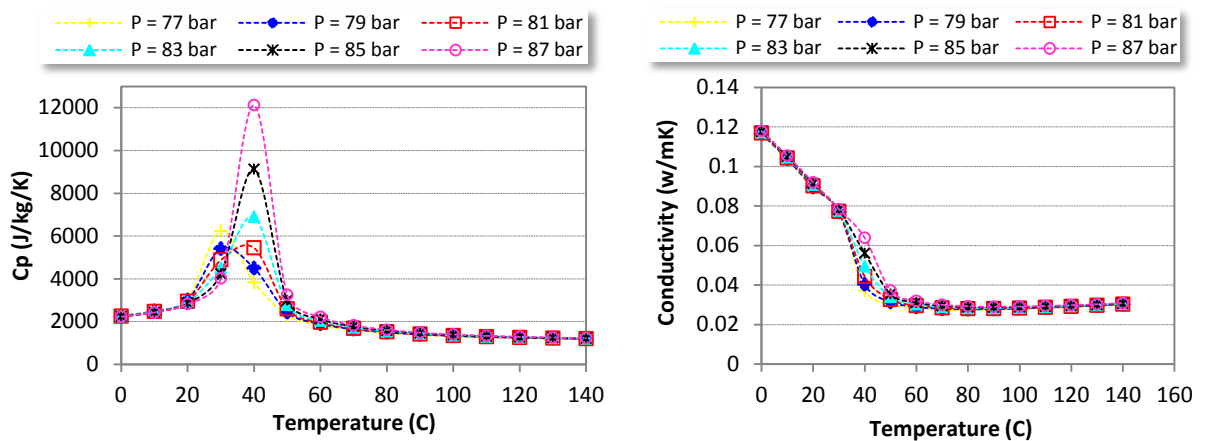


Figure 5.3 Variation of c_p and thermal conductivity of CO_2 with temperature for several working pressures
(Derived : EES®Program)

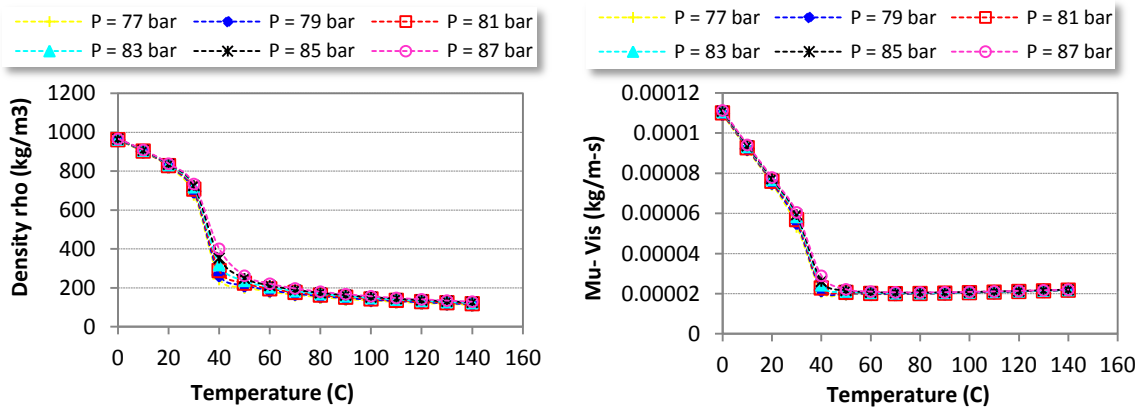


Figure 5.4 Variation of density and viscosity of CO_2 with temperature for several working pressures (Derived : EES®Program)

5.8 CFD geometry design of gas cooler heat exchanger

The main tube arrangement of the gas cooler in this study are gas cooler-A (3-row-4 circuit) and gas cooler-B (2- row- 2 circuit) as described in Chapter 4. To build the model geometry, individual segments from the entire gas cooler were considered in order to provide a representation of the gas cooler performance. It not possible to model the entire gas cooler because of the large number of fins and extensive computing resources required to model such complex gas coolers.

This model is designed to investigate the heat transfer coefficients of the heat exchanger. The heat transfer coefficients are crucial parameters to assess the heat exchanger performance, and the model was designed to enable the investigation of the air-side, refrigerant-side and overall/total heat transfer coefficients at each segment, for

individual pipes. This gas cooler model considers the air flow, refrigerant mass flow, fin wall and tube wall simultaneously, in order to adequately account for the interaction of the different aspects of the gas cooler. The wavy fin is made from aluminium with cooper tubes, and the design is shown in Figure. 5.5.

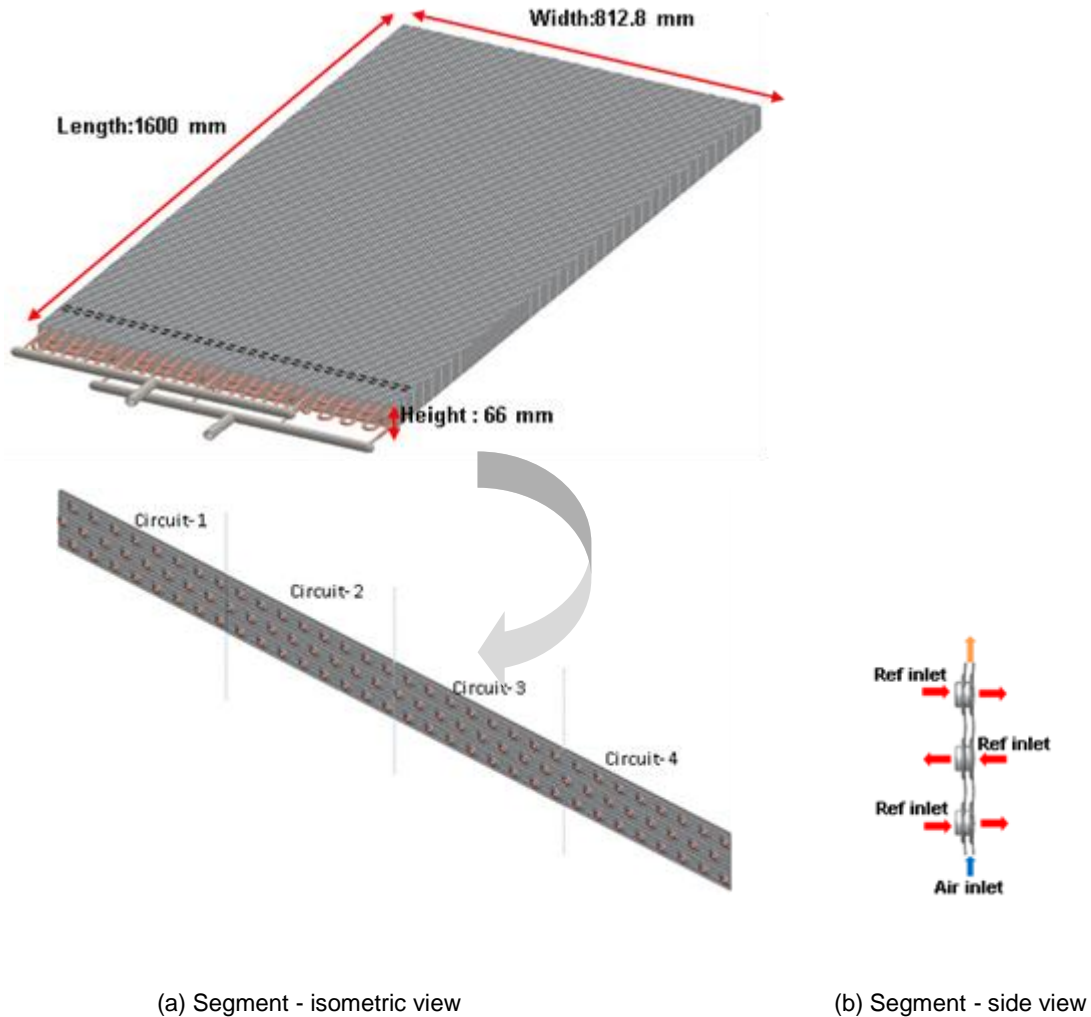


Figure 5.5 CFD Gas cooler geometry (i.e. gas cooler- A)

5.9 Meshing

The model was meshed using tetrahedral type elements and three different numbers of cells. The mesh sensitivity analysis was performed with respect to the residual convergence of the models. Using the coarse (1.2 million cells), medium (3.2 million cells) grids for gas cooler-A, and coarse (0.8 million), medium (2.1 million cells) for gas cooler-B, the residuals' convergence reached to a minimum of 10^{-4} for continuity, 10^{-7} for energy, 10^{-3} for x, y and z, 10^{-3} for k and 10^{-2} for ϵ , whilst the fine grid were found to have residuals in the order of 10^{-5} , 10^{-8} , 10^{-6} , 10^{-4} and 10^{-4} , respectively.

Following the satisfactory residuals obtained from the fine grid, the latter was used for subsequent simulations. However, this more refined grid also involved a higher computing time. The final mesh is shown in Figure 5.6 for gas cooler-A and Figure 5.7 for gas cooler-B, whereby high grid densities have been used in all areas where high temperature gradients were more likely to occur such as the fin collars and the close surroundings of the tube.

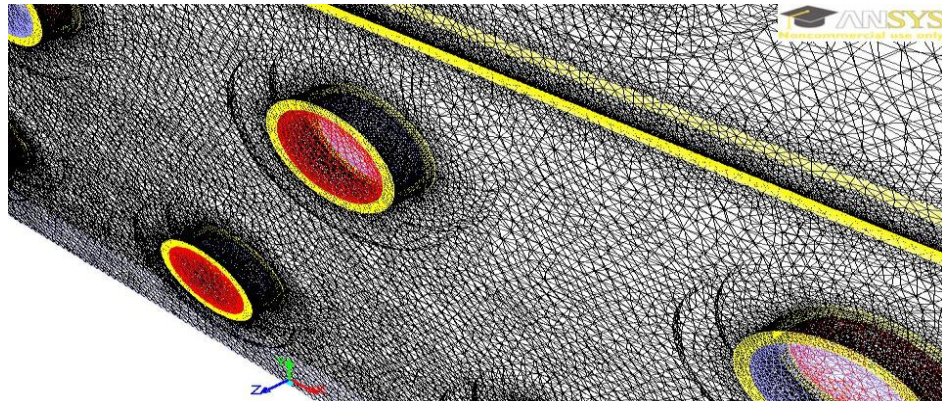


Figure 5.6 Mesh of gas cooler-A

Meshing was performed using tetrahedral type elements and the total number of cells for the fine grid was 4,238,766 cells and 2,825,844 cells for gas-cooler A and gas-cooler B, respectively. More cells could provide better accuracy but require significantly more computing time.

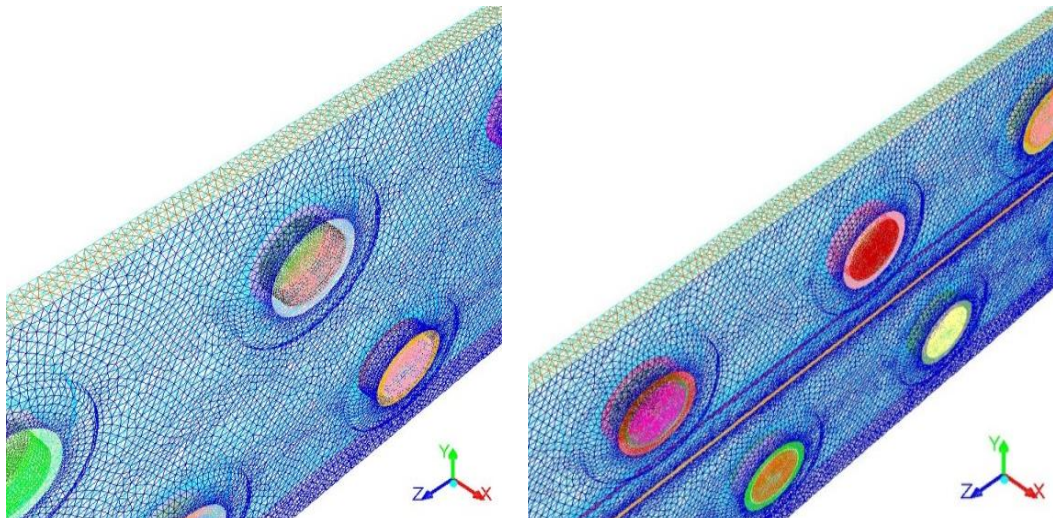


Figure 5.7 Mesh of gas-cooler B

5.10 CFD Boundary Conditions

The model consists of a 2.12 mm air gap between fins, a 0.16 mm thick wavy aluminium fin and 8 mm outer-diameter copper tubes, with a thickness of 1.68 mm and a refrigerant flow inner the tubes. The model simulated the heat transfer performance for five individual segments of the gas cooler, placed at five distances along the refrigerant tubes (0 m; 400 mm; 800 mm; 1200 mm; 1600 mm) from the inlet, as shown in Figure 5.8.

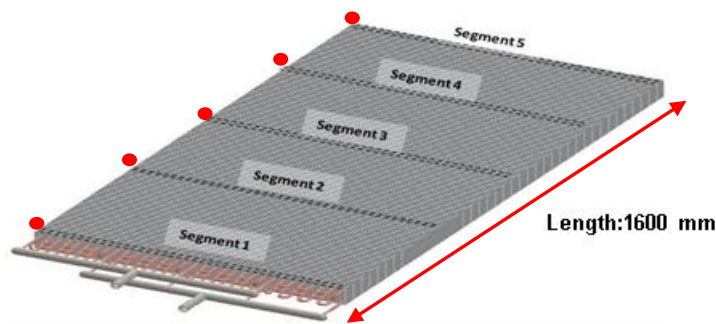


Figure 5.8 Segment positions along the 1600 mm length gas cooler

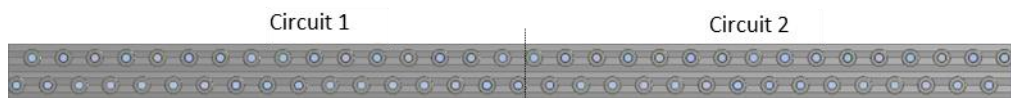
Since the fins are only 0.16 mm thick, the meshing of such a thin surface was found to be problematic in terms of the mesh type and size, especially when considered in the context of the overall gas cooler domain. Hence, the concept of thin-wall shell conduction available in ANSYS FLUENT® was employed (explained briefly in Section 5.6). This refers to the simplification of the material heat transfer discretisation to a single node within the thickness, therefore avoiding meshing to very small levels. This allows for a more convenient representation of heat conduction within the fin, and is also suggested by ANSYS FLUENT® to model such finned heat-exchangers (ANSYS FLUENT theory guide, 2013).

The boundary conditions used in the present study with reference to Figure 5.9 were defined as follows:

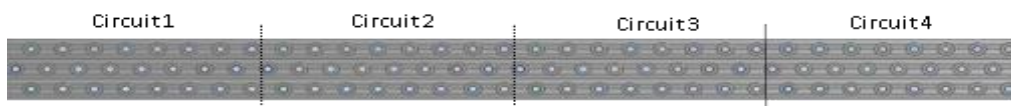
- The experimental refrigerant inlet mass flow rate, temperatures and pressure of each tube were input to the model segments. The temperatures were varied for the different locations of the segments along the refrigerant tubes (see Figure

5.10), whereby linear interpolation was assumed in order to define the refrigerant inlet temperatures in the inner segments.

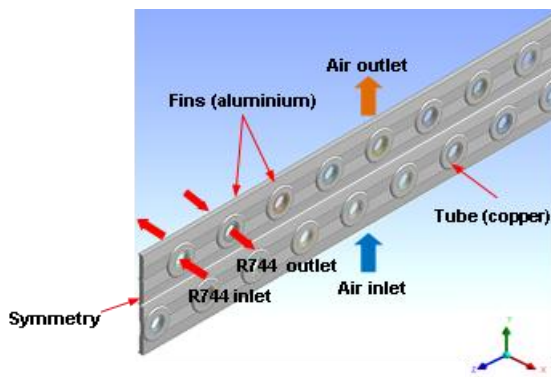
- The air enters between two fins (y-direction), at a constant velocity of 1.0 m/s, 1.3 m/s, 1.7 m/s, 2.0 m/s, 2.4 m/s and the respective inlet air temperature, similar to the experimental parameters.
- The fins and fin collar were modelled as thin-walls.
- The thermo-physical properties (density, viscosity, specific heat capacity, thermal conductivity) of air and refrigerant (R744) as a function of temperature and pressure were obtained using the Engineering Equation Solver (EES) software as shown in Figure 5.3 ad 5.4 and Table 5.1. These were incorporated using the piecewise-linear formulation in FLUENT®
- The thermo-physical properties of copper and aluminium are obtained from the FLUENT® database.



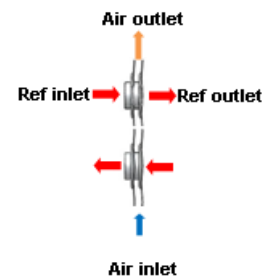
(a) Gas cooler-B (front view)



(b) Gas cooler-A (front view)



(c) Gas cooler-B (isometric view)



(d) Gas cooler-B (side view)

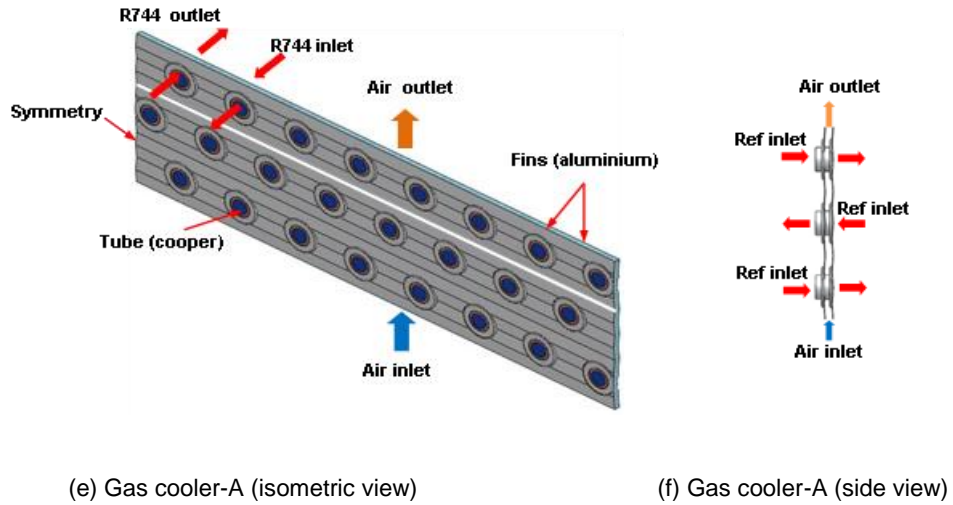


Figure 5.9 Boundary condition for gas coolers-A and B

The simulations were conducted on a 2.6GHz, 32GB RAM, Intel Xeon[®] Processor with 16 parallel threads, with a mean computing time of 4 hours. The simulations were carried out under steady-state and 3-dimensional conditions.

The inlet refrigerant temperature was taken from experimental tests on a finned tube gas cooler operating in supercritical mode. An example temperatures profiles along the tube for gas cooler-A and B at identical test conditions is shown in Figure 5.10 and for more detailed the input data for the CFD model is given in Appendix F.

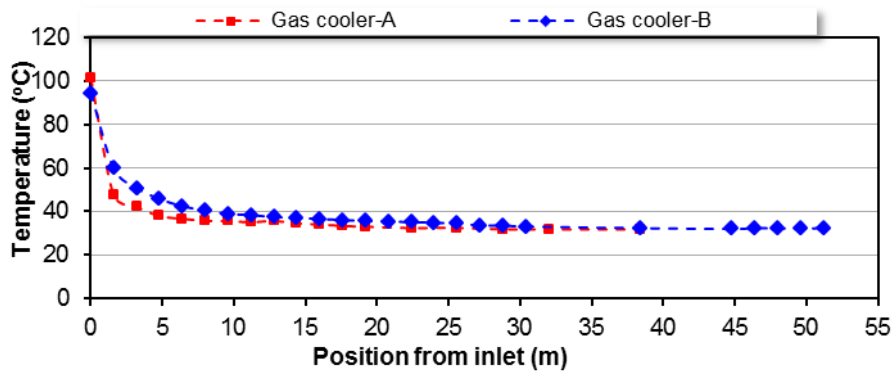


Figure 5.10 Coil tube temperature for inlet refrigerant boundary condition for gas cooler-A and gas cooler-B at identical test procedure

In addition to having simulations with adequate convergence criteria, the turbulence model influences the final simulation results (Bhutta et al, 2012). In this regards, the models' sensitivities were further analysed using different turbulence model available in

the FLUENT® package. These turbulence models include Standard, Realizable and Renormalisation Group (RNG) $k-\epsilon$ models; Standard and SST $k-\omega$ models, and the laminar model. The numerical results with different turbulence models are compared with experimental data, in order to determine the validity of each turbulence model as explained in Section 5.11.1.

5.11 Validation of the CFD Models against Experimental Results

The validation study is based on three main parameters, consisting firstly of determining the performance of the turbulence model, secondly of the comparison of the experimental and numerical fin temperatures, and lastly obtaining model errors for different test conditions. The validation process was conducted with respect to the heat rejection rate (Q) in the gas coolers and temperature air-off (outlet) for different experimental test conditions. Both the air-off temperature ($T_{\text{air-off}}$) and the heat rejection rate (Q) were obtained from the mean values of the five simulated segments for each experimental condition as described in Section 5.12.2 and 5.12.3. The validation procedure includes comparison between predicted CFD parameters and the experimental results.

5.11.1 Turbulence model (k- ϵ Realizable) validation

In this validation stage, two parameters of the heat exchanger performance were investigated: the heat rejection (Q) and the temperature of air –off ($T_{\text{air-off}}$). Figure 5.11 shows the comparison of the different turbulence models applied in the model against the test results for certain test condition (velocity 1.7 m/s) (other conditions had similar performances). The $k-\epsilon$ turbulence models were found to have better performance for both the heat released with relative error (%) and air-off temperatures with absolute error (Standard: 8.7%, 0.49°C errors; RNG: 7%, 0.17°C errors; Realizable: 5.9%, 0.14°C errors); the $k-\omega$ models showed slightly worse performance (Standard: 9.3%, 0.63°C errors and SST: 9.5%, 0.65°C errors) compared to the $k-\epsilon$ models; whilst the laminar model had errors of 38.3%, 2.62°C. The laminar model has the highest error, as it does not account for the turbulent effects in refrigerant flow. Hence, as the Realizable $k-\epsilon$ model showed the lowest error, it has been adopted for the simulations.

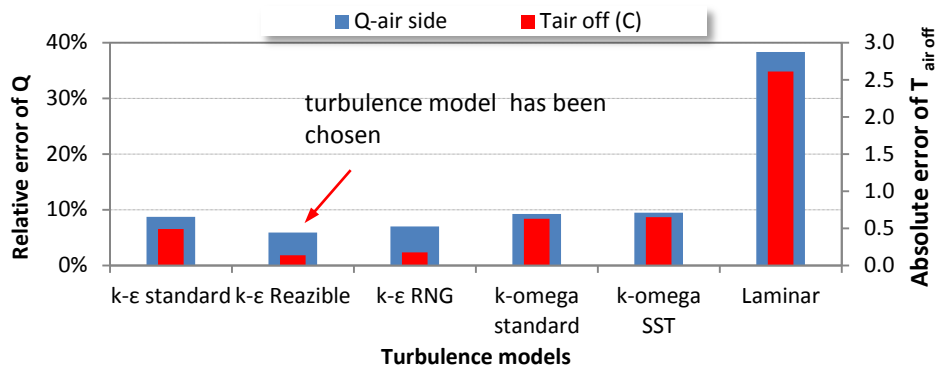


Figure 5.11 Turbulence model errors

5.11.2 Fin temperature validation

Figure 5.12 shows the diagram of the locations of the thermocouples in the gas cooler at the fin tips and fin collars.

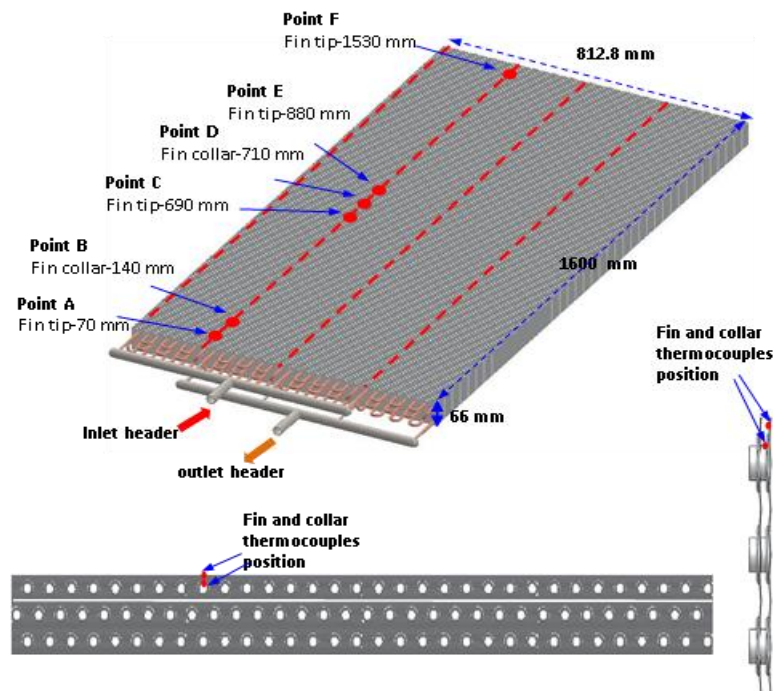


Figure 5.12 Fin temperature measurement positions – experimental tests

The model considered an air-inlet boundary temperature of 32.77 °C, operational pressure 84 bar_g and an air-inlet velocity of 1.7 m/s. The model resulted in temperature profiles of the fin tip (T_t) at fin segment distances of 70 mm, 690 mm, 880mm and 1530 mm from the inlet along line A (fin tip) and temperature profiles of fin collar (T_c) at fin segment distances of 140 mm, 710 mm is investigated along line B. Line A is positioned at 64 mm from the bottom or 2 mm from the top, which is similar to the

thermocouple positions. Line B is positioned at 59 mm from the bottom, as shown in Figure 5.13.

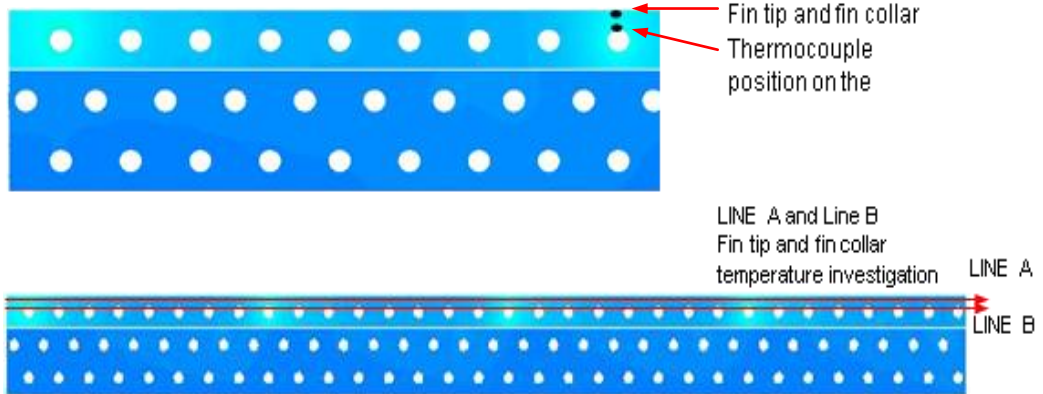


Figure 5.13 Fin temperature investigation with CFD

The model results of the fin tip temperature profiles (Line A) at 70 mm (Point A), 690 mm (Point C), 880 mm (Point E) and 1530 (Point F) mm segments position from the inlet are shown Figure 5.14.

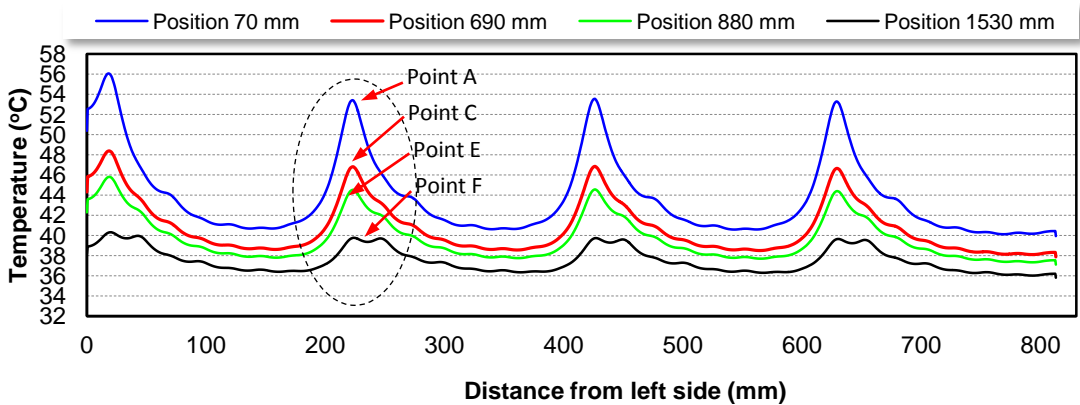


Figure 5.14 Temperature profile along each fin - LINE A

The modelled fin collar temperature profiles along Line B, 140 mm (Point B) and 710 mm (Point D) distances from the inlet, are shown in Figure 5.15.

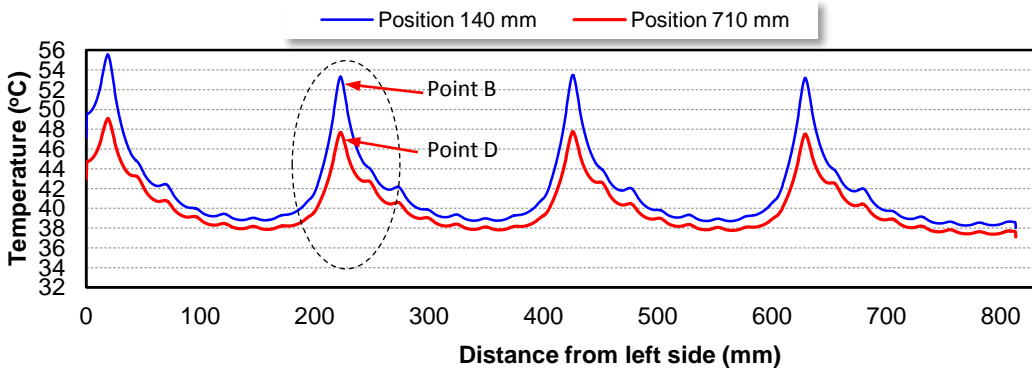


Figure 5.15 Temperature profile of fin collar-LINE B

The temperatures of fin-tip and fin-collar, obtained from the model at similar positions with the test are tabulated in Table 5.2.

Table 5.2 Comparison between experimental and model results for fin temperature

Points - distance of fin segment from inlet	Point A (70 mm)		Point B (140 mm)		Point C (690mm)		Point D (710 mm)		Point E (880 mm)		Point F (1530 mm)	
	Fin tip	Fin collar	Fin tip	Fin collar	Fin tip	Fin collar	Fin tip	Fin collar	Fin tip	Fin collar	Fin tip	Fin collar
Temp. Test results (°C)	56.8	-	-	55.4	47.9	-	-	48.3	45.2	-	41.2	-
Temp. Model results (°C)	53.6	-	-	53	46.5	-	-	47	44	-	39.8	-
Errors	3.2	-	-	2.4	1.4	-	-	1.3	1.2	-	1.4	-

The maximum absolute error of fin tip temperature is 3.2 °C, occurring at point A. This is due to Point A being located in the front position of the gas cooler, which may infer that the uneven air distribution in the experiment, the velocity and temperature may be different compared to the constant parameter input in the CFD model. In other positions, the absolute errors are lower than 1.5 °C.

5.11.3 Errors in prediction of heat rejection (Q) and air-off temperature ($T_{\text{air-off}}$)

This section compares the simulation results with experimental data with respect to the relative and absolute errors for heat rejection and air-off temperature, respectively, for different experimental test conditions. Both the air-off temperature and the heat rejection rate were obtained from the mean values of the five simulated segments for each experimental condition. The validation procedure consists of the comparison between predicted CFD parameters and the experimental results. The validation results are shown in Figure 5.16.

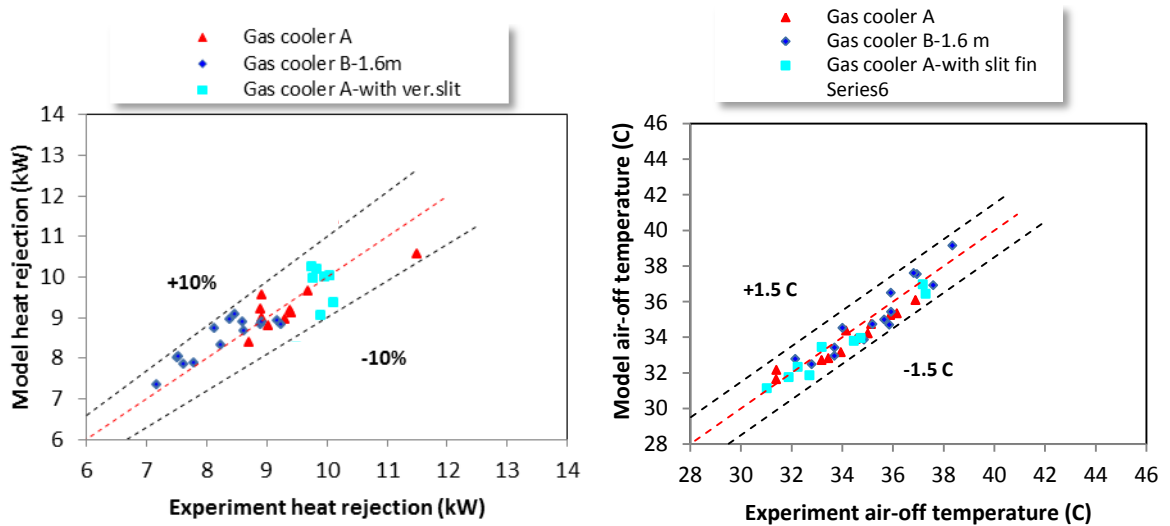


Figure 5.16 Model validation using heat rejection and air-off (outlet) temperature parameters

It can be seen from Figure 5.16 that the maximum error in the prediction of heat rejection was in the region of $\pm 10\%$ relative to the experimental heat rejection rates in the gas cooler, and a maximum absolute error of 1.5°C in the air-off temperatures. However, the mean heat rejection rate error was found to be 4.7% , and the mean air-off temperature was 0.57°C . Hence, for the purpose of this study, as the mean temperature error is within the uncertainty of the thermocouples and the relative mean error for the heat rejection rate is less than 5% , the simulation results are deemed to provide an accurate depiction of the air temperature changes across the heat exchanger. The model is therefore able to adequately predict the performance of the heat exchanger.

5.12 Post-Processing

As explained in Section 5.10, the gas cooler is divided in five segments to provide a representation of the entire gas cooler. The post processing results below display the fluid flow and temperature in each segment. Figure 5.17 shows a fin wall, tube wall temperature contours, air-flow path line and refrigerant-flow vectors of the gas cooler-A which was obtained from the first segment (refer to Figure 5.18). Three different fin designs consisting of continuous, horizontal and vertical & horizontal slit fins as explained in Section 4.2 is shown.

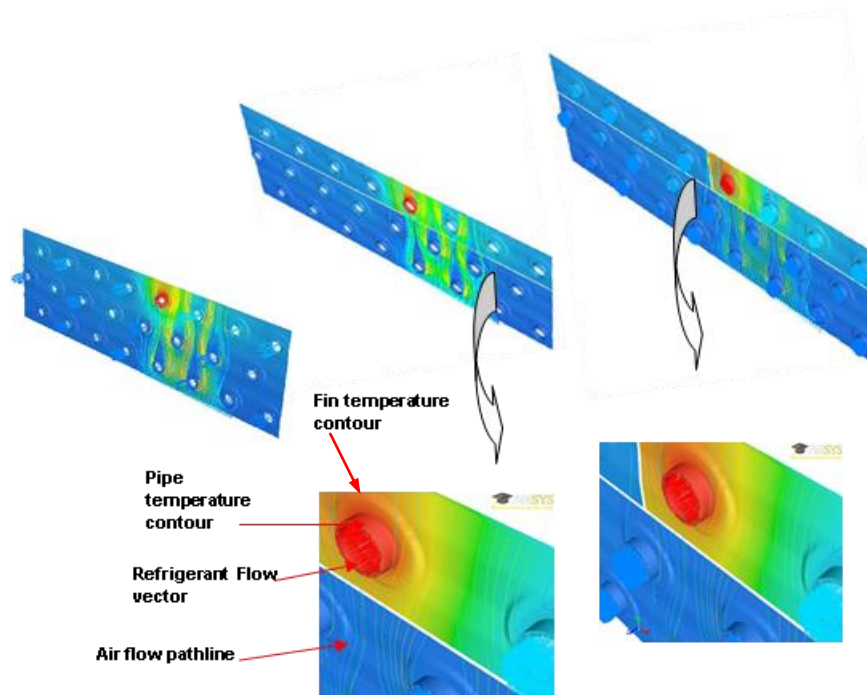


Figure 5.17 Temperature contour, velocity vector and path line of the CFD-post processing

5.12.1 Fin and pipe temperatures contours in five segments

Figure 5.18 and Figure 5.19 shows temperature contours for different segments along the coil length for a horizontal slit fin gas cooler. The segment position is corresponding to Figure 5.8.

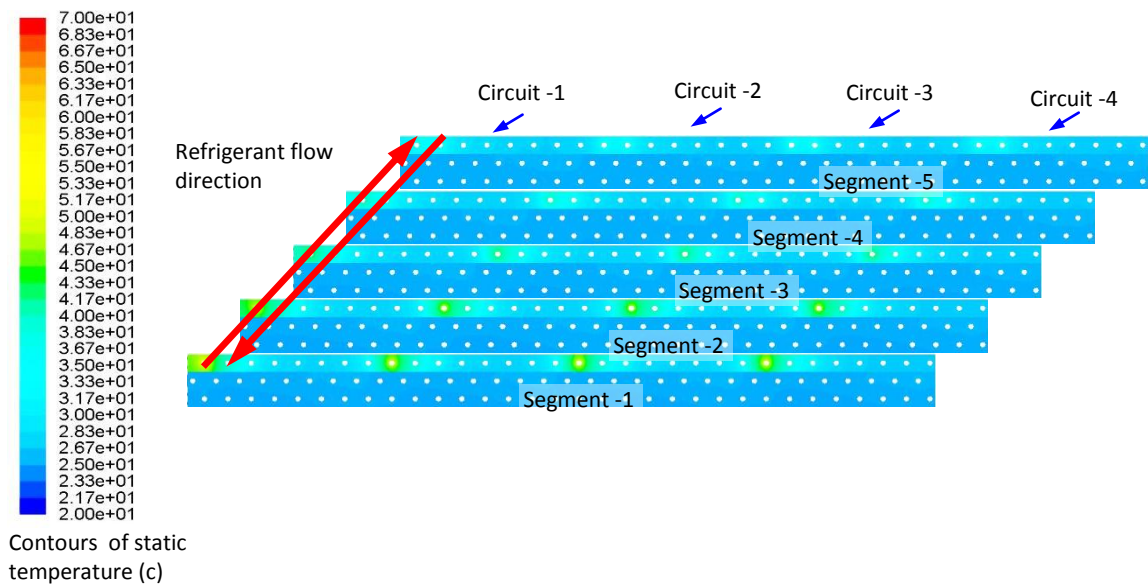


Figure 5.18 Fin temperature contour in each segment (gas cooler A)

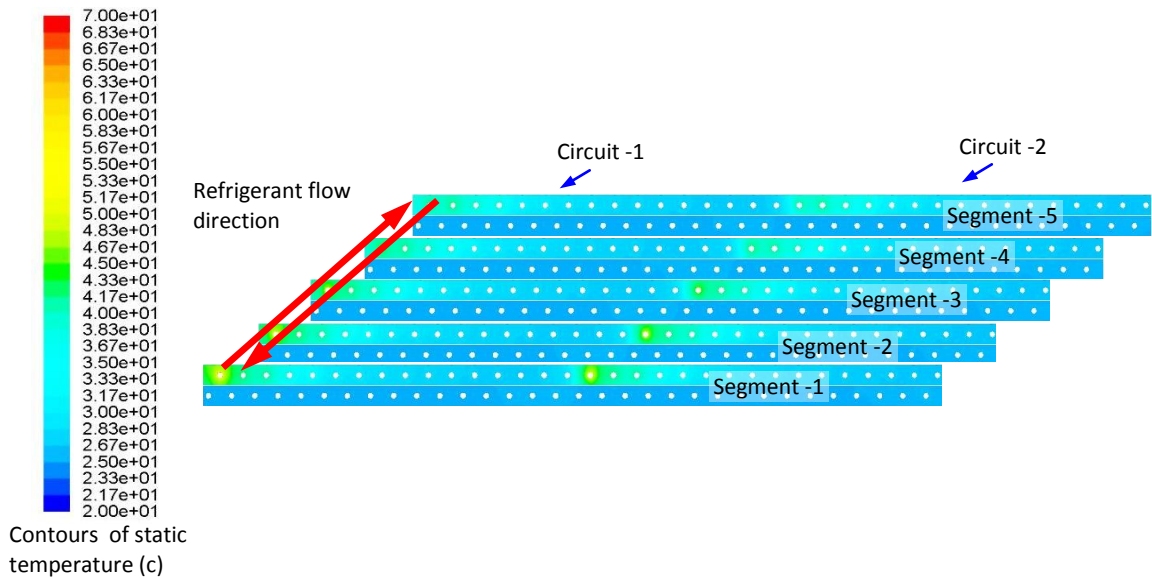


Figure 5.19 Fin temperature contour in each segment (gas cooler B)

The fin temperature contours were found to be identical for the different boundary conditions. As portrayed in Figures 5.18 and 5.19, gas cooler-A comprises 4-circuits and 2-circuits for gas cooler-B (basing the observation on the temperature contours). These figures also illustrate that only the first pipe of gas cooler-A and first three pipes of gas cooler-B have significantly higher temperature comparing than the others pipes.

From segment-1 to segment-5, the temperature gradually decreases as the refrigerant loses heat to the surrounding air. Between gas cooler-A and B, the temperature drop between each segment is faster in gas cooler-A, as confirmed by the temperature drop profile in the pipe shown in Figure 5.10. The detailed explanation on the fin temperature profile was explained in Section 5.11.2 (Fin validation temperature).

5.12.2 Air temperature and velocity contours

The air temperature profile was plotted according to row positions, in the direction of the air-inlet to outlet, gas coolers-A and B, as shown in Figures 5.20 and Figure 5.21, respectively. The variations of the air temperature profile in each row of gas cooler-A is shown in Figure 5.20 and this temperature profile will be used to calculate the heat rejection (Q) in each segment in order to investigate the heat transfer coefficient for the Chapter 6 and Chapter 7.

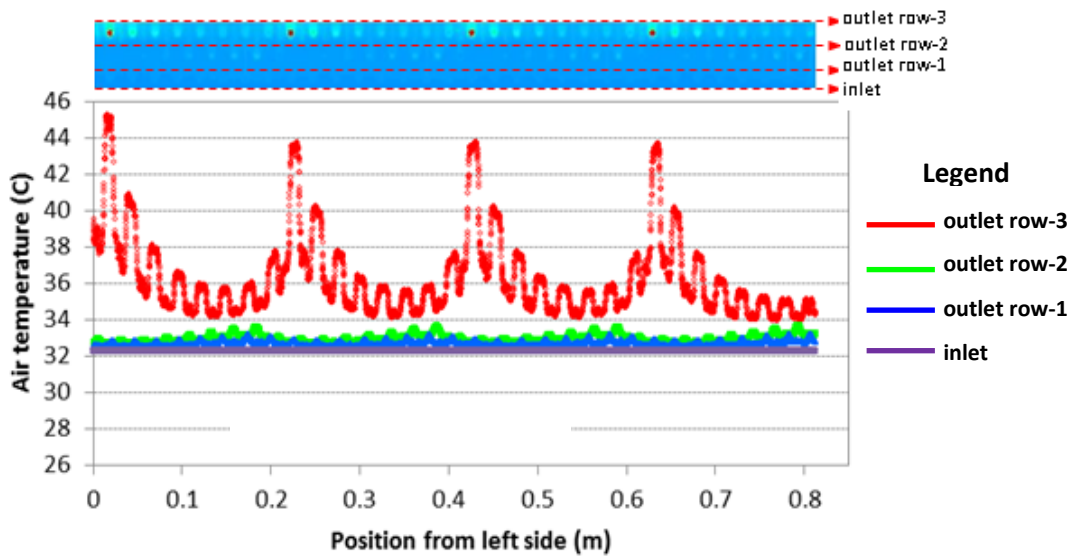


Figure 5.20 Air temperature contour and plot of gas cooler-A
 (This result based on horizontal slit fin-Figure 5.17-segment-3)

The row positions for gas cooler-B are described as inlet, middle and outlet temperature as shown in Figure 5.21. The inlet condition is similar with the condition that explained in Figure 5.19-segment 3.

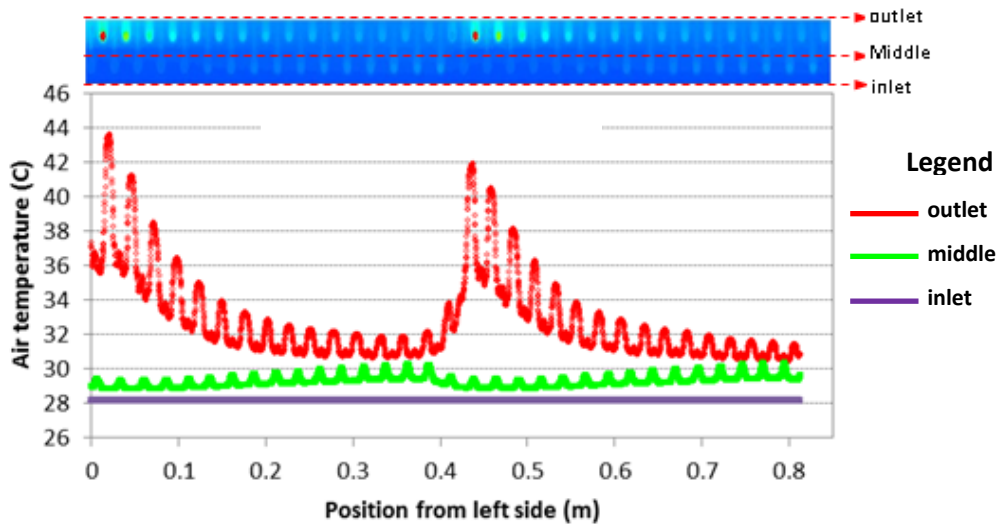
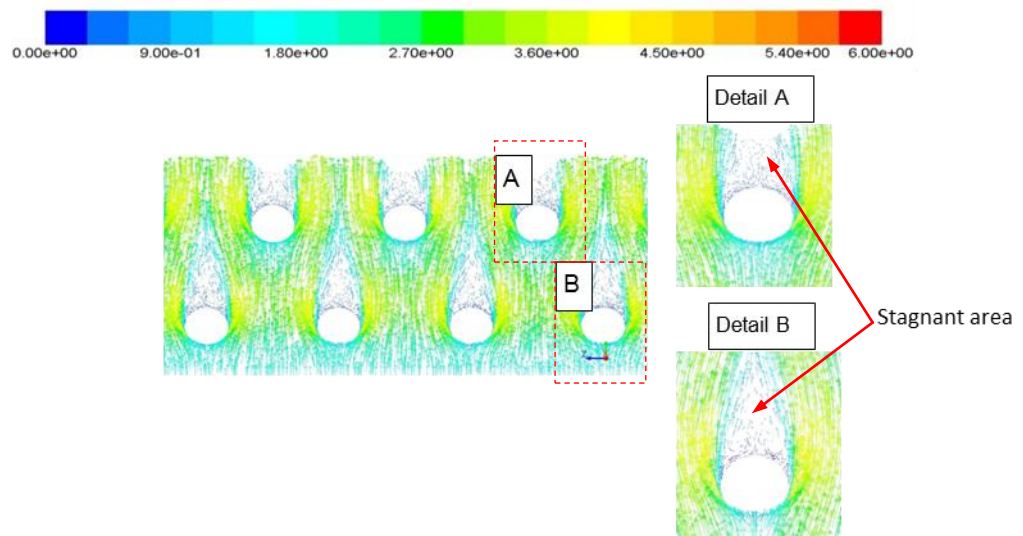


Figure 5.21 Air temperature contour and plot of gas cooler-B
 (This result based on horizontal slit fin-Figure 5.18-segment-3)

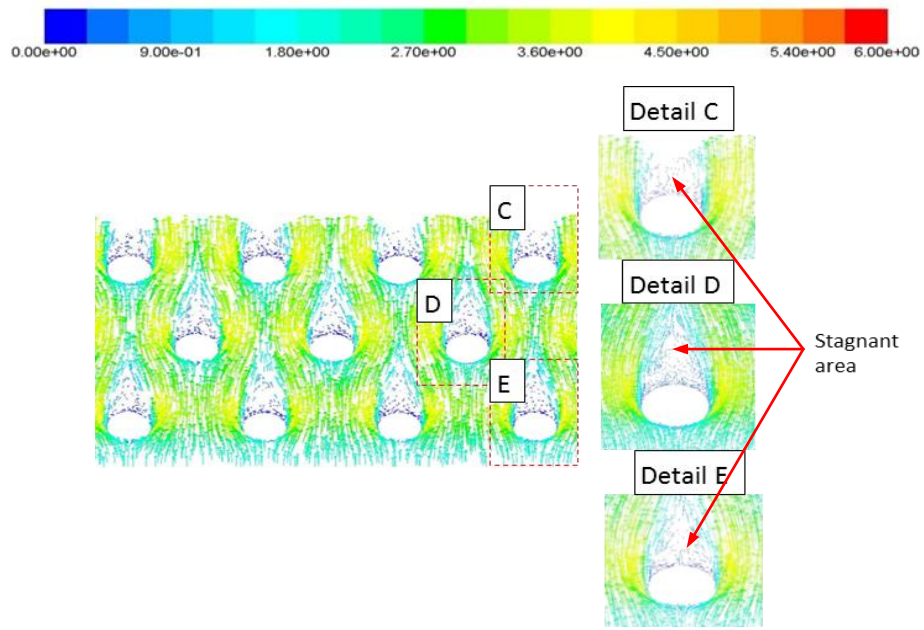
Figure 5.22 shows the air velocity vector on the heat exchanger with the colour depicting the velocity magnitudes, with an inlet air velocity of 2 m/s for gas cooler –A and gas cooler-B. It can be seen that because of the turbulence effect around the tube,

led to the velocity increasing after the air reach the tube and there is vortex around the tube.

The flow characteristics in the heat exchanger flow passage are strongly affected by the presence of both cylinders and fin. Flow of fluid between adjacent fins and around the tube results is naturally complex. In order to explain this phenomenon, in the Figure 5.22 also presents flow characteristic in each row of the gas cooler. Each row has a weak/stagnant formation on the rear pipe/tube. The larger stagnant area occurs at the row-2 of gas cooler-B, whilst for gas cooler-A, the middle row has the best vortex/turbulence flow and at row-3 also has the largest stagnant area. Heat transfer problem in the heat exchangers is strongly related to the flow structure (Sahin et al., 2006). In the each row better vortex may provide a better mixing of the air flow and (Wang et al., 1999) implied that higher heat transfer performance is likely due to the vortex shedding.



(a) Air flow characteristic of gas cooler-B



(b) Air flow characteristic of gas cooler-A

Figure 5.22 Velocity vector of gas cooler-B and A at air velocity inlet of 2 m/s

Figure 5.23 shows the average air-off (outlet) temperatures at all segments of gas coolers A and B. It can be seen that the average of outlet temperatures gradually decreased from segment-1 to segment-5 (segment refer to Figure 5.18 and 5.19), due to the temperature in pipe-1 dominating the mean segment temperature. To calculate the outlet temperature of the whole gas cooler was done by calculate the average of outlet temperature at all segments.

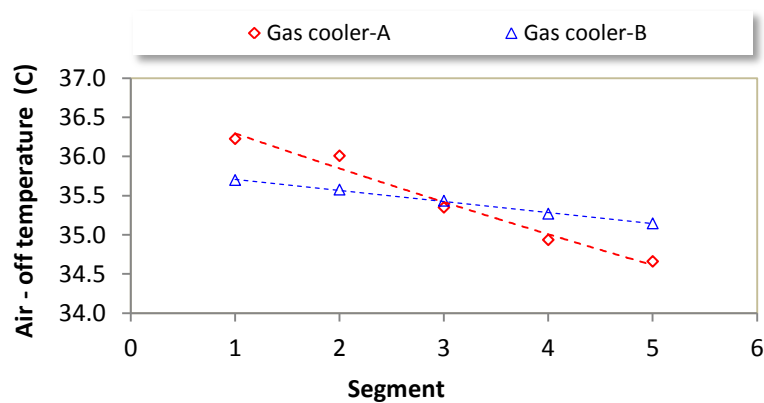


Figure 5.23 Average air - off temperature in each segment
 (Air on : GC-A=32.2°C, GC-B=32.4°C, \dot{m}_{air} : 0.00334 kg/s)

When comparing gas coolers-A and B, it can be inferred that the temperature drop in each segment is higher for gas cooler-A, due to the temperature profile of the refrigerant along the coil and the higher heat rejection capacity of gas cooler-A, compared to gas cooler-B (as describe in Section 4.6.4)

5.12.3 Heat Rejection (Q) in the CFD model

Similar with the outlet temperature in each segment described in Section 5.12.2, the heat rejection rates (Q) from segment-1 to segment-5 for both gas coolers-A and B are shown in Figure 5.24 (refer to Figure 5.18 and 5.19 for the location of the segment numbers). It can be seen that the heat rejection also decreased gradually from the front to the rear segments, where the drop gradient increased for gas cooler-A. This trend is also observed with the temperature contour in Figure 5.18 and 5.19.

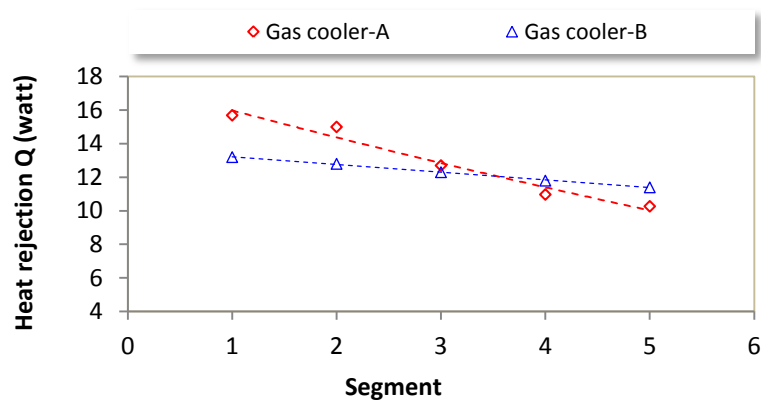


Figure 5.24 Average heat rejection (Q) at each segment
(Air on: Gas cooler-A=32.2°C, Gas cooler-B=32.4°C, \dot{m}_{air} : 0.00334 kg/s)

Since the segment is a controlled volume of the entire gas cooler, so that the heat rejection of the entire gas cooler model is calculated with equation as follows:

$$Q_{\text{gas cooler}} = \text{Avg.}Q_{\text{segment}} \times \text{Ratio} \quad (\text{Watt}) \quad (5.10)$$

Where, the ‘Avg. Q_{segment} ’ is average of heat rejection rate of all segments as shown in Figure 5.24. Furthermore, the ratio is the entire gas cooler volume divided by the segment volume. Based on the volume between segment and whole gas cooler, it was found that the ratio is 656 (gas cooler has 1600 mm length and segment has 2.44 mm total length with similar cross-sectional area as shown in Figure 5.5).

5.13 Summary

This chapter described the CFD models and simulation methodology for evaluating the performance of the finned- tube gas cooler with CO₂ as the working fluid and operating in supercritical condition. The gas coolers were modelled in individual segments at different distances to mimic the entire gas cooler. The CFD solves the discretized governing flow equations in a particular flow domain, in order to provide mainly temperature and velocity fields.

The model has been validated against experimental data obtained from the test results. The k- ϵ turbulence models were found have better performance than k- ω models and laminar model. Realizable k- ϵ turbulence has the best performance among k- ϵ turbulence models (Standard and RNG). The maximum error in the prediction of heat rejection was $\pm 10\%$ relative to the experimental heat rejection rates in the gas cooler, and a maximum absolute error of 1.5°C in the air-off temperatures. However, the mean heat rejection rate error was found to be 4.7%, and the mean air-off temperature error was 0.57 °C. The CFD results showed that by modelling segments, the overall performance of the gas cooler can be obtained with adequate accuracy, as depicted the mean errors obtained. The post processing results of the CFD model also obtained the segment temperature contour and the air flow characteristics which will be useful to investigate the heat transfer coefficient for the next chapters.

Chapter 6 deals with the investigation of the air-side heat transfer coefficients using the CFD models. The air side heat transfer coefficient investigated in segment in order to get a profile along the gas coolers.

CHAPTER VI – INVESTIGATION OF THE AIR-SIDE HEAT TRANSFER COEFFICIENT

6.1 Introduction

This chapter presents the air-side heat transfer coefficients (hc_a) for gas cooler B continuous and horizontal slit fins, and gas cooler-A continuous, horizontal slit fins and vertical & horizontal slit fins. The hc_a was investigated for individual segments of the gas cooler, and the specification of gas cooler- A and gas cooler- B described in Chapter 4. The hc_a in this study are calculated implicitly in the CFD model explained and validated in Chapter 5. The average heat transfer coefficient correlation of the gas coolers with respect to collar diameter Reynolds Number (Re_{D_c}) are then determined and employed to explain the performance of the gas cooler.

6.2 Calculation of air side -heat transfer coefficient

The finned and tube heat exchanger type is one of the most favourable heat exchanger for industrial application. In general, flow parameter (Re , Pr), material and fluid properties, tube bank parameter and fin spacing are parameters that can be altered to improve the air- side heat transfer coefficient (hc_a) (Shah and Seculic,2009). However, changing the fin geometry is one of the favoured methods to improve the gas cooler performance (Pongsoi et al., 2012). The performance of the finned-tube heat exchanger is limited by the air side heat transfer resistance because the air side heat transfer coefficient is significantly lower than the refrigerant side heat transfer coefficient. Many researches are being conducted to develop enhanced fin designs to improve the air side heat transfer performance of the finned-tube heat exchanger (Choi et al., 2010).

In this study, the air side heat transfer coefficients are determined according to the equation described by Wen and Ho (2009), equation (6.1). The heat transfer coefficient of the tube bundles/fin walls in each segment are deduced from the total heat transfer rate, the total heat transfer-surface area and the difference between the average wall and fluid bulk.

$$h_{ca} = \frac{Q}{(A_t + A_f)(T_w - T_b)} \quad (6.1)$$

The heat transfer rate (Q-Watt) in the gas cooler segment was calculated based on the air enthalpy difference as described by equation (6.2) as follows:

$$Q = \dot{m}_{air} \cdot \Delta h_{air} \quad (6.2)$$

The value of the thermo-physical properties of air were obtained at fluid film temperature (T_f) = 0.5 ($T_w + T_b$). The value of T_w is an average of the wall temperature of the tube bundles/fins, and T_b is the average of the air inlet and outlet temperatures. The example of air side heat transfer coefficient calculation is given in Appendix F.

6.3 Air side heat transfer coefficient of gas cooler-B

The diagram of the gas cooler is schematically shown in Figure 6.1. The pipe arrangement of gas cooler-B comprises 2-row and 2 circuits in parallel, with each circuit consisting of 32 pipes in a staggered arrangement. Air flows from bottom to top direction and the refrigerant flows in the counter cross direction to the air.

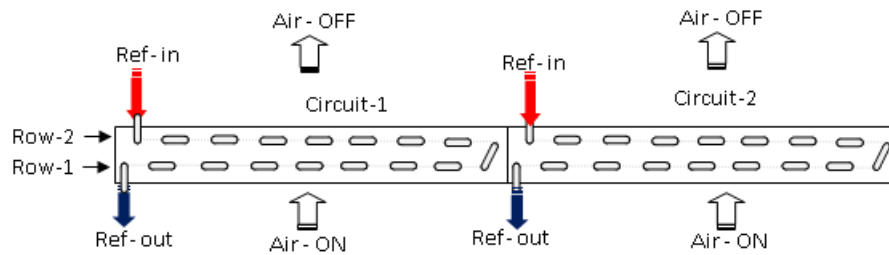


Figure 6.1 Schematic diagram of gas cooler-B design

For gas cooler-B, the study focused on the impact of fin designs on the air-side heat transfer coefficient in the segments, and the fin designs investigated comprised of continuous fin and horizontal slit fin. The investigated air inlet (air-on) velocities were: 1m/s, 1.3 m/s, 1.7 m/s, 2.0 m/s and 2.4 m/s, similar to the experimental test condition.

6.3.1 Segment air side heat transfer coefficient for gas cooler-B with continuous fin

Each segment is defined as one pipe, two fins, and the simulation of the air and refrigerant flows. The CFD post processing results of gas cooler-B with continuous fin

temperature contour is shown in Figure 6.2 (a). It can be seen that the temperature of the fin area near to the inlet of the CO₂ (see pipe-1) was much higher than the others, this cause heat conduction from the hotter pipe to the adjacent pipes through by fins. This heat conduction between pipes has the effect of decreasing the gas cooler performance (Park and Hrnjak, 2006). Figure 6.2(b) describes gas cooler-B segments which are divided by 32 segments in each circuit according to pipe reference 1 – 32.

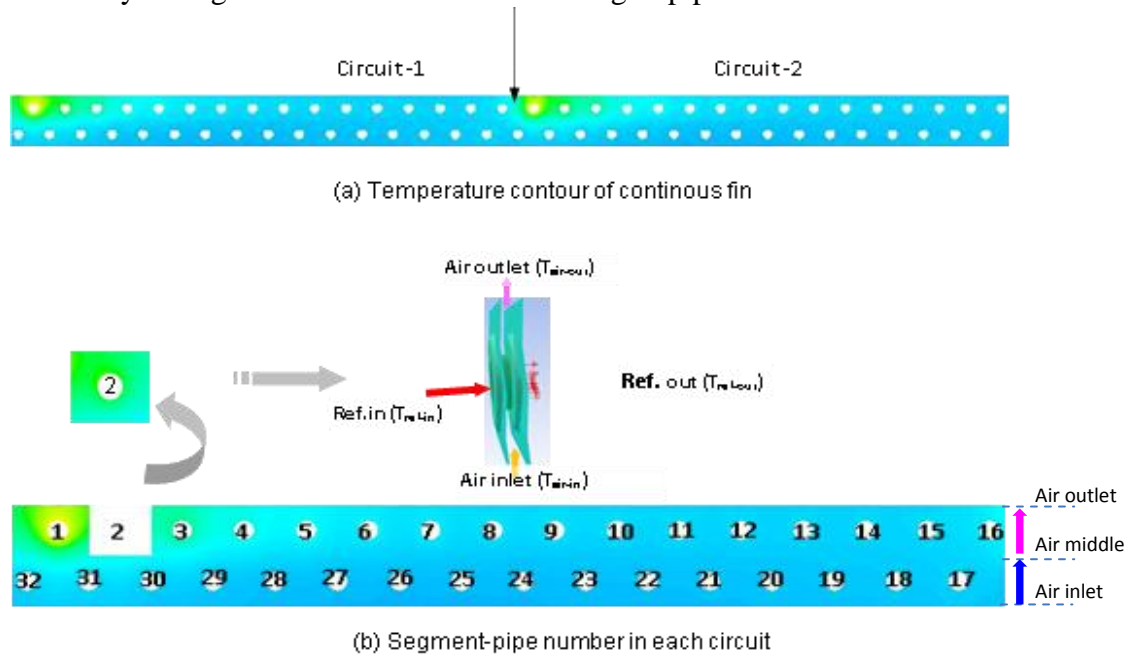
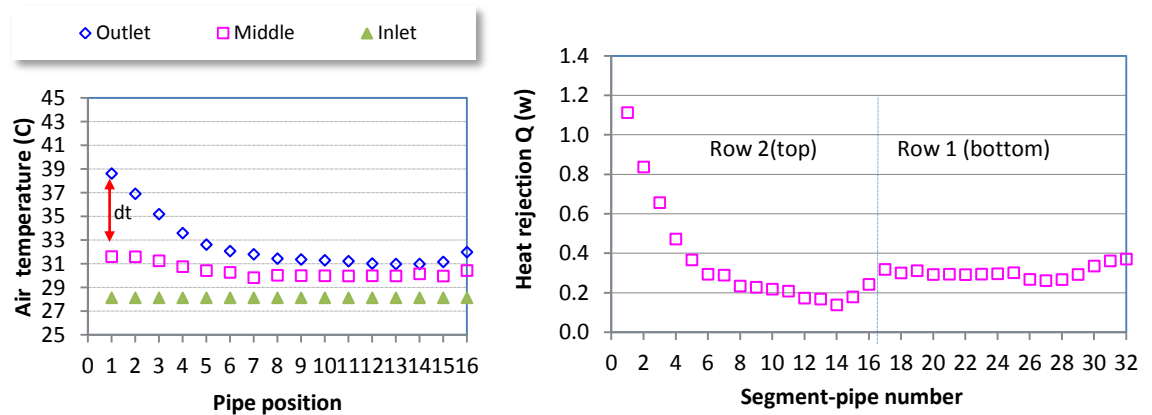
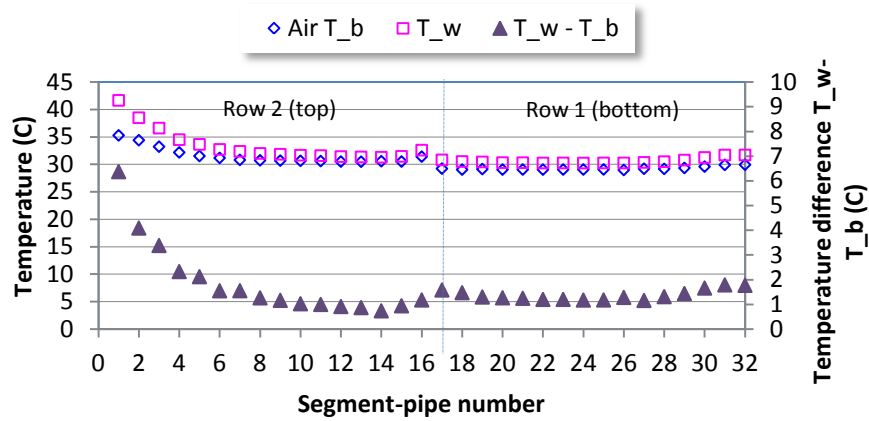


Figure 6.2 CFD post processing results and calculation methods for each segment

The air outlet temperature in each row and heat rejection (\dot{Q}) in each segment based for each pipe position reference are plotted in Figure 6.3 (a), whilst the temperature profile for the wall (fin and pipe), bulk temperature and temperature difference (TD) are shown in Figure 6.3 (b).



(a) Air temperature and heat rejection at pipe reference segments



(b) Wall temperature and temperature difference at segments

Figure 6.3 Average air, wall temperature and heat rejection in each segment for continuous fin

(Test condition: air inlet velocity:1.3 m/s, T_{air-ON}: 28.3°C)

The segment air side heat transfer coefficient (hc_a) of the continuous fin is shown in Figure 6.4. The air heat transfer coefficient (hc_a) is seen to be increasing in pipes 1-7 due to the faster reduction in the temperature difference ($T_w - T_b$) compared to the heat rejected (\dot{q}), as shown in Figures 6.3 (a) and (b). The heat transfer coefficient (hc_a) then stabilises in pipes 8-13, after which hc_a decreases. The increase in temperature and heat-rejected at pipes 15-16 is due to its proximity to the neighbouring hot pipe-1 where the two circuits meet in the gas cooler and this condition leads the air heat transfer coefficient (hc_a) at pipes 15-16 decreases. In the second row, hc_a is found to be slightly lower between pipes 17-18 as getting bad conduction from the neighbouring hot refrigerant pipe-1. Pipes 19-25 has a uniform hc_a as the temperature and heat rejection are similar, whilst after pipe 26, the hc_a decreases due to the relatively higher increase in the temperature difference ($T_w - T_b$) compared to the heat rejection rate. The mean heat transfer coefficient is found to be slightly higher for the bottom row this is due to the flow characteristic of the air flow better in the bottom row lead slightly average higher Reynolds Number in bottom row as described in Section 5.12.2.

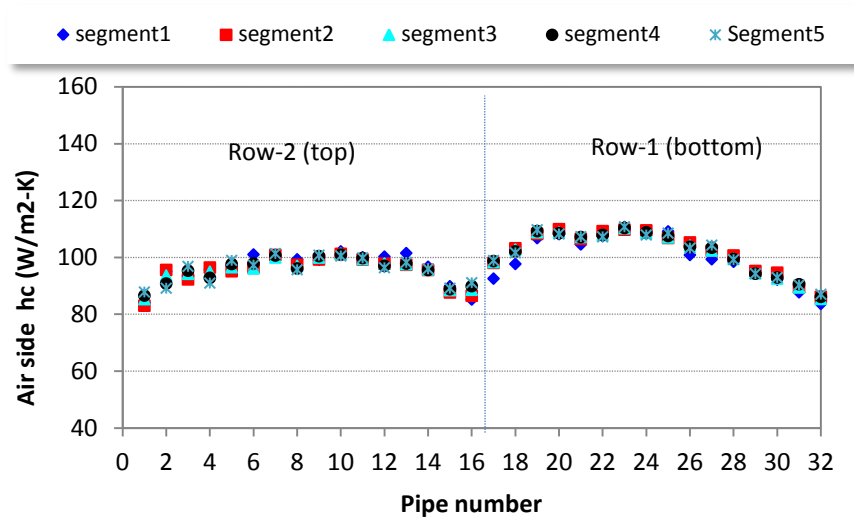


Figure 6.4 Air side heat transfer coefficient of the continuous fin configuration
(Test condition: air inlet velocity:1.3 m/s, T_{air-ON} : 28.3°C)

6.3.2 Segment air side heat transfer coefficient for gas cooler-B with slit fin

Slit-fin design of gas cooler-B is a horizontal slit mid-way between the first and second rows. Figure 6.5(a) shows the temperature contour for the slit-fin. It seems that the temperature in row-1(bottom) is significantly lower than the top row. It can also be observed that the temperature in the bottom row is relatively constant. Figure 6.5 (b) shows the hc_a investigation in one circuit, consisting of 32 pipes.

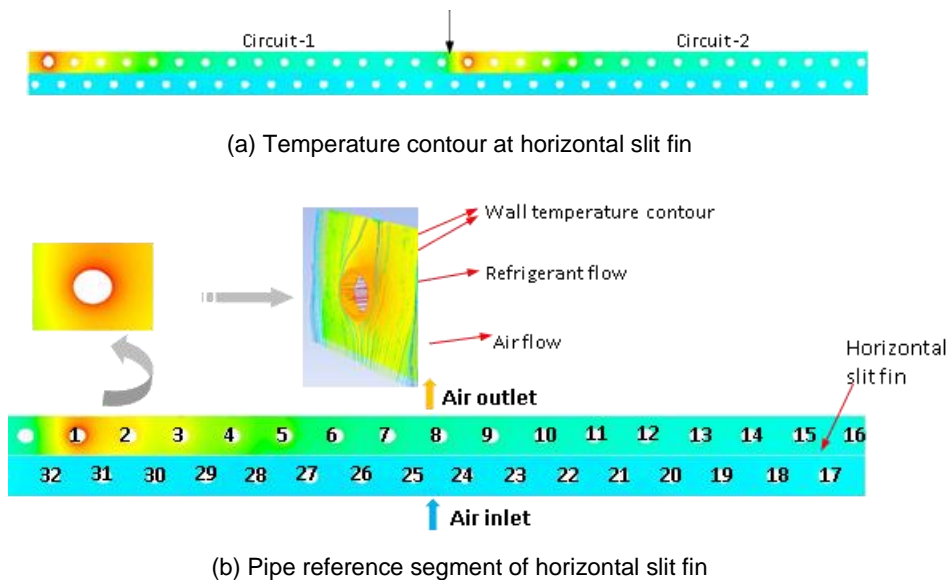
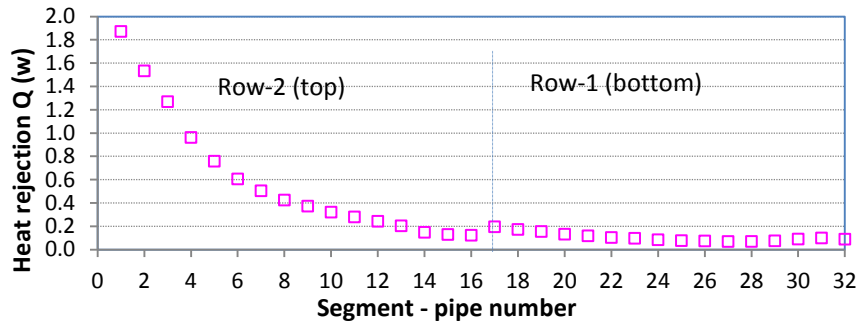
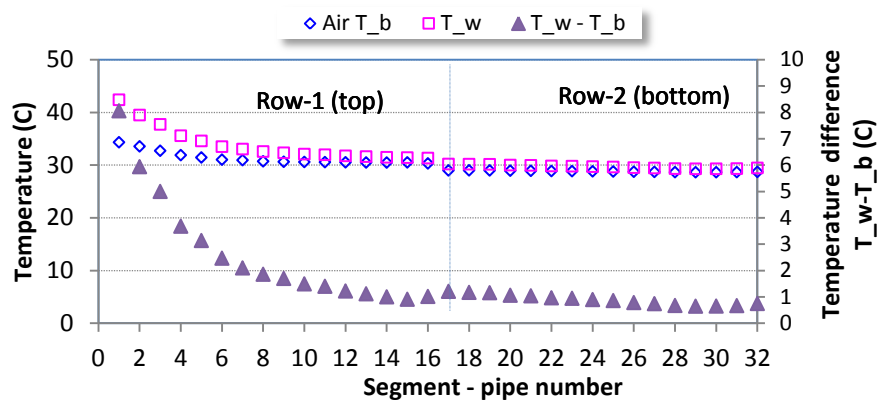


Figure 6.5 Air side CFD post processing results of gas cooler-B with horizontal slit fin

In order to support the analysis of the hc_a trends in one circuit, Figures 6.6 (a) and (b) show the heat rejection rate and temperature profiles in the segment.



(a) Variation of heat rejection at segments



(b) Temperature different, air bulk temperature and wall temperature at segments

Figure 6.6 Average air, wall temperature and heat rejection in each segment of slit fin design
(Test condition: air inlet velocity: 1.3 m/s, T_{air-ON}: 28.3°C)

The heat transfer coefficient is seen to be relatively constant for the bottom row, conversely the top row shows a decreasing trend in hc_a from the fourth pipe to the sixteenth (last pipe in the top row) as shown in Figure 6.7. The reducing trend can be attributed to the fact the heat rejection rate reduces from pipes 1 to 16, but the difference in temperature between T_w and T_b reduces at a slower rate than the heat rejected (refer to equation 6.1). Similarly, for the pipes in the bottom row, where the heat rejection rate and the difference between T_w and T_b are similar for pipes 17-32, the heat transfer coefficients are also uniform for all pipes in the bottom row. This is a consequence of the slit within the fin, whereby the lack of heat conduction between the top and bottom rows produces a relatively uniform temperature and heat rejection rate in the bottom row. As a result, the mean heat transfer coefficient is found to be higher for the bottom row.

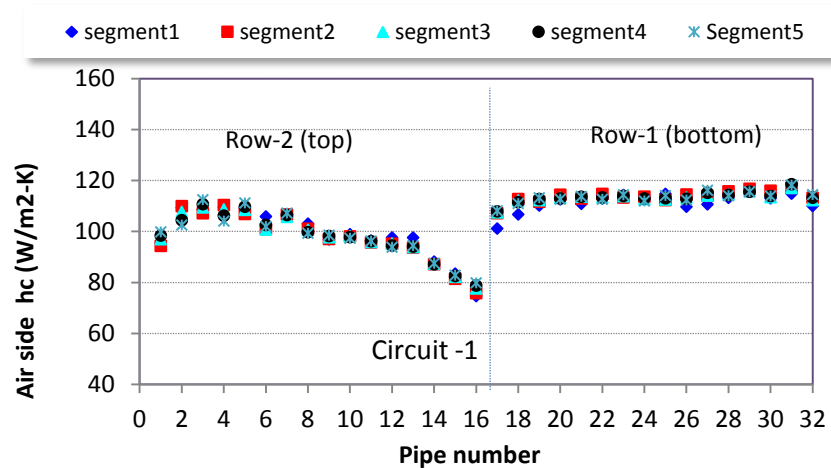


Figure 6.7 Segment air side heat transfer coefficient for circuit -1 and -2 for the slit fin
(Test condition: air inlet velocity:1.3 m/s, T_{air-on} : 28.3°C)

6.3.3 Average air-side heat transfer coefficient with respect to air velocity

The average CFD results were compared with experimental result from Wen and Ho (2009). However, Wen and Ho's experiment uses water as a working fluid for hot side and also has slightly different specification, especially tube outlet diameter, fin spacing, and number of pipes in a circuit as described in Table 6.1.

Table 6.1 Comparison heat exchanger specification between the CFD model and Wen and Ho (2009) experiment

Specification	CFD Model	Experiment of Wen and Ho, (2009)
Fin type	Wavy fin	Wavy fin
Number of row	2	2
Tube outer diameter	8 mm	10.30 mm
Inlet diameter	6.32 mm	10.10 mm
Fin spacing	2.11 mm	2.54 mm
Fin thickness	0.16 mm	0.12 mm
Number of pipe investigation in circuit	32	20
Working fluid	CO ₂	water

Figure 6.8 shows the variation of average the heat transfer coefficients with air inlet velocity investigated: 1m/s,1.3m/s,1.7 m/s, 2 m/s and 2.4 m/s. Figure 6.8 also indicated that as the air velocity increases the heat transfer coefficient also increase.

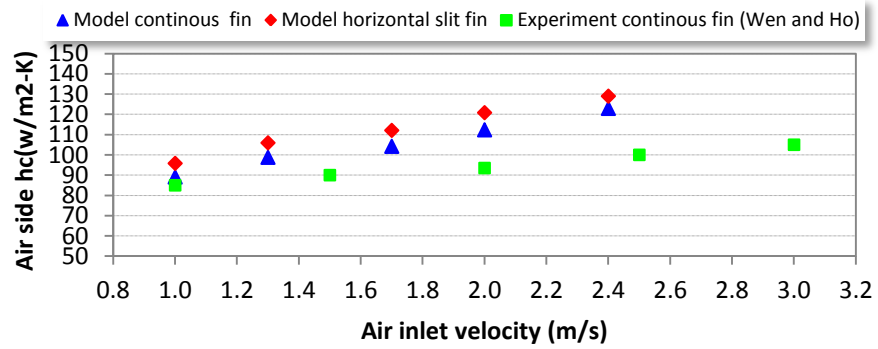


Figure 6.8 Variation of average air-side heat transfer coefficient with air inlet velocity

It can be seen that there is slightly deviation between model and Wen and Ho's experimental results especially at higher air velocity, this is most possible due to difference of the specification especially, collar diameter and fin spacing which can influence the vortex characteristic in the upstream and the downstream and lead a mixing quality of the airflow (Wang *et al.*,1999). However, according to this hc_a value comparison it can be considered that that CFD was adequate to calculate the air side heat transfer coefficient.

6.3.4 Average air-side heat transfer coefficient correlation for gas cooler-B

In this section, a correlation of average heat transfer coefficient were developed for gas cooler-B with respect to the Reynolds Number for the two different fin design (i) continuous fin, (ii) horizontal slit. The values of the thermo-physical properties of air were obtained at the film temperature (i.e. the average of T_b and T_w) with all the parameters used to calculate the heat transfer coefficients obtained from the CFD results. ' Re_{Dc} ', ' Pr_{Dc} ' and ' Nu_{Dc} ' are calculated based on the collar diameter. The correlations are shown in Figure 6.9.

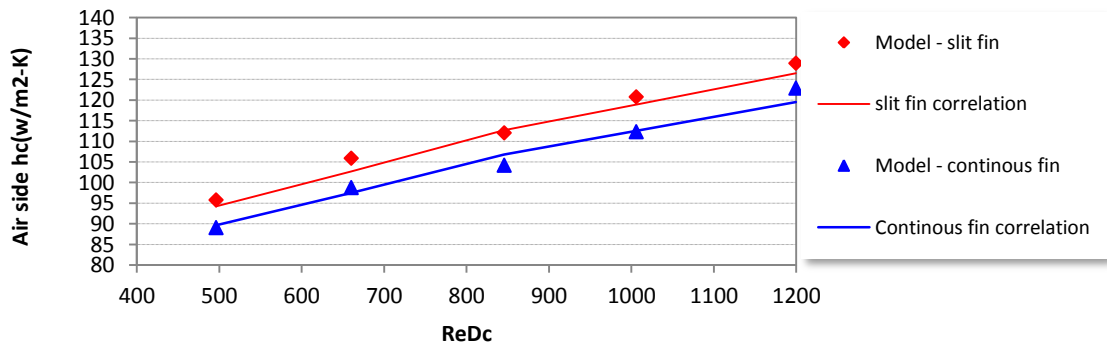


Figure 6.9 Average air side heat transfer coefficient correlation of gas cooler-B for horizontal slit fin and continuous fin

The respective correlations for the average air-side heat transfer coefficients for the slit and continuous fins were found to be:

Gas cooler-B with continuous fin design:

$$Nu_{DC} = 4 Re_{DC}^{0.33} Pr^{1/3} \quad (6.3)$$

Regression coefficient (R^2) = 0.990

Gas cooler-B with horizontal slit fin design:

$$Nu_{DC} = 4 Re_{DC}^{0.338} Pr^{1/3} \quad (6.4)$$

Regression coefficient (R^2) = 0.992

These correlations were developed by using the template provided in Chang and Kim (2006), and the coefficients and powers were adjusted to maximise the regression coefficients and provide minimum errors. It indicates that as Re increases, the heat-transfer coefficients also increase. The heat-transfer coefficients were found to vary between 95 W/m²K – 127 W/m²K for the slit fin design and 88 W/m²K – 120 W/m²K for the continuous fin design. The higher average heat transfer coefficient for the slit fin design can be attributed to the fact that the conduction effect from the hottest pipe through the fin is mitigated by the slit. The wall temperature T_w in the bottom row (row-1) of the gas cooler therefore decreases relative to the continuous fin, consequently reducing the temperature difference ($T_w - T_b$) for the slit fin. Conversely, the heat rejected by the bottom row in the slit fin configuration is also lower, but the relative change in \dot{q} from the continuous to the slit fin configurations is smaller than the reduction in ($T_w - T_b$). Hence the hc_a increases for the bottom row. Conversely in the top row (row-2), the both fin design seem have the same average hc_a , however the trend line is slightly different. Thus, as the bottom row hc_a are higher for the slit-fin configuration relative to continuous fin, the average heat transfer coefficients are also higher for the slit-fin configuration.

6.4 Air side -heat transfer coefficient of gas cooler-A

The schematic diagram of gas cooler-A with the refrigerant and air flow directions is shown in Figure 6.10. The pipe arrangement of gas cooler-A comprises 3-row and 4 circuits in parallel, with each circuit consisting of 24 pipes in a staggered arrangement. Air flows from in bottom-up direction and the refrigerant flow are counter-cross to the air direction, similar to gas cooler-B construction.

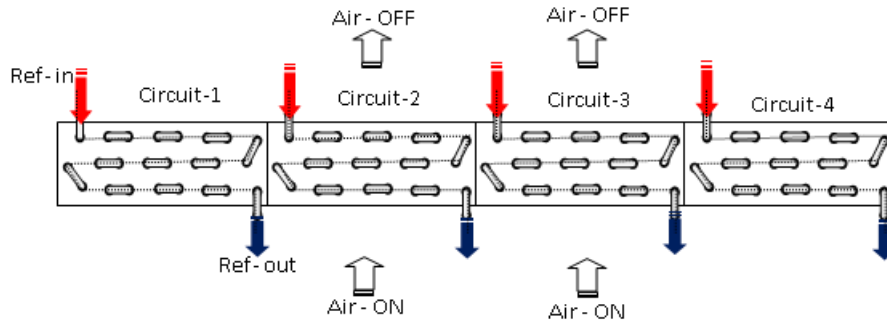


Figure 6.10 Schematic diagram of gas cooler-A

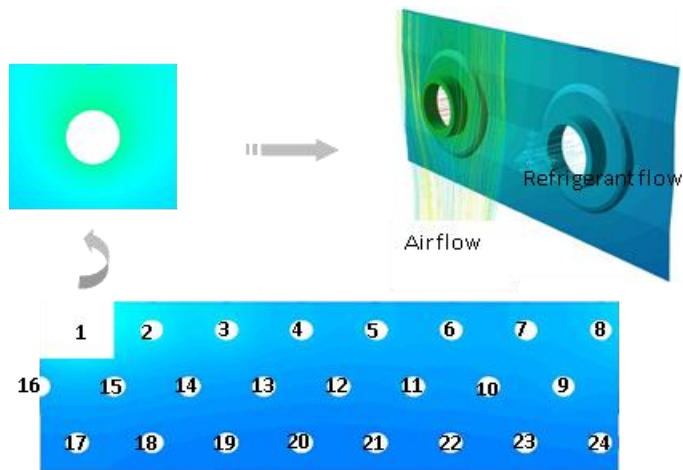
Air-side heat transfer coefficient was calculated by the same method as gas cooler-B, described in equations (6.1) and (6.2). For gas cooler-A, there are three different fin designs were investigated: the continuous fin, the horizontal slit fin and the horizontal and vertical slit fin. The gas cooler analysis consisted of firstly investigating the hc_a parameter for each segment (1-24) and secondly, developing a correlation of average heat transfer coefficient for the entire gas cooler with respect to the Reynolds Number (Re_{DC}). The test conditions considered different air-on velocities varying between 1.7 m/s, 2.0 m/s and 2.4 m/s.

6.4.1 Segment air side heat transfer coefficient of gas cooler –A continuous fin

Figure 6.11 (a) shows the fin temperature contour for the continuous fin design obtained from CFD. It is clear that there is heat conduction through the fin from the hottest pipe - 1 to the adjacent pipes. Figure 6.11 (b) shows the segment number in one circuit which is consist of 24 segments. It is also illustrated segment model with one tube, fins, air flow and refrigerant flow simulation.



(a) Temperature contour of gas cooler-A with continuous fin



(b) Segment in one circuit of gas cooler-A with continuous fin

Figure 6.11 Temperature contour and segment investigation of gas cooler-A

In order to provide an illustration of the heat rejection rates at different segments, Figure 6.12 shows the heat rejection rate for different segments and rows. The heat rejection rates fluctuate in each row, especially there are increasing at segment 8 and segment 16 and also slightly increases at segment 24, this is due to the fin continuous and there is an effect of the heat conduction from the their adjacent hotter pipes which lead the heat gain in those segments.

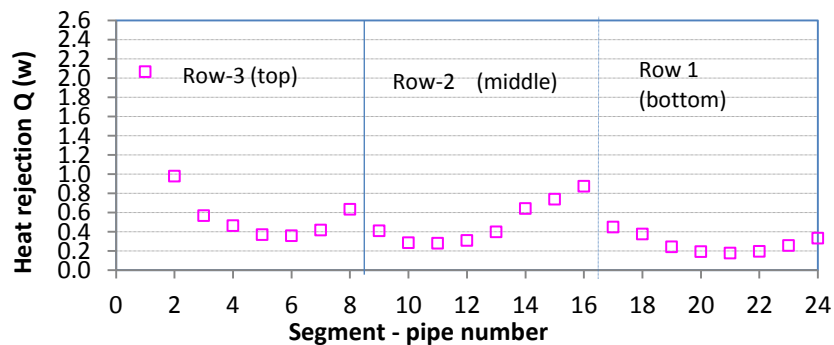


Figure 6.12 Heat rejection at pipe-reference segment
(Test condition: Air-on Velocity : 2.0 m/s , T air-ON: 31 ° C) –Segment-3)

Figure 6.13 describes the wall temperature profile and air bulk temperature in each segment as well as the temperature difference (TD). The variation of temperature profiles appears similar with the heat rejection rate variation shown in Figure 6.12.

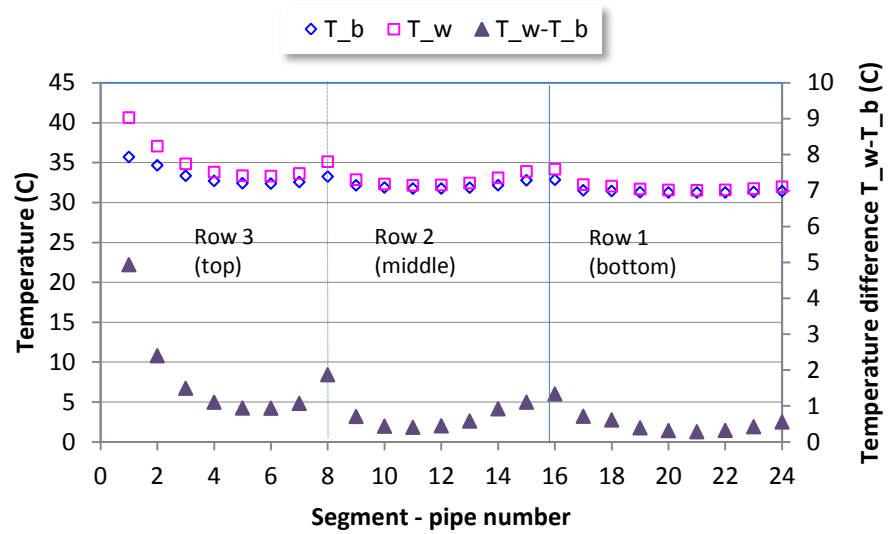


Figure 6.13 Variation of wall temperature, bulk temperature and temperature difference (TD) with segment number of gas cooler-A
 (Test condition: Air-on velocity: 2.0 m/s, T_{air-ON} : 31 °C –Segment-3)

The air side heat transfer coefficients for gas cooler-A with continuous fin design is shown in Figure 6.14. Related to the heat rejection and temperature difference ($T_w - T_b$) phenomena as described for gas cooler B, as a result in the top row (row-3) the hc_a slightly decrease from pipe-1 to pipe-8, the middle row pipe-9 until pipe-13 increasing and slightly decreasing from pipe-14 to pipe-16, conversely in the first row (bottom) the hc_a remained constant. In term of average hc_a in each row, the hc_a are slightly higher in the middle row than the bottom row, due to the turbulence produced by the tube, such that the mean turbulence intensity in the middle row is slightly greater than the bottom first row. Furthermore, at the third (top) row the heat transfer coefficient getting lowest since the air flow characteristic (as described in Section 5.12.2). And with regards to segments along the pipe length from front to rear (segment 1- segment 5), the hc_a appears generally constant, with minor variations for individual segments.

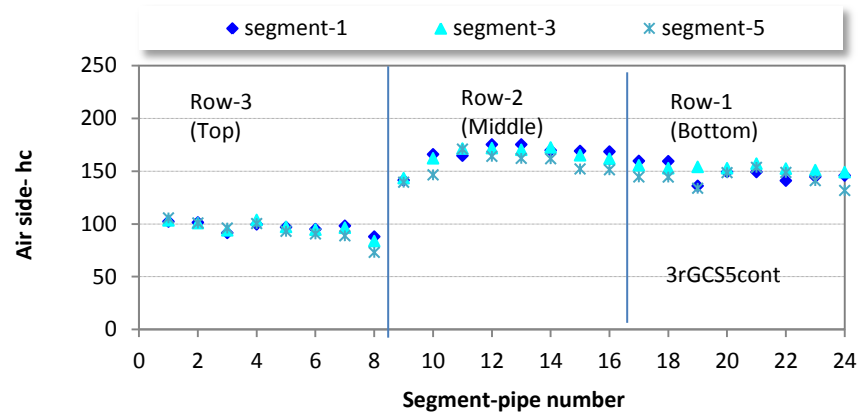


Figure 6.14 Air-side heat transfer coefficient at segment
(Test condition: Air-on velocity: 2.0 m/s, T air-ON: 31 °C)

6.4.2 Segment air side heat transfer coefficient of gas cooler-A with horizontal slit fin

Similar to gas cooler-B with horizontal fin design, one of the alterations to gas cooler-A fin design also include a horizontal slit mid-way between the top row and the middle row. The effects of the slit are described with reference to the temperature contour in the fin as shown in Figure 6.15 (a). It can be seen that with the horizontal slit the heat transfer across the fin between the top and middle row of tubes would reduce significantly particularly around the hottest tubes. Figure 6.15 (b) shows the 24 segments in one circuit.

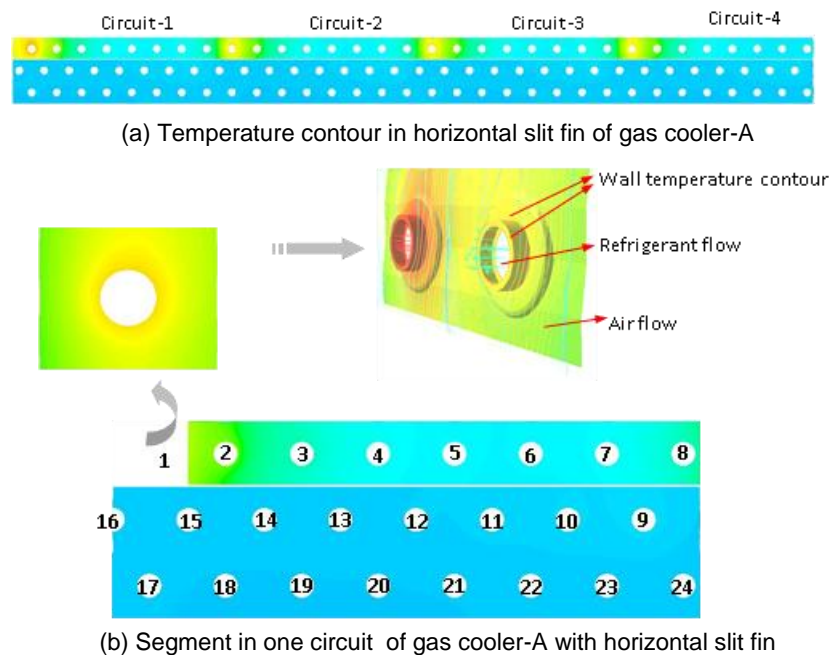


Figure 6.15 Post processing of CFD simulation results for gas cooler-A with horizontal slit

The heat transfer coefficient results with horizontal slit fin are shown in Figure 6.16, where it can be seen that, the slit affects the middle row of the gas cooler, such that the highest heat transfer coefficients are obtained in the middle row. The horizontal slit fin was found to have no effects on the bottom row and the top row.

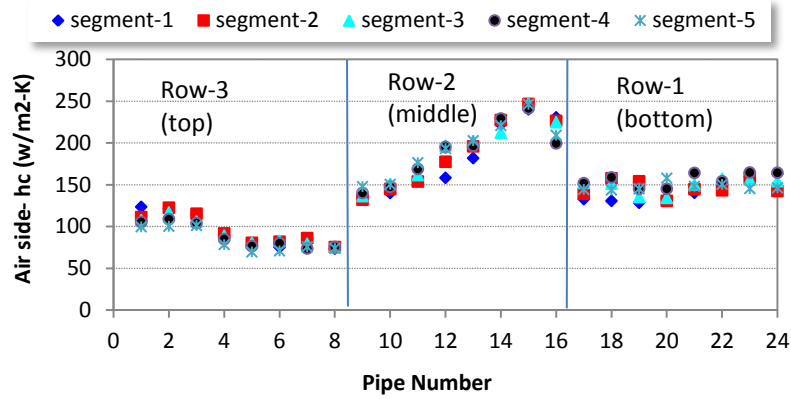


Figure 6.16 Air-side heat transfer coefficient for the gas cooler-A with horizontal slit fin (Test condition: Air-ON velocity: 2.0 m/s, Tair-ON : 31.8°C)

6.4.3 Segment air side heat transfer coefficient of gas cooler-A with vertical and horizontal slit fin

This slit design consists of a horizontal slit mid-way between row-3(top) and row-2(middle) and a vertical slit positioned between pipe- 1 and pipe-8 as shown in Figure 6.17. The vertical slit was intended to block heat conduction from the hottest tube-1 to the tube- 8, hence minimising the interaction of the different circuits with each other.

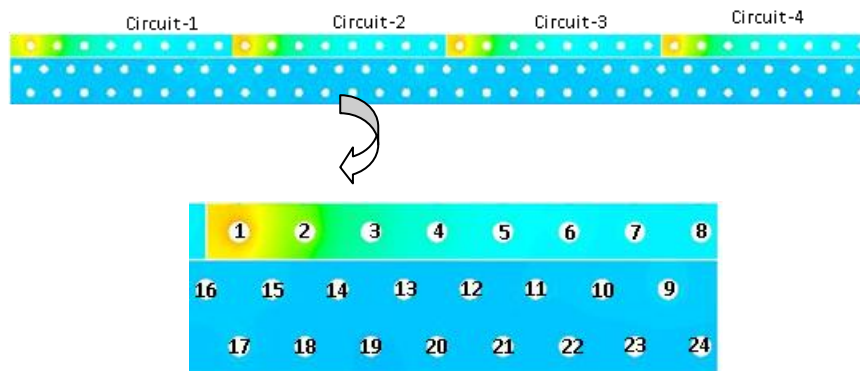


Figure 6.17 Post processing of CFD simulation results for gas cooler-A with horizontal and vertical slit fin

Figure 6.17 shows that the behaviour of each circuit is similar to each other, which was the intended effect of the vertical slit. It was found that the heat transfer coefficient variation increases only for pipe 8 with the hc_a was recorded approximately $82.7 \text{ W/m}^2\text{-K}$, comparing with only $74.8 \text{ w/m}^2\text{-K}$ for horizontal slit fin at the same position and operating condition.

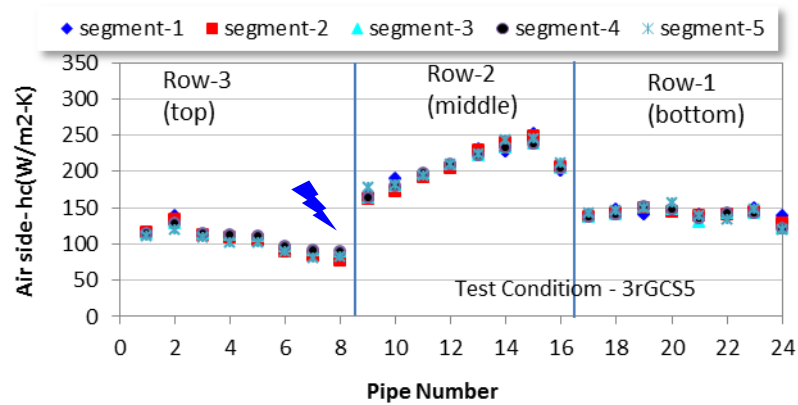


Figure 6.18 Air-side heat transfer coefficient of gas cooler-A with vertical and horizontal slit fins
(Test condition: Air-on velocity : 2.0 m/s , T air-on: 31 ° C)

6.4.4 Average air-side heat transfer coefficient correlation for gas cooler-A

With similar methodology with gas cooler-B correlation, the correlation of average heat transfer coefficient were developed for gas cooler-A for the three different fin design (i) continuous fin, (ii) horizontal slit and (iii) vertical and horizontal slit. The correlations are illustrated in Figure 6.19 below.

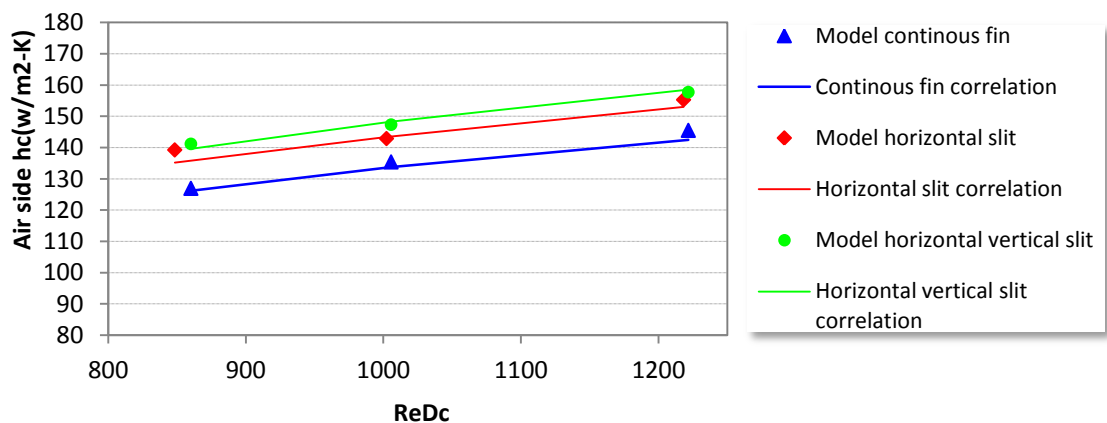


Figure 6.19 Correlation of average air-side heat transfer coefficient of gas cooler-A

The respective correlations for the average air-side heat transfer coefficients for the slit and continuous fin were found to be:

Gas cooler-A continuous fin design:

$$Nu_{DC} = 4 Re_{DC}^{0.355} Pr^{1/3} \quad (6.5)$$

Regression coefficient (R^2) = 0.998

Gas cooler-A with horizontal slit fin design:

$$Nu_{DC} = 4 Re_{DC}^{0.365} Pr^{1/3} \quad (6.6)$$

Regression coefficient (R^2) = 0.957

Gas cooler-A with horizontal and vertical fin design:

$$Nu_{DC} = 4 Re_{DC}^{0.37} Pr^{1/3} \quad (6.7)$$

Regression coefficient (R^2) = 0.998

Figure 6.19 and the correlations equations (6.5-6.7) indicate that as Re_{DC} increases, the heat-transfer coefficients also increase. The heat-transfer coefficients were found to vary between 141 W/m²K – 157 W/m²K for the vertical and horizontal slit fin, 139 W/m²K – 155 W/m²K for the horizontal fin and 126 W/m²K – 145 W/m²K continuous fin design.

The improvement in heat transfer coefficient with the slit fin configuration (horizontal, vertical and horizontal) lead the higher performance of the gas cooler. Comparing with the continuous fin, the horizontal slit fin improves the hc_a by approximately 6%-8%, whilst the addition of the vertical slit to horizontal slit fin contributed an additional 1%-2 % to the performance gain. It can be concluded that the slit fin is effective to increase the performance of the finned and tube gas cooler for CO₂ refrigeration system.

6.5 Comparison of the average air-side heat transfer coefficient for gas cooler-A and gas cooler-B

This section compares the hc_a of the two gas cooler designs investigated in this study. Figure 6.20 shows mean heat transfer coefficients with respect to the inlet Reynolds Number (Re_{Dc}).

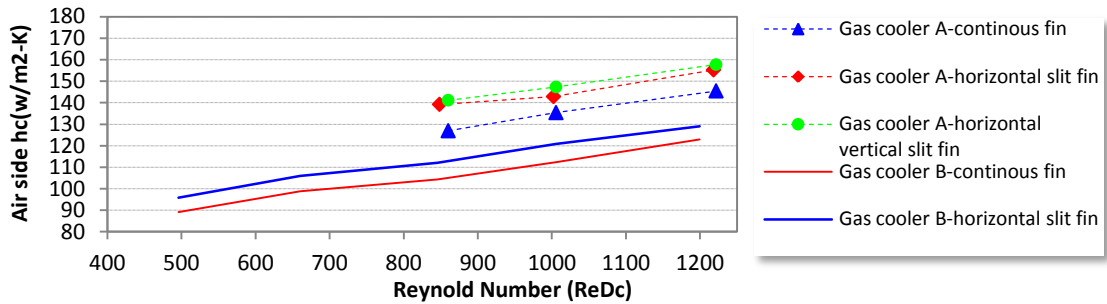


Figure 6.20 Variation of average air-side heat transfer coefficient of gas cooler-B and gas cooler-A

It can be seen that gas cooler-A has better performance than gas cooler-B. This is corresponding to the gas cooler design, especially combination of number of the pipe and circuit in entire gas cooler. It can be conclude that in the gas cooler mode operation, as the number of circuit more in gas cooler, the performance will be increased. This is due to the number of circuit will allow the better temperature distribution in the fin entire gas cooler. The more number of circuits enable to mitigate the heat gain of the colder adjacent pipes which caused by the heat conduction through the fin from the hotter pipe but will lead to increase size of the gas cooler, in this case the physical size of gas cooler A was 33% higher than that of gas cooler B.

6.6 Summary

This chapter investigated the air-side heat transfer (hc_a) properties at segments in order to adequately evaluate and explain the performance of the gas cooler. The evaluation was done both in terms of the mean and local hc_a values, with the development of heat transfer correlations for each gas cooler designs, with respect to the Pr and Re Numbers. The horizontal slit fin from the continuous can increases heat transfer coefficient by approximately 6%-8%, whilst the addition of the vertical slit to horizontal slit fin contributed an additional 1%-2% to the performance gain. In addition, the heat transfer profile in segments has shown that the hc_a is varied along the gas cooler depend on to the temperature profile and gas cooler construction.

Chapter 7 will evaluate and describe the refrigerant-side heat transfer coefficients (hc_r) and overall heat transfer coefficient (U -value) with the same gas coolers employed in this section.

CHAPTER VII - INVESTIGATION OF THE REFRIGERANT AND OVERALL HEAT TRANSFER COEFFICIENTS OF GAS COOLERS

7.1 Introduction

This chapter deals with the investigation of the refrigerant-side (hc_r) and overall heat transfer coefficients ($U-LMTD$) of the gas cooler. The methodology employed to calculate the heat transfer coefficient is similar to the air-side heat transfer coefficient calculation, explained in Chapter 6. Furthermore, the refrigerant-side heat transfer coefficients are presented as a function of bulk-temperature and the refrigerant mass flux, G , in order to allow comparisons with past studies. The overall heat transfer coefficients ($U-LMTD$) calculations from the experimental results are also presented in order to validate the CFD model.

7.2 Refrigerant-side heat transfer coefficient (hc_r)

The refrigerant-side heat transfer coefficient (hc_r) was determined from individual segments of CFD results using equation (7.1) as follows:

$$h_{cr} = \frac{q_{ref} \left(\frac{W}{m^2} \right)}{(T_{w,i} - T_{bulk}) K} \quad (7.1)$$

Where, q is refrigerant heat flux (W/m^2), $T_{w,i}$ is the temperature of inner pipe surface (copper), T_{bulk} is mean refrigerant pipe inlet and outlet temperature at each segment. The example of refrigerant side heat transfer coefficient calculation is given in Appendix F.

The temperature and velocity profiles from the CFD post processing results in a heat exchanger segment is shown in Figure 7.1. It shows the inner wall temperature contours and the refrigerant-flow vectors of pipe-1 and pipe-2 (refer to i.e. Figure 6.5 for gas cooler-B and i.e. Figure 6.15 for gas cooler-A), where the heat flux, inner wall temperature, refrigerant and air outlet temperatures are implicitly calculated by CFD. In addition to the refrigerant flow vectors, Figure 7.1 also shows the air flow path-line in the bottom-up direction of the heat exchanger.

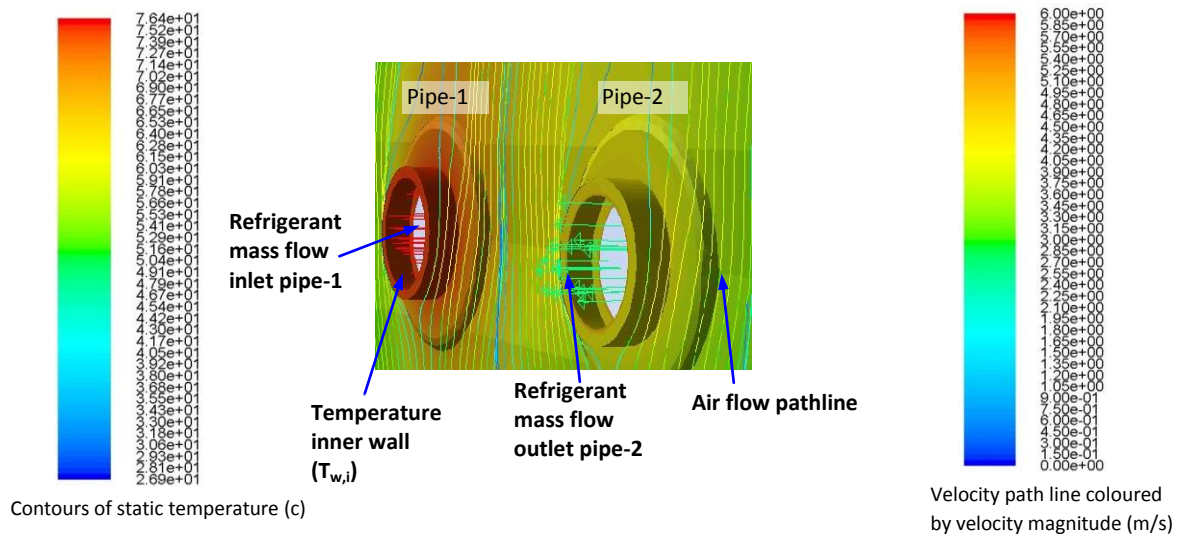


Figure 7.1 Refrigerant- side post processing results for a segment

7.2.1 Refrigerant-side heat transfer coefficient of gas cooler-B

This section presents the refrigerant-side heat transfer coefficient (hc_r) of gas cooler-B as a function of bulk temperature (T_b), together with the hc_r profiles in different segment as shown in Figure 7.2 and Figure 7.4 (the segment refer to Figures 5.18 and 6.5(b)).

The variation of hc_r as shown in Figure 7.2 is obtained from a specific operating conditions of: pressure of 82 bar_g; refrigerant mass flow rate of 0.0195 kg/s; and mass-flux (G) of 620 kg/s-m². It can be seen that the maximum hc_r is approximately 3600 W/m²-K at bulk temperatures at approximately 40°C. The lowest hc_r of 1700 W/m²-K occurs at the highest bulk temperature of 98 °C. This is due to the thermo-physical properties especially c_p properties of CO₂ is varied by temperature and the highest hc_r characterised by the pseudo-critical area and according to Dang and Hihara (2004) that pseudo-critical region is the region of the maximum in heat transfer coefficient and coincides with the region where the specific heat (c_p) is maximum. The variation of c_p with temperature is shown in Figure 7.3.

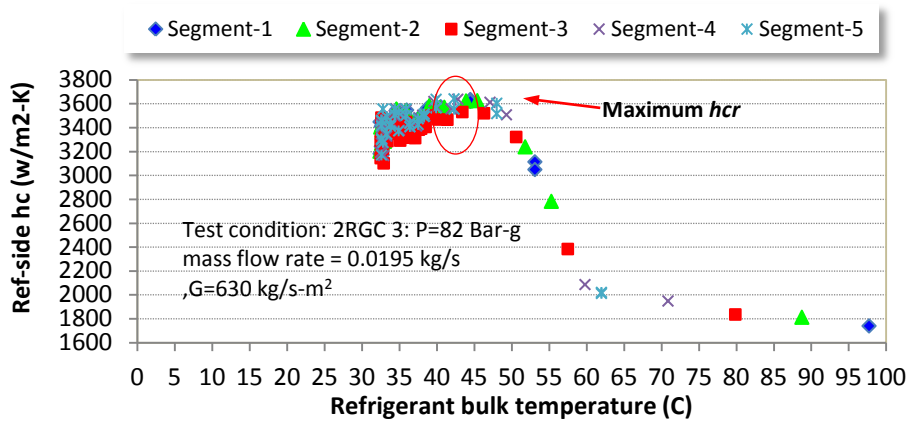


Figure 7.2 Variation of refrigerant side-heat transfer coefficients with refrigerant bulk temperature of gas cooler-B
(Operating conditions of mass flow rate: 0.0195 kg/s, gas pressure: 82 bar_g)

Figure 7.3 shows the variation of c_p with temperature under identical operation condition with the $h_{c,r}$ described in Figure 7.2. It also explains the piecewise-linear relation/equation of the refrigerant c_p in the CFD model, where it can be seen that the maximum c_p in this operating condition is at around 40 °C, portraying that the maximum of the c_p coincides with the maximum of the $h_{c,r}$ profile in Figure 7.2.

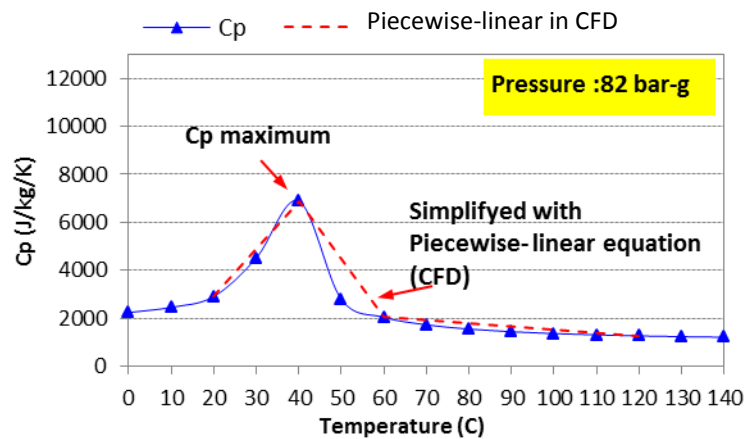
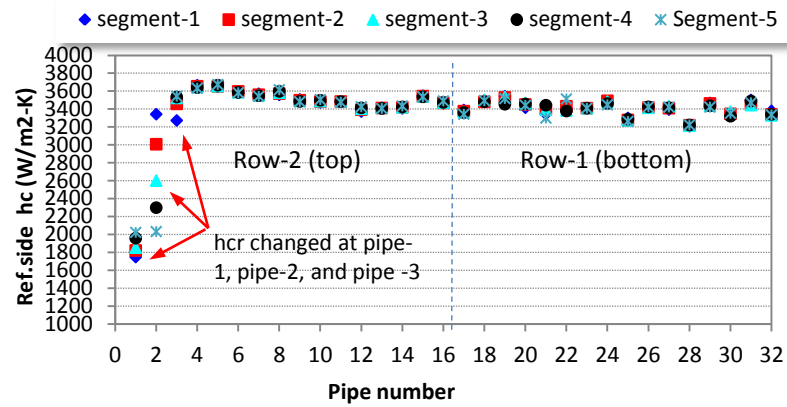


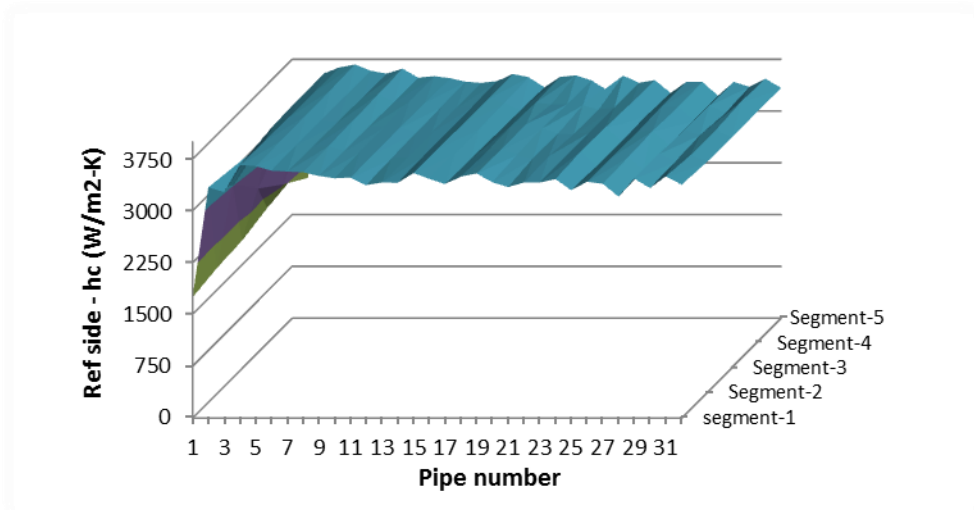
Figure 7.3 Variation of CO₂ c_p with temperature at a pressure: 82 bar_g
(Derived from EES®)

The $h_{c,r}$ profile in segment of the gas cooler is shown in Figure 7.4 (a), where the 3D map of these coefficients is shown in Figure 7.4 (b). The heat transfer coefficient along pipe-1 and pipe-3 increases slightly, whilst in pipe-2 the $h_{c,r}$ increases significantly from its gas cooler inlet to outlet. This is due to the refrigerant temperatures variation within the pipe being near the pseudo-critical, and the temperature changed rapidly from inlet to outlet in this pipe only in these pipes as described in experimental results in section

4.6.4. Furthermore, from pipe-4 to pipe-32 the h_{cr} within the pipes are generally uniform, as the temperature change is very small.



(a) Refrigerant heat transfer coefficient in segment



(b) Refrigerant heat transfer coefficient in segment in 3D chart

Figure 7.4 The h_{cr} profile in segment of gas cooler-B
(Operating condition: mass flow rate : 0.0195, gas pressure : 82 bar_g)

7.2.2 Refrigeration-side heat transfer coefficient of gas cooler-A

The variation of h_{cr} within gas cooler-A with bulk temperature range is shown in Figure 7.5. The bulk temperature range is taken for a certain operating condition: pressure: 83 bar_g; and mass-flow rate 0.0095 kg/s. Similar to the gas cooler-B investigation in section 7.2.1, Figure 7.6 shows the c_p of CO₂ and the linear-equation for the same operating condition with h_{cr} in Figure 7.5. It was found that the maximum h_{cr} is 2200 w/m²-K at approximately 40 °C and the maximum c_p also shows at the similar

temperature. For gas cooler-A, the mass flow rate in the circuits is approximately half than gas cooler-B, as a result the hc_r significantly lower than gas cooler-B.

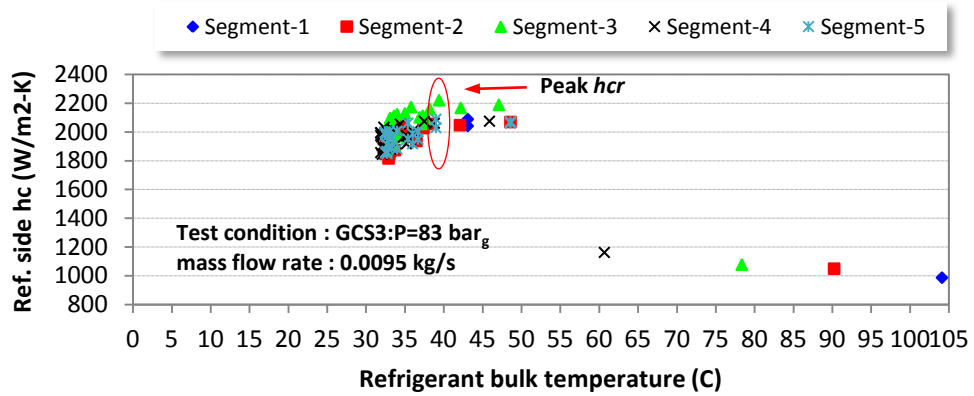


Figure 7.5 Variation of refrigerant-side heat transfer coefficient with bulk temperature of gas cooler-A

(Operating conditions of mass flow rate: 0.0095 kg/s and pressure of 83 bar_g)

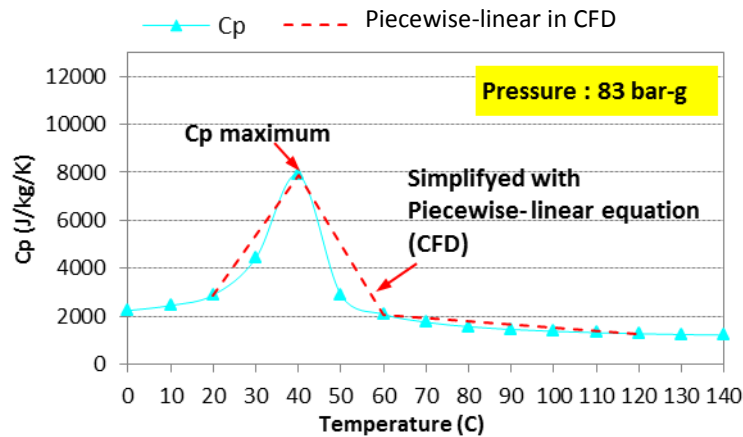
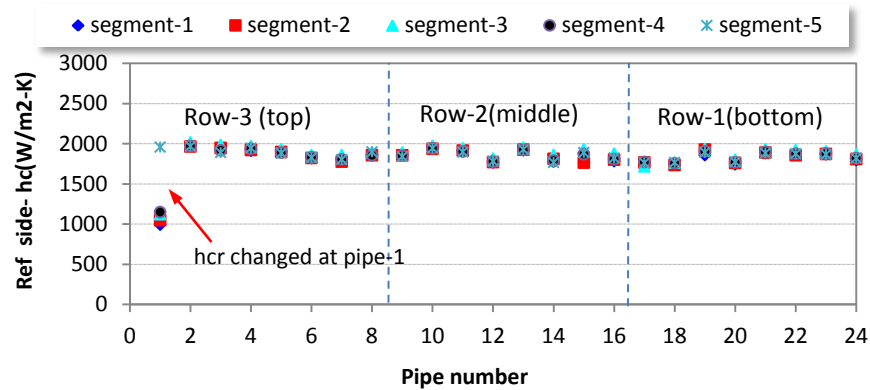


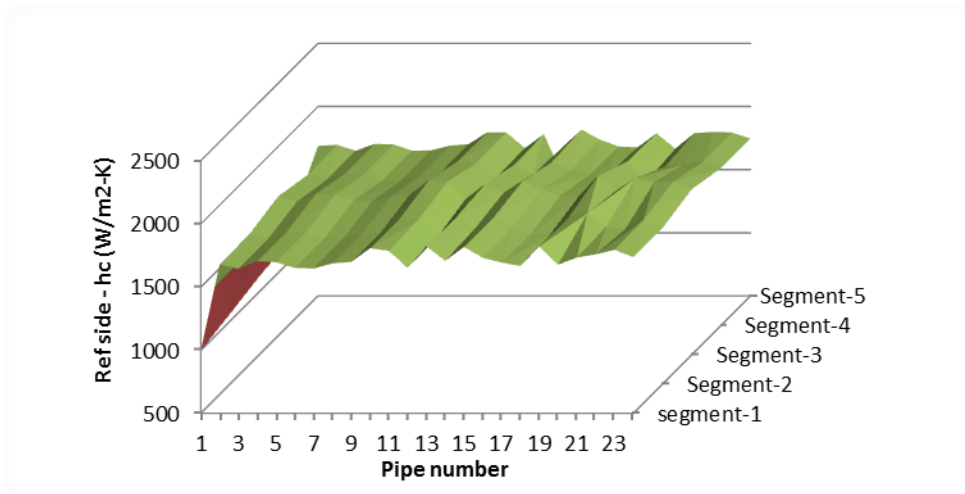
Figure 7.6 Variation of CO₂ c_p with temperature at pressure: 83 bar_g
(Derived from EES)

The hc_r profiles for each segment of gas cooler-A is shown in Figure 7.7 (a), together with the 3D map of the coefficients for the whole gas cooler in Figure 7.7 (b). It can be seen that the hc_r changed only in pipe -1, where the refrigerant temperature reduces rapidly, whilst the other pipes have relatively uniform hc_r . For gas cooler-A, the temperature drops significantly only in pipe-1 (inlet temperature: 105 °C and outlet temperature: 45 °C) as the c_p of the refrigerant changes rapidly from the lowest value (at 105 °C) to the maximum value near the critical temperature. A higher c_p produces a higher hc_r as the Pr number significantly increased from 0.96 to 3.4 between pipe-1 and pipe-2, respectively, causing the hc_r to change from 1000 W/m²K to 2000 W/m²K. The

subsequent pipes have refrigerant temperatures between 45 °C and 34 °C, whereby the c_p and hence the hc_r do not experience much variation.



(a) Refrigerant heat transfer coefficient in segment



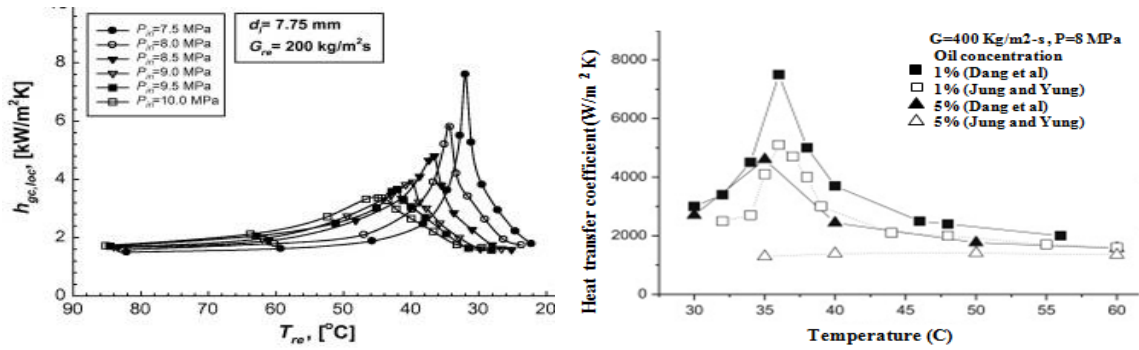
(b) Refrigerant heat transfer coefficient 3D chart

Figure 7.7 Variation of refrigerant- side heat transfer coefficient at segment of gas cooler-A
(Operating condition: mass flow rate= 0.0095 kg/s; pressure= 83 bar_g)

7.2.3 Comparison of h_{cr} for gas coolers-A and B with previous studies

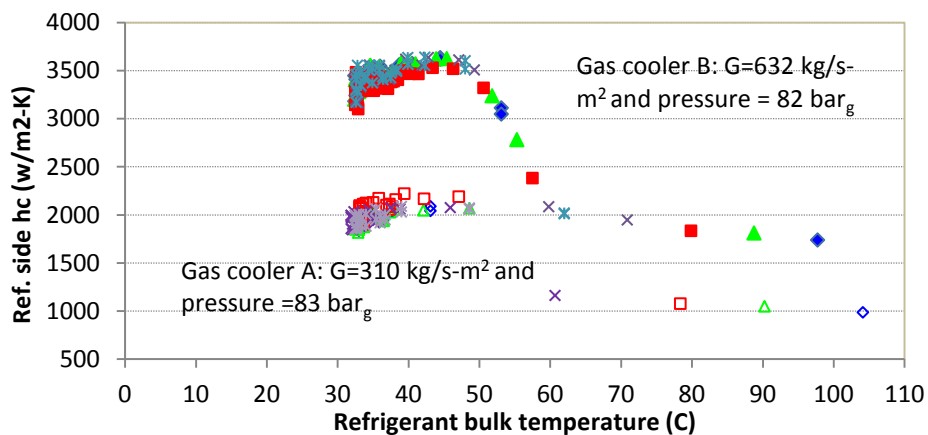
Dang and Hihara (2004) showed that the heat-transfer characteristics of CO₂ at supercritical pressures differ from those of fluids with constant properties. CO₂ has a better heat-transfer performance owing to its low viscosity and high specific heat, especially within the pseudo-critical temperature region. An experimental results from Oh and Son (2010), Dang *et al.* (2012) and Yun and Jung (2013) are presented in Figures 7.8(a) and (b). The Figure 7.8(a) presents the variation of CO₂ heat transfer coefficient (hc_r) with bulk temperature at supercritical pressure between 7.5 MPa to 10

MPa, whilst in Figure 7.8(b) illustrates the effect of oil concentration with the hc_r at supercritical pressure (8MPa). And the CFD model results from this current study are presented in Figure 7.8(c) to compare the hc_r profile from this study and the literature.



(a) Pure CO₂ heat transfer coefficient (Oh and Son, 2010)

(b) CO₂ with oil heat transfer coefficient (Jun and Yung, 2013)



(c) Variation of heat transfer coefficient with bulk temperature from CFD Result of gas cooler-A and B

Figure 7.8 The heat transfer coefficient from Oh and Son (2010), Dang *et al.* (2012), Jun and Yung (2013) and this study's results

The past experimental study carried out the test in a horizontal long pipe and indicated that the gas cooling pressure, of CO₂ have significant effects on the heat transfer coefficients. It reaches a peak near the pseudo-critical temperature and the value is damped with increasing pressure. The heat transfer coefficient of the CO₂ –lubricating oil mixture seem large deviations occur between Dang *et al.* (2012), and Jung and Yung (2013) results, especially in the pseudo–critical area. Dang *et al.*(2012) have got much higher hc_r in the near pseudo-critical area (from 30°C to 40°C), whilst after a

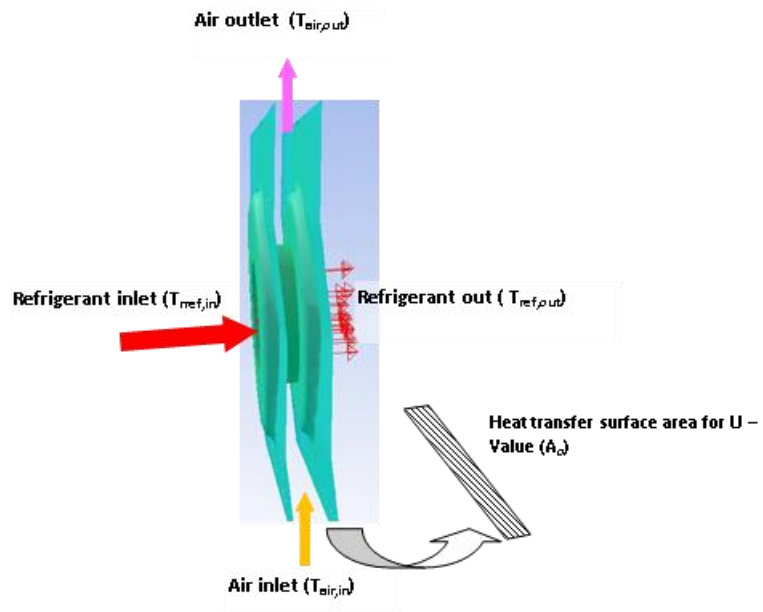
temperature of 50°C, the deviation seem to be closer. The large deviation seems due to the significant c_p increasing in the pseudo-critical region.

On the other hand, the CFD model from this current study investigated the segments in two actual gas-coolers, 2.44 mm long with finned-tubes, under mass flow rates of 0.0095 kg/s and 0.0195 kg/s and pressures of 82 bar_g and 83 bar_g. It was observed that the maximum hc_r also occurs at the temperature approximately 40°C, whereby the hc_r decreases significantly from temperatures 50 °C to 105 °C. Hence, it can be justified that the CFD model provided satisfactory trends compared with both the literature and actual experimental data. However, the usefulness of using CFD lies in its flexibility to act as a design and evaluation tool, as opposed to requiring expensive and time-consuming experimental setups.

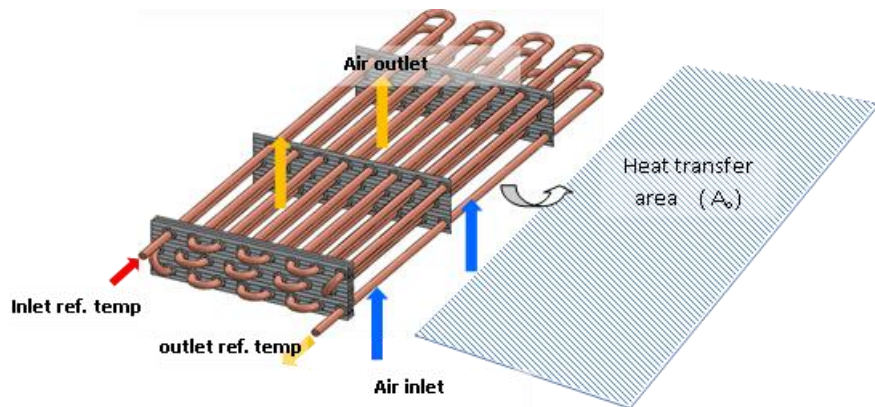
7.3 Overall heat transfer coefficient (U)-Log Mean Temperature Difference (LMTD) of gas coolers

Since the inlet and outlet temperatures of working fluid in gas coolers were specified by CFD in the segment, so that become to be easily to determine overall heat transfer coefficient using the U-LMTD method. In this study, the U-LMTD was investigated for each segment (using CFD) and compared with the U-LMTD in entire gas cooler from the experimental results.

Figure 7.9(a) shows a gas cooler segment which consists of the refrigerant pipe and two fins, which allow the determination of the air-flow parameters and heat transfer area (A_o) in order to calculate the overall heat transfer coefficient (U-LMTD) for each segment. Figure 7.9 (b) shows one circuit of gas cooler construction which allows the calculation of the U-LMTD from the experimental test.



(a) U-LMTD calculation in segment



(b) U-LMTD calculation from experimental result of one circuit coil of gas cooler-A

Figure 7.9 Overall heat transfer area

The overall heat transfer coefficient (U) was evaluated using Equation (7.2), heat rejection rate (Q -Watt) calculated using Equation (7.3), and the external heat transfer area (A_o) defined according to Figure 7.9.

$$U = \frac{Q}{A_o \Delta LM} \quad (7.2)$$

$$Q = \dot{m}_{air} \cdot \Delta h_{air} \quad (7.3)$$

where, ΔT_{LM} = Log mean temperature different, calculated from the following Equation (7.4):

$$\Delta T_{LM} = \frac{\Delta T_2 - \Delta T_1}{\ln\left(\frac{\Delta T_2}{\Delta T_1}\right)} \quad (7.4)$$

where ΔT_1 and ΔT_2 are defined as follows:

$$\Delta T_1 = T_{ref,i} - T_{air,o} \text{ and } \Delta T_2 = T_{ref,o} - T_{air,i} \quad (7.5)$$

where subscripts i and o represent inlet and outlet, respectively. The example of overall heat transfer coefficient calculation is given in Appendix F.

Since the gas cooler-B and gas cooler-A have different numbers of circuit, i.e. 2-circuits and 4-circuits, respectively, the heat transfer area (A_o) of one circuit of the gas cooler-B is doubled that of the gas cooler-A. The heat transfer area (A_o) for both gas coolers is illustrated in Figure 7.10.

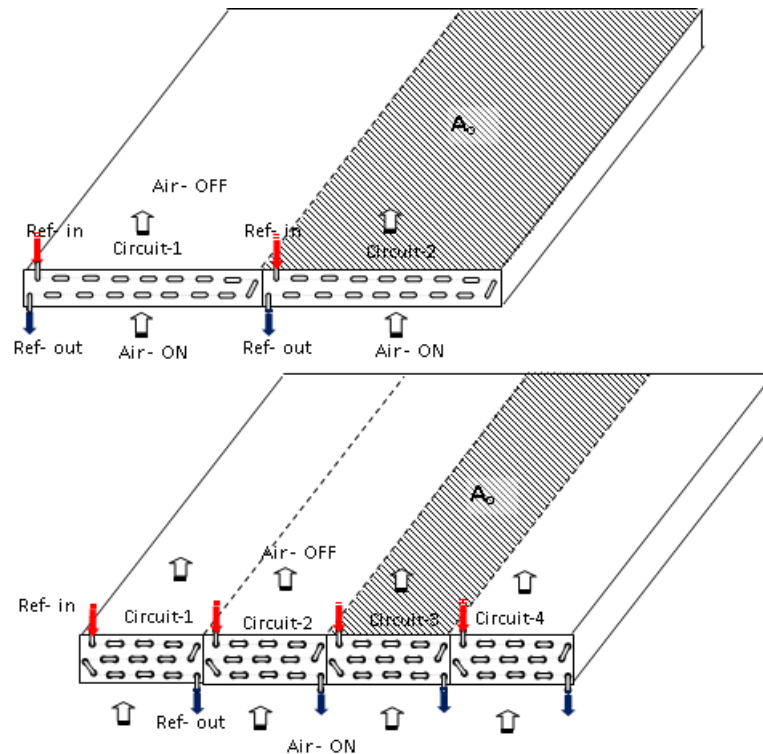
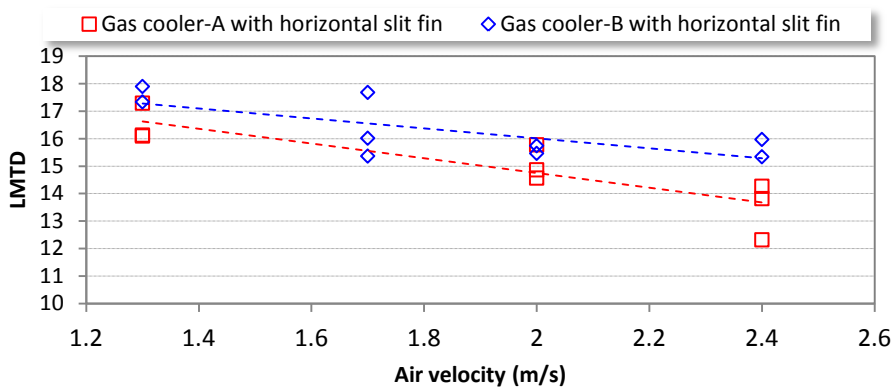


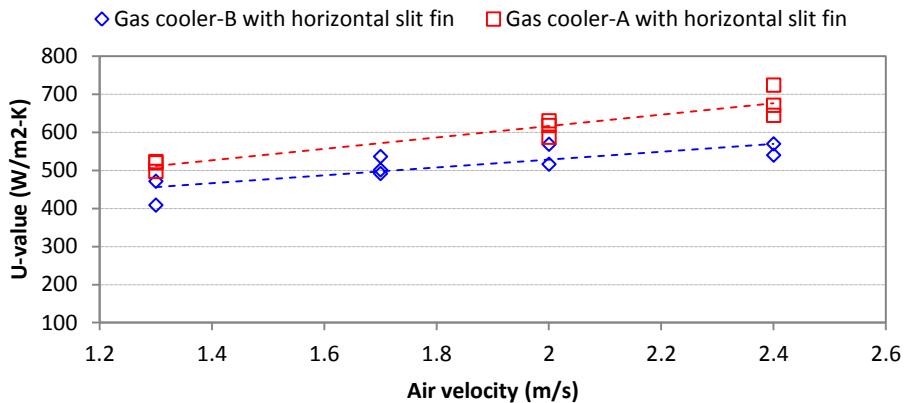
Figure 7.10 Schematic diagram of heat transfer area (A_o) of gas cooler-B and gas cooler-A from experimental result

7.3.1 The U-LMTD from the experimental results

In this section, the U-LMTD from the experimental result toward both gas-cooler types with horizontal slit fin in one circuit are investigated and illustrated in Figures 7.11 (a) and (b), referring to the schematic diagram of the gas cooler in Figure 7.10. The results of U-LMTD are presented in respect to the air velocity.



(a) Variation of LMTD profile with air velocity in entire gas cooler –experimental result



(b) Variation of U-value profile with air velocity in entire gas cooler –experimental result

Figure 7.11 Experimental U-LMTD results for gas cooler-A and B with horizontal slit fin

The average *U-value* of gas cooler-A is higher than gas cooler-B, although, gas cooler-B has refrigerant-side heat transfer coefficient almost doubled than that of gas cooler-A. However, the heat transfer area (A_o) in one circuit of gas cooler-B is also twice than that of gas cooler-A. The better performance of gas cooler-A seems to be due to the better design especially for the number of circuit and row configuration as already explained in Section 6.5.

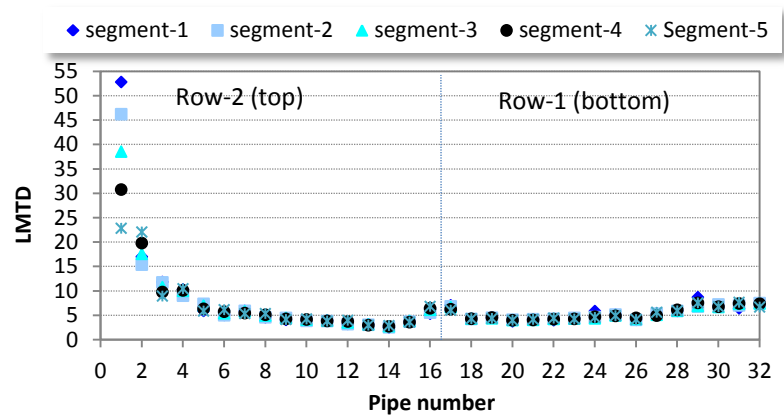
7.3.2 The U-LMTD from the CFD model results

The U-LMTD investigations using CFD are conducted at segments refers to segments which were presented in Chapter VI. In following section presents the U-LMTD for gas cooler-B with continuous and horizontal-slit fin configurations, in addition for the case of the horizontal-slit fin, the U-LMTD from experimental results for whole gas cooler in one circuit is also examined in order to compare the numerical result. Gas cooler-A has three different fin designs as described in Chapter 6, whereby the U-LMTD was also investigated using the same methodology with the air side heat transfer coefficient investigation. Both numerical and experimental results are shown in this section.

7.3.2.1 The U-LMTD for gas cooler-B with continuous fin

Figure 7.12(a) shows the LMTD variation for each segment and Figure 7.12(b) shows the U-value profile in the segments, with these results obtained from the numerical CFD model.

It can be seen that the LMTD changed significantly along pipe-1 until pipe-3. From pipe -4 until pipe 32 LMTD slightly uniform, only there are some gains especially, at pipe 16 and slightly at pipe 30-32. These heat gains are related to the heat transfer from the other adjacent hot pipes. The LMTD changes significantly in pipe-1 to pipe-4 seem effected by the refrigerant side heat transfer coefficient effect which also occur significant changed in these pipes, the effect of the refrigerant side in the pipe location was explain in the Section 7.2.1.



(a) LMTD profile in segment

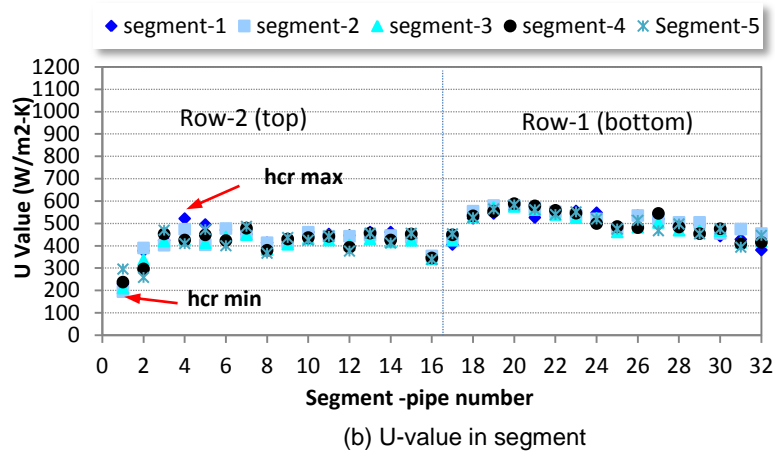
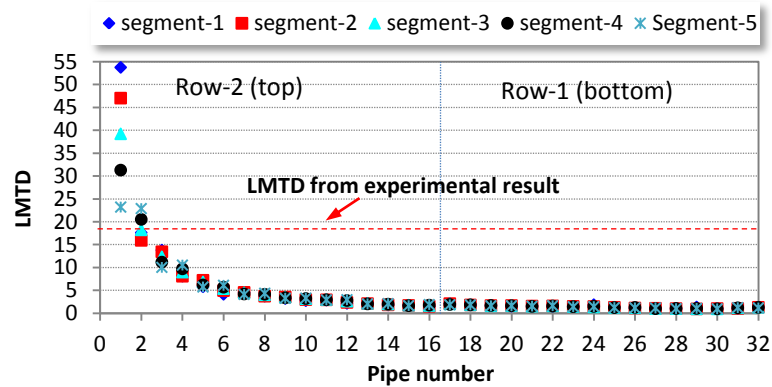


Figure 7.12 U- LMTD profile in gas cooler-B with continuous fin configuration
(Test condition air velocity: 1.3 m/s)

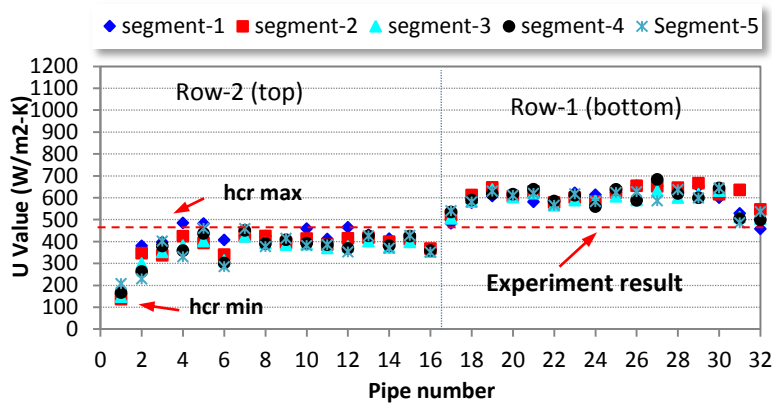
For the Figure 7.12(b) shows the U-values in pipe-1 to pipe-3 change with the pipe numbers, while from pipe-4 to pipe-16, the U-value is relatively uniform. It also shows the refrigerant-side heat transfer coefficient ($h_{c,r}$) effect which minimum at pipe-1 and maximum at pipe-4 (see Figure 7.4). In addition, at several segments, especially in pipes 16, 17, 30, 31, and 32, the U-value decreased and the average U-value in the bottom row seems to be slightly higher than the top row, due to the air-side heat transfer coefficient effect. As the fin is continuous, some heat gains occur especially, in pipe-16 and pipe-17 and also in pipes 30-32. This is related to the heat transfer conduction as described in experimental results Section 4.6.4.

7.3.2.2 U-value for gas cooler –B horizontal-slit fin segments

Figure 7.13 shows the LMTD – U value profile of gas cooler-B with horizontal-slit fin and the red straight line indicate the average U-value from the experimental test. Figure 7.13(a) confirms that the LMTD decreased significantly in the bottom row-1, when compared to the continuous fin design, mainly due to the slit, since the heat from row-2 can be blocked properly. As a result, Figure 7.13(b) shows the horizontal slit configuration contributes to an increase in the U-value in row-1 (the average percentage of improvement explained in Section 7.3.3).



(a) LMTD profile in segment



(b) U-value in segment

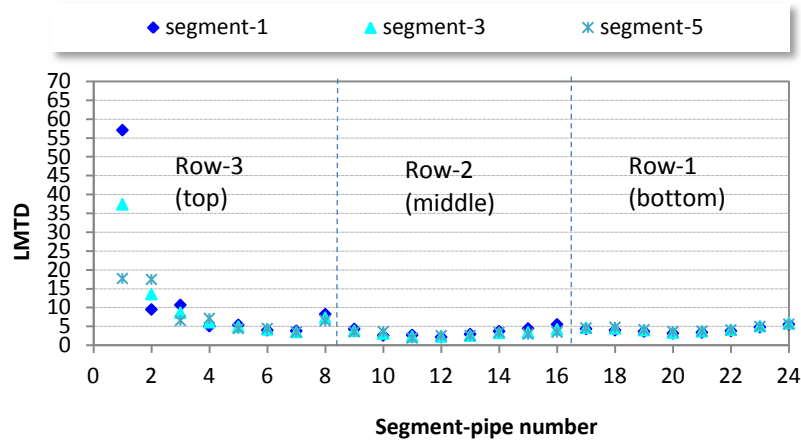
Figure 7.13 U-LMTD of gas cooler – B with horizontal-slit fin
(Test condition: air velocity: 1.3 m/s)

In summary, The U-LMTD profiles of gas cooler-B with the continuous and horizontal-slit fins show that the individual U-values did not remain constant and uniform in the entire heat exchanger but varied across the exchanger surface area. The overall heat transfer coefficient (U-value) trend line seems more as an effect of air-sides heat transfer coefficient rather than the refrigerant-side (the refrigerant side only effected more in pipe 1, pipe 2 and 3). The model has been able to show that reasonably accurate results can be obtained when compared with U-value calculation from tests conducted on a gas cooler in the laboratory with the errors is only 1%-7% (average the model and experimental errors are explained in Section 7.3.3).

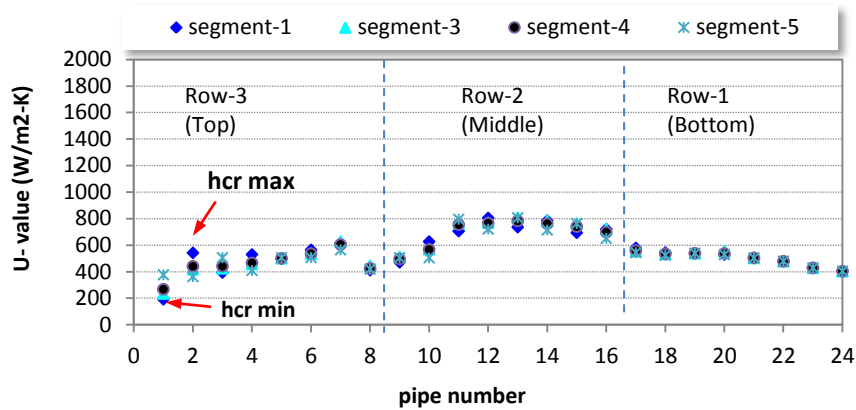
7.3.2.3 U-LMTD value for gas cooler-A continuous fin segments

Figure 7.14 (a) and (b) show the U- LMTD profiles of gas cooler-A with the continuous fin segments. The LMTD, because of the continuous fin construction, there is a heat

gain in pipe-8, pipe-16 and slightly in pipe-24. And the LMTD is significant high in the pipe-1 and 2, this is corresponded to refrigerant temperature profile along first pipe lead to changed significantly of the refrigerant side heat transfer coefficient (hc_r) which the trend in the pipe explained in the Section 7.2.2.



(a) LMTD profile in segment



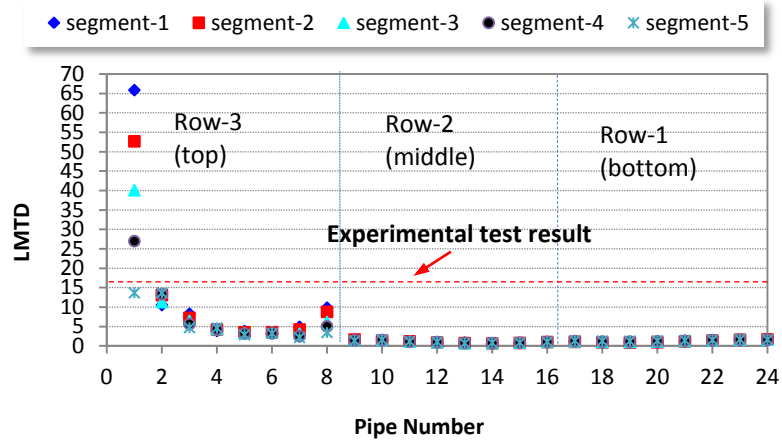
(b) U-value profile in segment

Figure 7.14 U-LMTD of gas cooler-A with continuous fin
(Test condition: air velocity: 1.7 m/s)

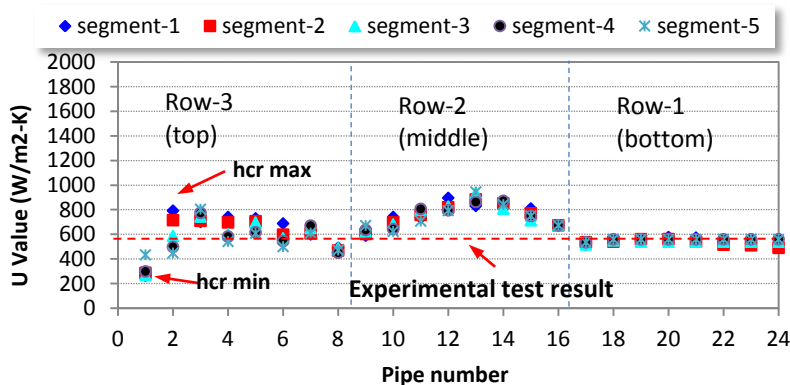
Similar with gas cooler-B investigation, the U value trend line seem to be more influenced by the air side heat transfer coefficient trend line. The U-value of the middle row shows slightly higher values than row-1 and row-3, due to the air-side effect that in the middle row the best air turbulence occurs which was explained in the Section 5.12.2 and Section 6.4.1. In addition at the position that the hc_r (refrigeration side heat transfer coefficient) getting maximum and minimum also seem effected to the U-value as shown in Figure 7.14.

7.3.2.4 U-LMTD value in segment of gas cooler-A with horizontal slit fin

The LMTD and U-values of the horizontal-slit fin design for gas cooler-A are shown in Figure 7.15 (a) and (b), with the experimental result highlighted by the dotted red-line. Because of the slit, the LMTD in the middle row and bottom row are become lower compared with the continuous fin in Figure 7.14, but in pipe-8 still get the heat gain from the first pipe that caused the LMTD increased.



(a) LMTD profile in segment



(a) LMTD profile in segment

Figure 7.15 U-LMTD of gas cooler-A with horizontal-slit fin
(Test condition: air velocity 1.7 m/s)

As a result because of the horizontal slit fin configuration, the U-value increased in the some segment of the top and middle row of the gas cooler comparing with the continuous fin, however in the bottom row the U also increases slightly, especially at the pipe 23 and pipe 24 . This is due to the better air side heat transfer and affected to the U-value trend line. The effect of the maximum and minimum of refrigerant side heat transfer coefficient (h_{c_r}) also seem clearly in the Figure 7.15.

7.3.2.5 U-LMTD value for gas cooler-A with horizontal and vertical slit fin segments

The effects of the vertical slit are shown in the Figure 7.16(a), where it can be seen that there is no LMTD gain in pipe-8, resulting in the U-value also increasing in this segment as shown in Figure 7.16(b). The average experimental LMTD and U-value for the entire circuit gas cooler is also shown, represented by the dotted red straight line.

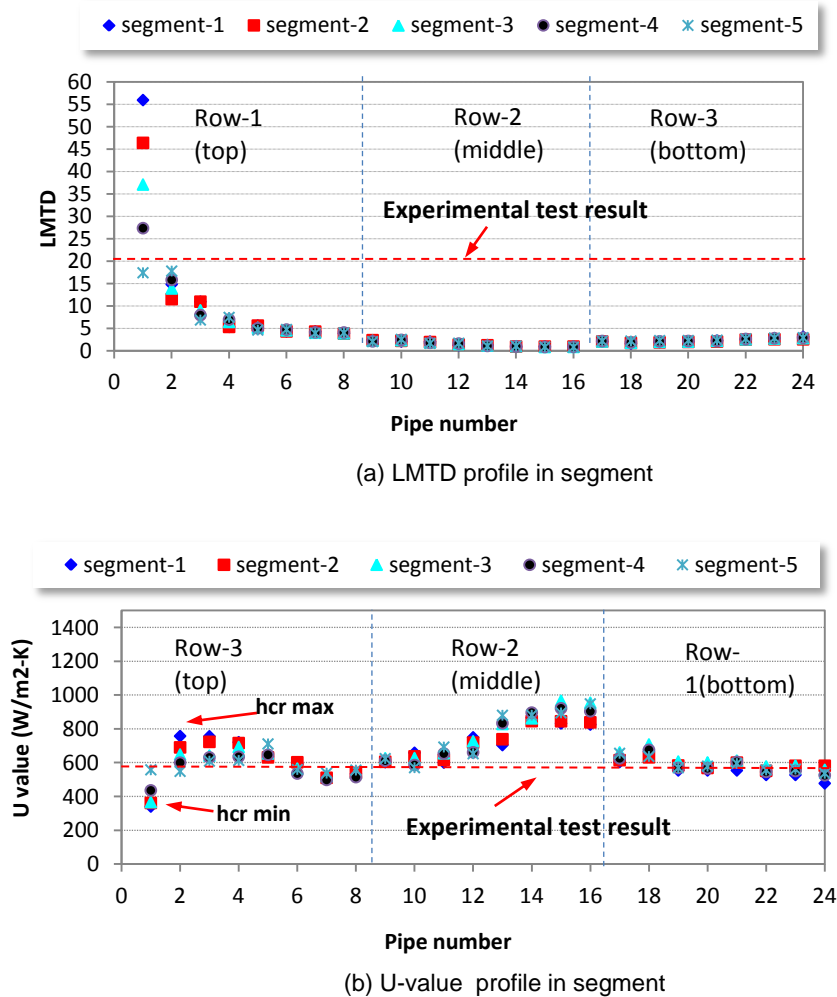


Figure 7.16 U-LMTD of gas cooler A with horizontal and vertical slit fin
(Test condition: air velocity 1.7 m/s)

The vertical slit fin only slightly contributes to increase U – value in the pipe-8 and overall average contribution is not high only maximum 1% contributed the performance.

In summary, the U-value profiles of gas cooler-A in each segment show strong relation with the air-side heat transfer coefficients and also slightly refrigerant side heat transfer coefficient especially in the top row within the pipe-1 and pipe-2.

7.3.3 Variation of mean U-value with air velocity in entire gas coolers

Figure 7.17 presents the U-value with respect the air velocity (m/s), for the results from the average CFD model and experiments results as described in section 7.3.1. Figure 7.18 presents the percentage of error the model result comparing with the experimental result for the average U-value in entire gas cooler.

The overall heat transfer coefficient increases as air velocity increases, due to an increase in the Reynolds Number. An increase in Reynold Number implies that more energy will be transferred from the refrigerant due to higher bulk movement (convection) of the air. In addition, the slit-fin design contributes positively to the overall heat transfer coefficient improvement.

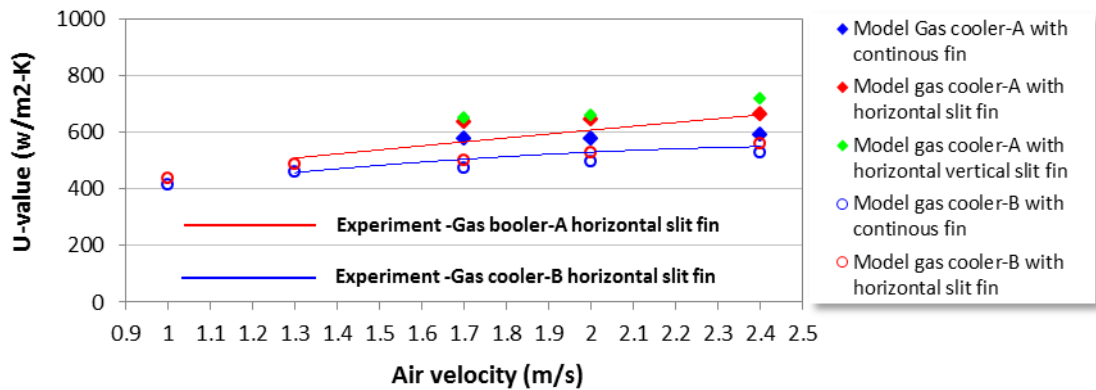


Figure 7.17 Variation of air side heat transfer coefficient with air-velocity for different gas cooler types

The mean overall heat-transfer coefficients of gas cooler-A from the model were found to vary between 650 W/m²K – 718 W/m²K for the ‘vertical and horizontal’ slit fin, 638 W/m²K – 665 W/m²K for the horizontal fin and 576 W/m²K – 592 W/m²K continuous fin design with the air velocity varies from 1.7 m/s to 2.4 m/s. Furthermore, for gas cooler-B were found vary between 438 W/m²K – 558 W/m²K for the horizontal slit fin, 413 W/m²K – 526 W/m²K for the continuous fin design with the air velocity vary from 1 m/s to 2.4 m/s . Comparing with the experimental investigations, deviations of around 8%-9.7% and 1%- 7% were observed for gas cooler-A and gas cooler-B, respectively. Gas cooler-A model get more error that gas cooler B because of temperature refrigerant on the bottom row of the gas cooler slightly fluctuate. However, it can be considered that the CFD model results have a good agreement with the experimental results since the error is less than 10%.

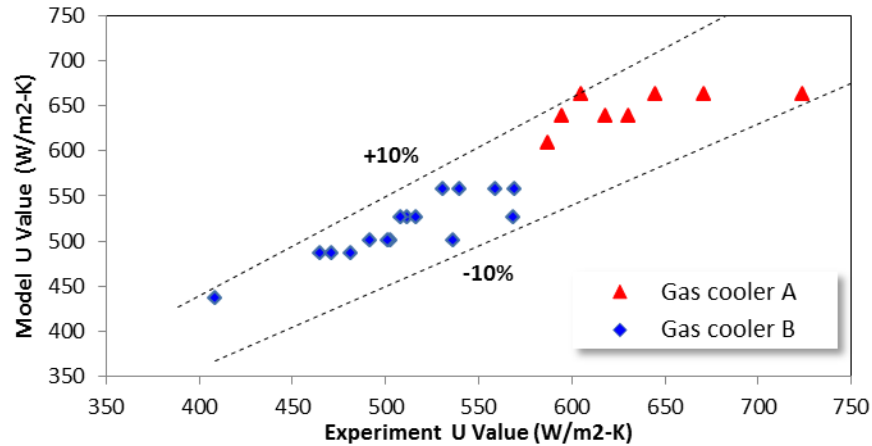


Figure 7.18 U Value errors of the CFD results compared with the experimental results

The improving gas cooler geometry with higher number of row and circuit (2 rows - 2 circuits to 3 rows - 4 circuits) obtained increases in the overall heat transfer coefficient of the gas cooler by 20%-25%, but will lead to increased size and capital cost.

7.4 Summary

This chapter used the CFD model to investigate the refrigerant-side (hc_r) and the overall heat transfer coefficients ($U-LMTD$) for individual segments of the gas cooler. The bulk temperature and refrigerant mass flow rate are significant influence to the refrigerant side heat transfer coefficient (hc_r) and the variation show coincide with the variation of the specific heat (c_p) with temperature. In the special operating condition (at operating pressures are 82 bar_g and 83 bar_g), the hc_r reach peak at bulk temperature of 40°C and the lowest hc_r occurs at the highest bulk temperature.

The U-LMTD was also calculated from experimental results for a circuit of the entire gas cooler to compare the U-value and LMTD obtained from the model. Compared with the experimental results, maximum deviations around 9.7% observed for the gas coolers. The CFD model enable evaluate more deeply the overall heat transfer coefficient segment by segment along the gas cooler. The results have shown that the overall heat transfer coefficient is influenced by both air-side and refrigerant-side heat transfer coefficient. In this investigation also found that better gas cooler construction such as higher number of row and number of circuit can improve the overall heat transfer coefficient by 20%-25%.

Chapter 8 will summarise the results of the investigations in this study and will provide some recommendations for future work.

CHAPTER VIII - CONCLUSIONS AND RECOMMENDATIONS FOR FUTURE WORK

The use of Carbon dioxide (CO₂) as a refrigerant has become more popular in recent years because of environmental concerns. In general, for supermarket refrigeration systems, greenhouse gas emissions are indirect due to electricity used to drive them and direct from refrigerant leakage. The use of CO₂ as refrigerant is a way of reducing direct emissions from refrigeration plant.

Finned tube heat exchangers are the most common type of gas cooler/condenser in CO₂ refrigeration systems because of the flexibility in their manufacture and direct heat rejection to the ambient.

In this thesis, the performance of gas coolers was investigated both experimentally in the laboratory and through numerically using Computational Fluid Dynamics (CFD) modelling. The experiments were carried out at both sub-critical and supercritical operating conditions and the tests involved four gas cooler designs. The experimental test facilities involved a 'booster' CO₂ refrigeration system with hot gas bypass and a specially designed and fabricated gas cooler test rig.

In more detail, the research involved:

- A literature review of carbon dioxide (CO₂) as a natural refrigerant including its thermophysical properties; the different types and designs of CO₂ refrigeration systems (i.e., booster with hot gas bypass, internal heat exchanger (IHX), and the use of ejectors); discharge pressure optimisation and control in the supercritical mode of operation; heat transfer and pressure drop in finned-tube heat exchangers.
- The development of a gas cooler test rig and improvement of the existing CO₂ refrigeration system in the laboratory through the installation of a medium temperature (MT) additional load, MT display cabinet and MT air cooler to provide additional refrigeration load for the system.

- Experimental investigations to determine the performance of different gas cooler coils over a range of sub-critical and supercritical operating conditions including a range of air flow velocities, refrigerant mass flow rate and degree of sub-cooling.
- Analytical investigation of the gas cooler design and sizing to determine the effect of the number of rows and circuits and the use of slit fin configuration to enhance performance.
- Development of a CFD modelling approach to simulate the performance of the gas cooler within reasonable computational time and validation of the model with experimental data.
- Investigation of air-side, refrigerant-side and overall heat transfer coefficients using the CFD model.

The findings from the research and recommendations for future work are given below.

8.1 Conclusions

8.1.1 The literature review revealed that:

- As a natural refrigerant, carbon dioxide (CO₂) has very good thermophysical properties and can provide high heat transfer rates in heat exchangers. It is also environmentally friendly with zero Ozone Depletion Potential (ODP) and negligible Global Warming Potential (GWP) of 1.0.
- CO₂ refrigeration systems are becoming more popular with several design options for supermarket applications.
- In the supercritical mode of operation there is an optimum pressure that maximises system COP. This pressure is mostly a function of the outlet gas cooler refrigerant temperature.
- The refrigerant side heat transfer coefficient is significantly influenced by mass flux and temperature of the CO₂.

8.1.2 Test facilities were designed and built to facilitate the experimental programme. They involved a CO₂ booster refrigeration system with hot gas bypass with two parallel variable speed compressors at medium level evaporating temperature and refrigeration load of the order of 14.5 kW. At maximum capacity, heat rejection by the gas cooler was around 15 kW. The system provided stable operating conditions for the test

programme. The main controller of the CO₂ refrigeration system enabled stable control of gas cooler pressure, compressor speed, degree of sub-cooling and MT evaporating pressure to provide the required refrigerant test conditions for the gas cooler.

A specially designed gas cooler test rig enabled the variation of air flow rate and air-on temperature of the gas cooler. The air-on temperature range enabled the simulate from subcritical mode to supercritical mode operation. The air velocity variation was regulated by the fan speed and got accuracy correlation of percentage (%) of fan full speed with air velocity (m/s).

8.1.3 A series of tests were carried out to investigate the performance of four gas cooler types. The performance of the gas coolers was mainly established from the heat rejection rate (Q), and approach temperature (AT). The experimental results indicated that:

- The performance of the supercritical mode was found to be lower than the subcritical mode this is indicated by heat rejection decrease as the air-on temperature increased. This is because with higher air-on temperature the heat transfer rate in the heat exchanger is reduced due to the fact that some important thermal physical properties of CO₂ (such as specific heat, density, viscosity) are strongly dependent on its temperature and pressure.
- Pressure drop of refrigerant in the gas cooler was found to reduce with increasing gas cooling pressure due to a reduction in refrigerant density. The pressure drop also reduced with reducing refrigerant mass flow rate and pipe flow length. The refrigerant side pressure drop in the gas cooler for fixed pipe length can be kept within acceptable limits by using appropriate number of pipe circuits, thus varying the refrigerant mass flow through each circuit.
- Air-side pressure drop correlations for the tested gas coolers were developed using the experimental test data. As expected, the air side pressure drop was found to increase with increasing air velocity and number of rows in the air flow direction.
- The slit fin design can improve the performance of the gas cooler by eliminating conduction across the fin between the first and second row of tubes. This was demonstrated using an infrared camera and through CFD modelling.

8.1.4 Computational Fluid Dynamics (CFD) modelling was employed to investigate heat transfer in the gas cooler. The main conclusions are as follows:

- The k- ϵ realizable turbulence model was found to provide the best performance in comparison to test results from the turbulence models investigated.
- Due to the complexity of the problem for CFD simulation of the whole heat exchanger, the gas cooler was modelled in segments using experimental data as inputs to each segment. This was found to be a reasonable compromise between modelling complexity and simulation accuracy.
- Maximum error in the simulation of the heat rejection (Q) of the gas cooler was found to be lower than 10% and mean error 4.7 % compared to data from the experimental tests. Maximum error in the simulation of the air temperature at the outlet of the gas cooler (air off) was found to be 1.5 °C, and the mean error 0.57 °C. CFD results of the simulation of the fin temperature showed average error of less than 1.5 °C. These errors were considered acceptable considering the uncertainty of the experimental measurements.

8.1.5 The air-side heat transfer coefficient (hc_a) was investigated using the CFD model with the following results:

- The local air side heat transfer coefficient in a segment is influenced by the position in the heat exchanger in the direction of air flow and the local conditions of air temperature and velocity.
- A correlation relating the average air side heat transfer coefficient to the Reynolds Number showed the air side heat transfer coefficient increases with increasing Reynolds number.
- The slit fin configuration contributed to increasing the air side heat transfer coefficient. A horizontal slit increased the heat transfer coefficient by 6%-8% and a vertical slit by an additional 1%-2%.

8.1.6 The refrigerant side heat transfer coefficient (hc_r) was investigated in the gas cooling process. The results are as follows:

- The variation of the refrigerant heat transfer coefficient follows the variation of the specific heat (c_p) with temperature. For pressures in the region of 82 bar_g -83

bar_g the maximum hc_r occurred at a bulk refrigerant temperature of approximately 40 °C.

- In this study, the significant change in the refrigerant heat transfer coefficient occurred in the first three pipes.
- The CFD methodology employed was found to adequately represent the heat transfer characteristics of the gas cooler, as well as act as an effective simulation tool to determine local refrigerant-side heat transfer coefficient.

8.1.7 In this study, the overall heat transfer coefficient (*U-value*) was investigated using the Log Mean Temperature Difference (*LMTD*) approach from experimental data and CFD simulation results. The findings are as follows:

- Experimental results showed that the overall heat transfer coefficient of the gas cooler increased almost linearly with gas cooler face air velocity.
- Results for the overall heat transfer coefficient obtained from CFD modelling showed good agreement with results obtained from the test data - the maximum error was found to be 9.7%.
- The modelling approach can be used to investigate the influence of the gas cooler design and operating parameters on overall heat transfer and heat rejection parameters.

8.2 Recommendations for future work

Due to limitations of the test rig and safety considerations, tests at high pressures were limited. Tests at pressures up to 120 bar will be useful in providing a wider range of data for model development and validation. It is therefore recommended that the test facility be improved to enable operation at pressures up to 120 bar.

To improve the reliability of the test results, tests should also be conducted at better controlled environmental test conditions, for example in an environmental test chamber.

In addition, a more comprehensive instrumentation should be used to enable measurement of pipe, fin and air temperatures at many more positions than what was achieved in this study.

Regarding the numerical simulation portion of this study, although providing validated results, there are further improvements possible for the CFD model. The model has been developed based on the assumption of non-slip conditions for the fin and pipe surfaces, and as a result the pressure drops across the fins and pipes involve small errors. This consideration of surface topology for frictional studies was not performed in this study, due to unavailability of data. Hence, future modelling studies should aim at also quantifying the surface topology and characteristics of the gas cooler in order to ensure pressure drop predictions with less error, and therefore also allow more accurate predictions of fan power requirements.

CFD simulations are very appropriate for air-flow predictions as they directly solve the discretised Navier-Stokes equations, however a major drawback is the large time considerations for the simulations. For instance, the mean simulation time in this study was 4-5 hours using a computer with capacity of 2.6GHz, 32GB RAM, Intel Xeon[®] Processor with 16 parallel threads. These large simulation times therefore limit the performance of parametric analyses for gas coolers, which are especially important in the design phases of the gas cooler. In this respect, a possible improvement to this simulation strategy would be to employ CFD models to generate enough data so as to formulate correlations, as done in this study, and henceforth employ these correlations in simple nodal models. Such models can be developed in platforms such as EES, MATLAB or TRNSYS, and would require a lot less time to run parametric analyses.

REFERENCES

- Ahammed, M.E., Bhattacharyya, S., Ramgopal, M., 2014. Thermodynamic design and simulation of a CO₂ based transcritical vapour compression refrigeration system with an ejector. *International Journal of Refrigeration* 45, 177-188.
- ANSYS FLUENT User's Guide, 2013. Release 13.0, P.699
- Aprea, C, and Maiorino, A, 2008. An experimental evaluation of the transcritical CO₂ refrigerator performances using an internal heat exchanger. *International Journal of Refrigeration* 31, 1006-1011.
- ASHRAE, 2010. ASHRAE Handbook of Refrigeration. ASHRAE, Inc., Atlanta, 749 pgs.
- ASHRAE, 2014. ASHRAE Handbook of Refrigeration. ASHRAE, Inc., Atlanta, 749 pgs.
- Asinari, P, Cecchinato, L, Fornasieri, E, 2004. Effect of thermal conduction in microchannel gas coolers for carbon dioxide. *International Journal of Refrigeration* 27, 577-586.
- Beaver, A.C., Yin, J.M., Bullard, C.W., Hrnjak, P.S., 1999. An experimental investigation of transcritical carbon dioxide systems for residential air-conditioning. *ACRC Report CR-18. University of Illinois at Urbana-Champaign, Urbana, USA.*
- Bhutta, M.M.A.B., Hayat, N., Bashir, M.H., Khan, A.R., 2012. CFD applications in various heat exchangers design: A review. *Applied Thermal Engineering* 32, 1 –12.
- Bilirgen, H., Dunbar, S., Levy, E.K., 2013. Numerical modelling of finned heat exchangers. *Applied Thermal Engineering* 61, 278 – 288.
- Cang, Y., and Kim, M., 2006. Modeling and performance simulation of gas cooler for CO₂ heat pump system. *Proc. International Refrigeration and Air Conditioning Conference, Purdue University, paper 764.*
- Cen, J., Liu, P., Jiang, F., 2012. A novel transcritical CO₂ refrigeration cycle with two ejectors. *International Journal of Refrigeration* 35, 2233-2239.
- Chen, Y., and Gu, J., 2005. The optimum high pressure for CO₂ transcritical refrigeration systems with internal heat exchangers. *International Journal of Refrigeration* 28, 1238-1249.
- Choi, J.M., Kim, Y., Lee, M., 2010. Air side heat transfer coefficients of discrete plate finned-tube heat exchangers with large fin pitch. *Applied Thermal Engineering* 30, 174 – 180.
- Danfoss, 2009. Product catalogue. Available from: www.danfoss.co.uk.
- Danfoss, 2010. Product catalogue. Available from: www.danfoss.co.uk.
- Danfoss-Optyma OP-MCHC034GSA01G. Product catalogue, available from: www.danfoss.co.uk

- Dang, C., and Hihara, E. , 2004. In-tube cooling heat transfer of supercritical carbon dioxide. Part 1. Experimental measurement. *International Journal of Refrigeration* 27, 736 – 747.
- Dang, C., Hoshika, K., Hihara, E., 2012. Effect of lubricating oil on the flow and heat-transfer characteristics of supercritical carbon dioxide. *International Journal of Refrigeration* 35, 1410 – 1417.
- Dang, C., Iino, K., Fukuoka, K., Hihara, E., 2007. Effect of lubricating oil on cooling heat transfer of supercritical carbon dioxide. *International Journal of Refrigeration* 30, 724 – 731.
- EES, 2013. Engineering Equation Solver. www.fChart.com
- Elbel, S., and Hrnjak, P., 2008. Experimental validation of a prototype ejector designed to reduce throttling losses encountered in transcritical R744 system operation. *International Journal of Refrigeration* 31,411-422.
- Fangtian, S., and Yitai, M. , 2011. Thermodynamic analysis of transcritical CO₂ refrigeration cycle with an ejector. *Applied Thermal Engineering* 31, 1184-1189.
- Fillipini, S., and Merlo, U., 2011. New finned heat exchanger development with low refrigerant charge. *Proc. on ICR*, Prague, Czech Republic, ID:296.
- Finckh, O, Schrey, R., Wozny, M., 2011. Energy and efficiency comparison between standardized HFC and CO₂ transcritical systems for supermarket applications. *23rd Int. Congr. of Refrig.*, Prague.
- Ge, Y.T, and Tassou, S.A., 2009. Control optimisation of CO₂ cycles for medium temperature retail food refrigeration systems. *International Journal of Refrigeration* 32,1376-1388.
- Ge, Y.T, and Tassou, S.A., 2011a. Thermodynamic analysis of transcritical CO₂ booster refrigeration systems in supermarket. *Energy Conversion and Management* 52,1868-1875.
- Ge, Y.T, and Tassou, S.A., 2011b. Performance evaluation and optimal design of supermarket refrigeration systems with supermarket model “SuperSim”. Part II: Model applications. *International Journal of Refrigeration* 34,540-549.
- Ge, Y.T., and Cropper, R.T., 2009. Simulation and performance evaluation of finned-tube CO₂ gas coolers for refrigeration systems. *Applied Thermal Engineering* 29,957-965.
- Gnielinski V., 1976. New equation for heat and mass transfer in turbulent pipe and channel flow. *Int. J. Chem. Eng.* 16, 359-368.
- Gowreesunker, B.L., and Tassou S.A., 2013. Effectiveness of CFD simulation for the performance prediction of phase change building boards in the thermal environment control of indoor spaces. *Building and Environment* 59, 612-625.
- Gupta, D.K., and Dasgupta, M.S.,2014. Simulation and performance optimization of finned tube gas cooler for trans-critical CO₂ refrigeration system in Indian context. *International Journal of Refrigeration* 38,153-167.
- Gupta, K, Singh, D.K., Dasgupta, M.S., 2010. Environmental effect on gas cooler design for transcritical carbon dioxide refrigeration system in India context. *Journal of Advanced Research in Mechanical Engineering* , pp.147-152.

- He, Y.L., Chu, P., Tao, W.Q., Zhang, Y.W., Xie, T., 2013. Analysis of heat transfer and pressure drop for fin-and-tube heat exchangers with rectangular winglet-type vortex generators. *Applied Thermal Engineering* 61, 770 – 783.
- Hwang, Y., Jin, D.H., Radermacher, Hutchins, J.W., 2005. Performance measurement of CO₂ heat exchangers. *ASHRAE Transactions* 111(2).
- IIR Guide., CO₂ as a refrigerant. Editor by Dr A. B. Pearson, International Institute of Refrigeration, ISBN: 978-2-36215-006-7. 2014.
- Incropera F.P., DeWitt D.P. Introduction to Heat Transfer. third ed. New York John: Wiley and Sons; 1996.
- Jung, J.Y., and Yun, R., 2013. Prediction of gas cooling heat transfer coefficients for CO₂- oil mixtures. *International Journal of Refrigeration* 36, 129 – 135.
- Kim, Y., 2005. Heat transfer characteristics of flat plate finned-tube heat exchangers with large fin pitch. *International of Refrigeration* 28, 851-858.
- KIMO,2013. available at www.kimo.co.uk
- Lauder, B.E., and Spalding, D.B., 1972. Lectures in mathematical models of turbulence. academic press, London, England
- Liao, S.M., Zhaoa, T.S., Jakobsen, A., 2000. A correlation of optimal heat rejection pressures in transcritical carbon dioxide cycles. *Applied Thermal Engineering* 20,831-841.
- Lucas, C., and Koehler, J., 2012. Experimental investigation of the COP improvement of a refrigeration cycle by use of an ejector. *International Journal of Refrigeration* 35, 1595-1603
- Nakagawa, M., Marasigan, A.R., Matsukawa, T., 2011. Experimental analysis on the effect of internal heat exchanger in transcritical CO₂ refrigeration cycle with two-phase ejector. *International Journal of Refrigeration* 34,1577-1586.
- Oh, H.K., and Son, C.H., 2010. New correlation to predict the heat transfer coefficient in-tube cooling of supercritical CO₂ in horizontal macro-tube. *Experimental Thermal and Fluid Science* 34,1230-1241.
- Ommen, T., and Elmegaard, B., 2012. Numerical model for thermoeconomic diagnosis in commercial transcritical/subcritical booster refrigeration system. *Energy Conversion and Management* 60, 161-169.
- Park, C.Y., and Hrnjak P., 2006. Effect of heat conduction through the fins of a microchannel serpentine gas cooler of transcritical CO₂ system. *International Journal of Refrigeration* 30, 389-397.
- Perrotin, T., and Clodic, D., 2004. Thermal-hydraulic CFD study in louvered fin-and-flat-tube heat exchangers. *International Journal of Refrigeration* 27, 422 – 432.
- Petrov, N.E., and Popov, V.N., 1985. Heat transfer and resistance of carbon dioxide being cooled in the supercritical region. *Thermal Engineering* 32(3), 131–134.
- Pitla, S.S., Groll, E.A., Ramadhyani, S., 2002. New correlation to predict the heat transfer coefficient during in-tube cooling of turbulent supercritical CO₂. *International Journal of Refrigeration* 25, 887 – 895.

- Pongsoi, P., Pikulkajorn, S., Wongwises, S., 2012. Experimental study on the air-side performance of a multipass parallel and counter cross-flow L-footed spiral fin-and-tube heat exchanger, *Heat transfer Engineering*. Taylor and Francis Group 33(15),1251–1263, available at : <http://www.tandfonline.com/loi/uhte20>
- Pu, H., Ding, G., Ma, X., Hu, H., Gao, Y., 2009. Effects of biofouling on air-side heat transfer and pressure drop for finned tube heat exchangers. *International Journal of Refrigeration* 32,1032-1040.
- Reynolds, O., 1895. On the dynamical theory of incompressible viscous fluids and the determination of the criterion. *Phil. Trans. Of the royal society London, Series A, Vol.186:123-164.*
- Rigola, J., Ablangue, Segarra, C.D., Olivia, A., 2010. Numerical simulation and experimental validation of internal heat exchanger influence on CO₂ trans-critical cycle performance. *International Journal of Refrigeration* 33,664-674.
- Sahin, B., Akkoca, A., Ozturk, N.A., Akili, H., 2006. Investigation of flow characteristic in a plate fin and tube heat exchanger model composed of single cylinder. *International Journal of Heat and Fluid Flow* 27, 522-530
- Sánchez, D., Patiño, J., Llopis, R., Cabello, R., Torrella, E., 2014. New positions for an internal heat exchanger in a CO₂ supercritical refrigeration plant. Experimental analysis and energetic evaluation. *Applied Thermal Engineering* 63,129-139.
- Santosa, ID.M.C., Suamir, IN., Ge, Y.T., Tsamos, K., Tassou, S.A., 2013. Modelling and analysis of CO₂ gas coolers for commercial refrigeration applications. *Proc. 2nd Conference on Sustainability and the Cold Chain*. Paris, France, ISBN: 978-2-913149-97-7 paper S12-P2.
- Sawalha, S, 2008. Theoretical evaluation of trans-critical CO₂ systems in supermarket refrigeration. Part I: Modeling, simulation and optimization of two system solutions. *International Journal of Refrigeration* 31,516-524.
- Shah, R.K., and Sekulic, D.P., 2003. Fundamentals of heat exchanger design. John Wiley & Sons, New Jersey, ISBN: 0-471-32171-0
- Singh, V., Abdelaziz, O., Aute, V., Radermacher, R., 2011. Simulation of air-to-refrigerant fin-and-tube heat exchanger with CFD-based air propagation. *International Journal of Refrigeration* 34, 1883 – 1897.
- Singh, V., Aute, V., Radermacher, R., 2008. Numerical approach for modeling air-to-refrigerant fin-and-tube heat exchanger with tube-to-tube heat transfer. *International Journal of Refrigeration* 31, 1414 – 1425.
- Singh, V., Aute, V., Radermacher, R., 2010. Investigation of effect of cut fins on carbon dioxide gas cooler performance. *HVAC&R Research* Volume 16, Number:4
- Son, C.H., and Park, S.J., 2006. An experimental study on heat transfer and pressure drop characteristics of carbon dioxide during gas cooling process in a horizontal tube. *International Journal of Refrigeration* 29, 539 – 546.
- Sun, L., and Zhang, C.L., 2014. Evaluation of elliptical finned-tube heat exchanger performance using CFD and response surface methodology. *International Journal of Thermal Sciences* 75, 45-53.

- Taler, D., and Oclo P., 2014. Thermal contact resistance in plate fin-and-tube heat exchangers determined by experimental data and CFD simulations. *International Journal of Thermal Sciences* 84, 309 – 322.
- Tao, Y.B., He, Y.L, Tao,W.Q, 2010. Exergetic analysis of transcritical CO₂ residential air-conditioning system based on experimental data. *Applied Energy* 87,3065-3072.
- Tassou, S.A., 2002. Comparison between direct and indirect refrigeration systems in UK supermarkets. *Internal Report for IEA Annex, 26, Brunel University*, 30 pgs.
- Tassou, S.A., Ge, Y., Hadawey, A., Marriot, D., 2011. Energy consumption and conservation in food retailing. *Applied Thermal Engineering* 31, 147 – 156.
- Torrella, E, Sa'nchez, D, Llopis, R, Cabello, R, 2011. Energetic evaluation of an internal heat exchanger in a CO₂ transcritical refrigeration plant using experimental data. *International Journal of Refrigeration* 34,40-49.
- Wang, C.C., Tao, W.H., Chang, C.J., 1999. An investigation of the airside performance of the slit fin-and-tube heat exchangers. *International Journal of Refrigeration* 22, 595-630.
- Wen, M.Y., and Ho, C.Y., 2009. Heat-transfer enhancement in fin-and-tube heat exchanger with improved fin. *Applied Thermal Engineering* 29, 1050 – 1057.
- Yaïci, W., Ghorab, M., Entchev, E., 2014. 3D CFD analysis of the effect of inlet air flow maldistribution on the fluid flow and heat transfer performances of plate-fin-and-tube laminar heat exchangers. *International Journal of Heat and Mass Transfer* 74, 490 – 500.
- Yoon, S.H., Kim, J.H., Hwang, Y.W., Kim, M.S., 2003. Heat transfer and pressure drop characteristic during the in-tube cooling process of carbon dioxide in the supercritical region. *International Journal of Refrigeration* 26, 857 – 864.
- Yun, R., Kim, Y.B., Kim, Y.C., 2009. Air side heat transfer characteristics of plate finned tube heat exchangers with slit fin configuration under wet conditions. *Applied Thermal Engineering* 29, 3014 – 3020.
- Zhang, W.J., and Zhang C.L., 2011. A correlation-free on-line optimal control method of heat rejection pressures in CO₂ transcritical systems. *International Journal of Refrigeration* 34,844-850.
- Zilio, C., Cecchinato, L., Corradi, M., Schiochet, G., 2007. An assessment of heat transfer through fins in a fin-and-tube gas cooler for transcritical carbon dioxide cycles. *HCAC&R Research* Vol.13, 3.

Appendix A: Mechanical components of test rig

This appendix provides drawing of the identification and numbering of the mechanical component of the CO₂ refrigeration system, with all of the valve number and measurement point. The system improvements and the gas coolers test rig design pictures were also presented.

Legend for the symbol used in the mechanical components drawing:

IHX	Internal Heat Exchanger	Acc	Accumulator
L/HPS	Low/high pressure switch	OF	Oil Filter
OS	Oil separator	LF	Liquid filter
OR	Oil receiver		PT (Pressure transducer)
TXV	Thermostatic expansion valve		Temperature sensor (thermocouple)
AKV	Automatic expansion valve		PRV (Pressure relief valve)
SV	Solenoid Valve		Pressure switch
SF	Filter	D,M,R	Number of the valve

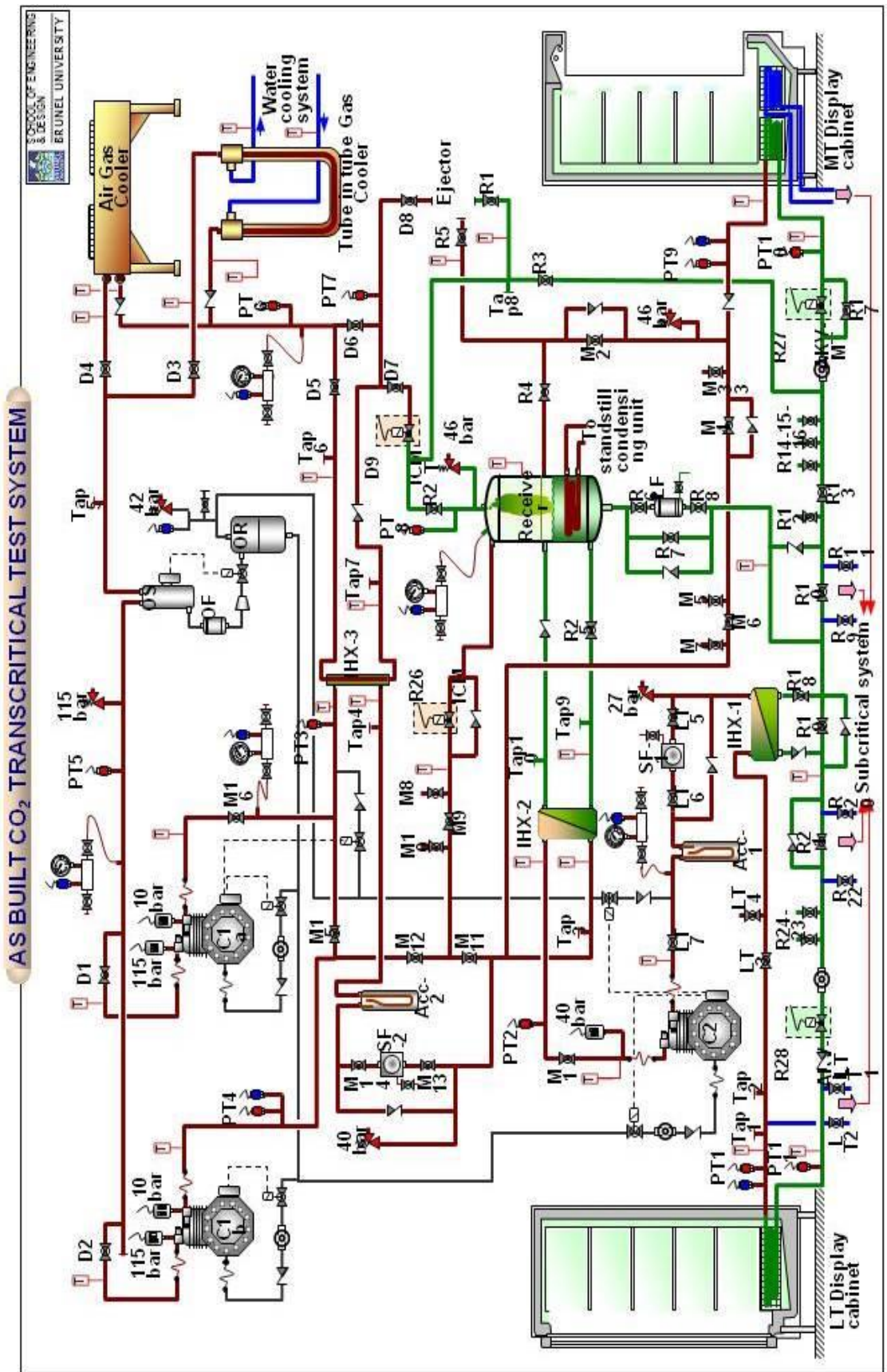


Figure A-1 Schematic diagram of CO₂ refrigeration as built in Refrigeration Laboratory-Brunel University

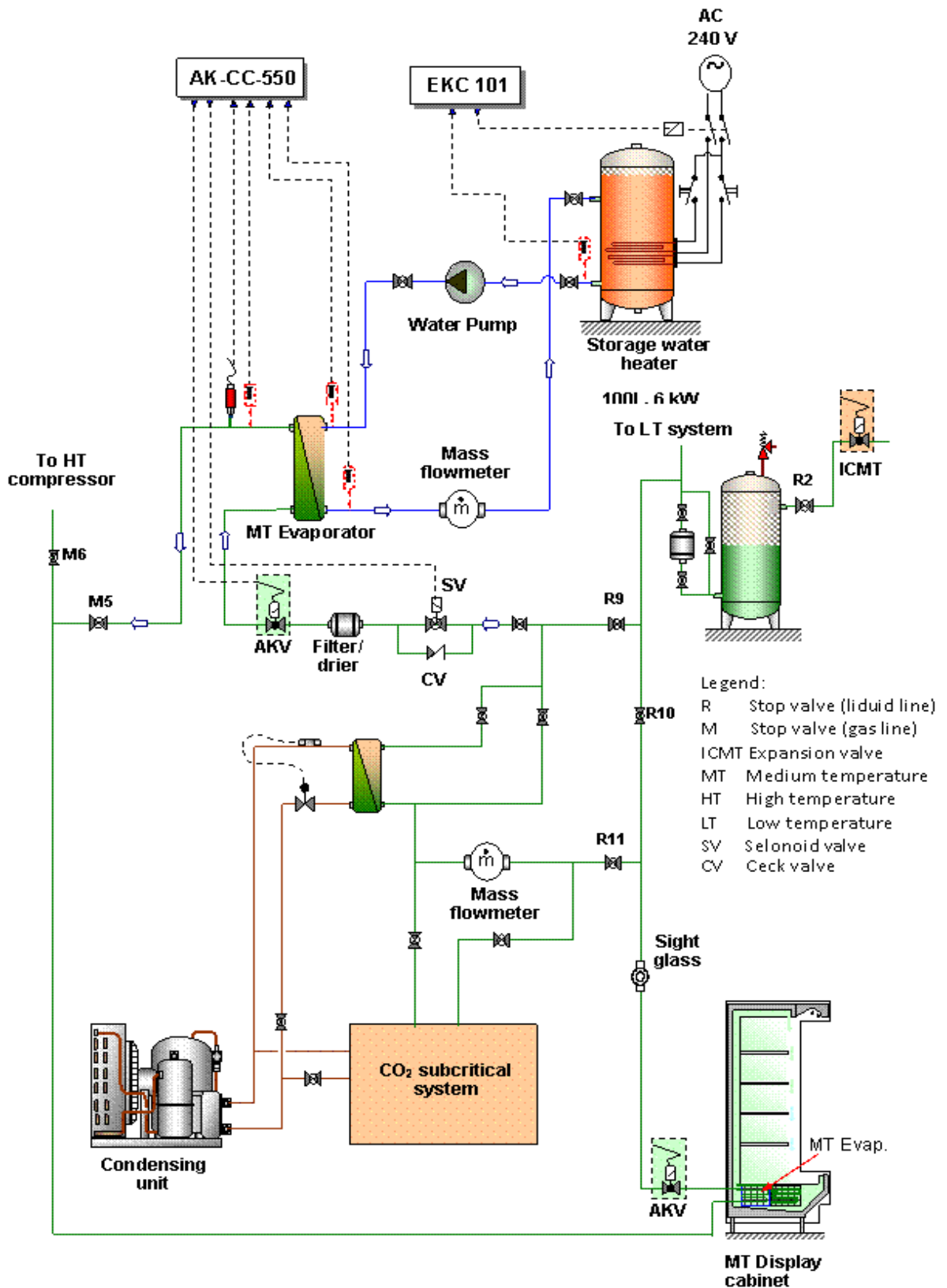


Figure A-2 Schematic diagram of the MT additional load and sub-cooler for CO₂ refrigeration system

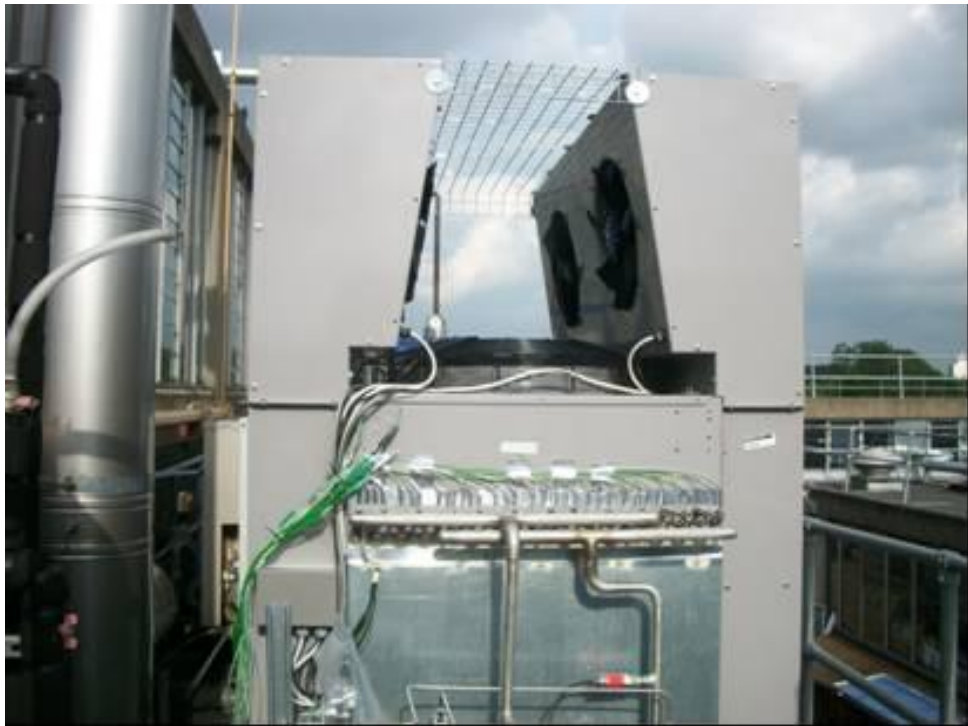


Figure A-3 Photograph of gas cooler test rig

Appendix B: Instrumentation and data logging systems of gas cooler test rig

This appendix provides the positions of the measurement points in the gas cooler test rig, monitor display of both gas cooler test rig and the CO₂ refrigeration system, identification of the measurement points and calibration equations of the thermocouples, pressure transducers, pressure different transducer, as well as flow meter.

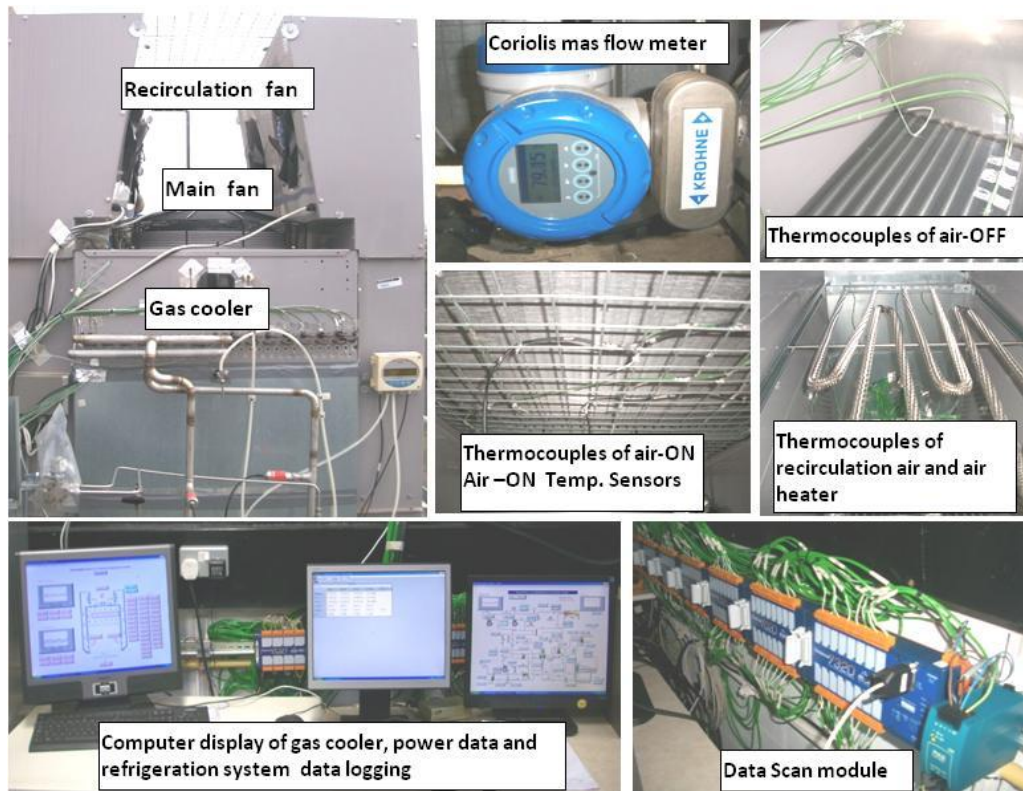


Figure B-1 Instrumentation and data logging system

Identification of the measurement points of the gas cooler measurement data logger is presented in Table B-1 and the display of the data logger illustrated at Figure B-2 up to Figure B-6. Legend for Table B-1:

- T = temperature
- DP-Air = pressure different transducer for air side
- P1 = pressure transducer at gas cooler inlet header
- P2 = pressure transducer at gas cooler outlet header
- PIN = pressure transducer at gas cooler inlet coil
- POUT = pressure transducer at gas cooler outlet coil

Table B-1 Channel identification on the Data Scan logger

Datascan Logger Configuration:			Gas Cooler		
Channel No.	Sensor No.	Description	Channel No.	Sensor No.	Description
Box 1: All OFF	T1	T. Air Off-1	49	T53	T. Recirculated Air-13
	T2	T. Air Off-2	50	T54	T. Recirculated Air-14
	T3	T. Air Off-3	51	T55	T. Recirculated Air-15
	T4	T. Air Off-4	52	T56	T. Recirculated Air-16
	T5	T. Air Off-5	53	T57	T. Inlet Air-1
	T6	T. Air Off-6	54	T58	T. Inlet Air-2
	T7	T. Air Off-7	55	T59	T. Outlet Air-1
	T8	T. Air Off-8	56	T60	T. Outlet Air-2
	T9	T. Air Off-9	57	T61	T. Outlet Air-3
	T10	T. Air Off-10	58	T62	T. Outlet Air-4
	T11	T. Air Off-11	59	T63	T. Coil Pipe-C1-1
	T12	T. Air Off-12	60	T64	T. Coil Pipe-C1-2
	T17	T. Air On-1	61	T65	T. Coil Pipe-C1-3
	T18	T. Air On-2	62	T66	T. Coil Pipe-C1-4
	T19	T. Air On-3	63	T67	T. Coil Pipe-C1-5
	T20	T. Air On-4	64	T68	T. Coil Pipe-C1-6
Box 2: S6 ON	T21	T. Air On-5	65	T69	T. Coil Pipe-C1-7
	T22	T. Air On-6	66	T70	T. Coil Pipe-C1-8
	T23	T. Air On-7	67	T71	T. Coil Pipe-C1-9
	T24	T. Air On-8	68	T72	T. Coil Pipe-C2-1
	T25	T. Air On-9	69	T73	T. Coil Pipe-C2-2
	T26	T. Air On-10	70	T74	T. Coil Pipe-C2-3
	T27	T. Air On-11	71	T75	T. Coil Pipe-C2-4
	T28	T. Air On-12	72	T76	T. Coil Pipe-C2-5
	T29	T. Air On-13	73	T77	T. Coil Pipe-C2-6
	T30	T. Air On-14	74	T78	T. Coil Pipe-C2-7
	T31	T. Air On-15	75	T79	T. Coil Pipe-C2-8
	T32	T. Air On-16	76	T80	T. Coil Pipe-C2-9
	T33	T. Air On-17	77	T81	T. Coil Pipe-C3-1
	T34	T. Air On-18	78	T82	T. Coil Pipe-C3-2
	T35	T. Air On-19	79	T83	T. Coil Pipe-C3-3
	T36	T. Air On-20	80	T84	T. Coil Pipe-C3-4
Box 3: S5 ON	T37	T. Air On-21	81	T85	T. Coil Pipe-C3-5
	T38	T. Air On-22	82	T86	T. Coil Pipe-C3-6
	T39	T. Air On-23	83	T87	T. Coil Pipe-C3-7
	T40	T. Air On-24	84	T88	T. Coil Pipe-C3-8
	T41	T. Recirculated Air-1	85	T89	T. Coil Pipe-C3-9
	T42	T. Recirculated Air-2	86	T90	T. Coil Pipe-C4-1
	T43	T. Recirculated Air-3	87	T91	T. Coil Pipe-C4-2
	T44	T. Recirculated Air-4	88	T92	T. Coil Pipe-C4-3
	T45	T. Recirculated Air-5	89	T93	T. Coil Pipe-C4-4
	T46	T. Recirculated Air-6	90	T94	T. Coil Pipe-C4-5
	T47	T. Recirculated Air-7	91	T95	T. Coil Pipe-C4-6
	T48	T. Recirculated Air-8	92	T96	T. Coil Pipe-C4-7
T49	T. Recirculated Air-9	93	T97	T. Coil Pipe-C4-8	
T50	T. Recirculated Air-10	94	T98	T. Coil Pipe-C4-9	
T51	T. Recirculated Air-11	95			
T52	T. Recirculated Air-12	96			

Table B-1 Channel identification on the Data Scan logger (Continued)

Datascan Logger Configuration:			Gas Cooler	
Channel No.	Sensor No.	Description		
Box 7: S4 & S5 ON	97	DP-AIR	P. Differential	
	98	P1	P. Gas Cooler-Inlet (header)	
	99	P2	P. Gas Cooler-Out (header)	
	100	PIN1	P. Gas Cooler in 1 (coil)	
	101	PIN2	P. Gas Cooler in 2 (coil)	
	102	POUT1	P. Gas Cooler out 1 (coil)	
	103	POUT2	P. Gas Cooler out 2 (coil)	
Box 8: S4, S5 & S6 ON	104			
	105			
	106			
	107			
	108			
	109			
	110			
	111			
	112			

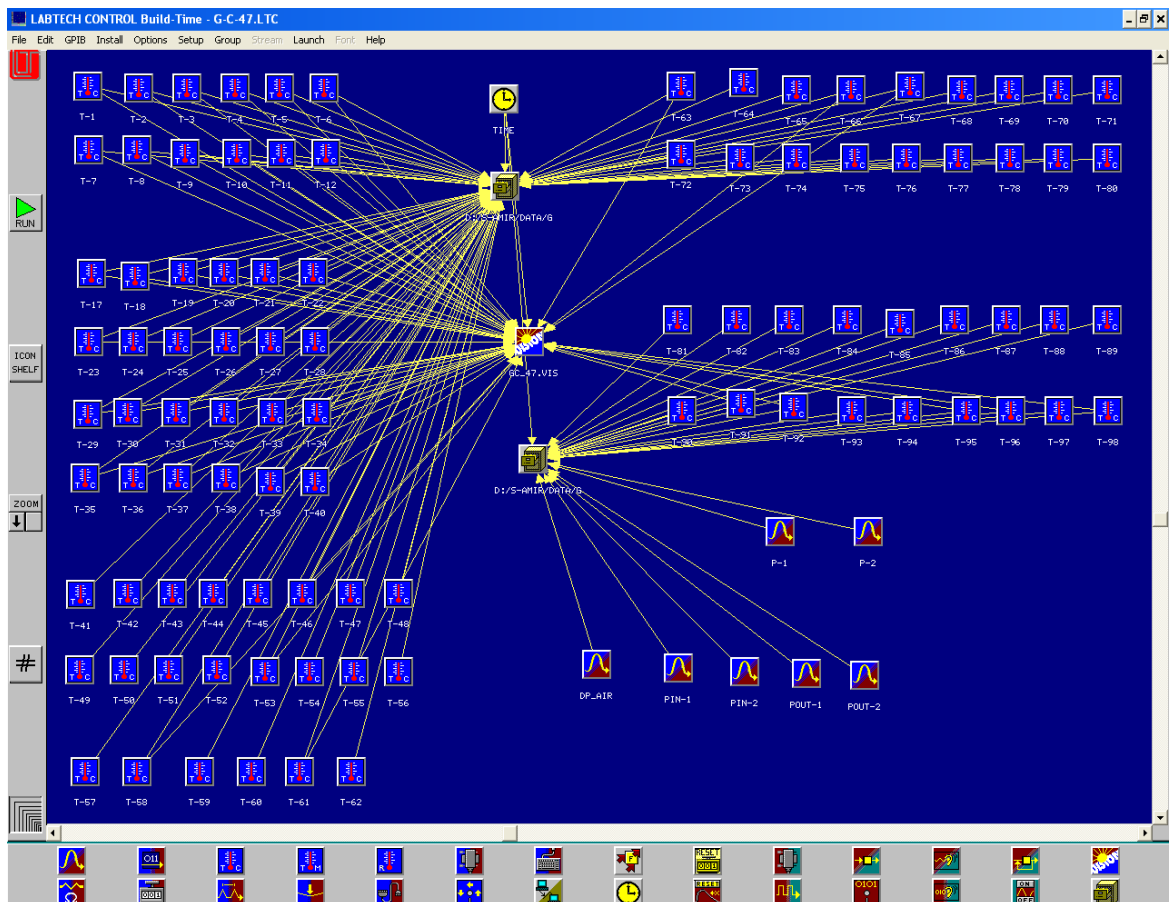


Figure B-2 Control build in Labtech of gas cooler data logger

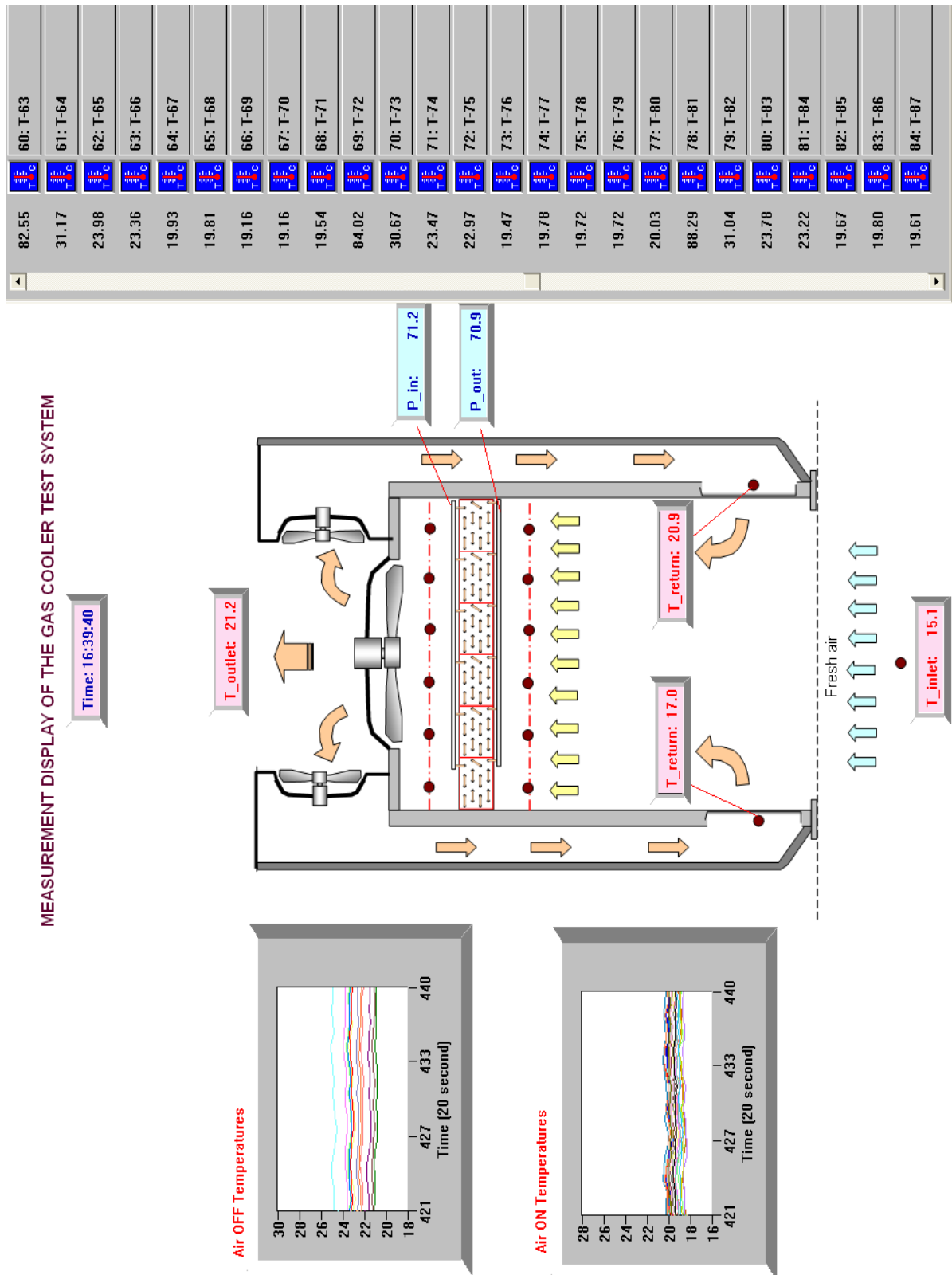


Figure B-3 A display of gas cooler measurement in starting up load (Air ON = 20 °C)

MEASUREMENT DISPLAY OF THE GAS COOLER TEST SYSTEM

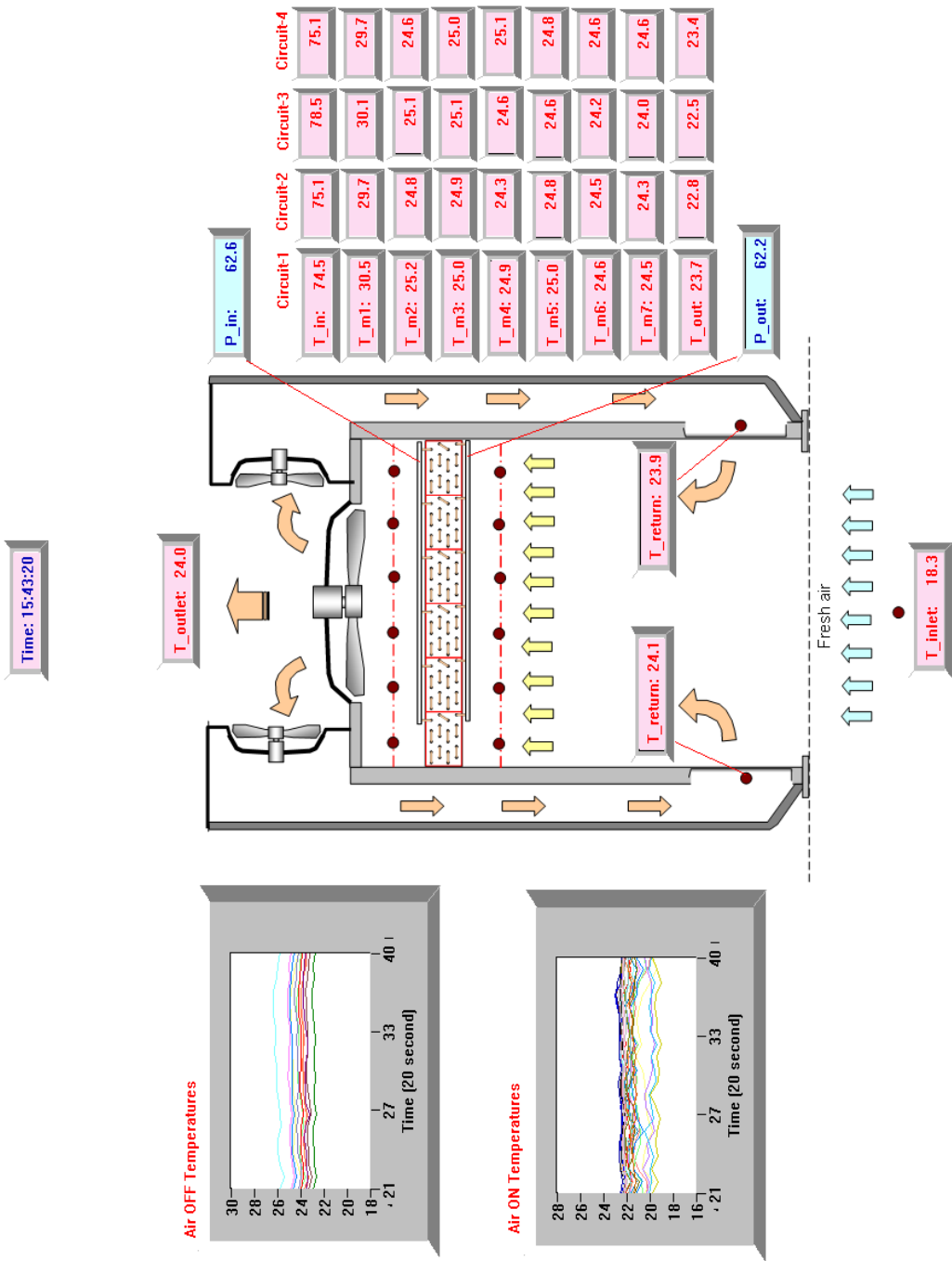


Figure B-4 A display of gas cooler measurement in steady state load air-ON 22°C

The calibration equations of the thermocouples are presented in following Table B-2.

Table B-2 Calibration equations of the thermocouples of gas cooler test rig

Calibration Equation of the Thermocouples

General Equation:

$$Y = mX + b$$

Legend:

Y = estimated actual temperature °C

X = thermocouple reading (°C)

SE-m = Standard error of m

SE-b = standard error of b

m = slope of Y and X corelation (linear regression)

b = constant or Y intercept

R² = coefficient of determination

SE-Y = standard error of estimated Y

Thermocouples	m	b	R ²	SE-m	SE-b	SE-Y
T1	1.006422	-0.224810	0.9985330	0.0146	0.2444	0.4872
T2	1.006125	-0.244091	0.9985090	0.0147	0.2465	0.4928
T3	1.006529	-0.313855	0.9985720	0.0144	0.2417	0.4781
T4	1.007656	-0.377674	0.9986530	0.0140	0.2350	0.4586
T5	1.005240	-0.378429	0.9985730	0.0144	0.2419	0.4779
T6	1.009519	-0.678186	0.9985610	0.0145	0.2444	0.4806
T7	1.016917	-0.800334	0.9985780	0.0145	0.2437	0.4766
T8	1.009174	-0.691975	0.9985770	0.0144	0.2432	0.4770
T9	1.009185	-0.643462	0.9985540	0.0145	0.2449	0.4823
T10	1.008918	-0.643991	0.9986170	0.0142	0.2395	0.4674
T11	1.009030	-0.610201	0.9986200	0.0142	0.2390	0.4665
T12	1.010024	-0.676273	0.9986120	0.0142	0.2401	0.4686
T17	1.010466	-0.684766	0.9986350	0.0141	0.2382	0.4631
T18	1.010357	-0.663061	0.9985890	0.0144	0.2420	0.4740
T19	1.010123	-0.649104	0.9986580	0.0140	0.2359	0.4573
T20	1.010484	-0.652083	0.9986050	0.0143	0.2406	0.4703
T21	1.010261	-0.669156	0.9986460	0.0141	0.2371	0.4604
T22	1.007995	-0.665754	0.9986660	0.0139	0.2353	0.4554
T23	1.007786	-0.641638	0.9985790	0.0144	0.2428	0.4765
T24	1.008126	-0.638037	0.9986000	0.0143	0.2409	0.4714
T25	1.006584	-0.752051	0.9986900	0.0138	0.2337	0.4496
T26	1.008799	-0.759998	0.9985920	0.0143	0.2423	0.4734
T27	1.008531	-0.728030	0.9985940	0.0143	0.2419	0.4728
T28	1.007630	-0.666963	0.9987040	0.0137	0.2320	0.4460
T29	1.008354	-0.810320	0.9986340	0.0141	0.2389	0.4632
T30	1.008062	-0.561418	0.9986670	0.0139	0.2347	0.4550
T31	1.008026	-0.590051	0.9986690	0.0139	0.2346	0.4545
T32	1.007922	-0.627917	0.9986930	0.0138	0.2327	0.4487
T33	1.009413	-0.642028	0.9987500	0.0135	0.2277	0.4345
T34	1.008360	-0.648860	0.9986610	0.0140	0.2357	0.4567
T35	1.008591	-0.734869	0.9985970	0.0143	0.2417	0.4721
T36	1.009206	-0.781258	0.9985920	0.0143	0.2424	0.4734
T37	1.009126	-0.817441	0.9985700	0.0144	0.2444	0.4785
T38	1.008841	-0.837981	0.9985830	0.0144	0.2435	0.4755
T39	1.001583	1.203327	0.9986680	0.0138	0.2269	0.4550
T40	1.002716	1.175075	0.9986130	0.0141	0.2316	0.4682
T41	1.004092	1.157879	0.9986800	0.0138	0.2259	0.4518
T42	1.001583	-0.195296	0.9984050	0.0151	0.2548	0.5167
T43	1.002734	3.721418	0.9985910	0.0142	0.2262	0.4735
T44	1.002238	3.720344	0.9986310	0.0140	0.2230	0.4639
T45	1.002008	3.737103	0.9986220	0.0141	0.2237	0.4661
T46	1.002419	3.738011	0.9985330	0.0145	0.2308	0.4873
T47	1.002695	3.747141	0.9985900	0.0142	0.2263	0.4738
T48	1.001976	3.762256	0.9986020	0.0142	0.2253	0.4710
T49	1.000440	3.783498	0.9985820	0.0143	0.2268	0.4758
T50	1.001188	3.770771	0.9985990	0.0142	0.2255	0.4716
T51	1.002815	0.399485	0.9986230	0.0141	0.2340	0.4660

Table B-2 Calibration equations of the thermocouples of gas cooler test rig (continued)

Thermocouples	m	b	R ²	SE-m	SE-b	SE-Y
T52	1.003458	0.416978	0.9986340	0.0140	0.2329	0.4632
T53	1.002706	0.420698	0.9986460	0.0140	0.2319	0.4602
T54	1.005028	0.411832	0.9986450	0.0140	0.2321	0.4606
T55	1.005153	0.483058	0.9986430	0.0140	0.2319	0.4611
T56	1.005713	0.485195	0.9986630	0.0139	0.2302	0.4561
T57	1.005694	0.500755	0.9987160	0.0136	0.2255	0.4431
T58	1.003502	1.098576	0.9987090	0.0136	0.2237	0.4448
T59	1.003063	1.100321	0.9986720	0.0138	0.2269	0.4539
T60	1.000417	1.157030	0.9986110	0.0141	0.2318	0.4688
T61	1.003079	1.124538	0.9987310	0.0135	0.2217	0.4393
T62	1.000264	1.185578	0.9986590	0.0139	0.2276	0.4571
T63	1.005678	-0.581317	0.9985830	0.0143	0.2421	0.4755
T64	1.006373	-0.637317	0.9986110	0.0142	0.2400	0.4688
T65	1.008531	-0.728030	0.9985940	0.0143	0.2419	0.4728
T66	1.008854	-0.713885	0.9986640	0.0139	0.2357	0.4559
T67	1.008062	-0.561418	0.9986670	0.0139	0.2347	0.4550
T68	1.008650	-0.554843	0.9987360	0.0136	0.2285	0.4380
T69	1.009185	-0.643462	0.9985540	0.0145	0.2449	0.4823
T70	1.008868	-0.656974	0.9985640	0.0145	0.2441	0.4800
T71	1.016917	-0.800334	0.9985780	0.0145	0.2437	0.4766
T72	1.016260	-0.804837	0.9985310	0.0147	0.2477	0.4878
T73	1.002380	-0.259961	0.9984280	0.0150	0.2533	0.5115
T74	1.005240	-0.378429	0.9985730	0.0144	0.2419	0.4779
T75	1.007656	-0.377674	0.9986530	0.0140	0.2350	0.4586
T76	1.006125	-0.244091	0.9985090	0.0147	0.2465	0.4928
T77	1.006869	-0.227677	0.9985090	0.0147	0.2465	0.4929
T78	1.005325	0.050396	0.9985550	0.0145	0.2413	0.4821
T79	1.005148	0.043130	0.9985630	0.0144	0.2406	0.4802
T80	1.003983	0.047941	0.9985220	0.0146	0.2440	0.4898
T81	1.011714	0.764923	0.9987190	0.0137	0.2241	0.4422
T82	1.011096	0.691332	0.9987210	0.0137	0.2242	0.4417
T83	0.998481	0.793385	0.9986510	0.0139	0.2299	0.4590
T84	0.998970	1.058034	0.9986390	0.0139	0.2299	0.4621
T85	0.998530	1.070330	0.9986370	0.0139	0.2300	0.4625
T86	0.995816	1.066011	0.9986650	0.0138	0.2276	0.4556
T87	0.996806	0.994470	0.9986300	0.0140	0.2308	0.4641
T88	1.001412	1.146833	0.9985590	0.0144	0.2361	0.4811
T89	1.000665	1.096362	0.9985940	0.0142	0.2334	0.4728
T90	0.998242	1.051715	0.9985770	0.0142	0.2350	0.4769
T91	0.996903	1.020488	0.9985730	0.0142	0.2355	0.4779
T92	0.996485	1.007307	0.9985510	0.0143	0.2374	0.4831
T93	0.997392	0.926840	0.9985340	0.0144	0.2391	0.4870
T94	1.006029	-0.584418	0.9985790	0.0143	0.2425	0.4765
T95	1.004779	-0.744378	0.9986340	0.0140	0.2385	0.4631
T96	1.004826	-0.757554	0.9987110	0.0136	0.2318	0.4443
T97	1.004027	-0.614769	0.9986430	0.0140	0.2371	0.4610
T98	1.008126	-0.638037	0.9986000	0.0143	0.2409	0.4714



Pressure transmitter

Type: MBS33

Measuring range: 0 -160 Bar

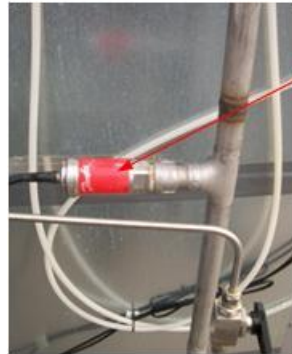
Pressure connection : G ½ A (EN 837)

Code: 060 G 3067

Cable version : 2m

Type no: MBS 33-3211-3ABo8

Resistor : 500 Ω



**Pressure Transducer
on Inlet Header**

**Pressure Transducer
on outlet Header**

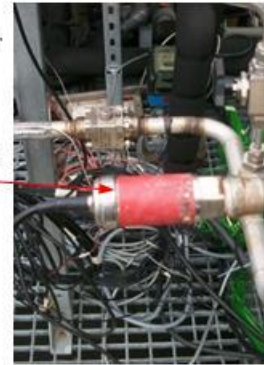


Figure B-7 Pressure transducers type on gas cooler

As explained in the thermocouples calibration, for the pressure transmitters, pressure difference transmitter and flow meter calibration also using similar equation. A general equation between the measured pressure and the output voltage of the pressure transmitters is as follows:

$$y = mx + b$$

where y = measured pressure (bar_g), x = output voltage (Volt), b = constant and m =rate pressure change. And the calibration graphs and equations of the six pressure transmitters of the gas cooler test rig, pressure difference transmitter and flow meter present in following Figures B-8, Figure B-9, Figure B-10, respectively.

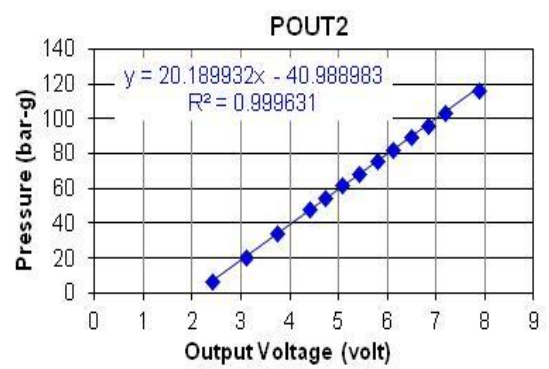
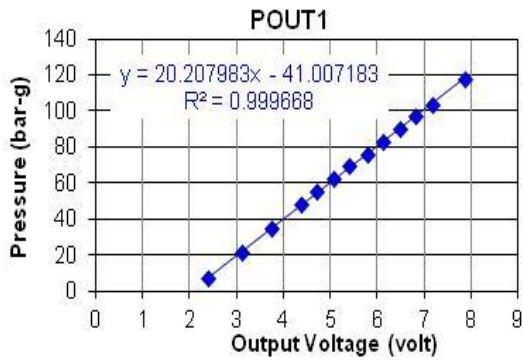
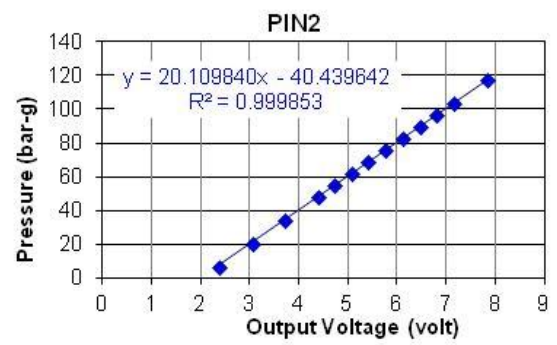
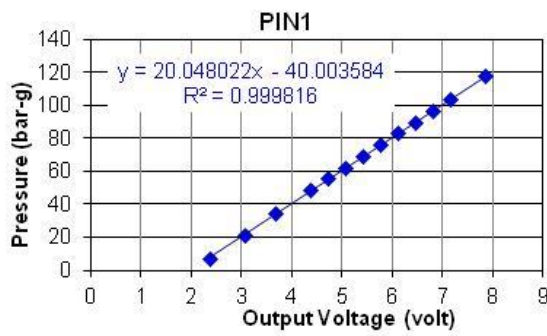
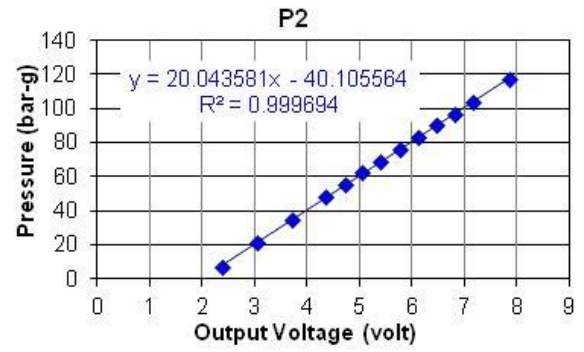
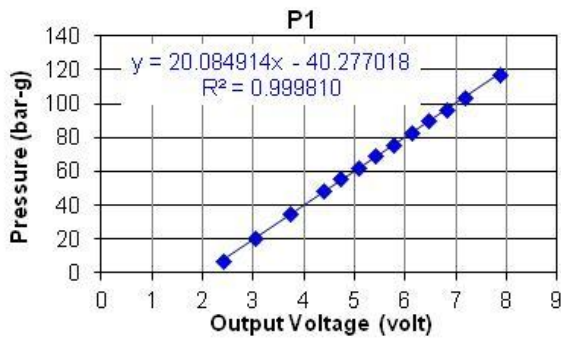


Figure B-8 Calibration graph and equation of the pressure transducers

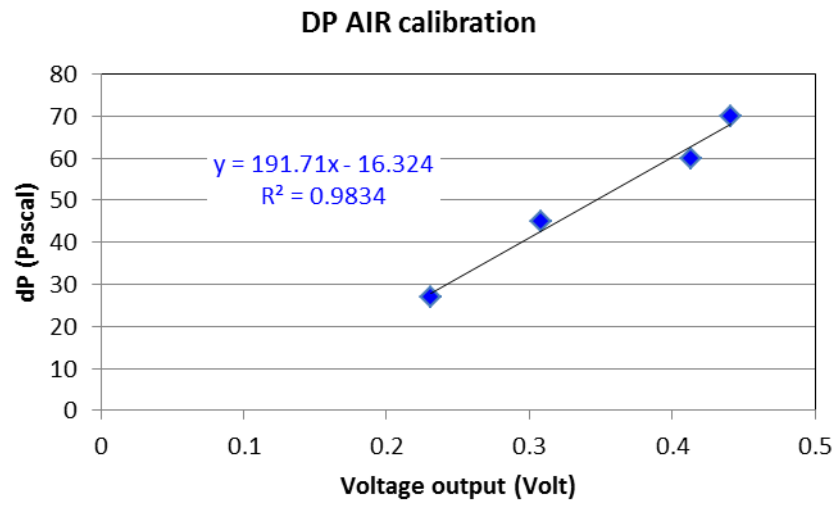


Figure B-9 Calibration graph and equation of the air pressure difference transducers

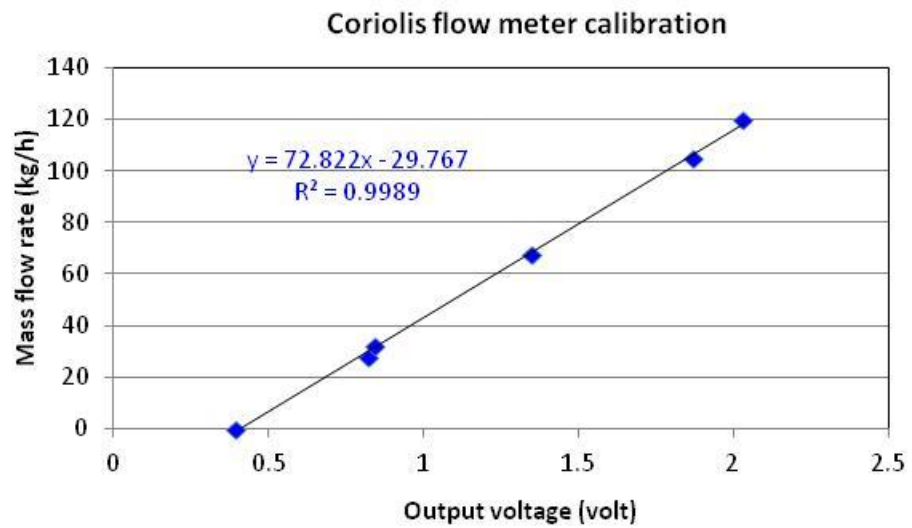


Figure B-10 Calibration graph and equation of the pressure transducers

Appendix C: Operational procedures

This appendix describes CO₂ refrigeration system, and the system operated on booster hot gas bypass mode and only on Medium Temperature (MT) system.

C.1 Operational procedure of CO₂ refrigeration system –booster hot gas bypass-Medium Temperature (MT) system

This appendix describes booster bypass hot gas modes of system operation For the gas cooler test condition, the system operated in Medium Temperature (MT) system. Operational procedures and some precautions are also presented. The explanations in this appendix refer to Figure A-1 (Appendix A). The operational procedures are as follows.

1. Choose Mode-2 switch on the main control panel to satisfy the booster mode operation and only the High Temperature (HT) compressors (number 1 or/and 2) operated as described in following figure.

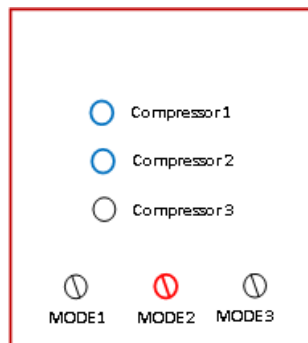
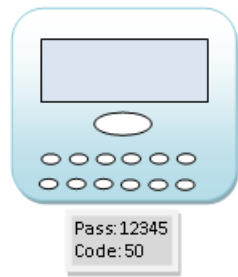


Figure C-1 Main control panel of CO₂ refrigeration system

2. Set operational condition according to control strategies which explained in the chapter 3 on the main controller (AK-SC-255) and showed in the following figure.



- Many items should be controlled :**
- Timer management
 - Compressor speed (%)
 - Pressure control : Receiver pressure: 32 Bar, High Pressure: 115 Bar, medium Pressure: 25-28 Bar , this is related to the optimum operation
 - Condensing unit control , etc (**see manual book**)

Figure C-2 Main controller (AK-SC-255)

3. Valve arrangement for the operational mode and the number of the valve refers to Figure A-1.

Table C.1 Valve arrangement of the operation mode

Valve no.	M1	M2	M3	M4	M5	M5	M6	M7	M8	M9	M10	M11
Position	√	X	X	√	X	X	√	X	X	√	X	√
Valve no.	M12	M13	M14	M15	M16							
Position	X	√	√	X	√							
Valve no.	D1	D2	D3	D4	D5	D6	D7	D8	D9			
Position	√	√	X	√	X	√	√	X	√			
Valve no.	R1	R2	R3	R4	R5	R6	R7	R8	R9	R10	R11	R12
Position	X	√	X	X	X	√	X	√	√	X	√	X
Valve no.	R13	R14	R15	R16	R17	R18	R19	R20	R21	R22	R23	R24
Position	√	X	X	X	X	X	X	X	X	X	X	X
Valve no.	LT1	LT2	LT3	LT4	LT5	LT6	LT7					
Position	X	X	X	X	X	X	X					

x = closed; √ = fully open

4. The procedures consist of three stages which include starting up, testing and shutting down. The test system is assumed to be fully charged; in standby conditions; the standstill condensing unit is in operation to keep the CO₂ refrigerant in the system and the pressure set up at 32 bar.

4.1.Starting up procedure

- a. Prepare the gas cooler test rig and check the setting point of fan speeds and the thermostat of the electrical air heater.
- b. Recheck the parameter settings of the main controller , and then increasing the standstill condensing unit pressure set become 32.5 bar (on standstill condition the pressure at 26 bar) match with the running condition of receiver pressure set at 32 bar
- c. Recheck the parameter settings of the display cabinets and the additional load.
- d. Ensure the oil level of the MT compressor in the range and there is sufficient oil in the oil reservoir- check trough by sigh glass.
- e. Start up the monitoring and the data logging system.
- f. Switch on the display cabinets and the additional load system and ensure fans, lights, water-glycol pump, flow meter and expansion valve are in good working order.
- g. Switch on the gas cooler main fan, recirculation fan and electrical air heater.
- h. Switch on the HT compressor (number 1 or number 2) and observe the operation.
- i. Monitor the temperature and pressure of the whole system including the liquid level in the receiver to ensure the system is working in stable conditions to ensure the system can maintain the set point.
- j. Regularly observe the oil level of the compressor to ensure the oil management system can work properly.

And then the experimental tests can be arranged.

4.2.Experimental test procedure

- a. Previous performing the experimental tests the starting up procedure needs to be finished and the system is kept running.
- b. Rearrange the CO₂ refrigeration system and the gas cooler set point control according to the test condition. The fan speed and ambient temperature are set at

the gas cooler control panel, and the compressor speed at the main controller (AK-CS-255), and sub-cooler set at the main control panel.

- c. Monitor and record the performance parameters by restarting the data logging system.
- d. The test procedure should be repeated for other test conditions.
- e. When the tests have been completed the test rig must be shut down.

4.3. Shutting down procedure

- a. Before shutting down, the CO₂ refrigeration system must be pumped down in order to store the liquid CO₂ back to the receiver through by close the valve R18.
- b. Switch off the electrical air heater for the gas cooler.
- c. Keep the HT compressor in operation until all liquid CO₂ is pump out from the liquid line. The compressor is automatically switched off when the system has been pumped down.
- d. The compressor controller is safe to switch off.
- e. Turn off the display cabinets and the additional load system.
- f. Switch off the gas cooler fans.
- g. The liquid CO₂ is then kept in the system by the standstill condensing unit. To ensure the receiver condition during standstill, the condensing cut-in set at 26 bar, so the tank pressure will keep in the properly pressure and temperature and then ensure the condensing unit work smoothly during standstill condition.

C.2 Precautions

For safety purposes, the test rig was designed to enable the CO₂ refrigerant to be released to the atmosphere when the pressure in the system is above the pressure limits in each region, which are high pressure: 115 bar, intermediate pressure: 46 bar, medium pressure: 40 bar and low pressure: 27 bar (*see Figure A-1*). In the running operation, it is always a risk that the CO₂ refrigerant released from the system due to system pressure going up above pressure limits. The pressure in the system can rise quickly and the standstill condensing unit cannot prevent suddenly. To minimize risks of injury the following precautions need to be taken:

- The machine room must be sufficiently ventilated by keeping the door open.

- Turn off the electrical air heater of gas cooler, display cabinets and the additional load system.
- Close the valve R 18 to pump down the system.
- By keeping the compressor running, the suction pressure can be maintained below the bursting pressure of the safety valve. The CO₂ refrigerant release to the atmosphere from the pressure relief valve (PRV).
- The compressor is automatically switched off by the low pressure switch. After that, switch off manually the compressor controller. The condensing unit is then gradually able to decrease the pressure of the system.
- The CO₂ refrigerant will also escape from the system during standby conditions if the standstill condensing unit getting fails. In this case, the CO₂ refrigerant is released gradually from the pressure relief valve of the receiver.

Appendix D: Examples of test results

This appendix describes the some experimental result for the gas cooler test rig and illustrated at Figure D-1 until Figure D-7.

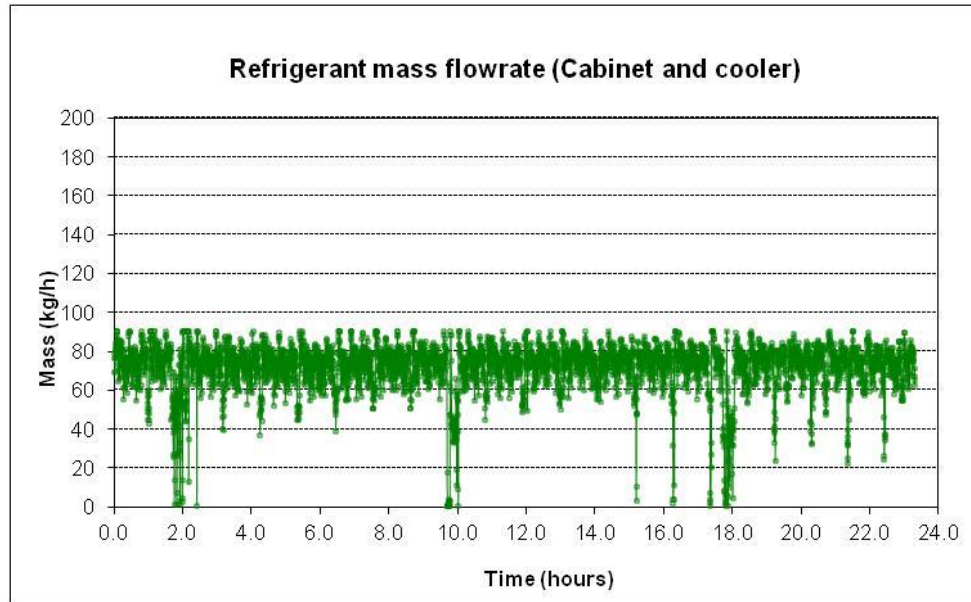


Figure D-1 Mass flow rate on cabinet and air cooler (kg/h) recorded from mass flow meter, test condition: air –ON temperature 24°C, 40% fan speed , 65-100% compressor speed , Approach Temperature 3.7-3.9 K

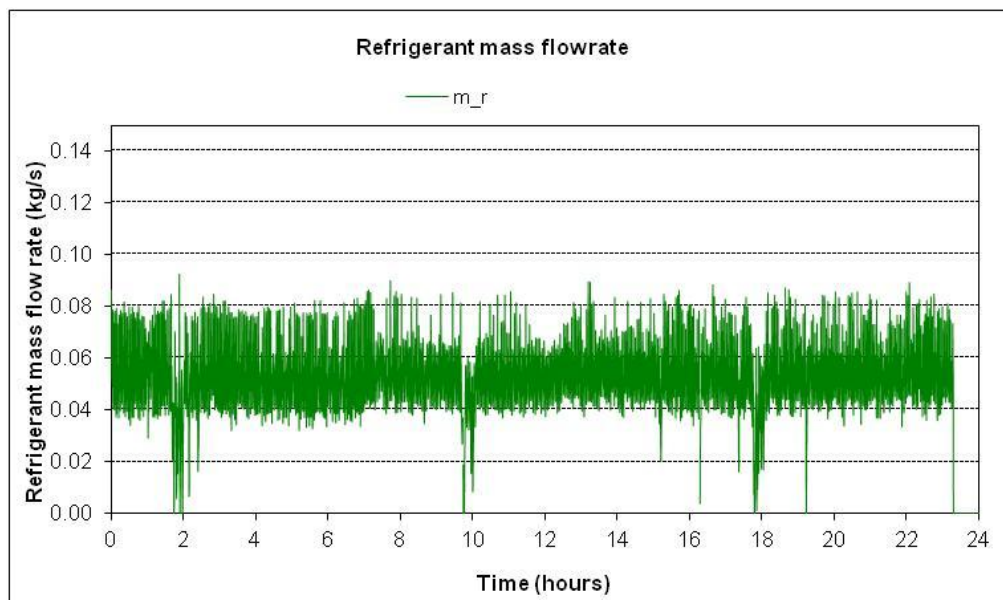


Figure D-2 Mass flow rate on gas cooler (kg/s) depend on heat balance in gas cooler test condition: air –ON temperature 24°C, 40% fan speed , 65-100% compressor speed , Approach Temperature 3.7-3.9 K

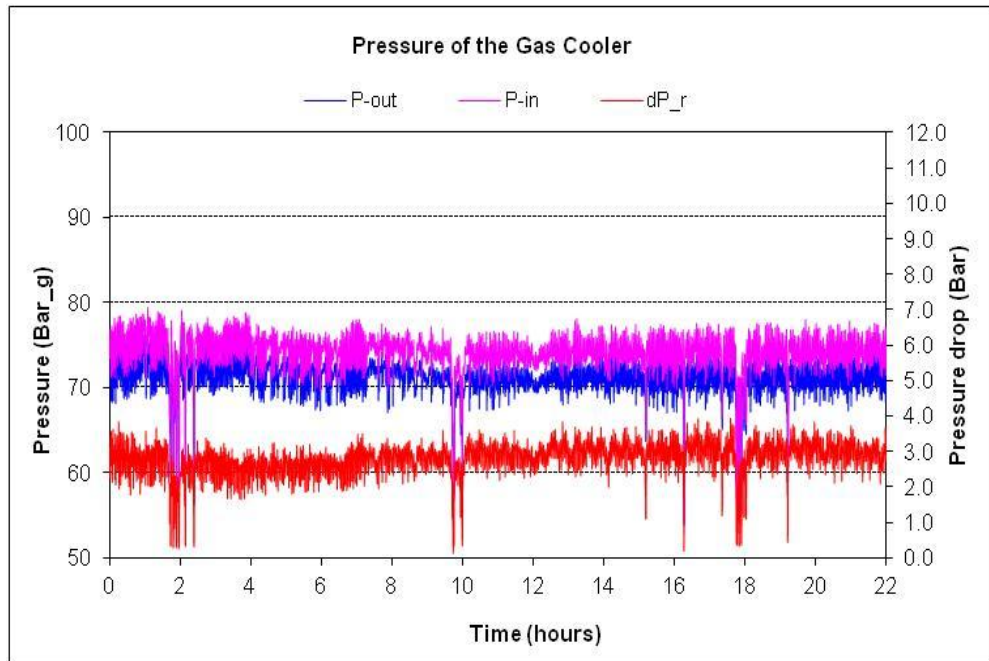


Figure D-3 Pressure of gas cooler , test condition: air –ON temperature 24°C, 40% fan speed , 65-100% compressor speed , Approach Temperature 3.7-3.9 K

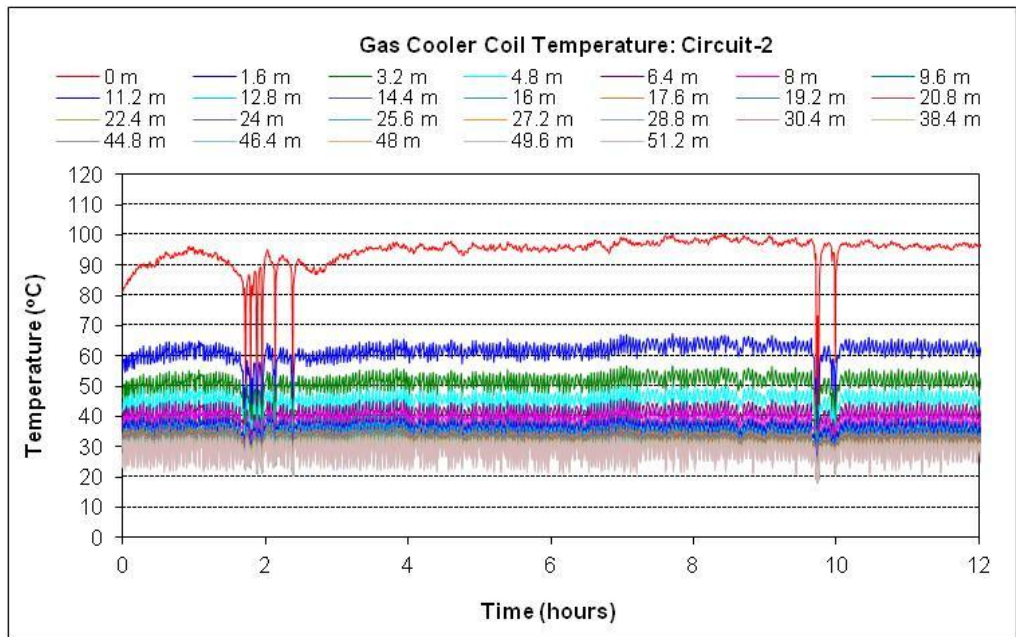


Figure D-4 Coil temperature of gas cooler circuit-2, test condition: air –ON temperature 24 °C, 40% fan speed , 65-100% compressor speed , Approach Temperature 3.7-3.9 K

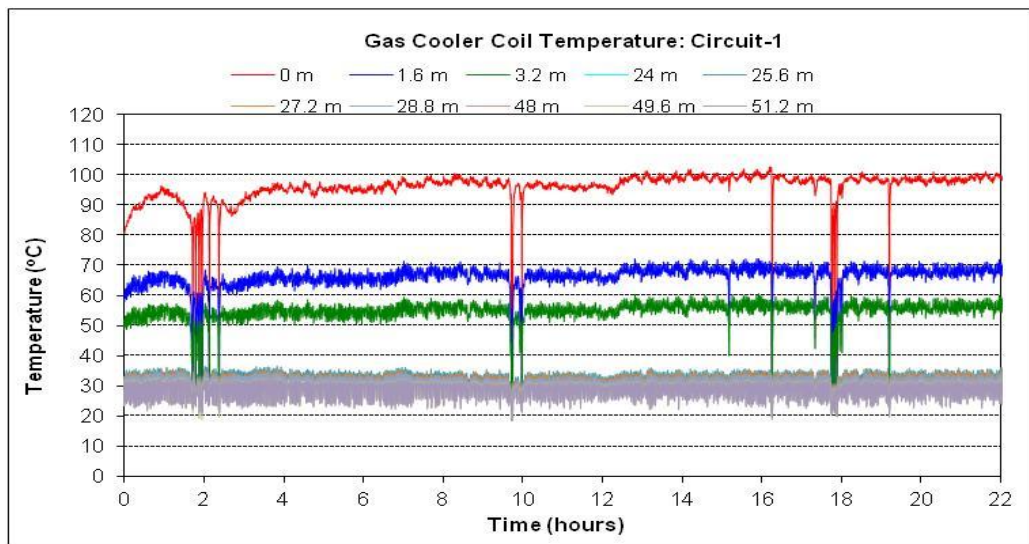


Figure D-5 Coil temperature of gas cooler circuit-1, test condition: air –ON temperature 24 °C, 40% fan speed , 65-100% compressor speed , Approach Temperature 3.7-3.9 K

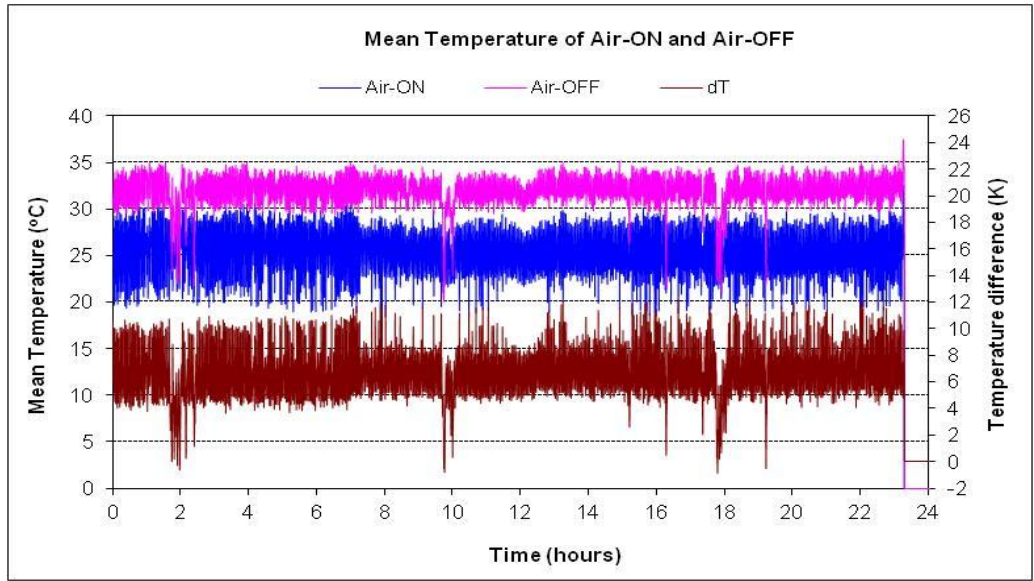


Figure D-6 Mean temperature of air-ON and air-OFF and dT of gas cooler, test condition: air –ON temperature 24 °C, 40% fan speed , 65-100% compressor speed , Approach Temperature 3.7-3.9 K

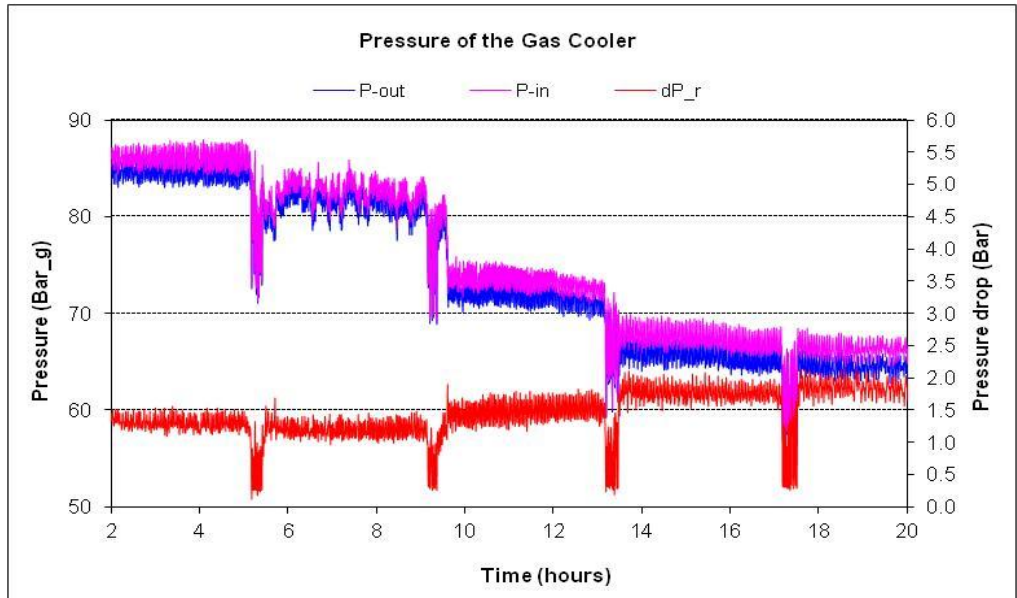


Figure D-7 Gas cooler pressure and pressure drop at test condition : air-ON temperature 20°C-34°C

Appendix E: Uncertainty analysis

In the analysis of test results, key parameters such as: heat rejection is not directly measured. It is calculated as a function of one or more variables that are directly measured. Each measured variable has a random variability which is referred to as its “uncertainty”. This appendix describes the calculations of uncertainty propagation of measured variables into the calculated parameters which include: heat rejection.

The uncertainty propagation was determined using the EES software with an assumption that individual measurements are uncorrelated and random. In general, uncertainty of the calculated parameters can be determined from (EES, 2013):

$$U_Y = \sqrt{\sum_i \left(\frac{\partial Y}{\partial X_i} \right)^2 U_{X_i}^2} \quad (\text{E.1})$$

Where:

Y = calculated parameter; X_i = measured variables; U_Y = uncertainty of calculated parameter; U_{X_i} = uncertainty of measured variables

The heat rejection calculation as a function of :

$$Q = f(V_{air}, T_{airout}, T_{air\ out}, A, \rho, Cp)$$

The calculation using EES presents as follows:

Unit Settings: SI C bar J mass deg

Variable±Uncertainty	Partial derivative	% of uncertainty
$Q = 12978 \pm 827 \text{ [w]}$		
$A = 1.186 \pm 1.000\text{E-}07 \text{ [m}^2\text{]}$	$\partial Q / \partial A = 10944$	0.00 %
$P_1 = 1 \pm 1.000\text{E-}08 \text{ [bar]}$	$\partial Q / \partial P_1 = 12978$	0.00 %
$T_{in} = 32 \pm 0.5 \text{ [}^\circ\text{C]}$	$\partial Q / \partial T_{in} = -3265$	49.22 %
$T_{out} = 36 \pm 0.5 \text{ [}^\circ\text{C]}$	$\partial Q / \partial T_{out} = 3224$	47.98 %
$Vel = 2.4 \pm 0.072 \text{ [m/s]}$	$\partial Q / \partial Vel = 5407$	2.80 %

$\rho = 1.134 \pm 0.003645$ [kg/m ³]		
<hr/>		
A = 1.186 ± 0.0001 [m ²]	$\partial \rho / \partial A = 0$	0.00 %
P ₁ = 1 ± 0.003 [bar]	$\partial \rho / \partial P_1 = 1.134$	87.17 %
T _{in} = 32 ± 0.5 [°C]	$\partial \rho / \partial T_{in} = -0.001846$	6.42 %
T _{out} = 36 ± 0.5 [°C]	$\partial \rho / \partial T_{out} = -0.001846$	6.42 %
Vel = 2.4 ± 0.015 [m/s]	$\partial \rho / \partial Vel = 0$	0.00 %

No unit problems were detected.

Calculation time = .0 sec.

Unit Settings: SI C bar J mass deg

Variable ± Uncertainty	Partial derivative	% of uncertainty
cp = 1005 ± 0.019		
<hr/>		
A = 1.186 ± 0.0001 [m ²]	$\partial cp / \partial A = 0$	0.00 %
P ₁ = 1 ± 0.003 [bar]	$\partial cp / \partial P_1 = 0$	0.00 %
T _{in} = 32 ± 0.5 [°C]	$\partial cp / \partial T_{in} = 0.02686$	50.00 %
T _{out} = 36 ± 0.5 [°C]	$\partial cp / \partial T_{out} = 0.02686$	50.00 %
Vel = 2.4 ± 0.015 [m/s]	$\partial cp / \partial Vel = 0$	0.00 %

No unit problems were detected.

Calculation time = .0 sec.

Appendix F: CFD model input data and calculation

This appendix provides the input of the working fluid properties and then formulated as a piecewise linier equation for CFD model. The appendix also presents temperature inlet of refrigerant at segments and some CFD result for heat transfer coefficient calculations, as follows.

F-1. Air properties

The air properties of the gas cooler cold fluid has been used which is moisture air at 50% RH which derived from the EES program, the properties of air is tabulated in following Table F-1

Table F-1 Air properties

Temperature (K)	Density ρ (kg/m ³)	Specific heat c_p (j/kg-K)	Viscosity μ (kg/m-s)	Thermal conductivity k (W/m-K)
0	1.248	1031	1.73e-5	0.02368
100	0.9138	1035	2.18e-5	0.03106

(Properties values were derived from EES program at pressure 103.3 kPa)

F.2 Refrigerant (CO₂-R744) properties and piecewise linier graph

Furthermore, properties of the refrigerant were also derived from EES over a temperature range between 40 °C and 120 °C (i.e. pressure 80.9 Bar). The properties are as a function of pressure and temperature are shown in following Figures.

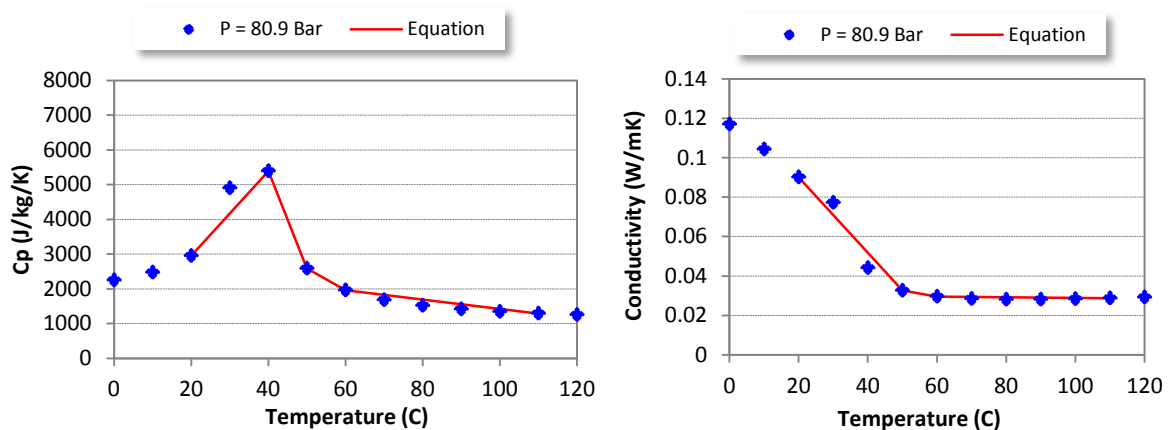


Figure F.1 Variation of c_p and conductivity of CO₂ with temperature at pressure=80.9 bar and a piecewise linier equation (Derived: EES Program)

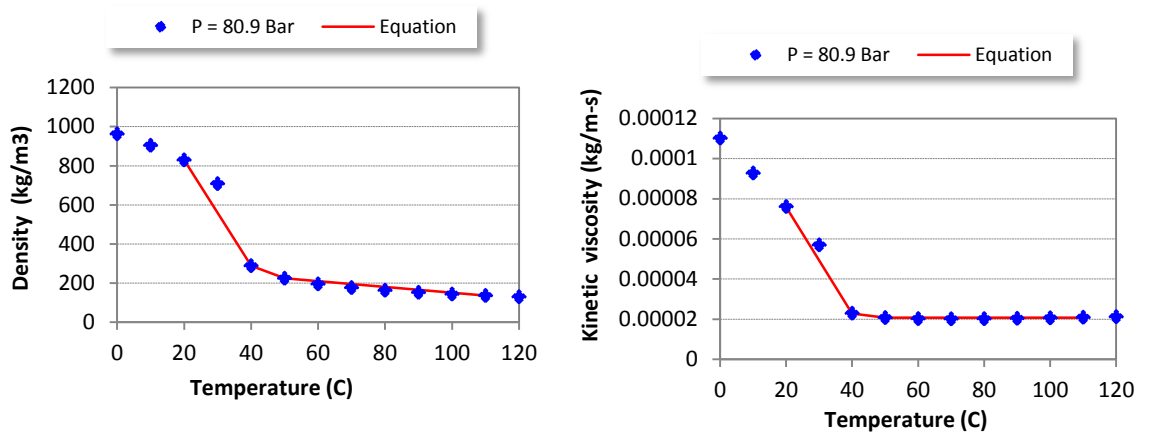


Figure F.2 Variation of density and viscosity of CO₂ with temperature at pressure=80.9 bar and a piecewise linier graph (Derived: EES Program)

F.3 Temperature inlet refrigerant in segment

The inlet boundaries of refrigerant temperature at certain test condition for 3-row gas cooler and 2-row gas cooler present at following figures and tables , and the segment 1 until the segment 5 refer to Figure F-5.

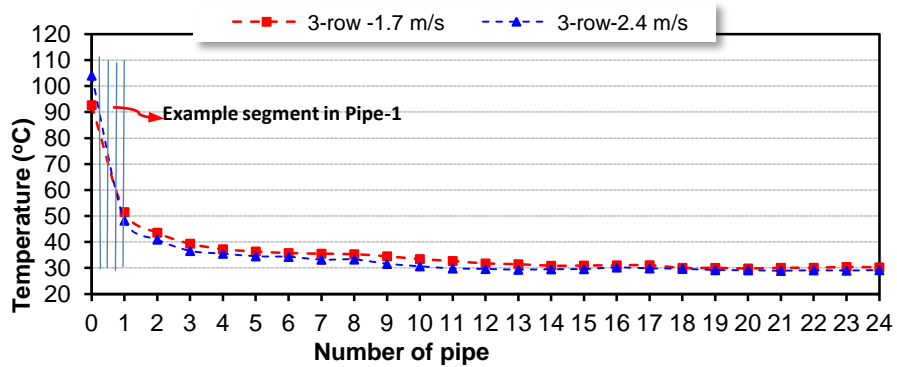


Figure F.3 Temperature profile along the pipe of gas cooler-A with horizontal and vertical slit fin (example: segment in pipe-1)

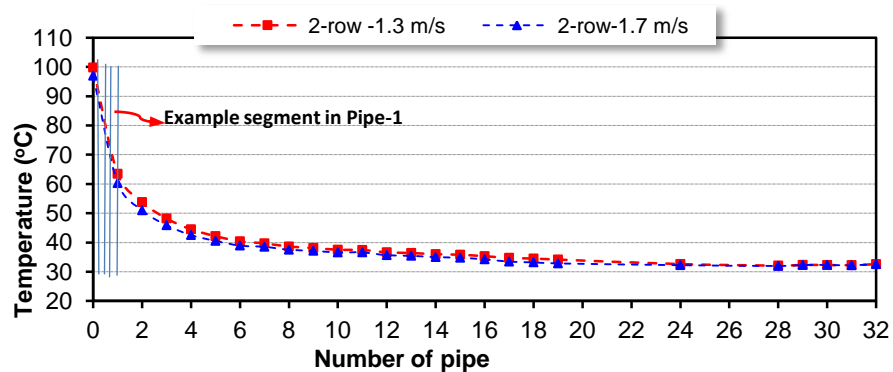


Figure F.4 Temperature profile along the pipe of gas cooler-B with horizontal slit fin (example: segment in pipe-1)

And then the temperature inlet in each segment calculated by interpolation equation and provide at following tables.

Table F-2 Temperature refrigerant inlet at segments of gas cooler-A with horizontal and vertical slit fin (Test condition : $T_{air-ON}=29\text{ }^{\circ}\text{C}$, $V_{air}=1.7\text{ m/s}$)

Pipe Number	Segment 1 position mm	0 Temp C	Segment2 Position mm	400.00 Temp C	Segment 3 Position mm	800.0 Temp C	Segment 4 Position mm	1200 Temp C	Segment 5 Position mm	1600.00 Temp C
1	0	92.7	400	82.4	800	72.1	1200	61.8	1600	51.5
2	3200	43.6	2800	45.6	2400	47.6	2000	49.5	1600	51.5
3	3200	43.6	3600	42.5	4000	41.5	4400	40.4	4800	39.4
4	6400	37.2	6000	37.8	5600	38.3	5200	38.8	4800	39.4
5	6400	37.2	6800	37.0	7200	36.8	7600	36.6	8000	36.3
6	9600	35.8	9200	35.9	8800	36.1	8400	36.2	8000	36.3
7	9600	35.8	10000	35.7	10400	35.6	10800	35.6	11200	35.5
8	12800	35.3	12400	35.4	12000	35.4	11600	35.5	11200	35.5
9	12800	35.3	13200	35.1	13600	34.9	14000	34.7	14400	34.5
10	16000	33.4	15600	33.7	15200	34.0	14800	34.2	14400	34.5
11	16000	33.4	16400	33.2	16800	33.1	17200	32.9	17600	32.7
12	19200	31.8	18800	32.0	18400	32.2	18000	32.5	17600	32.7
13	19200	31.8	19600	31.7	20000	31.6	20400	31.5	20800	31.5
14	22400	30.9	22000	31.0	21600	31.2	21200	31.3	20800	31.5
15	22400	30.9	22800	30.9	23200	30.9	23600	30.9	24000	31.0
16	25600	31.0	25200	31.0	24800	31.0	24400	31.0	24000	31.0
17	25600	31.0	26000	31.0	26400	31.0	26800	31.1	27200	31.1
18	28800	30.1	28400	30.3	28000	30.6	27600	30.8	27200	31.1
19	28800	30.1	29200	30.1	29600	30.1	30000	30.1	30400	30.1
20	32000	29.8	31600	29.9	31200	29.9	30800	30.0	30400	30.1
21	32000	29.8	32400	29.9	32800	30.0	33200	30.0	33600	30.1
22	35200	30.1	34800	30.1	34400	30.1	34000	30.1	33600	30.1
23	35200	30.1	35600	30.2	36000	30.3	36400	30.3	36800	30.4
24	38400	30.2	38000	30.3	37600	30.3	37200	30.4	36800	30.4

Table F-3 Temperature refrigerant inlet at segments of gas cooler-B with horizontal slit fin
 (Test condition : $T_{\text{air-ON}} = 31.3 \text{ }^{\circ}\text{C}$, $V_{\text{air}} = 1.3 \text{ m/s}$)

Pipe number	Segment 1	0	Segment 2	400	Segment 3	800	Segment 4	1200	Segment 5	1600
	position mm	Temp C								
1	0	99.8	400	90.7	800	81.6	1200	72.5	1600	63.5
2	3200	53.8	2800	56.2	2400	58.6	2000	61.0	1600	63.5
3	3200	53.8	3600	52.4	4000	51.0	4400	49.6	4800	48.2
4	6400	44.5	6000	45.4	5600	46.3	5200	47.2	4800	48.2
5	6400	44.5	6800	43.9	7200	43.3	7600	42.7	8000	42.1
6	9600	40.4	9200	40.8	8800	41.2	8400	41.7	8000	42.1
7	9600	40.4	10000	40.2	10400	40.0	10800	39.8	11200	39.7
8	12800	38.6	12400	38.9	12000	39.1	11600	39.4	11200	39.7
9	12800	38.6	13200	38.5	13600	38.3	14000	38.2	14400	38.1
10	16000	37.5	15600	37.6	15200	37.8	14800	37.9	14400	38.1
11	16000	37.5	16400	37.5	16800	37.4	17200	37.4	17600	37.4
12	19200	36.6	18800	36.8	18400	37.0	18000	37.2	17600	37.4
13	19200	36.6	19600	36.6	20000	36.5	20400	36.4	20800	36.4
14	22400	36.0	22000	36.1	21600	36.2	21200	36.3	20800	36.4
15	22400	36.0	22800	35.9	23200	35.9	23600	35.8	24000	35.8
16	25600	35.3	25200	35.4	24800	35.5	24400	35.7	24000	35.8
17	25600	35.3	26000	35.1	26400	35.0	26800	34.9	27200	34.7
18	28800	34.5	28400	34.5	28000	34.6	27600	34.7	27200	34.7
19	28800	34.5	29200	34.4	29600	34.3	30000	34.2	30400	34.1
20	32000	33.8	31600	33.9	31200	34.0	30800	34.1	30400	34.1
21	32000	33.8	32400	33.7	32800	33.7	33200	33.6	33600	33.5
22	35200	33.2	34800	33.3	34400	33.4	34000	33.4	33600	33.5

Table F-4 Temperature refrigerant inlet at segments of gas cooler-B with horizontal slit fin
 (Test condition : $T_{\text{air-ON}} = 31.3 \text{ }^{\circ}\text{C}$, $V_{\text{air}} = 1.3 \text{ m/s}$) (Continued)

Pipe number	Segment 1 position mm	0 Temp C	Segment2 Position mm	400 Temp C	Segment 3 Position mm	800 Temp C	Segment 4 Position mm	1200 Temp C	Segment 5 Position mm	1600 Temp C
23	35200	33.2	35600	33.1	36000	33.0	36400	33.0	36800	32.9
24	38400	32.6	38000	32.7	37600	32.7	37200	32.8	36800	32.9
25	38400	32.6	38800	32.6	39200	32.5	39600	32.5	40000	32.5
26	41600	32.3	41200	32.4	40800	32.4	40400	32.4	40000	32.5
27	41600	32.3	42000	32.3	42400	32.3	42800	32.2	43200	32.2
28	44800	32.1	44400	32.1	44000	32.1	43600	32.2	43200	32.2
29	44800	32.1	45200	32.1	45600	32.2	46000	32.2	46400	32.3
30	48000	32.2	47600	32.3	47200	32.3	46800	32.3	46400	32.3
31	48000	32.2	48400	32.2	48800	32.2	49200	32.2	49600	32.2
32	51200	32.6	50800	32.5	50400	32.4	50000	32.3	49600	32.2

F.3 Heat transfer coefficient calculation

The heat transfer calculations from the CFD program are tabulated in following tables F.5 until F.8.

Table F.5 Air side heat transfer coefficient of gas cooler-B

Test cond	Row Number	Pipe number	Segment 1- fin area (4 circuit)	Total segment pipe outer area	Mass flow rate	Total area	Air T_in	Air T_ot	dT_air	Air T_b	T_fin	T_pipe	T_w	Q_dot	hc
			m ²	m ²	kg/s	m ²	°C	°C	°C	°C	°C	°C	°C	°C	W
GC16-S2	Row-1	Pipe 1	0.00103	0.000053	8.0782E-05	0.00108	29.28	39.38	10.10	34.33	39.00	45.77	42.39	0.80	92.00
		Pipe 2	0.00103	0.000053	8.0782E-05	0.00108	29.19	37.91	8.71	33.55	37.57	41.41	39.49	0.69	107.19
		Pipe 3	0.00103	0.000053	8.0782E-05	0.00108	29.16	36.28	7.12	32.72	36.04	39.40	37.72	0.56	104.50
		Pipe 4	0.00103	0.000053	8.0782E-05	0.00108	29.16	34.61	5.45	31.89	34.44	36.69	35.57	0.43	107.60
		Pipe 5	0.00103	0.000053	8.0782E-05	0.00108	29.19	33.70	4.51	31.44	33.57	35.59	34.58	0.35	104.22
		Pipe 6	0.00103	0.000053	8.0782E-05	0.00108	29.27	32.78	3.50	31.03	32.76	34.23	33.49	0.21	78.93
		Pipe 7	0.00103	0.000053	8.0782E-05	0.00108	29.34	32.53	3.19	30.94	32.35	33.72	33.03	0.24	106.93
		Pipe 8	0.00103	0.000053	8.0782E-05	0.00108	29.43	32.00	2.57	30.71	32.00	33.14	32.57	0.20	98.57
		Pipe 9	0.00103	0.000053	8.0782E-05	0.00108	29.50	31.76	2.27	30.63	31.80	32.86	32.33	0.17	94.63
		Pipe 10	0.00103	0.000053	8.0782E-05	0.00108	29.56	31.61	2.04	30.58	31.61	32.54	32.08	0.15	95.61
		Pipe 11	0.00103	0.000053	8.0782E-05	0.00108	29.61	31.50	1.90	30.55	31.51	32.40	31.95	0.14	93.29
		Pipe 12	0.00103	0.000053	8.0782E-05	0.00108	29.69	31.36	1.67	30.52	31.36	32.13	31.75	0.12	92.83
		Pipe 13	0.00103	0.000053	8.0782E-05	0.00108	29.74	31.24	1.49	30.49	31.26	31.95	31.61	0.11	91.31
		Pipe 14	0.00103	0.000053	8.0782E-05	0.00108	29.84	31.11	1.27	30.48	31.17	31.79	31.48	0.09	84.97
		Pipe 15	0.00103	0.000053	8.0782E-05	0.00108	29.88	31.14	1.26	30.51	31.12	31.71	31.42	0.09	89.16
		Pipe 16	0.00103	0.000053	8.0782E-05	0.00108	29.85	30.78	0.93	30.31	30.93	31.45	31.19	0.07	74.41
	Row-2	Pipe 17	0.00103	0.000053	8.0782E-05	0.00108	28.13	29.85	1.72	28.99	29.73	30.67	30.20	0.14	104.52
		Pipe 18	0.00103	0.000053	8.0782E-05	0.00108	28.13	29.88	1.75	29.00	29.77	30.58	30.17	0.14	109.91
		Pipe 19	0.00103	0.000053	8.0782E-05	0.00108	28.13	29.84	1.71	28.99	29.74	30.55	30.14	0.14	108.90
		Pipe 20	0.00103	0.000053	8.0782E-05	0.00108	28.13	29.74	1.61	28.94	29.63	30.36	30.00	0.13	111.55
		Pipe 21	0.00103	0.000053	8.0782E-05	0.00108	28.13	29.69	1.56	28.91	29.59	30.31	29.95	0.12	110.10
		Pipe 22	0.00103	0.000053	8.0782E-05	0.00108	28.13	29.61	1.48	28.87	29.51	30.16	29.83	0.12	111.87
		Pipe 23	0.00103	0.000053	8.0782E-05	0.00108	28.13	29.56	1.43	28.85	29.47	30.12	29.79	0.11	110.52
		Pipe 24	0.00103	0.000053	8.0782E-05	0.00108	28.13	29.50	1.37	28.81	29.41	30.02	29.71	0.11	110.82
		Pipe 25	0.00103	0.000053	8.0782E-05	0.00108	28.13	29.43	1.30	28.78	29.35	29.93	29.64	0.10	109.52
		Pipe 26	0.00103	0.000053	8.0782E-05	0.00108	28.13	29.34	1.21	28.73	29.26	29.78	29.52	0.09	111.65
		Pipe 27	0.00103	0.000053	8.0782E-05	0.00108	28.13	29.27	1.14	28.70	29.19	29.70	29.44	0.09	111.17
		Pipe 28	0.00103	0.000053	8.0782E-05	0.00108	28.13	29.19	1.06	28.66	29.11	29.55	29.33	0.08	112.84
		Pipe 29	0.00103	0.000053	8.0782E-05	0.00108	28.13	29.16	1.03	28.64	29.08	29.50	29.29	0.08	113.83
		Pipe 30	0.00103	0.000053	8.0782E-05	0.00108	28.13	29.16	1.03	28.64	29.08	29.51	29.30	0.08	113.09
		Pipe 31	0.00103	0.000053	8.0782E-05	0.00108	28.13	29.19	1.06	28.66	29.12	29.54	29.33	0.08	114.20
		Pipe 32	0.00103	0.000053	8.0782E-05	0.00108	28.13	29.28	1.15	28.70	29.20	29.70	29.45	0.09	110.41

(Test condition: air velocity =1.7 m/s, air –ON temperature = 32.4 °C, pressure=82.4 bar)

Table F.6 Air –side heat transfer coefficient of gas cooler-A calculation

Test cond	Row Number	Pipe Number	Fin area	Outer pipe area	Air mass flow rate	Total area	Air T_in	Air T_ot	dT_air	Air T_b	T_fin	T_pipe	T_w	Q_dot	hc
			m ²	m ²	kg/s	m ²	°C	°C	°C	°C	°C	°C	°C	°C	W
GCS5-S2	Row 1	Pipe 1	0.00103021	5.3125E-05	0.00012323	0.001	31.58	42.09	10.51	36.84	43.43	51.56	47.49	1.29	111.64
		Pipe 2	0.00103021	5.3125E-05	0.00012323	0.001	31.49	37.20	5.71	34.35	37.75	40.84	39.30	0.69	128.92
		Pipe 3	0.00103021	5.3125E-05	0.00012323	0.001	31.41	34.59	3.18	33.00	35.09	37.25	36.17	0.37	108.64
		Pipe 4	0.00103021	5.3125E-05	0.00012323	0.001	31.35	33.27	1.92	32.31	33.57	35.16	34.37	0.22	99.59
		Pipe 5	0.00103021	5.3125E-05	0.00012323	0.001	31.35	32.77	1.43	32.06	32.94	34.41	33.67	0.16	89.45
		Pipe 6	0.00103021	5.3125E-05	0.00012323	0.001	31.45	32.43	0.98	31.94	32.52	33.83	33.18	0.10	77.26
		Pipe 7	0.00103021	5.3125E-05	0.00012323	0.001	31.58	32.39	0.81	31.99	32.28	33.61	32.95	0.08	78.54
		Pipe 8	0.00103021	5.3125E-05	0.00012323	0.001	31.75	32.20	0.45	31.98	32.10	33.00	32.55	0.05	73.55
	Row 2	Pipe 9	0.00103021	5.3125E-05	0.00012323	0.001	31.43	31.69	0.26	31.56	31.49	32.26	31.88	0.05	157.19
		Pipe 10	0.00103021	5.3125E-05	0.00012323	0.001	31.39	31.58	0.19	31.49	31.60	31.79	31.70	0.04	166.34
		Pipe 11	0.00103021	5.3125E-05	0.00012323	0.001	31.31	31.45	0.14	31.38	31.43	31.62	31.52	0.03	184.65
		Pipe 12	0.00103021	5.3125E-05	0.00012323	0.001	31.25	31.35	0.10	31.30	31.40	31.43	31.41	0.02	196.40
		Pipe 13	0.00103021	5.3125E-05	0.00012323	0.001	31.24	31.35	0.12	31.30	31.37	31.44	31.40	0.03	217.99
		Pipe 14	0.00103021	5.3125E-05	0.00012323	0.001	31.28	31.41	0.13	31.35	31.40	31.50	31.45	0.03	231.49
		Pipe 15	0.00103021	5.3125E-05	0.00012323	0.001	31.34	31.49	0.15	31.42	31.48	31.59	31.54	0.03	239.97
		Pipe 16	0.00103021	5.3125E-05	0.00012323	0.001	31.42	31.58	0.16	31.50	31.53	31.78	31.66	0.03	196.01
	Row 3	Pipe 17	0.00103021	5.3125E-05	0.00012323	0.001	31.06	31.42	0.36	31.24	31.31	31.64	31.47	0.03	119.43
		Pipe 18	0.00103021	5.3125E-05	0.00012323	0.001	31.06	31.34	0.28	31.20	31.20	31.48	31.34	0.02	137.58
		Pipe 19	0.00103021	5.3125E-05	0.00012323	0.001	31.06	31.28	0.22	31.17	31.12	31.41	31.27	0.02	151.22
		Pipe 20	0.00103021	5.3125E-05	0.00012323	0.001	31.06	31.24	0.18	31.15	31.13	31.30	31.22	0.01	135.29
		Pipe 21	0.00103021	5.3125E-05	0.00012323	0.001	31.06	31.25	0.19	31.15	31.15	31.29	31.22	0.01	133.15
		Pipe 22	0.00103021	5.3125E-05	0.00012323	0.001	31.06	31.31	0.25	31.18	31.23	31.37	31.30	0.02	135.78
		Pipe 23	0.00103021	5.3125E-05	0.00012323	0.001	31.06	31.39	0.33	31.22	31.36	31.43	31.40	0.03	135.07
		Pipe 24	0.00103021	5.3125E-05	0.00012323	0.001	31.06	31.43	0.37	31.24	31.47	31.47	31.47	0.03	124.11

(Test condition: Air velocity =2.0 m/s, Air-ON temperature = 31.06°C, Pressure : 82.5 bar)

Table F.7 Refrigerant-side heat transfer coefficient calculation

Row	Tube Reference	2RGC3-S1				2RGC7-S1				2RGC16-S1			
		Bulk Ref temp (C)	Pipe wall inner temp (C)	Heat Flux (W/m ²)	Refrigerant side hc (W/m ² -K)	Bulk Ref temp (C)	Pipe wall inner temp (C)	Heat Flux (W/m ²)	Refrigerant side hc (W/m ² -K)	Bulk Ref temp (C)	Pipe wall inner temp (C)	Heat Flux (W/m ²)	Refrigerant side hc (W/m ² -K)
Row-1	1	97.73	54.64	74930.8	1739.1	90.01	51.22	66469.1	1713.5	96.92	53.11	76552.4	1747.0
	2	53.09	46.71	19875.0	3113.0	47.74	43.02	14865.9	3155.8	51.65	45.28	21312.0	3342.9
	3	53.09	45.36	23570.6	3048.5	47.73	41.42	19512.5	3090.4	51.65	44.05	24899.1	3273.0
	4	44.47	41.75	9897.2	3635.1	39.46	37.70	5727.4	3250.0	43.25	40.43	10327.9	3666.2
	5	44.47	40.96	12687.2	3618.8	39.46	37.58	6080.1	3239.9	43.25	39.74	12815.8	3648.6
	6	40.51	38.89	5800.4	3574.7	35.82	36.25	-1373.9	3195.6	39.76	37.96	6453.7	3582.6
	7	40.51	38.41	7480.6	3563.3	35.82	35.25	1824.4	3193.8	39.76	37.59	7757.7	3571.7
	8	38.74	37.43	4666.4	3564.0	34.39	33.72	2195.9	3270.3	38.33	36.83	5329.9	3559.4
	9	38.74	37.17	5517.9	3516.3	34.39	33.21	3805.1	3227.7	38.33	36.63	5967.7	3507.9
	10	37.59	36.56	3591.5	3473.0	33.59	32.69	2951.3	3264.1	37.39	36.17	4236.0	3473.7
	11	37.59	36.38	4212.2	3481.4	33.59	32.52	3504.7	3270.7	37.39	36.02	4761.7	3483.4
	12	36.57	35.91	2237.1	3373.6	32.78	32.10	2211.5	3231.7	36.34	35.54	2697.9	3372.4
	13	36.57	35.78	2705.6	3418.5	32.78	32.00	2539.4	3267.1	36.34	35.44	3088.3	3414.9
	14	35.97	35.49	1635.2	3406.6	32.36	31.79	1898.0	3307.7	35.66	35.11	1887.3	3407.0
	15	35.97	35.42	1948.2	3546.7	32.36	31.73	2147.5	3435.2	35.66	35.05	2175.0	3549.0
	16	35.30	35.14	547.4	3473.6	31.83	31.54	996.2	3405.3	34.92	34.76	538.1	3465.2
Row-2	17	35.30	34.25	3567.1	3394.8	31.83	30.71	3727.4	3329.8	34.92	34.07	2895.0	3389.8
	18	34.61	34.02	2069.2	3510.4	31.33	30.58	2621.5	3498.1	33.86	33.64	755.1	3497.1
	19	34.61	33.95	2326.9	3549.2	31.33	30.54	2787.7	3540.9	33.86	33.57	1023.9	3543.4
	20	34.12	33.69	1486.3	3491.6	30.89	30.32	2016.8	3509.6	33.36	33.34	78.4	3315.6
	21	34.12	33.60	1775.9	3442.4	30.89	30.27	2153.1	3453.5	33.36	33.28	273.8	3345.7
	22	33.56	33.31	863.2	3412.5	30.62	30.15	1618.0	3459.3	33.11	33.14	-116.2	3410.6
	23	33.56	33.22	1158.7	3379.5	30.62	30.22	1365.0	3421.0	33.11	33.11	-3.5	3410.4
	24	32.99	32.93	212.8	3467.7	30.35	30.49	-501.4	3567.1	32.85	32.98	-453.7	3462.7
	25	32.99	32.86	424.4	3264.5	30.35	32.54	-7332.7	3348.8	32.85	32.96	-372.5	3301.0
	26	32.70	32.71	-27.1	3170.4	73.17	46.58	50142.3	3086.3	32.75	32.91	-548.9	3422.6
	27	32.70	32.67	105.0	3304.5	73.17	46.49	50081.3	3077.1	32.75	32.90	-513.3	3394.1
	28	32.41	32.54	-426.3	3181.6	29.50	32.09	-8464.7	3270.4	32.64	32.87	-729.3	3208.7
	29	32.41	32.55	-475.7	3447.8	29.50	29.93	-1508.5	3507.7	32.64	32.89	-859.1	3468.9
	30	32.58	32.65	-223.5	3242.1	29.52	29.51	21.4	2809.5	33.00	33.06	-199.5	3330.9
	31	32.58	32.72	-493.3	3409.6	29.52	29.43	314.7	3492.7	33.00	33.11	-384.3	3501.9
	32	33.03	33.08	-166.2	3340.5	29.67	29.61	181.4	3275.9	33.22	33.30	-259.7	3380.0
Average Hc (W/m ² -K)					3361.1				3255.2				3389.0
Row	Tube Reference	GC3-S5				GC8-S5				GC13-S5			
		Bulk Ref temp (C)	Pipe wall inner temp (C)	Heat Flux (W/m ²)	Refrigerant side hc (W/m ² -K)	Bulk Ref temp (C)	Pipe wall inner temp (C)	Heat Flux (W/m ²)	Refrigerant side hc (W/m ² -K)	Bulk Ref temp (C)	Pipe wall inner temp (C)	Heat Flux (W/m ²)	Refrigerant side hc (W/m ² -K)
Row-1	1	48.59	39.93	17865.2	2062.4	47.19	39.09	15872.2	1959.0	47.89	39.57	16293.7	1957.9
	2	48.59	40.09	17620.2	2072.4	47.19	39.26	15628.3	1969.3	47.89	39.76	16013.4	1968.1
	3	39.00	37.08	3902.6	2030.5	37.80	36.12	3180.5	1891.1	38.20	36.41	3401.2	1902.0
	4	39.00	36.49	5243.1	2089.0	37.80	35.48	4514.4	1946.9	38.20	35.67	4940.1	1957.6
	5	36.70	35.74	1925.7	2002.3	35.80	34.75	1982.3	1884.7	36.00	34.85	2166.8	1889.4
	6	36.70	35.64	2072.5	1949.6	35.80	34.65	2101.8	1827.2	36.00	34.73	2327.4	1836.8
	7	36.00	35.58	805.2	1918.9	35.10	34.59	928.4	1805.2	35.10	34.63	843.2	1806.3
	8	36.00	36.15	-297.6	1988.6	35.10	35.20	-194.0	1899.7	35.10	35.33	-431.0	1858.4
Row-2	9	35.40	33.74	3246.0	1952.0	34.50	33.00	2760.9	1842.2	34.50	32.93	2899.7	1844.9
	10	35.40	33.78	3347.7	2062.6	34.50	33.04	2839.9	1945.0	34.50	32.97	2976.8	1944.1
	11	34.00	33.46	1088.6	2007.5	33.30	32.77	1005.8	1898.2	33.40	32.72	1289.1	1904.2
	12	34.00	33.39	1140.1	1882.2	33.30	32.70	1062.6	1782.5	33.40	32.66	1314.4	1778.6
	13	33.30	33.22	151.9	1968.4	32.60	32.52	157.5	1929.6	32.90	32.52	720.9	1922.5
	14	33.30	33.19	199.6	1892.5	32.60	32.49	191.3	1767.4	32.90	32.49	739.9	1821.5
	15	33.00	33.14	-271.4	2003.4	32.30	32.43	-246.7	1891.5	32.50	32.41	180.0	1918.0
	16	33.00	33.19	-356.2	1900.5	32.30	32.48	-331.1	1823.1	32.50	32.45	83.9	1792.3
Row-3	17	32.70	32.97	-501.1	1865.5	32.20	32.33	-223.0	1762.4	32.30	32.24	98.8	1746.1
	18	32.70	32.96	-472.3	1850.1	32.20	32.31	-202.7	1767.3	32.30	32.23	117.3	1735.4
	19	32.50	32.92	-830.2	1997.6	31.90	32.25	-660.6	1893.6	32.10	32.20	-182.7	1906.4
	20	32.50	32.95	-842.3	1858.8	31.90	32.28	-673.4	1774.9	32.10	32.22	-221.2	1782.5
	21	32.50	32.97	-927.4	1995.0	31.90	32.30	-743.7	1883.9	32.20	32.26	-121.1	1865.5
	22	32.50	33.01	-1002.1	1982.6	31.90	32.34	-816.8	1876.5	32.20	32.30	-200.0	1916.9
	23	32.70	33.06	-711.9	1969.4	32.10	32.40	-551.0	1867.0	32.40	32.36	71.2	1903.1
	24	32.70	33.02	-615.5	1913.8	32.10	32.36	-467.4	1820.4	32.40	32.32	145.3	1787.8
Average Hc (W/m ² -K)					1967.3				1862.9				1864.4

Table F.8 Overall heat transfer coefficient (U-LMTD)

Test cond	Row number	Pipe number	Face area	Air T _{in}	Air T _{ot}	Q _{dot}	Ref Tin	Ref Tout	LMTD	U	
			m ²	°C	°C	W	°C	°C	K	W/m ² K	
2RGC7-S2	Row-1	Pipe 1	0.000124	29.28	39.38	0.80	81.60	81.51	47.05241	137.08	
		Pipe 2	0.000124	29.19	37.91	0.69	49.90	49.88	15.94801	347.24	
		Pipe 3	0.000124	29.16	36.28	0.56	46.50	46.49	13.46479	337.56	
		Pipe 4	0.000124	29.16	34.61	0.43	40.30	40.29	8.109724	424.91	
		Pipe 5	0.000124	29.19	33.70	0.35	38.90	38.90	7.222796	393.89	
		Pipe 6	0.000124	29.27	32.78	0.21	36.20	36.20	4.96892	340.98	
		Pipe 7	0.000124	29.34	32.53	0.24	35.70	35.70	4.578763	426.21	
		Pipe 8	0.000124	29.43	32.00	0.20	34.60	34.60	3.742775	425.79	
		Pipe 9	0.000124	29.50	31.76	0.17	34.30	34.30	3.550917	393.98	
		Pipe 10	0.000124	29.56	31.61	0.15	33.70	33.70	2.999384	414.12	
		Pipe 11	0.000124	29.61	31.50	0.14	33.60	33.60	2.945138	386.27	
		Pipe 12	0.000124	29.69	31.36	0.12	33.00	33.00	2.378208	415.31	
		Pipe 13	0.000124	29.74	31.24	0.11	32.70	32.70	2.122604	418.00	
		Pipe 14	0.000124	29.84	31.11	0.09	32.40	32.40	1.85044	399.85	
		Pipe 15	0.000124	29.88	31.14	0.09	32.30	32.30	1.717482	410.92	
		Pipe 16	0.000124	29.85	30.78	0.07	31.90	31.90	1.539833	368.49	
		Row-2	Pipe 17	0.000124	28.13	29.85	0.14	31.70	31.70	2.117685	519.61
			Pipe 18	0.000124	28.13	29.88	0.14	31.30	31.30	1.821586	614.39
			Pipe 19	0.000124	28.13	29.84	0.14	31.30	31.30	1.703395	644.00
			Pipe 20	0.000124	28.13	29.74	0.13	30.90	30.90	1.697276	607.33
			Pipe 21	0.000124	28.13	29.69	0.12	30.90	30.90	1.582633	629.50
			Pipe 22	0.000124	28.13	29.61	0.12	30.60	30.60	1.621792	578.83
			Pipe 23	0.000124	28.13	29.56	0.11	30.60	30.60	1.501209	606.34
			Pipe 24	0.000124	28.13	29.50	0.11	30.40	30.40	1.483845	583.26
			Pipe 25	0.000124	28.13	29.43	0.10	30.30	30.30	1.325158	617.90
			Pipe 26	0.000124	28.13	29.34	0.09	30.00	30.00	1.162173	655.09
			Pipe 27	0.000124	28.13	29.27	0.09	29.90	29.90	1.100147	652.74
			Pipe 28	0.000124	28.13	29.19	0.08	29.60	29.60	1.030206	641.92
			Pipe 29	0.000124	28.13	29.16	0.08	29.50	29.50	0.959408	668.23
			Pipe 30	0.000124	28.13	29.16	0.08	29.50	29.50	1.039637	616.44
			Pipe 31	0.000124	28.13	29.19	0.08	29.50	29.50	1.049454	632.98
			Pipe 32	0.000124	28.13	29.28	0.09	29.60	29.60	1.308306	548.99

(Test condition: air velocity = 1.3 m/s, air-ON temperature = 28.1°C, pressure = 75.7 bar)